


國立交通大學

機械工程學系

碩士論文

FC-72 流量震盪對一可變功率小圓型加熱面之週期性
流動沸騰熱傳及氣泡特性研究



Time periodic flow boiling heat transfer and bubble characteristics of FC-72 over a small heated circular plate due to simultaneous refrigerant flow rate and heat flux oscillations

研究生：陳文慶

指導教授：林清發博士

中華民國九十八年六月

**FC-72 流量震盪對一可變功率小圓型加熱面之週期性
流動沸騰熱傳及氣泡特性研究**

Time periodic flow boiling heat transfer and bubble characteristics of FC-72 over a small heated circular plate due to refrigerant flow rate and heat flux oscillation

研 究 生：陳文慶

Student: Wun Ching Chen

指 導 老 師：林清發

Advisor: Tsing-Fa Lin

國立交通大學



Submitted to Department of Mechanical Engineering

College of Engineering

National Chiao Tung University

In partial Fulfillment of the Requirements

For the Degree of

Master of Science

In Mechanical Engineering

June 2009

Hsinchu, Taiwan, Republic of China

中華民國 九十八 年 六 月

誌謝

幕然回首兩年前的此時，對於離家到新竹交大求學的我而言，心中真是充滿了既期待又害怕的複雜心情。來到交大這充滿學術研究氣息的生活，讓我覺得在此讀書做研究是一種享受。然而，一想到即將要離開這可愛的校園，不禁令人懷念起在此的點點滴滴。

能獲得碩士學位，首先很榮幸能接受林清發教授的指導，從文獻資料的蒐集、實驗系統的構思設計到最後物理觀念的闡述分析，都令我受益匪淺。而老師對我們在研究上嚴謹的要求，更深深地影響到我日後的處事態度。而能夠順利地完成我的碩士論文，要感謝實驗室博士班文瑞學長以及建安學長的幫忙及指導使得我的論文能順利完成。同學譚徵、書磊的互相砥礪幫忙，當然也少不了一群為實驗室注入活力、帶來歡樂的學弟們：游象麟、許書豪、熊宏嘉及陳俊州的幫忙。得之於人者太多，在此一同向所有幫助過我的人致謝。

即將踏出交大校門邁向另一求學生涯的我，回首來時路，很慶幸並沒辜負當初父母對我的期望；在今年能如期獲得碩士學位。我想今天若我有任何些微的成就，爺爺奶奶和父母對我的教養及支持鼓勵，是我能一路來的原動力，僅將我的榮耀獻給我摯愛的家人。

陳文慶
2009/6 於風城交大

FC-72 流量震盪對一可變功率小圓型加熱面之週期性流動沸騰熱傳及氣泡特性研究

研究生：陳文慶 指導教授：林清發 博士

國立交通大學機械工程學系

摘要

這項研究目的探索 FC-72 在矩形流道中流過一小圓型加熱塊同步時間週期性蓄冷劑震盪和熱通量震盪對沸騰熱傳以及氣泡特徵研究。流量震盪為三角波震盪以及熱通量震盪為正旋波震盪。探討流量以及熱通量同向以及反向震盪研究。實驗參數為流量為 200, 300 以及 400 kg/m²s 震幅為 5%, 10% 以及 15%, 熱通量範圍為 0.1 到 10W/cm² 震幅為 10%, 30% 以及 50% 週期為 10 到 30 秒, 次冷度為 0 到 15K, 壓力為常壓。

實驗結果顯示在單向流中流量和熱通量同向震盪時會有抑制壁溫震盪的效果然而在雙相流中流量和熱通量反向震盪才能有效抑制壁溫的震盪, 由於熱通量以及流量對壁溫的反應時間有延遲因此在加以考慮延遲的因素後確實能驗證說單向流中流量和熱通量同向震盪以及雙相流中流量和熱通量反向震盪能有效的防止壁溫的震盪。



**Time periodic flow boiling heat transfer and bubble characteristics of FC-72
over a small heated circular plate due to simultaneous refrigerant flow rate
and heat flux oscillation**

Student : Wun Ching Chen Advisor : Prof. Tsing-Fa Lin

Department of Mechanical Engineering

National Chiao Tung University

ABSTRACT

This study intends to explore how simultaneously imposed time periodic coolant flow rate and heat flux oscillations affect the temporal flow boiling heat transfer and associated bubble characteristics of FC-72 over a small circular heated copper plate flush mounted on the bottom of a horizontal rectangular channel. The oscillations of the coolant flow rate and heat flux are respectively in the forms of nearly triangular and sinusoidal waves. Both the in-phase and out-of-phase mass flux and heat flux oscillations are investigated. In the experiment the time-average coolant mass flux \bar{G} is varied from 300 to 400 kg/m²s and the amplitude of the coolant mass flux oscillation is mainly fixed at 5, 10 and 15% of \bar{G} . The mean heat flux ranges from 0.1 to 10W/cm² with the amplitude of the heat flux oscillation set at 10, 30 and 50% of \bar{q} for the same period of the heat flux and mass flux oscillations varied from 10 to 30 seconds Besides, the time-average liquid subcooling at the inlet of the test section ranges from 0 to 15K and the system is at slightly subatmospheric pressure.

The transient oscillatory flow boiling heat transfer characteristics are illustrated by presenting the measured time variations of the heated plate temperature and boiling heat transfer coefficient. The experimental results show that the heated surface temperature also oscillates periodically in time at the same frequency as the mass and heat flux oscillations. Besides, the amplitude of the T_w oscillation is generally smaller in the flow boiling when the out-of-phase G and q oscillations are imposed. But in the single-phase flow the T_w oscillation is normally weaker by imposing in-phase G and q oscillations. These results indicate that the oscillation in T_w caused by the heat flux oscillation

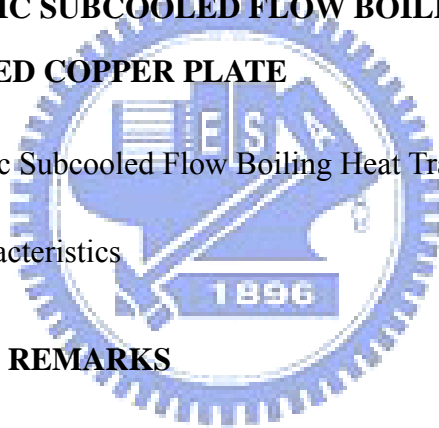
can be suppressed by the in-phase G oscillation in the single-phase flow and by the out-of-phase G oscillation in the boiling flow. It is further noted that by imposing the G oscillation at the time instant equal to the difference between the time lags in T_w resulting respectively from the q oscillation only behind the q oscillation, and G oscillation only behind the q oscillation, the T_w oscillation can be significantly suppressed and even completely wiped out.



TABLE OF CONTENTS

ABSTRACT	i
TABLE OF CONTENTS	ii
LIST OF TABLE	iii
LIST OF FIGURE	iv
CHAPTER 1 INTRODUCTION	
1.1 Motive of the Present Study	1
1.2 Literature Review	2
1.2.1 Steady Single-Phase Force Convection Heat Transfer	2
1.2.2 Transient pool boiling heat transfer	3
1.2.3 Transient single-phase forced convection heat transfer	4
1.2.4 Transient flow boiling heat transfer	5
1.2.5 Bubble Characteristics	7
1.3 Objective of This Study	9
CHAPTER 2 EXPERIMENTAL APPARATUS AND PROCEDURES	12
2.1 Degassing Unit	12
2.2 Coolant Loop	12
2.3 Test Section	13
2.4 Hot-water Loop	14
2.5 Cold-water Loop	15
2.6 DC Power Supply	15
2.7 Data Acquisition	15
2.8 Optical Measurement Technique	16
2.9 Experimental Procedures	16
2.10 Experimental Parameters	17

CHAPTER 3 DATA REDUCTION	28
3.1 Single Phase Heat Transfer	28
3.2 Two Phase Flow Boiling Heat Transfer	30
3.3 Uncertainty Analysis	31
CHAPTER 4 TIME PERIODIC SATURATED FLOW BOILING OF FC-72 OVER A SMALL HEATED COPPER PLATE	33
4.1 Single-phase Liquid Convective Heat Transfer	34
4.2 Time Periodic Saturated Flow Boiling Heat Transfer Characteristics	34
4.3 Bubble Characteristics	38
CHAPTER 5 TIME PERIODIC SUBCOOLED FLOW BOILING OF FC-72 OVER A SMALL HEATED COPPER PLATE	100
5.1 Time Periodic Subcooled Flow Boiling Heat Transfer Characteristics	101
5.2 Bubble Characteristics	104
CHAPTER 6 CONCLUDING REMARKS	169
REFERENCES	171



LIST OF TABLES

Table 1.1 Thermodynamic properties for FC-72	12
Table 1.2 Some single-phase convection heat transfer correlations for electronic cooling	13
Table 2.1 Experimental parameters	18
Table 2.2 Thermodynamic and transport properties of the dielectric refrigerant FC-72 list	19
Table 3.1 Summary of the uncertainty analysis	32
Table 4.1 Amplitudes of T_w oscillation and relative time lags in transient oscillatory saturated flow boiling for various \bar{q} at $\Delta q/\bar{q} = 30\%$, $\Delta G/\bar{G} = 10\%$ and $t_p = 20$ sec. for $\bar{G} = 200$ kg/m ² s.	40
Table 4.2 Amplitudes of T_w oscillation and relative time lags in transient oscillatory saturated flow boiling for various \bar{q} at $\Delta q/\bar{q} = 10, 30, 50\%$, $\Delta G/\bar{G} = 5\%$ and $t_p = 20$ sec. for $\bar{G} = 300$ kg/m ² s.	41
Table 4.3 Amplitudes of T_w oscillation and relative time lags in transient oscillatory saturated flow boiling for various \bar{q} at $\Delta q/\bar{q} = 10, 30, 50\%$, $\Delta G/\bar{G} = 10\%$ and $t_p = 20$ sec. for $\bar{G} = 300$ kg/m ² s.	42
Table 4.4 Amplitudes of T_w oscillation and relative time lags in transient oscillatory saturated flow boiling for various \bar{q} at $\Delta q/\bar{q} = 30\%$, $\Delta G/\bar{G} = 15\%$ and $t_p = 20$ sec. for $\bar{G} = 300$ kg/m ² s.	43
Table 4.5 Amplitudes of T_w oscillation and relative time lags in transient oscillatory saturated flow boiling for various \bar{q} at $\Delta q/\bar{q} = 30\%$, $\Delta G/\bar{G} = 10\%$ and $t_p = 20$ sec. for $\bar{G} = 400$ kg/m ² s.	43
Table 4.6 Amplitudes of T_w oscillation and relative time lags in transient oscillatory saturated flow boiling for various \bar{q} at $\Delta q/\bar{q} = 10, 30, 50\%$, $\Delta G/\bar{G} = 5\%$ and $t_p = 30$ sec. for $\bar{G} = 300$ kg/m ² s.	44
Table 4.7 Amplitudes of T_w oscillation and relative time lags in transient oscillatory saturated flow boiling for various \bar{q} at $\Delta q/\bar{q} = 10, 20\%$, $\Delta G/\bar{G} = 15\%$ and $t_p = 20$ sec. for $\bar{G} = 300$ kg/m ² s.	45
Table 4.8 Amplitudes of T_w oscillation and relative time lags in transient oscillatory saturated flow boiling for various \bar{q} at $\Delta q/\bar{q} = 10, 15\%$, $\Delta G/\bar{G} = 20\%$ and $t_p = 30$ sec. for $\bar{G} = 300$ kg/m ² s.	45

Table 5.1 Amplitudes of T_w oscillation and relative time lags in transient oscillatory subcooled flow boiling for various \bar{q} for $\Delta q/\bar{q}=30\%$, $\Delta G/\bar{G}=10\%$ and $t_p=20\text{sec}$. at $\bar{G}=300\text{kg/m}^2\text{s}$ and $\Delta\bar{T}_{sub}=5\text{K}$.	106
Table 5.2 Amplitudes of T_w oscillation and relative time lags in transient oscillatory subcooled flow boiling for various \bar{q} for $\Delta q/\bar{q}=30\%$, $\Delta G/\bar{G}=10\%$ and $t_p=20\text{sec}$. at $\bar{G}=200\text{kg/m}^2\text{s}$ and $\Delta\bar{T}_{sub}=10\text{K}$.	106
Table 5.3 Amplitudes of T_w oscillation and relative time lags in transient oscillatory subcooled flow boiling for various \bar{q} for $\Delta q/\bar{q}=30\%$, $\Delta G/\bar{G}=5\%$ and $t_p=20\text{sec}$. at $\bar{G}=300\text{kg/m}^2\text{s}$ and $\Delta\bar{T}_{sub}=10\text{K}$.	107
Table 5.4 Amplitudes of T_w oscillation and relative time lags in transient oscillatory subcooled flow boiling for various \bar{q} for $\Delta q/\bar{q}=30\%$, $\Delta G/\bar{G}=15\%$ and $t_p=20\text{sec}$. at $\bar{G}=300\text{kg/m}^2\text{s}$ and $\Delta\bar{T}_{sub}=10\text{K}$.	107
Table 5.5 Amplitudes of T_w oscillation and relative time lags in transient oscillatory subcooled flow boiling for various \bar{q} for $\Delta q/\bar{q}=10,30,50\%$, $\Delta G/\bar{G}=10\%$ and $t_p=20\text{sec}$ at $\bar{G}=300\text{kg/m}^2\text{s}$ and $\Delta\bar{T}_{sub}=10\text{K}$.	108
Table 5.6 Amplitudes of T_w oscillation and relative time lags in transient oscillatory subcooled flow boiling for various \bar{q} for $\Delta q/\bar{q}=30\%$, $\Delta G/\bar{G}=10\%$ and $t_p=20\text{sec}$ at $\bar{G}=400\text{kg/m}^2\text{s}$ and $\Delta\bar{T}_{sub}=10\text{K}$.	109
Table 5.7 Amplitudes of T_w oscillation and relative time lags in transient oscillatory subcooled flow boiling for various \bar{q} for $\Delta q/\bar{q}=30\%$, $\Delta G/\bar{G}=10\%$ and $t_p=20\text{sec}$ at $\bar{G}=300\text{kg/m}^2\text{s}$ and $\Delta\bar{T}_{sub}=15\text{K}$.	109
Table 5.8 Amplitudes of T_w oscillation and relative time lags in transient oscillatory subcooled flow boiling for various \bar{q} for $\Delta q/\bar{q}=30\%$, $\Delta G/\bar{G}=10\%$ and $t_p=30\text{sec}$ at $\bar{G}=300\text{kg/m}^2\text{s}$ and $\Delta\bar{T}_{sub}=10\text{K}$.	110
Table 5.9 Amplitudes of T_w oscillation and relative time lags in transient oscillatory subcooled flow boiling for various \bar{q} for $\Delta q/\bar{q}=5,10,23\%$, $\Delta G/\bar{G}=5\%$ and $t_p=20\text{sec}$ at $\bar{G}=300\text{kg/m}^2\text{s}$ and $\Delta\bar{T}_{sub}=10\text{K}$.	110
Table 5.10 Amplitudes of T_w oscillation and relative time lags in transient oscillatory subcooled flow boiling for various \bar{q} for $\Delta q/\bar{q}=8,30,32,45\%$, $\Delta G/\bar{G}=10\%$ and $t_p=20\text{sec}$ at $\bar{G}=300\text{kg/m}^2\text{s}$ and $\Delta\bar{T}_{sub}=10\text{K}$.	111

Table 5.11 Amplitudes of T_w oscillation and relative time lags in transient oscillatory subcooled flow boiling for various \bar{q} for $\Delta q/\bar{q}=15,35,50\%$, $\Delta G/\bar{G}=15\%$ and $t_p=20\text{sec}$ at $\bar{G}=300\text{kg/m}^2\text{s}$ and $\Delta T_{sub}=10\text{K}$.

111



LIST OF FIGURES

Experiment Apparatus

Fig. 2.1 Schematic diagram of experimental apparatus	23
Fig. 2.2 Three-dimensional plots of test section along with inlet and outlet sections	24
Fig. 2.3 Three-dimensional plots illustrating the test section in the rectangular flow channel	25
Fig. 2.4 Three-dimensional pictures showing (a) hollow cylindrical Teflon block and (b) cylindrical Teflon bolt	26
Fig. 2.5 Locations of thermocouples	27
Fig. 2.6 Schematics of the copper plate module	28
Fig. 2.7 Locations of the thermocouples inside the cylindrical-hollow Teflon block	29
Fig. 2.8 Schematic diagram of heat flux oscillation control loop	30

Saturated Flow Boiling

Fig. 4.1 Comparison of the present steady single-phase liquid convection heat transfer data with the correlation of Gersey and Mudawar (1992) for (a) $h_{1\phi}$ vs. G and (b) Nu_L vs. Re_L .	46
Fig. 4.2 Time variations of the copper plate temperature in stable saturated flow boiling for various imposed heat fluxes at (a) $G=300\text{kg}/\text{m}^2\text{s}$ (b) $G=400\text{kg}/\text{m}^2\text{s}$	47
Fig. 4.3 Fig. 4.2 (a) Stable saturated flow boiling curve (b) Stable saturated flow boiling heat transfer coefficients.	48
Fig.4.4 Time variations of the measured instantaneous heated surface temperature for (a) imposed heat flux oscillation only, (b) in-phase G and q oscillations and (c) out-of-phase G and q oscillations at $\bar{G} = 200\text{kg}/\text{m}^2\text{s}$ and $\Delta G/\bar{G} = 10\%$ for $\Delta q/\bar{q} = 30\%$ and $t_p = 20\text{sec}$.	49
Fig.4.5 Time variations of the measured instantaneous heated surface temperature for (a) imposed heat flux oscillation only, (b) in-phase G and q oscillations and (c) out-of-phase G and q oscillations at $\bar{G} = 300\text{kg}/\text{m}^2\text{s}$ and $\Delta G/\bar{G} = 5\%$ for $\Delta q/\bar{q} = 10\%$ and $t_p = 20\text{sec}$.	50
Fig.4.6 Time variations of the measured instantaneous heated surface temperature for (a) imposed heat flux oscillation only, (b) in-phase G and q oscillations and (c) out-of-phase G and q oscillations at $\bar{G} = 300\text{kg}/\text{m}^2\text{s}$ and $\Delta G/\bar{G} = 5\%$ for $\Delta q/\bar{q} = 30\%$ and $t_p = 20\text{sec}$.	51
Fig.4.7 Time variations of the measured instantaneous heated surface temperature for (a) imposed heat	

flux oscillation only, (b) in-phase G and q oscillations and (c) out-of-phase G and q oscillations at $\bar{G} = 300kg/m^2s$ and $\Delta G/\bar{G} = 5\%$ for $\Delta q/\bar{q} = 50\%$ and $t_p = 20sec$. 52

Fig.4.8 Time variations of the measured instantaneous heated surface temperature for (a) imposed heat flux oscillation only, (b) in-phase G and q oscillations and (c) out-of-phase G and q oscillations at $\bar{G} = 300kg/m^2s$ and $\Delta G/\bar{G} = 10\%$ for $\Delta q/\bar{q} = 10\%$ and $t_p = 20sec$. 53

Fig.4.9 Time variations of the measured instantaneous heated surface temperature for (a) imposed heat flux oscillation only, (b) in-phase G and q oscillations and (c) out-of-phase G and q oscillations at $\bar{G} = 300kg/m^2s$ and $\Delta G/\bar{G} = 10\%$ for $\Delta q/\bar{q} = 30\%$ and $t_p = 20sec$. 54

Fig.4.10 Time variations of the measured instantaneous heated surface temperature for (a) imposed heat flux oscillation only, (b) in-phase G and q oscillations and (c) out-of-phase G and q oscillations at $\bar{G} = 300kg/m^2s$ and $\Delta G/\bar{G} = 10\%$ for $\Delta q/\bar{q} = 50\%$ and $t_p = 20sec$. 55

Fig.4.11 Time variations of the measured instantaneous heated surface temperature for (a) imposed heat flux oscillation only, (b) in-phase G and q oscillations and (c) out-of-phase G and q oscillations at $\bar{G} = 300kg/m^2s$ and $\Delta G/\bar{G} = 15\%$ for $\Delta q/\bar{q} = 30\%$ and $t_p = 20sec$. 56

Fig.4.12 Time variations of the measured instantaneous heated surface temperature for (a) imposed heat flux oscillation only, (b) in-phase G and q oscillations and (c) out-of-phase G and q oscillations at $\bar{G} = 400kg/m^2s$ and $\Delta G/\bar{G} = 10\%$ for $\Delta q/\bar{q} = 30\%$ and $t_p = 20sec$. 57

Fig.4.13 Time variations of the measured instantaneous heated surface temperature for (a) imposed heat flux oscillation only, (b) in-phase G and q oscillations and (c) out-of-phase G and q oscillations at $\bar{G} = 300kg/m^2s$ and $\Delta G/\bar{G} = 5\%$ for $\Delta q/\bar{q} = 10\%$ and $t_p = 30sec$. 58

Fig.4.14 Time variations of the measured instantaneous heated surface temperature for (a) imposed heat flux oscillation only, (b) in-phase G and q oscillations and (c) out-of-phase G and q oscillations at $\bar{G} = 300kg/m^2s$ and $\Delta G/\bar{G} = 5\%$ for $\Delta q/\bar{q} = 30\%$ and $t_p = 30sec$. 59

Fig.4.15 Time variations of the measured instantaneous heated surface temperature for (a) imposed heat flux oscillation only, (b) in-phase G and q oscillations and (c) out-of-phase G and q oscillations at $\bar{G} = 300kg/m^2s$ and $\Delta G/\bar{G} = 5\%$ for $\Delta q/\bar{q} = 50\%$ and $t_p = 30sec$. 60

Fig.4.16 Time variations of the measured instantaneous heated surface temperature for (a) imposed heat flux oscillation only, (b) imposed mass flux oscillation only, and (c) in-phase or out-of-phase G and q oscillations at $\bar{G} = 300kg/m^2s$ and $\Delta G/\bar{G} = 15\%$ for various \bar{q} at $t_p = 20sec$. 61

Fig.4.17 Time variations of the measured instantaneous heated surface temperature for (a) imposed heat flux oscillation only, (b) imposed mass flux oscillation only, and (c) in-phase or out-of-phase G

and q oscillations at $\bar{G} = 300 \text{ kg/m}^2 \text{ s}$ and $\Delta G/\bar{G} = 20\%$ for various \bar{q} at $t_p = 30 \text{ sec}$. 62

Fig. 4.18 Time variations of the heat transfer coefficient for (a) imposed heat flux oscillation only, (b) in-phase G and q oscillations and (c) out-of-phase G and q oscillations at $\bar{G} = 200 \text{ kg/m}^2 \text{ s}$ and $\Delta G/\bar{G} = 10\%$ for $\Delta q/\bar{q} = 30\%$ and $t_p = 20 \text{ sec}$. 63

Fig. 4.19 Time variations of the heat transfer coefficient for (a) imposed heat flux oscillation only, (b) in-phase G and q oscillations and (c) out-of-phase G and q oscillations at $\bar{G} = 300 \text{ kg/m}^2 \text{ s}$ and $\Delta G/\bar{G} = 5\%$ for $\Delta q/\bar{q} = 10\%$ and $t_p = 20 \text{ sec}$. 64

Fig. 4.20 Time variations of the heat transfer coefficient for (a) imposed heat flux oscillation only, (b) in-phase G and q oscillations and (c) out-of-phase G and q oscillations at $\bar{G} = 300 \text{ kg/m}^2 \text{ s}$ and $\Delta G/\bar{G} = 5\%$ for $\Delta q/\bar{q} = 30\%$ and $t_p = 20 \text{ sec}$. 65

Fig. 4.21 Time variations of the heat transfer coefficient for (a) imposed heat flux oscillation only, (b) in-phase G and q oscillations and (c) out-of-phase G and q oscillations at $\bar{G} = 300 \text{ kg/m}^2 \text{ s}$ and $\Delta G/\bar{G} = 5\%$ for $\Delta q/\bar{q} = 50\%$ and $t_p = 20 \text{ sec}$. 66

Fig. 4.22 Time variations of the heat transfer coefficient for (a) imposed heat flux oscillation only, (b) in-phase G and q oscillations and (c) out-of-phase G and q oscillations at $\bar{G} = 300 \text{ kg/m}^2 \text{ s}$ and $\Delta G/\bar{G} = 10\%$ for $\Delta q/\bar{q} = 10\%$ and $t_p = 20 \text{ sec}$. 67

Fig. 4.23 Time variations of the heat transfer coefficient for (a) imposed heat flux oscillation only, (b) in-phase G and q oscillations and (c) out-of-phase G and q oscillations at $\bar{G} = 300 \text{ kg/m}^2 \text{ s}$ and $\Delta G/\bar{G} = 10\%$ for $\Delta q/\bar{q} = 30\%$ and $t_p = 20 \text{ sec}$. 68

Fig. 4.24 Time variations of the heat transfer coefficient for (a) imposed heat flux oscillation only, (b) in-phase G and q oscillations and (c) out-of-phase G and q oscillations at $\bar{G} = 300 \text{ kg/m}^2 \text{ s}$ and $\Delta G/\bar{G} = 10\%$ for $\Delta q/\bar{q} = 50\%$ and $t_p = 20 \text{ sec}$. 69

Fig. 4.25 Time variations of the heat transfer coefficient for (a) imposed heat flux oscillation only, (b) in-phase G and q oscillations and (c) out-of-phase G and q oscillations at $\bar{G} = 300 \text{ kg/m}^2 \text{ s}$ and $\Delta G/\bar{G} = 15\%$ for $\Delta q/\bar{q} = 30\%$ and $t_p = 20 \text{ sec}$. 70

Fig. 4.26 Time variations of the heat transfer coefficient for (a) imposed heat flux oscillation only, (b) in-phase G and q oscillations and (c) out-of-phase G and q oscillations at $\bar{G} = 400 \text{ kg/m}^2 \text{ s}$ and $\Delta G/\bar{G} = 10\%$ for $\Delta q/\bar{q} = 30\%$ and $t_p = 20 \text{ sec}$. 71

Fig. 4.27 Time variations of the heat transfer coefficient for (a) imposed heat flux oscillation only, (b)

in-phase G and q oscillations and (c) out-of-phase G and q oscillations at $\bar{G} = 300\text{kg}/\text{m}^2\text{s}$ and $\Delta G/\bar{G} = 5\%$ for $\Delta q/\bar{q} = 10\%$ and $t_p = 30\text{sec}$. 72

Fig. 4.28 Time variations of the heat transfer coefficient for (a) imposed heat flux oscillation only, (b) in-phase G and q oscillations and (c) out-of-phase G and q oscillations at $\bar{G} = 300\text{kg}/\text{m}^2\text{s}$ and $\Delta G/\bar{G} = 5\%$ for $\Delta q/\bar{q} = 30\%$ and $t_p = 30\text{sec}$. 73

Fig. 4.29 Time variations of the heat transfer coefficient for (a) imposed heat flux oscillation only, (b) in-phase G and q oscillations and (c) out-of-phase G and q oscillations at $\bar{G} = 300\text{kg}/\text{m}^2\text{s}$ and $\Delta G/\bar{G} = 5\%$ for $\Delta q/\bar{q} = 50\%$ and $t_p = 30\text{sec}$. 74

Fig. 4.30 Time variations of the heat transfer coefficient for (a) imposed heat flux oscillation only, (b) imposed mass flux oscillation only and (c) out-of-phase G and q oscillations at $\bar{G} = 300\text{kg}/\text{m}^2\text{s}$ and $\Delta G/\bar{G} = 15\%$ for $\Delta q/\bar{q} = 10, 20\%$ and $t_p = 20\text{sec}$. 75

Fig. 4.31 Time variations of the heat transfer coefficient for (a) imposed heat flux oscillation only, (b) imposed mass flux oscillation only and (c) out-of-phase G and q oscillations at $\bar{G} = 300\text{kg}/\text{m}^2\text{s}$ and $\Delta G/\bar{G} = 20\%$ for $\Delta q/\bar{q} = 10, 15\%$ and $t_p = 20\text{sec}$. 76

Fig. 4.32 Photos of stable saturated flow boiling at certain time instants in statistical state for various imposed heat fluxes for (a) $G = 200\text{kg}/\text{m}^2\text{s}$, (b) $G = 300\text{kg}/\text{m}^2\text{s}$ and (c) $G = 400\text{kg}/\text{m}^2\text{s}$. 77

Fig. 4.33 Photos of saturated flow boiling at certain time instants in a typical time periodic cycle for an imposed constant mass flux at $\bar{q} = 4.03\text{W}/\text{cm}^2$, $\Delta q/\bar{q} = 30\%$, $G = 200\text{kg}/\text{m}^2\text{s}$ and $t_p = 20\text{sec}$. 78

Fig. 4.34 Photos of saturated flow boiling at certain time instants in a typical time periodic cycle for imposed in-phase G & q oscillations at $\bar{G} = 200\text{kg}/\text{m}^2\text{s}$, $\Delta G/\bar{G} = 10\%$, $\bar{q} = 4.03\text{W}/\text{cm}^2$ and $\Delta q/\bar{q} = 30\%$ with $t_p = 20\text{sec}$. 79

Fig. 4.35 Photos of saturated flow boiling at certain time instants in a typical time periodic cycle for imposed out-of-phase G & q oscillations at $\bar{G} = 200\text{kg}/\text{m}^2\text{s}$, $\Delta G/\bar{G} = 10\%$, $\bar{q} = 4.03\text{W}/\text{cm}^2$ and $\Delta q/\bar{q} = 30\%$ with $t_p = 20\text{sec}$. 80

Fig. 4.36 Photos of saturated flow boiling at certain time instants in a typical time periodic cycle for an imposed constant mass flux at $\bar{q} = 4.03\text{W}/\text{cm}^2$, $\Delta q/\bar{q} = 30\%$, $G = 300\text{kg}/\text{m}^2\text{s}$ and $t_p = 20\text{sec}$. 81

Fig. 4.37 Photos of saturated flow boiling at certain time instants in a typical time periodic cycle for imposed in-phase G & q oscillations at $\bar{G} = 300\text{kg}/\text{m}^2\text{s}$, $\Delta G/\bar{G} = 10\%$, $\bar{q} = 4.03\text{W}/\text{cm}^2$ and $\Delta q/\bar{q} = 30\%$ with $t_p = 20\text{sec}$. 82

Fig. 4.38 Photos of saturated flow boiling at certain time instants in a typical time periodic cycle for

imposed out-of-phase G & q oscillations at $\bar{G}=300\text{kg/m}^2\text{s}$, $\Delta G/\bar{G}=10\%$, $\bar{q}=4.03\text{W/cm}^2$ and $\Delta q/\bar{q}=30\%$ with $t_p = 20\text{sec}$. 83

Fig. 4.39 Photos of saturated flow boiling at certain time instants in a typical time periodic cycle for imposed in-phase G & q oscillations at $\bar{G}=300\text{kg/m}^2\text{s}$, $\Delta G/\bar{G}=15\%$, $\bar{q}=4.03\text{W/cm}^2$ and $\Delta q/\bar{q}=30\%$ with $t_p = 20\text{sec}$. 84

Fig. 4.40 Photos of saturated flow boiling at certain time instants in a typical time periodic cycle for imposed out-of-phase G & q oscillations at $\bar{G}=300\text{kg/m}^2\text{s}$, $\Delta G/\bar{G}=15\%$, $\bar{q}=4.03\text{W/cm}^2$ and $\Delta q/\bar{q}=30\%$ with $t_p = 20\text{sec}$. 85

Fig. 4.41 Photos of saturated flow boiling at certain time instants in a typical time periodic cycle for an imposed constant mass flux at $\bar{q}=4.03\text{W/cm}^2$, $\Delta q/\bar{q}=50\%$, $G = 300\text{kg/m}^2\text{s}$ and $t_p = 20\text{sec}$. 86

Fig. 4.42 Photos of saturated flow boiling at certain time instants in a typical time periodic cycle for imposed in-phase G & q oscillations at $\bar{G}=300\text{kg/m}^2\text{s}$, $\Delta G/\bar{G}=10\%$, $\bar{q}=4.03\text{W/cm}^2$ and $\Delta q/\bar{q}=50\%$ with $t_p = 20\text{sec}$. 87

Fig. 4.43 Photos of saturated flow boiling at certain time instants in a typical time periodic cycle for imposed out-of-phase G & q oscillations at $\bar{G}=300\text{kg/m}^2\text{s}$, $\Delta G/\bar{G}=10\%$, $\bar{q}=4.03\text{W/cm}^2$ and $\Delta q/\bar{q}=50\%$ with $t_p = 20\text{sec}$. 88

Fig. 4.44 Photos of saturated flow boiling at certain time instants in a typical time periodic cycle for an imposed constant mass flux at $\bar{q}=4.03\text{W/cm}^2$, $\Delta q/\bar{q}=30\%$, $G = 300\text{kg/m}^2\text{s}$ and $t_p = 30\text{sec}$. 89

Fig. 4.45 Photos of saturated flow boiling at certain time instants in a typical time periodic cycle for imposed in-phase G & q oscillations at $\bar{G}=300\text{kg/m}^2\text{s}$, $\Delta G/\bar{G}=10\%$, $\bar{q}=4.03\text{W/cm}^2$ and $\Delta q/\bar{q}=30\%$ with $t_p = 30\text{sec}$. 90

Fig. 4.46 Photos of saturated flow boiling at certain time instants in a typical time periodic cycle for imposed out-of-phase G & q oscillations at $\bar{G}=300\text{kg/m}^2\text{s}$, $\Delta G/\bar{G}=10\%$, $\bar{q}=4.03\text{W/cm}^2$ and $\Delta q/\bar{q}=30\%$ with $t_p = 30\text{sec}$. 91

Fig. 4.47 Photos of subcooled flow boiling at certain time instants in a typical time periodic cycle for an imposed constant mass flux at $\bar{q}=4.01\text{W/cm}^2$, $\Delta q/\bar{q}=15\%$, $G = 300\text{kg/m}^2\text{s}$ with $t_p = 20\text{sec}$. 92

Fig. 4.48 Photos of subcooled flow boiling at certain time instants in a typical time periodic cycle for an imposed constant heat flux at $\bar{q}=4.01\text{W/cm}^2$, $G = 300\text{kg/m}^2\text{s}$, $\Delta G/\bar{G}=10\%$ with $t_p = 20\text{sec}$. 93

Fig. 4.49 Photos of subcooled flow boiling at certain time instants in a typical time periodic cycle for imposed out-of-phase G & q oscillations at $\bar{G}=300\text{kg/m}^2\text{s}$, $\Delta G/\bar{G}=10\%$, $\bar{q}=4.01\text{W/cm}^2$ and $\Delta q/\bar{q}=15\%$ with $t_p = 20\text{sec}$. 94

Fig. 4.50 Photos of subcooled flow boiling at certain time instants in a typical time periodic cycle for an imposed constant mass flux at $\bar{q}=4.01\text{W/cm}^2$, $\Delta q/\bar{q}=20\%$, $G = 300\text{kg/m}^2\text{s}$ with $t_p = 20\text{sec}$. 95

Fig. 4.51 Photos of subcooled flow boiling at certain time instants in a typical time periodic cycle for an imposed constant heat flux at $\bar{q}=4.01\text{W/cm}^2$, $G = 300\text{kg/m}^2\text{s}$, $\Delta G/\bar{G}=15\%$ with $t_p = 20\text{sec}$. 96

Fig. 4.52 Photos of subcooled flow boiling at certain time instants in a typical time periodic cycle for imposed out-of-phase G & q oscillations at $\bar{G}=300\text{kg/m}^2\text{s}$, $\Delta G/\bar{G}=15\%$, $\bar{q}=4.01\text{W/cm}^2$ and $\Delta q/\bar{q}=20\%$ with $t_p = 20\text{sec}$. 97

Fig. 4.53 Time period oscillatory saturated flow boiling of FC-72 with $\bar{q}=4.03\text{W/cm}^2$, $\Delta q/\bar{q}=30\%$, $G=300\text{kg/m}^2\text{s}$, $\Delta G/\bar{G}=10\%$ and $t_p=20\text{sec}$. for the time variations of bubble characteristics: (a) bubble departure diameter (b) bubble departure frequency (c) active nucleation site density. 98

Fig. 4.54 Time period oscillatory saturated flow boiling of FC-72 with $\bar{q}=4.03\text{W/cm}^2$, $\Delta q/\bar{q}=30\%$, $G=300\text{kg/m}^2\text{s}$, $\Delta G/\bar{G}=15\%$ and $t_p=20\text{sec}$. for the time variations of bubble characteristics: (a) bubble departure diameter (b) bubble departure frequency (c) active nucleation site density. 99

Subcooled Flow Boiling

Fig. 5.1 Time variations of the copper plate temperature in stable subcooled flow boiling for various imposed heat fluxes at (a) $G=300\text{kg/m}^2\text{s}$ and (b) $G=400\text{kg/m}^2\text{s}$ 112

Fig. 5.2 (a) Stable subcooled flow boiling curve and (b) stable subcooled flow boiling heat transfer coefficient. 113

Fig. 5.3 Time variations of the measured instantaneous heated surface temperature for (a) imposed heat flux oscillation only, (b) in-phase G and q oscillations and (c) out-of-phase G and q oscillations at $\bar{G} = 300\text{kg/m}^2\text{s}$ and $\Delta G/\bar{G} = 10\%$ for $\Delta q/\bar{q} = 30\%$ and $t_p = 20\text{sec}$. for $\Delta T_{sub} = 5\text{K}$. 114

Fig. 5.4 Time variations of the measured instantaneous heated surface temperature for (a) imposed heat flux oscillation only, (b) in-phase G and q oscillations and (c) out-of-phase G and q oscillations at $\bar{G} = 200\text{kg/m}^2\text{s}$ and $\Delta G/\bar{G} = 10\%$ for $\Delta q/\bar{q} = 30\%$ and $t_p = 20\text{sec}$. for $\Delta T_{sub} = 10\text{K}$. 115

Fig. 5.5 Time variations of the measured instantaneous heated surface temperature for (a) imposed heat flux oscillation only, (b) in-phase G and q oscillations and (c) out-of-phase G and q oscillations at $\bar{G} = 300\text{kg/m}^2\text{s}$ and $\Delta G/\bar{G} = 5\%$ for $\Delta q/\bar{q} = 30\%$ and $t_p = 20\text{sec}$. for $\Delta T_{sub} = 10\text{K}$. 116

Fig. 5.6 Time variations of the measured instantaneous heated surface temperature for (a) imposed heat flux oscillation only, (b) in-phase G and q oscillations and (c) out-of-phase G and q oscillations

at $\bar{G} = 300 \text{ kg/m}^2\text{s}$ and $\Delta G/\bar{G} = 10\%$ for $\Delta q/\bar{q} = 10\%$ and $t_p = 20 \text{ sec}$. for $\Delta \bar{T}_{sub} = 10 \text{ K}$. 117

Fig. 5.7 Time variations of the measured instantaneous heated surface temperature for (a) imposed heat flux oscillation only, (b) in-phase G and q oscillations and (c) out-of-phase G and q oscillations

at $\bar{G} = 300 \text{ kg/m}^2\text{s}$ and $\Delta G/\bar{G} = 10\%$ for $\Delta q/\bar{q} = 30\%$ and $t_p = 20 \text{ sec}$. for $\Delta \bar{T}_{sub} = 10 \text{ K}$. 118

Fig. 5.8 Time variations of the measured instantaneous heated surface temperature for (a) imposed heat flux oscillation only, (b) in-phase G and q oscillations and (c) out-of-phase G and q oscillations

at $\bar{G} = 300 \text{ kg/m}^2\text{s}$ and $\Delta G/\bar{G} = 10\%$ for $\Delta q/\bar{q} = 50\%$ and $t_p = 20 \text{ sec}$. for $\Delta \bar{T}_{sub} = 10 \text{ K}$. 119

Fig. 5.9 Time variations of the measured instantaneous heated surface temperature for (a) imposed heat flux oscillation only, (b) in-phase G and q oscillations and (c) out-of-phase G and q oscillations

at $\bar{G} = 300 \text{ kg/m}^2\text{s}$ and $\Delta G/\bar{G} = 15\%$ for $\Delta q/\bar{q} = 30\%$ and $t_p = 20 \text{ sec}$. for $\Delta \bar{T}_{sub} = 10 \text{ K}$. 120

Fig. 5.10 Time variations of the measured instantaneous heated surface temperature for (a) imposed heat flux oscillation only, (b) in-phase G and q oscillations and (c) out-of-phase G and q oscillations

at $\bar{G} = 400 \text{ kg/m}^2\text{s}$ and $\Delta G/\bar{G} = 10\%$ for $\Delta q/\bar{q} = 30\%$ and $t_p = 20 \text{ sec}$. for $\Delta \bar{T}_{sub} = 10 \text{ K}$. 121

Fig. 5.11 Time variations of the measured instantaneous heated surface temperature for (a) imposed heat flux oscillation only, (b) in-phase G and q oscillations and (c) out-of-phase G and q oscillations

at $\bar{G} = 300 \text{ kg/m}^2\text{s}$ and $\Delta G/\bar{G} = 10\%$ for $\Delta q/\bar{q} = 30\%$ and $t_p = 20 \text{ sec}$. for $\Delta \bar{T}_{sub} = 15 \text{ K}$. 122

Fig. 5.12 Time variations of the measured instantaneous heated surface temperature for (a) imposed heat flux oscillation only, (b) in-phase G and q oscillations and (c) out-of-phase G and q oscillations

at $\bar{G} = 300 \text{ kg/m}^2\text{s}$ and $\Delta G/\bar{G} = 10\%$ for $\Delta q/\bar{q} = 30\%$ and $t_p = 30 \text{ sec}$. for $\Delta \bar{T}_{sub} = 10 \text{ K}$. 123

Fig. 5.13 Time variations of the measured instantaneous heated surface temperature for (a) imposed heat flux oscillation only, (b) imposed mass flux oscillation only, and (c) in-phase or out-of-phase G and q oscillations

at $\bar{G} = 300 \text{ kg/m}^2\text{s}$ and $\Delta G/\bar{G} = 5\%$ for various \bar{q} at $t_p = 20 \text{ sec}$. for $\Delta \bar{T}_{sub} = 10 \text{ K}$. 124

Fig. 5.14 Time variations of the measured instantaneous heated surface temperature for (a) imposed heat flux oscillation only, (b) imposed mass flux oscillation only, and (c) in-phase or out-of-phase G and q oscillations

at $\bar{G} = 300 \text{ kg/m}^2\text{s}$ and $\Delta G/\bar{G} = 10\%$ for various \bar{q} at $t_p = 20 \text{ sec}$. for $\Delta \bar{T}_{sub} = 10 \text{ K}$. 125

Fig. 5.15 Time variations of the measured instantaneous heated surface temperature for (a) imposed heat flux oscillation only, (b) imposed mass flux oscillation only, and (c) in-phase or out-of-phase G and q oscillations

at $\bar{G} = 300 \text{ kg/m}^2\text{s}$ and $\Delta G/\bar{G} = 15\%$ for various \bar{q} at $t_p = 20 \text{ sec}$. for $\Delta \bar{T}_{sub} = 10 \text{ K}$. 126

Fig. 5.16 Time variations of the heat transfer coefficient for (a) imposed heat flux oscillation only, (b) in-phase G and q oscillations and (c) out-of-phase G and q oscillations at $\bar{G} = 300\text{kg} / \text{m}^2\text{s}$ and $\Delta G / \bar{G} = 10\%$ for $\Delta q / \bar{q} = 30\%$ and $t_p = 20\text{sec}$. for $\Delta \bar{T}_{sub} = 5\text{K}$. 127

Fig. 5.17 Time variations of the heat transfer coefficient for (a) imposed heat flux oscillation only, (b) in-phase G and q oscillations and (c) out-of-phase G and q oscillations at $\bar{G} = 200\text{kg} / \text{m}^2\text{s}$ and $\Delta G / \bar{G} = 10\%$ for $\Delta q / \bar{q} = 30\%$ and $t_p = 20\text{sec}$. for $\Delta \bar{T}_{sub} = 10\text{K}$. 128

Fig. 5.18 Time variations of the heat transfer coefficient for (a) imposed heat flux oscillation only, (b) in-phase G and q oscillations and (c) out-of-phase G and q oscillations at $\bar{G} = 300\text{kg} / \text{m}^2\text{s}$ and $\Delta G / \bar{G} = 5\%$ for $\Delta q / \bar{q} = 30\%$ and $t_p = 20\text{sec}$. for $\Delta \bar{T}_{sub} = 10\text{K}$. 129

Fig. 5.19 Time variations of the heat transfer coefficient for (a) imposed heat flux oscillation only, (b) in-phase G and q oscillations and (c) out-of-phase G and q oscillations at $\bar{G} = 300\text{kg} / \text{m}^2\text{s}$ and $\Delta G / \bar{G} = 10\%$ for $\Delta q / \bar{q} = 10\%$ and $t_p = 20\text{sec}$. for $\Delta \bar{T}_{sub} = 10\text{K}$. 130

Fig. 5.20 Time variations of the heat transfer coefficient for (a) imposed heat flux oscillation only, (b) in-phase G and q oscillations and (c) out-of-phase G and q oscillations at $\bar{G} = 300\text{kg} / \text{m}^2\text{s}$ and $\Delta G / \bar{G} = 10\%$ for $\Delta q / \bar{q} = 30\%$ and $t_p = 20\text{sec}$. for $\Delta \bar{T}_{sub} = 10\text{K}$. 131

Fig. 5.21 Time variations of the heat transfer coefficient for (a) imposed heat flux oscillation only, (b) in-phase G and q oscillations and (c) out-of-phase G and q oscillations at $\bar{G} = 300\text{kg} / \text{m}^2\text{s}$ and $\Delta G / \bar{G} = 10\%$ for $\Delta q / \bar{q} = 50\%$ and $t_p = 20\text{sec}$. for $\Delta \bar{T}_{sub} = 10\text{K}$. 132

Fig. 5.22 Time variations of the heat transfer coefficient for (a) imposed heat flux oscillation only, (b) in-phase G and q oscillations and (c) out-of-phase G and q oscillations at $\bar{G} = 300\text{kg} / \text{m}^2\text{s}$ and $\Delta G / \bar{G} = 15\%$ for $\Delta q / \bar{q} = 30\%$ and $t_p = 20\text{sec}$. for $\Delta \bar{T}_{sub} = 10\text{K}$. 133

Fig. 5.23 Time variations of the heat transfer coefficient for (a) imposed heat flux oscillation only, (b) in-phase G and q oscillations and (c) out-of-phase G and q oscillations at $\bar{G} = 400\text{kg} / \text{m}^2\text{s}$ and $\Delta G / \bar{G} = 10\%$ for $\Delta q / \bar{q} = 30\%$ and $t_p = 20\text{sec}$. for $\Delta \bar{T}_{sub} = 10\text{K}$. 134

Fig. 5.24 Time variations of the heat transfer coefficient for (a) imposed heat flux oscillation only, (b) in-phase G and q oscillations and (c) out-of-phase G and q oscillations at $\bar{G} = 300\text{kg} / \text{m}^2\text{s}$ and $\Delta G / \bar{G} = 10\%$ for $\Delta q / \bar{q} = 30\%$ and $t_p = 20\text{sec}$. for $\Delta \bar{T}_{sub} = 15\text{K}$. 135

Fig. 5.25 Time variations of the heat transfer coefficient for (a) imposed heat flux oscillation only, (b) in-phase G and q oscillations and (c) out-of-phase G and q oscillations at $\bar{G} = 400\text{kg} / \text{m}^2\text{s}$ and

$\Delta G/\bar{G} = 10\%$ for $\Delta q/\bar{q} = 30\%$ and $t_p = 30\text{sec}$. for $\Delta\bar{T}_{sub} = 10\text{K}$. 136

Fig. 5.26 Time variations of the heat transfer coefficient for (a) imposed heat flux oscillation only, (b) imposed mass flux oscillation only and (c) out-of-phase G and q oscillations at $\bar{G} = 300\text{kg}/\text{m}^2\text{s}$ and $\Delta G/\bar{G} = 5\%$ for $\Delta q/\bar{q} = 5, 10, 23\%$ and $t_p = 20\text{sec}$. for $\Delta\bar{T}_{sub} = 10\text{K}$. 137

Fig. 5.27 Time variations of the heat transfer coefficient for (a) imposed heat flux oscillation only, (b) imposed mass flux oscillation only and (c) out-of-phase G and q oscillations at $\bar{G} = 300\text{kg}/\text{m}^2\text{s}$ and $\Delta G/\bar{G} = 10\%$ for $\Delta q/\bar{q} = 8, 30, 32, 45\%$ and $t_p = 20\text{sec}$. for $\Delta\bar{T}_{sub} = 10\text{K}$. 138

Fig. 5.28 Time variations of the heat transfer coefficient for (a) imposed heat flux oscillation only, (b) imposed mass flux oscillation only and (c) out-of-phase G and q oscillations at $\bar{G} = 300\text{kg}/\text{m}^2\text{s}$ and $\Delta G/\bar{G} = 15\%$ for $\Delta q/\bar{q} = 15, 35, 50\%$ and $t_p = 20\text{sec}$. for $\Delta\bar{T}_{sub} = 10\text{K}$. 139

Fig. 5.29 Photos of stable subcooled flow boiling at certain time instants in statistical state for various imposed heat fluxes for (a) $G = 200\text{kg}/\text{m}^2\text{s}$, (b) $G = 300\text{kg}/\text{m}^2\text{s}$ and (c) $G = 400\text{kg}/\text{m}^2\text{s}$ at $\Delta\bar{T}_{sub} = 10\text{K}$. 140

Fig. 5.30 Photos of subcooled flow boiling at certain time instants in a typical time periodic cycle for a constant imposed mass flux at $\bar{q} = 4.01\text{W}/\text{cm}^2$, $\Delta q/\bar{q} = 30\%$ and $G = 200\text{kg}/\text{m}^2\text{s}$ with $t_p = 20\text{sec}$. and $\Delta\bar{T}_{sub} = 10\text{K}$. 141

Fig. 5.31 Photos of subcooled flow boiling at certain time instants in a typical time periodic cycle for imposed in-phase G & q oscillations at $\bar{G} = 200\text{kg}/\text{m}^2\text{s}$, $\Delta G/\bar{G} = 10\%$, $\bar{q} = 4.01\text{W}/\text{cm}^2$ and $\Delta q/\bar{q} = 30\%$ with $t_p = 20\text{sec}$. and $\Delta\bar{T}_{sub} = 10\text{K}$. 142

Fig. 5.32 Photos of subcooled flow boiling at certain time instants in a typical time periodic cycle for imposed out-of-phase G & q oscillations at $\bar{G} = 200\text{kg}/\text{m}^2\text{s}$, $\Delta G/\bar{G} = 10\%$, $\bar{q} = 4.01\text{W}/\text{cm}^2$ and $\Delta q/\bar{q} = 30\%$ with $t_p = 20\text{sec}$. and $\Delta\bar{T}_{sub} = 10\text{K}$. 143

Fig. 5.33 Photos of subcooled flow boiling at certain time instants in a typical time periodic cycle for a constant imposed mass flux at $\bar{q} = 4.01\text{W}/\text{cm}^2$, $\Delta q/\bar{q} = 30\%$ and $G = 300\text{kg}/\text{m}^2\text{s}$ with $t_p = 20\text{sec}$. and $\Delta\bar{T}_{sub} = 10\text{K}$. 144

Fig. 5.34 Photos of subcooled flow boiling at certain time instants in a typical time periodic cycle for imposed in-phase G & q oscillations at $\bar{G} = 300\text{kg}/\text{m}^2\text{s}$, $\Delta G/\bar{G} = 10\%$, $\bar{q} = 4.01\text{W}/\text{cm}^2$ and $\Delta q/\bar{q} = 30\%$ with $t_p = 20\text{sec}$. and $\Delta\bar{T}_{sub} = 10\text{K}$. 145

Fig. 5.35 Photos of subcooled flow boiling at certain time instants in a typical time periodic cycle for

imposed out-of-phase G & q oscillations at $\bar{G}=300\text{kg/m}^2\text{s}$, $\Delta G/\bar{G}=10\%$, $\bar{q}=4.01\text{W/cm}^2$ and $\Delta q/\bar{q}=30\%$ with $t_p=20\text{sec}$. and $\Delta T_{sub}=10\text{K}$. 146

Fig. 5.36 Photos of subcooled flow boiling at certain time instants in a typical time periodic cycle for imposed in-phase G & q oscillations at $\bar{G}=300\text{kg/m}^2\text{s}$, $\Delta G/\bar{G}=15\%$, $\bar{q}=4.01\text{W/cm}^2$ and $\Delta q/\bar{q}=30\%$ with $t_p=20\text{sec}$. and $\Delta T_{sub}=10\text{K}$. 147

Fig. 5.37 Photos of subcooled flow boiling at certain time instants in a typical time periodic cycle for imposed out-of-phase G & q oscillations at $\bar{G}=300\text{kg/m}^2\text{s}$, $\Delta G/\bar{G}=15\%$, $\bar{q}=4.01\text{W/cm}^2$ and $\Delta q/\bar{q}=30\%$ with $t_p=20\text{sec}$. and $\Delta T_{sub}=10\text{K}$. 148

Fig. 5.38 Photos of subcooled flow boiling at certain time instants in a typical time periodic cycle for a constant imposed mass flux at $\bar{q}=4.01\text{W/cm}^2$, $\Delta q/\bar{q}=50\%$ at $G=300\text{kg/m}^2\text{s}$ with $t_p=20\text{sec}$. and $\Delta T_{sub}=10\text{K}$. 149

Fig. 5.39 Photos of subcooled flow boiling at certain time instants in a typical time periodic cycle for imposed in-phase G & q oscillations at $\bar{G}=300\text{kg/m}^2\text{s}$, $\Delta G/\bar{G}=10\%$, $\bar{q}=4.01\text{W/cm}^2$ and $\Delta q/\bar{q}=50\%$ with a $t_p=20\text{sec}$. and $\Delta T_{sub}=10\text{K}$. 150

Fig. 5.40 Photos of subcooled flow boiling at certain time instants in a typical time periodic cycle for imposed out-of-phase G & q oscillations at $\bar{G}=300\text{kg/m}^2\text{s}$, $\Delta G/\bar{G}=10\%$, $\bar{q}=4.01\text{W/cm}^2$ and $\Delta q/\bar{q}=50\%$ with a $t_p=20\text{sec}$. and $\Delta T_{sub}=10\text{K}$. 151

Fig. 5.41 Photos of subcooled flow boiling at certain time instants in a typical time periodic cycle for a constant imposed mass flux at $\bar{q}=4.01\text{W/cm}^2$, $\Delta q/\bar{q}=30\%$ at $G=300\text{kg/m}^2\text{s}$ with $t_p=30\text{sec}$. and $\Delta T_{sub}=10\text{K}$. 152

Fig. 5.42 Photos of subcooled flow boiling at certain time instants in a typical time periodic cycle for imposed in-phase G & q oscillations at $\bar{G}=300\text{kg/m}^2\text{s}$, $\Delta G/\bar{G}=10\%$, $\bar{q}=4.01\text{W/cm}^2$ and $\Delta q/\bar{q}=30\%$ with $t_p=30\text{sec}$. and $\Delta T_{sub}=10\text{K}$. 153

Fig. 5.43 Photos of subcooled flow boiling at certain time instants in a typical time periodic cycle for imposed out-of-phase G & q oscillations at $\bar{G}=300\text{kg/m}^2\text{s}$, $\Delta G/\bar{G}=10\%$, $\bar{q}=4.01\text{W/cm}^2$ and $\Delta q/\bar{q}=30\%$ with $t_p=30\text{sec}$. and $\Delta T_{sub}=10\text{K}$. 154

Fig. 5.44 Photos of subcooled flow boiling at certain time instants in a typical time periodic cycle for a constant imposed mass flux at $\bar{q}=5.03\text{W/cm}^2$, $\Delta q/\bar{q}=30\%$ at $G=300\text{kg/m}^2\text{s}$ with $t_p=20\text{sec}$. and $\Delta T_{sub}=15\text{K}$. 155

Fig. 5.45 Photos of subcooled flow boiling at certain time instants in a typical time periodic cycle for

imposed in-phase G & q oscillations at $\bar{G}=300\text{kg/m}^2\text{s}$, $\Delta G/\bar{G}=10\%$, $\bar{q}=5.03\text{W/cm}^2$ and $\Delta q/\bar{q}=30\%$ with $t_p=20\text{sec}$. and $\Delta T_{sub}=15\text{K}$. 156

Fig. 5.46 Photos of subcooled flow boiling at certain time instants in a typical time periodic cycle for imposed out-of-phase G & q oscillations at $\bar{G}=300\text{kg/m}^2\text{s}$, $\Delta G/\bar{G}=10\%$, $\bar{q}=5.03\text{W/cm}^2$ and $\Delta q/\bar{q}=30\%$ with $t_p=20\text{sec}$. and $\Delta T_{sub}=15\text{K}$. 157

Fig. 5.47 Photos of subcooled flow boiling at certain time instants in a typical time periodic cycle for a constant imposed mass flux at $\bar{q}=4.01\text{W/cm}^2$, $\Delta q/\bar{q}=10\%$ at $G=300\text{kg/m}^2\text{s}$ with $t_p=20\text{sec}$. and $\Delta T_{sub}=10\text{K}$. 158

Fig. 5.48 Photos of subcooled flow boiling at certain time instants in a typical time periodic cycle for a constant imposed heat flux at $\bar{q}=4.01\text{W/cm}^2$ at $G=300\text{kg/m}^2\text{s}$, $\Delta G/\bar{G}=5\%$ with $t_p=20\text{sec}$. and $\Delta T_{sub}=10\text{K}$. 159

Fig. 5.49 Photos of subcooled flow boiling at certain time instants in a typical time periodic cycle for imposed out-of-phase G & q oscillations at $\bar{G}=300\text{kg/m}^2\text{s}$, $\Delta G/\bar{G}=5\%$, $\bar{q}=4.01\text{W/cm}^2$ and $\Delta q/\bar{q}=10\%$ with $t_p=20\text{sec}$. and $\Delta T_{sub}=10\text{K}$. 160

Fig. 5.50 Photos of subcooled flow boiling at certain time instants in a typical time periodic cycle for a constant imposed mass flux at $\bar{q}=4.01\text{W/cm}^2$, $\Delta q/\bar{q}=22\%$ at $G=300\text{kg/m}^2\text{s}$ with $t_p=20\text{sec}$. and $\Delta T_{sub}=10\text{K}$. 161

Fig. 5.51 Photos of subcooled flow boiling at certain time instants in a typical time periodic cycle for a constant imposed heat flux at $\bar{q}=4.01\text{W/cm}^2$ at $G=300\text{kg/m}^2\text{s}$, $\Delta G/\bar{G}=10\%$ with $t_p=20\text{sec}$. and $\Delta T_{sub}=10\text{K}$. 162

Fig. 5.52 Photos of subcooled flow boiling at certain time instants in a typical time periodic cycle for imposed out-of-phase G & q oscillations at $\bar{G}=300\text{kg/m}^2\text{s}$, $\Delta G/\bar{G}=10\%$, $\bar{q}=4.01\text{W/cm}^2$ and $\Delta q/\bar{q}=22\%$ with $t_p=20\text{sec}$. and $\Delta T_{sub}=10\text{K}$. 163

Fig. 5.53 Photos of subcooled flow boiling at certain time instants in a typical time periodic cycle for a constant imposed mass flux at $\bar{q}=4.01\text{W/cm}^2$, $\Delta q/\bar{q}=35\%$ at $G=300\text{kg/m}^2\text{s}$ with $t_p=20\text{sec}$. and $\Delta T_{sub}=10\text{K}$. 164

Fig. 5.54 Photos of subcooled flow boiling at certain time instants in a typical time periodic cycle for a constant imposed heat flux at $\bar{q}=4.01\text{W/cm}^2$ at $G=300\text{kg/m}^2\text{s}$, $\Delta G/\bar{G}=15\%$ with $t_p=20\text{sec}$. and $\Delta T_{sub}=10\text{K}$. 165

Fig. 5.55 Photos of subcooled flow boiling at certain time instants in a typical time periodic cycle for

imposed out-of-phase G & q oscillations at $\bar{G}=300\text{kg/m}^2\text{s}$, $\Delta G/\bar{G}=15\%$, $\bar{q}=4.01\text{W/cm}^2$ and $\Delta q/\bar{q}=35\%$ with $t_p=20\text{sec}$. and $\Delta T_{sub}=10\text{K}$. 166

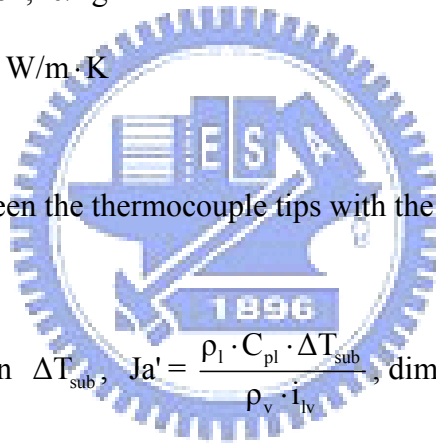
Fig. 5.50 Time period oscillatory subcooled flow boiling of FC-72 with $\bar{q}=4.01\text{W/cm}^2$, $\Delta q/\bar{q}=30\%$, $G=300\text{kg/m}^2\text{s}$, $\Delta G/\bar{G}=10\%$ and $t_p=20\text{sec}$. for the time variations of bubble characteristics: (a) bubble departure diameter (b) bubble departure frequency (c) active nucleation site density. 167

Fig.5.51 Time period oscillatory subcooled flow boiling of FC-72 with $\bar{q}=4.01\text{W/cm}^2$, $\Delta q/\bar{q}=30\%$, $G=300\text{kg/m}^2\text{s}$, $\Delta G/\bar{G}=15\%$ and $t_p=20\text{sec}$. for the time variations of bubble characteristics: (a) bubble departure diameter (b) bubble departure frequency (c) active nucleation site density. 168



NOMENCLATURE

A	area, m^2
B	element height, m
c_p	specific heat, $J/kg^\circ C$
D	hydraulic diameter of rectangular-channel, m
G	mass flux, kg/m^2s
g	acceleration due to gravity, m/s^2
H	height, m
h	heat transfer coefficient, $W/m^2 \cdot K$
I	measured current from DC power supply, A
i_{lv}	enthalpy of vaporization, $J/kg \cdot K$
k	thermal conductivity, $W/m \cdot K$
L	length, mm
l	vertical distance between the thermocouple tips with the copper surface
\dot{m}	mass flow rate, kg/s
Ja'	Jacob number based on ΔT_{sub} , $Ja' = \frac{\rho_l \cdot C_{pl} \cdot \Delta T_{sub}}{\rho_v \cdot i_{lv}}$, dimensionless
Nu	Nusselt number, $Nu = \frac{h \cdot L}{k}$, dimensionless
N_{ac}	Active nucleation site density, n/m^2
N_{conf}	Confinement number, $N_{conf} = \frac{(\sigma/g \cdot \Delta\rho)^{0.5}}{D_h}$, dimensionless
P	system pressure, kPa
Pr	Prandtl number, $Pr = \frac{\mu \cdot C_p}{k}$, dimensionless
Q	heat transfer rate, W
q	average imposed heat flux, W/cm^2
Re	Reynolds number, $Re = \frac{G \cdot D}{\mu}$, dimensionless



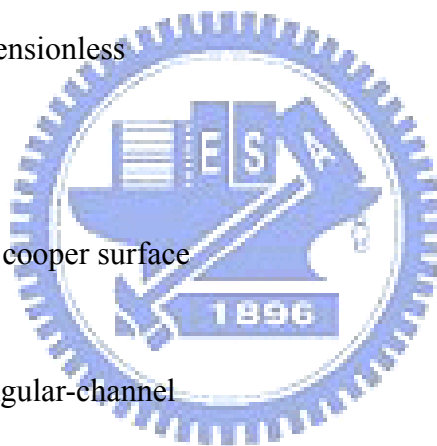
t_l	time lag, sec
t_p	heating period, sec
T	temperature, °C
V	coolant FC-72 flow velocity, m/s
V	measured voltage from DC power supply, V
W	width, m

Greek Symbols

ΔT	temperature difference, °C
μ	dynamic viscosity, $N \cdot s/m^2$
v	specific volume, m^3/kg
ρ	density, kg/m^3
ε	relative heat loss, dimensionless

Subscripts

ave	average
c,h	from heater surface to cooper surface
cu	copper
cs	cross-section of rectangular-channel
d	diameter
e	effective
g	gas
h	hydraulic
i	at the inlet of the test section
in	at the inlet of the test section
i,o	at inlet and exit of the test section
lv	liquid phase to vapor phase
m	average value for the two phase mixture or between the inlet and exit
M	mica
n	net power input to the coolant FC-72



o	at the outlet of the test section
p	preheater
r	coolant FC-72
s	surface
sat	saturated state for coolant FC-72
sp	single-phase convective heat transfer
sub	subcooled state for coolant FC-72
T	teflon
t	total
tp	two-phase boiling heat transfer
v	vapor
w	wall
w	water
1ϕ	single-phase
2ϕ	two-phase



CHAPTER 1

INTRODUCTION

1.1 Motive of the Present Study

With recent fast progress in the IC(Integrated Circuit) technology, the IC chips are currently designed to be relatively light, thin, short and small to enhance their performance. As the microelectronic systems become miniaturized, the density of the power dissipation in them increases significantly. It is also well known that the IC junction temperature must be kept under 85°C to avoid being damaged and to maintain its normal operation[1]. The heat removal method based on the gas cooling is usually not sufficiently effective for the high generation components. Besides, the use of the direct liquid cooling can greatly increase the heat removal rate. But it is still not higher enough for high power density in advanced CPUs. Moreover, the method utilizing the boiling of liquid is most effective because of the latent heat transfer involved in the process. Furthermore, the power dissipation in IC chips are often time dependent in practical operation. Therefore heat removal rate must be varied in time to meet the required time varying cooling load. To accommodate the time varying heat removal rate, the coolant flow rate is controlled instantly at the required level. Specifically, the coolant flow rate is often set to increase with the heat removal rate and vice versa. In stable flow boiling in which the coolant mass flux and heat flux are kept at constant levels, however, the boiling curves are known to be only slightly affected by the mass flux. How the flow boiling heat transfer characteristics are influenced by the simultaneous time varying imposed heat flux and mass flux remains largely unexplored.

In employing the liquid boiling in the electronics cooling the coolants must be chemically stable, inert and dielectric. The coolant FC-72, a fluorocarbon liquid manufactured by the 3M Company, meets the above requirements and is appropriate for the electronics cooling. However, our understanding of time dependent flow boiling due to time varying heating and coolant flow rate is poor. In the present study an initial attempt is made to unravel how the characteristics of FC-72

flow boiling heat transfer and bubble motion over a flush mounted small heated surface in a rectangular channel are affected by the simultaneous time periodic refrigerant flow rate and imposed heat flux. Some thermophysical properties for FC-72 are given in Table 1.1

1.2 Literature Review

In what follows the literature relevant to the present study is reviewed, especially on the use of boiling of dielectric liquids for cooling of electronic equipments including the single-phase and boiling heat transfer.

1.2.1 Steady single-phase and stable flow boiling heat transfer

Incropera et al. [2] investigated single-phase convective heat transfer of water and FC-77 from single array and four-row arrays of 12 flush-mounted heat sources in a horizontal rectangular channel for the channel Reynolds numbers ranging from 1,000 to 14,000. They developed a model to predict the relation between the Reynolds number and Nusselt number for the turbulent flow regime with $5,000 < Re_D < 14,000$. Unfortunately, the measured data were significantly under-predicted in the laminar flow regime. Investigation of single-phase and subcooled flow boiling heat transfer from a small heated patch with R-113 and FC-72 was carried out by Samant and Simon [3]. They combined the experimental data for R-113 and FC-72 to develop an empirical correlation. In addition, they observed large temperature excursions at the onset of nucleate boiling and a boiling hysteresis near the onset of nucleate boiling in the subcooled boiling. Garimella and Eibeck [4] analyzed the heat transfer characteristics of an six-row array of 30 heat sources in single-phase forced convection of water for the channel Reynolds number ranging from 150 to 5,150. They reported that the heat transfer coefficient decreased with decreasing Reynolds number and the Nusselt number decreased with increasing ratio of the channel height to protruding element height. Gersey and Mudawar [5] studied the orientation effect on the single-phase forced convection and subcooled flow boiling of FC-72 over a nine in-line microelectronic chips. They proposed an empirically generalized equation based on their experimental data. Heindel et al. [6,7] examined single-phase liquid convection and flow boiling of water and FC-72 over a 1 x 10 array of flush

mounted discrete heat sources in a horizontal rectangular channel. In investigating the critical heat flux of FC-72 for four in-line simulated electronic chips in vertical channel flow boiling experiments, Tso et al. [8] found that temperature of the chip surface decreased with the increases in the flow velocity and liquid subcooling in the partial boiling region and this result was opposed to that of Willingham and Mudawar [9]. The fluid velocity and subcooling temperature have smaller effect on the surface temperature in the fully-developed boiling region. They observed that increases in the fluid velocity and liquid subcooling resulted in a delay in the incipience of nucleate boiling and in an increase in the critical heat flux.

The single-phase heat transfer correlations proposed in some of the above studies are listed in Table 1.2.

1.2.2 Transient pool boiling heat transfer

Hohl et al. [10] conducted pool boiling of FC-72 subject to an increasing heating rate and found that CHF increased with the heating rate. Besides, the transient CHF is higher than the steady state CHF. Sakurai and Shiotsu [11] investigated transient pool boiling of water over a platinum wire of 1.2 mm in diameter and 97.9 mm in length to simulate a step input of reactivity in a nuclear reactor in which the reactor power rised exponentially with time. The incipient boiling heat flux was found to increase exponentially with time for the exponential period ranging from 5 ms to 10s. Besides, the wire surface temperature at first increases with the heat input. Moreover, the heat transfer coefficient and heat flux at the incipient boiling point are higher for a shorter heating period. Okuyama et al. [12] conducted pool boiling of R-113 at large stepwise power generation in a 7- μm thick copper foil focusing on the transient critical heat flux above which the effective heat removal in transient nucleate boiling could not be expected. They noted that the transient critical heat flux was lower than the critical heat flux in the steady state under a low system pressure. In the case of the low system pressure, the bubble near the transient critical heat flux has a peculiar shape like a “straw hat” which was considered to be due to the consumption of the nucleate boiling liquid layer. In the case of high system pressure, no more vapor bubble appears in transient nucleate boiling and

transition occurs due to filling of the fine initial bubbles on the heat transfer surface. Besides, at low heat generation rate the wall superheat drops for a moment after boiling incipience. But at high heat generation rate this becomes hard to see, because the duration of nucleate boiling becomes extremely short. Later Okuyama and Iida [13] moved further to investigate liquid nitrogen pool boiling over a platinum wire with a stepwise heat generation. In the case of a low heat generation rate, boiling transition was observed to occur due to the coalescence of nucleate boiling bubbles. While in the case of a high heat generation rate, a vapor sheath grows along the test wire since the excess superheat energy is stored in the liquid layer at boiling incipience. Besides, in the case of an extremely high heat generation rate, a lot of fine initial bubbles grow rapidly and simultaneously. Boiling transition occurs due to the filling of the bubbles on the heater.

Transient nucleate boiling of several highly wetting fluids on a thick flat sample and a wire also with a stepwise heat generation was experimentally studied by Duluc et al. [14]. They observed that for the cases with high thermal inertia, fewer transient pool boiling was developed owing to the large heat capacity of the heater. Besides for the transient experiments subject to very fast heating, the wall superheat at boiling onset may be higher than the steady condition. Auracher and Marquardt et al. [15] investigated transient pool boiling from a thick copper with FC-72. They observed a hysteresis between the heating and cooling transient conditions. Under steady boiling conditions and with a clean heater surface, no hysteresis was observed.

1.2.3 Transient single-phase forced convection heat transfer

Girault and Petit [16] investigated transient single-phase forced convection in a horizontal plane channel with different time varying imposed heat fluxes on the channel walls. On the bottom plate the imposed heat flux varies like a sinusoidal wave. While on the top plate the imposed heat flux is like a rectangular wave. During the power-on period both the top and bottom plate temperatures were found to vary smoothly. There is a small wall temperature oscillation for the power-off situation. This is considered to result from the existence of internal energy in the channel walls even when the power is turned off. Bhowmik and Tou [17, 18] performed an experiment to

study transient FC-72 forced convection heat transfer from a four-in-line chip module that is flush-mounted onto one wall of a vertical rectangular channel. The Reynolds number based on the heat source length ranges from 800 to 2,625 for the heat flux varying from 1 to 7 W/cm². Their data suggest that the transient characteristics of the overall heat transfer coefficient are both of importance in the thermal systems during the power-on and power-off periods. Besides, the heat transfer coefficient was noted to be affected strongly by the number of chips. In a similar experiment [19] they investigated the transient heat transfer characteristics from an array of 4 x 1 flush mounted simulated electronic chips using water as the working fluid during the power-off periods. The Reynolds number based on the heat source length ranges from 1,050 to 2,625. The transient heat transfer regime in the period of 75s after the heater power is cut-off is examined. They observed that the Nusselt numbers of the four chips at the beginning of power-off were close but then they diverged with time. However, the Nusselt number increases with time, due to the chip wall temperature decrease with time. When compared with water, an overall increase of 70% in the Nusselt number is obtained by using FC-72.

1.2.4 Transient flow boiling heat transfer

Kataoka et al. [20] investigated transient flow boiling of water over a platinum wire subject to an exponentially increasing heat input. The wire diameter and length respectively vary from 0.8 to 1.5 mm and from 3.93 to 10.4 cm. Two types of transient boiling were observed. In A-type (heating period is 20ms, 50ms, or 10s) boiling, the transient maximum critical heat flux increases with decreasing period at constant flow velocity. Whereas, in the B-type (heating period is 5ms, 10ms, or 14ms) boiling, the transient maximum heat flux decreases first with the period and then increases. Two-phase flow and heat transfer in a small tube of 1 mm internal diameter using R-141b as the working fluid were studied by Lin et al. [21]. At a low heat flux input, a relatively constant wall temperature was obtained. Besides, forced convection evaporation occurs towards the outlet end of the tube and the fluctuations in the wall temperature are small. With a high heat flux input, however, significant fluctuation in the wall temperature can be observed. This is caused by a

combination of time varying heat transfer coefficient and time varying local pressure and fluid saturation temperature.

Two-phase flow instability in the flow boiling of various liquids in a long heated channel has been recognized for several decades [22, 23]. On a certain operating condition significant temporal oscillations in pressure, temperature, mass flux and boiling onset occur. Recently, some detailed characteristics associated with these instabilities were investigated through experimental measurement and theoretical modeling. Specifically in flow boiling of refrigerant R-11 in a vertical channel, the pressure-drop and thermal oscillations were observed by Kakac et al. [24]. Two-phase homogeneous model along with the thermodynamic equilibrium assumption was used to predict the condition leading to the thermal oscillation. And their predicted periods and amplitudes of the oscillations were in a good agreement with their measured data. Kakac and his colleagues [25] further noted the presence of the density wave oscillation superimposed on the pressure-drop oscillations. Moreover, the drift flux model was employed in their numerical prediction. In a continuing study for R-11 in a horizontal tube of 106 cm long, Ding et al. [26] examined the dependence of the oscillation amplitude and period on the system parameters and located the boundary of various types of oscillations on the steady-state pressure-drop versus mass flux characteristic curves. A similar experimental study was carried out by Comakli et al. [27] for a 319.5 cm long tube. They showed that the channel length has an important effect on the two-phase flow dynamic instabilities.

The dynamic behavior for a horizontal boiling channel connected with a surge tank for liquid supply has also received some attention. Mawasha and Gross [28] used a constitutive model containing a cubic nonlinearity combined with a homogeneous two-phase flow model to simulate the pressure-drop oscillation. Their prediction is matched with the measured data. Later, the channel wall capacity effects was included [29] to allow the wall temperature and heat transfer coefficient to vary with time.

Wang et al. [30] noted that the boiling onset in a upward flow of subcooled water in a vertical

tube of 7.8-m long connected with a liquid surge tank could cause substantial flow pressure and density-wave oscillations. These boiling onset oscillations were attributed to a sudden increase of pressure-drop across the channel and a large fluctuation in the water flow rate at the onset of nucleate boiling. This in turn results from the feedback of the pressure-drop and flow rate by the system, causing the location of the boiling onset to move in and out of the channel.

Brutin et al. [31] reported the pressure-drop oscillations of n-pentane liquid in a vertical small rectangular channel ($D_h=0.889\text{mm}$, $L=50\text{mm}$ & 200mm). A non-stationary state of two-phase flow was observed. The effects of the inlet flow condition on the boiling instabilities were found to be relatively significant [32]. A similar study for subcooled flow boiling of deionized water was conducted by Shuai et al. [33] and the pressure-drop oscillations were also noted.

1.2.5 Bubble Characteristics

Literature relevant to the bubble characteristics in boiling flow is briefly reviewed. A recent experiment conducted by Chang et al. [34] focused on the behavior of near-wall bubbles in subcooled flow boiling of water. The population of the near-wall bubbles was found to increase with the increase in the heat flux and in the superheated liquid layer very small bubbles were noted to attach to the heated wall. In addition, the coalesced bubbles are smaller for a higher mass flux of the flow. Cornwell and Kew [35] examined various flow regimes for boiling of refrigerant R-113 in a vertical rectangular multi-channel with $D_h = 1.03$ and 1.64 mm. Based on visualization of the flow and measurement of the heat transfer, three flow regimes have been suggested, namely, the isolated bubble, confined bubble and annular-slug bubble flows. In the isolated bubble regime, heat transfer coefficient depends on the heat flux and hydraulic diameter. In the confined bubble regime, heat transfer coefficient depends on the heat flux, mass flux, vapor quality and hydraulic diameter. While in the annular-slug bubble regime, heat transfer coefficient depends on the mass flux, vapor quality and hydraulic diameter. Lie and Lin [36, 37] examined flow boiling heat transfer and associated bubble characteristics of R-134a in a narrow annular duct ($D_h=4, 2$ mm). They concluded that the bubbles are suppressed to become smaller and less dense by raising the refrigerant mass flux and

inlet subcooling. The mean bubble departure frequency increases with the increasing refrigerant mass flux and saturated temperature and with the decreasing duct size. Moreover, the active nucleation site density is much higher at a lower refrigerant mass flux particularly at a high imposed heat flux. Bang et al. [38] examined boiling of R-134a in a vertical rectangular channel focusing on the characteristic structures in the near-wall region. They noted the presence of the vapor remnants below the discrete bubbles and coalesced bubbles and the presence of an interleaved liquid layer between the vapor remnants and bubbles. Besides, the bubble layer was divided into two types, a near-wall bubble layer dominated by small bubbles and a following bubble layer prevailed by large coalesced bubbles. Kandlikar [39] examined the subcooled flow boiling of water in a rectangular horizontal channel. They concluded that the bubble growth was slow at high subcooling and the departure diameter decreased as the flow rate increased.

By using optical measurement techniques, Maurus et al. [40,41] examined the bubble size distribution and local void fraction in subcooling flow boiling of water at atmospheric pressure. They reported that the bubble size increased with an increase in the heat flux but reduced with an increase in the mass flux. The total bubble life time, the remaining lifetime after the detachment process and the waiting time between two bubble cycles decreased significantly as the mass flux increased. In a recent study Maurus and Sattelmayer [42] further defined the bubbly flow region by the ratio of the averaged phase boundary velocity to the averaged fluid velocity. On the other hand, an experimental analysis was carried out by Thorncroft et al. [43] to investigate the vapor bubble growth and departure in vertical upflow and downflow boiling of FC-87. They found that the bubble growth rate and bubble departure diameter increased with the Jacob number (increasing ΔT_{sat}) and decreased at increasing mass flux in both upflow and downflow. Bubble rise characteristics after the bubble departure from a nucleation site in vertical upflow tube boiling were investigated by Okawa et al. [44-46]. They noted that the flow inertia had a significant influence on the onset of detachment but the influence was gradually reduced with time. They also observed three different bubble rise paths after the departure from nucleation sites. Specifically, some bubbles slide upward along the vertical wall, some bubbles detach from the wall after sliding, and

other bubbles remain close to the wall and reattach to the wall. Forced convection boiling experiments conducted by Situ et al. [47,48] for water in a vertical annular channel revealed that the bubble departure frequency increased as the heat flux increased. Moreover, the experimental results indicate that bubble lift-off diameter increases at increasing inlet temperature and heat flux. In addition, Yin et al. [49] examined the subcooled flow boiling of R-134a in a horizontal annular duct and noted that both the bubble departure size and frequency reduced at increasing liquid subcooling. They found that only the liquid subcooling showed a large effect on the bubble size.

1.3 Objective of This Study

The above literature review clearly indicates that detailed characteristics of the time dependent flow boiling of liquids resulting from imposed time varying heat input and/or coolant flow rate are still poorly understood. In this study, an experiment will be carried out to investigate how simultaneously imposed time periodic heat flux and mass flux oscillations in the form of sinusoidal-like waves affect the temporal flow boiling heat transfer and associated bubble characteristics of FC-72 flow over a small heated circular plate flush mounted on the bottom of a horizontal rectangular channel. The imposed heat flux and mass flux oscillate at the same frequency. The use of this heated surface intends to simulate the power dissipating chip in an electronic system. In the experiment both the time periodic saturated and subcooled flow boiling will be examined. Effects of the mean level, period and amplitude of the imposed heat flux and mass flux oscillations on the boiling characteristics will be inspected in detail for FC-72. Besides, the effects of in-phase and out-of phase of the heat flux and mass flux oscillations on the flow boiling characteristics will be explored.

Table 1.1 Thermophysical properties for FC-72.

Properties	FC-72
Appearance	Clear, colorless
Average Molecular Weight	338
Boiling Point (1 atm)	55.7°C
Pour Point	-90°C
Estimated Critical Temperature	449K
Estimated Critical Pressure	1.83×10^6 pascals
Vapor Pressure	30.9×10^3 pascals
Latent Heat of Vaporization (at normal boiling point)	88 J/g
Liquid Density	1680 kg/m ³
Kinematic Viscosity	0.38 centistokes
Absolute Viscosity	0.64 centipoise
Liquid Specific Heat	1100 J kg ⁻¹ C ⁻¹
Liquid Thermal Conductivity	0.057 W m ⁻¹ °C ⁻¹
Coefficient of Expansion	0.00156 °C ⁻¹
Surface Tension	10 dynes/cm
Refractive Index	1.251
Water Solubility	10 ppmw
Solubility in Water	<5 ppmw
Ozone Depletion Potential	0

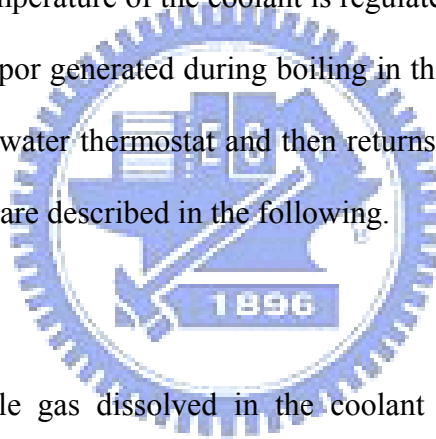
Table 1.2 Some single-phase convection heat transfer correlations for electronics cooling.

Reference	Working Fluid	Heat Transfer Correlation	Conditions
Samant and Simon [2]	R-113 & FC-72	$Nu_H = 0.47Re_H^{0.58}Pr^{0.5}$	Test patch size: 0.25mm × 2.0mm Bulk velocity: 2.05 ~ 16.86 m/s Pressure at the patch: 118.8 ~ 338.1 kPa
Garimella and Eibeck [3]	Water	$Nu = 1.31Re_a^{0.48}(LS/B)^{0.15}$	Heat sources size: 1.9 cm × 1.9 cm 150 < Re _H < 5150 Arrays: 5 row × 6 line
Incropera et al. [5]	Water & FC-77	$Nu_L = 0.13Re_D^{0.64}Pr^{0.38}(\mu_o/\mu_h)^{0.25}$	Heat sources size: 1.9 cm × 1.9 cm 150 < Re _H < 5150 Arrays: 5 row × 6 line
Gersey and Mudawar [8]	FC-72	$Nu_L = 0.362Re_L^{0.614}Pr^{1/3}$	Heat sources size: 10mm × 10mm Arrays: 9 row × 1 line Flow velocity: 13 ~ 400 cm/s

CHAPTER 2

EXPERIMENTAL APPARATUS AND PROCEDURES

The experimental system established in the present study to investigate the transient oscillatory flow boiling heat transfer and associated bubble characteristics of the dielectric coolant FC-72 over a small heated copper plate flush mounted on the bottom of a horizontal rectangular channel is depicted schematically in Fig. 2.1. This system includes four major parts, namely, a degassing unit, a coolant loop, a hot-water loop, and a cold water loop. The test section along with the entrance and exit sections are shown in Fig. 2.2 by three-dimensional plots. The liquid coolant FC-72 is driven by a gear pump and the inlet temperature of the coolant is regulated by a pre-heater with a hot water circulation in it. The coolant vapor generated during boiling in the test section is then condensed in a condenser cooled by another water thermostat and then returns to a receiver. The details of each part in the experimental system are described in the following.



2.1 Degassing Unit

Since any non-condensable gas dissolved in the coolant can significantly affect the heat transfer performance and nucleate boiling phenomena, we must degas the coolant before beginning the experiments. After each recharge of the coolant or re-arrangement of the piping system, the coolant must be degassed. The degassing unit consists of a tank of 8 liters patched with a flexible electric heater on its inside surface to heat the coolant to its boiling point. During the degassing process, the air and any non-condensable gas dissolved in the coolant escape from the liquid FC-72 in the tank and pass through the released valve on the top of the tank. Besides, a pressure transducer and a thermocouple are equipped in the tank to measure the pressure and temperature of FC-72.

2.2 Coolant Loop

After degassing the coolant, FC-72, we remove non-condensable gases possibly existing in the coolant-loop by using a vacuum pump and then fill the degassed FC-72 liquid into the coolant-loop.

The coolant loop is composed of a variable-speed gear pump, a filter, a volume flow meter, a pre-heater, a test section including the inlet and outlet sections, a condenser, and a receiver. The head of the gear pump is coupled with a magnet-driven disk sealed inside with an envelope to avoid any contamination from the shaft. The shaft is driven by a variable-speed AC induction motor which is in turn regulated by an inverter. The temporal oscillation of the coolant flow rate can be implemented by an optional external control of the inverter through a programmable DC current or voltage signal sequence. Besides, the mean coolant flow rate can be further adjusted by regulating the bypass valve.

The coolant FC-72 at the outlet of the magnetic micro-pump must be kept subcooled to avoid any vapor flow through the volume flow meter. The pre-heater is used to heat the subcooled coolant FC-72 to a preset temperature at the test section inlet by receiving heat from the hot water in the hot-water loop. Finally, the vapor-liquid coolant mixture is generated in the test section when the coolant flows over the heated copper plate. The vapor flow leaving the test section is re-liquefied by the condenser in the cold-water loop.

After leaving the condenser, the liquid FC-72 flows back to the receiver at the bottom of the system. An accumulator is connected to a high-pressure nitrogen tank to dampen the fluctuations of the time-average coolant flow rate and pressure. The filter is used to filter the impurities and non-condensable gases possibly existing in the loop. Varying the temperature and flow rate of the hot-water flowing through the pre-heater allows us to control the time-average pressure of the coolant loop. Two absolute pressure transducers are installed at the inlet and outlet of the test section with a resolution up to $\pm 2\text{kPa}$. All the refrigerant and water temperatures are measured by calibrated copper-constantan thermocouples (T-type) with a calibrated accuracy of $\pm 0.2^\circ\text{C}$. The test section is thermally insulated with a polyethylene insulation layer so that heat loss from it can be reduced significantly.

2.3 Test Section

The test section mainly consists of a circular copper plate flush mounted on the bottom of the

horizontal rectangular channel. The rectangular flow-channel includes a gradually diverging section, the main test section, and a gradually converging section (Fig. 2.3). They are all made of stainless steel plate. The installation of the inlet and exit sections intends to avoid the sudden change in the cross section of the channel. The test section is 20 mm in width, 5 mm in height, and 150 mm in length, and hence the aspect ratio of the test section is 4.0. The heated plate is placed around the geometric center of the bottom plate of the test section. A ladder-shaped acrylic window is installed on the upper lid of the test section right above the heated plate. The temperature and pressure of the FC-72 flow at the inlet and exit of the test section are measured by the calibrated thermocouples and pressure transducers, as schematically shown in Fig. 2.3.

The copper plate module schematically shown in Figs. 2.4 and 2.5 includes a hollow cylindrical Teflon block, a cylindrical Teflon bolt, a copper plate, two pieces of mica plates, a Teflon plate, and an electric-heater. The diameter of the copper plate is 10 mm and the plate is 2 mm thick and is heated by passing DC current through the electric-heater. Besides, three thermocouples are fixed at the back surface of the copper plate to estimate the temperature of the upper surface of the copper plate and another two thermocouples are fixed at the top and bottom surface of the electric-heater to measure their surface temperatures. The locations of the thermocouples at the backside of the copper plate and at the electric-heater surface are shown in Fig. 2.5. The mica plates are placed between the heater and copper plate and between the heater and Teflon plate, intending to prevent the DC current leaking to the copper plate. The detailed structure of the module is shown in Fig. 2.6. The magnitude of heat loss from each surface of the cylindrical-hollow Teflon block can be evaluated from the temperature measured at selected locations in the block. Locations of the thermocouples are schematically shown in Fig. 2.7.

2.4 Hot-water Loop

In order to maintain the dielectric coolant FC-72 at the preset temperature at the test section inlet, a hot-water loop is used to preheat the coolant before it arrives at the test section inlet. The hot-water loop for the pre-heater includes a thermostat with a 20-liter hot water container, a 2-kW

heater in it, and a 0.5-hp water pump which can drive the hot water at a specified flow rate to the pre-heater. Besides, a bypass valve in the loop can further adjust the water flow rate. The hot water passes through the container while the liquid coolant FC-72 flows through the inner coiled pipe in the pre-heater. The connecting pipe between the pre-heater and test section is thermally insulated with a 5-cm thick polyethylene layer to reduce the heat loss from the pipe.

2.5 Cold-water Loop

The cold-water loop is designed for condensing the liquid-vapor mixture of coolant FC-72 delivered from the test section. The maximum cooling capacity of the thermostat is 2,000 Kcal/hr. The cold water at a specific flow rate is driven by a 0.5-hp pump to the condenser and a bypass loop is provided to adjust the flow rate. By adjusting the temperature and flow rate of the cold water, the bulk temperature of FC-72 in the condenser can be controlled at a preset level.

2.6 Programmable DC Power Supply

The power generated in the electric-heater is provided by a programmable DC power supply (Chroma 6203-60). The power supply can deliver the chosen time variation of the power input to the heater. Here the power input is chosen to in a sinusoidal oscillation. This power supply provides a maximum rated D.C. power of 300 W for an output Voltage of 60 V and an output current of 5 A. The time periodic power input to the copper plate is transmitted through a GPIB interface to a personal computer as shown in Fig. 2.8. A Yokogawa WT210 digital power meter with an accuracy of $\pm 0.1\%$ is used to measure the DC current through the electric-heater and the voltage drop across the heater with an accuracy of $\pm 1.5\%$. Thus the power input to the heater can be calculated.

2.7 Data Acquisition

The data acquisition system employed to acquire and process the data from various transducers is a 30-channel data logger (YOKOGAWA MX-100) along with a personal computer. All the voltage signals from the T-type thermocouples, pressure transducers, and volume flow-meters are converted to the temperature, pressure, and volume flow rate by the internal calibration equations in

the computer and are displayed on the screen simultaneously.

2.8 Optical Measurement Technique

The optical measurement technique employed in the present study enables us to capture the bubble characteristics in the boiling flow near the copper plate. The photographic apparatus consists of a high speed digital video camera (IDT High-speed CMOS Digital Camera), a micro-lens (Optem Zoom160), a three-dimensional positioning mechanism, and a personal computer. The high-speed motion analyzer can take photographs up to 143,307 frames/s. Here, a recording rate of 5000 frames/s is adopted to obtain the images of the bubble ebullition processes. The positioning mechanism is used to hold the camera at the required accurate position. The data for the bubble characteristics are collected in the regions near the geometric center of the plate surface. After the experimental system reaches a statistical state at long time, we start recording the boiling activity. The high speed motion analyzer stores the images which are later downloaded to a personal computer. Then, the time variations of the space-average bubble departure diameter and frequency and active nucleation site density are calculated by viewing more than 500 frames for each case. In order to achieve the highest possible resolution and to eliminate errors in calibration, the camera lens is fixed at a constant focal length, resulting in a fixed viewing area. Typically, a total of over 150 bubble diameter measurements are used to construct the present data. The bubble departure frequency is measured by counting the total number of bubbles that emerge from the targeted heating surface area during a period of a second.

2.9 Experimental Procedures

In each time periodic flow boiling experiment, liquid FC-72 in the coolant container is degassed first. Besides, the non-condensable gases in the coolant loop are evacuated and the degassed liquid FC-72 is filled into the loop. Then, we turn on the controller for setting the required variable rotation rate of the AC motor to regulate the FC-72 flow rate to the preset mean level, period and amplitude of the mass flux oscillation. Due to the inertia of the coolant flow, the mass

flux oscillates like a triangular wave. Next, the water temperature and flow rate in the hot-water loop are adjusted so that the FC-72 temperature at the test section inlet can be maintained at a preset level. The heat flux to the coolant in the test section is provided by the programmable DC power supply. The programmable power supply allows us to impose the required temporal heat flux oscillation in the form of nearly sinusoidal waves. In addition, we can calculate the time variation of the heat transfer rate to the coolant by instantly measuring the voltage across the electric-heater and the current delivered to the electric-heater. Temperature and flow rate of the cold water in the cold-water loop can be adjusted to condense and subcool the liquid-vapor mixture of FC-72 from the test section. Meanwhile, we regulate the time-average FC-72 pressure at the test section inlet by adjusting the gate valve locating right after the outlet of the test section. All measurements proceed when the experimental system has reached statistical state after the initial transients have died out. Finally, the scanning rate for each data channel is chosen to be 2 Hz and all the data channels are scanned for a period of 180 seconds.

2.10 Experimental Parameters

The ranges of the experimental parameters to be covered in the present study are listed in Table 2.1. Moreover, the thermodynamic and transport properties of FC-72 are given in Table 2.2 [50].

Table 2.1 Experimental Parameters

Parameter	Range	Unit
Flow velocity (V)	16.7 ~ 30	cm/s
Mean mass flux (\bar{G})	200 ~ 400	kg/m ² s
Mass flux oscillation amplitude ($\Delta G/\bar{G}$)	±5%,±10%,±15%	
Heat flux oscillation amplitude ($\Delta q/\bar{q}$)	±10%, ±30%, ±50%	-
Oscillation period (t_p)	10 ~ 30	sec
Time-average subcooling temperature ($\Delta \bar{T}_{sub}$)	0 ~ 10	°C
Mean imposed heat flux (\bar{q})	0.1 ~ 10	W/cm ²
Time-average system pressure (P)	99.0	kPa

Table 2.2 Thermodynamic and transport properties of the dielectric coolant FC-72[50]

Temperature T		Pressure P	Latent heat h_{fg}	Density ρ		Dynamic viscosity μ		Specific heat C_p		Conductivity K		Thermal expansion coefficient β	Surface tension σ	Thermal diffusion coefficient α		Prandtl No. Pr	
°C	K	Mpa	kJ/kg	kg/m ³ (l)	kg/m ³ (v)	mPa*s(l)	uPa*s(v)	J/kg*K(l)	J/kg*K(v)	mW/mK(l)	mW/mK(v)	1/K(l)	mN/m(l)	m ² /s(l)	m ³ /s(v)	liquid	vapor
20	293.15	0.024	90.4	1687	3.43	0.69	10.76	1045	844	57.9	10.4	0.00157	10.9	3.29E-08	3.6	12.4	0.87
25	298.15	0.03	88.5	1674	4.28	0.64	10.94	1053	851	57.4	10.8	0.00159	10.47	3.26E-08	3	11.8	0.86
30	303.15	0.038	86.7	1660	5.27	0.6	11.11	1061	858	56.9	11.1	0.0016	10.04	3.23E-08	2.5	11.2	0.86
35	308.15	0.046	84.8	1647	6.44	0.56	11.29	1068	866	56.3	11.5	0.00161	9.62	3.20E-08	2.1	10.6	0.85
40	313.15	0.057	82.9	1634	7.78	0.53	11.47	1076	873	55.8	11.8	0.00162	9.2	3.17E-08	1.7	10.2	0.85
45	318.15	0.069	81.1	1621	9.31	0.5	11.64	1084	880	55.2	12.2	0.00164	8.78	3.14E-08	1.5	9.7	0.84
50	323.15	0.083	79.1	1607	11.06	0.47	11.82	1092	887	54.7	12.5	0.00165	8.36	3.12E-08	1.3	9.3	0.84
54.3	327.45	0.097	77.5	1596	12.75	0.44	11.97	1098	892	54.3	12.8	0.00166	8.01	3.09E-08	1.1	9	0.83
55	328.15	0.099	77.2	1594	13.03	0.44	12	1099	893	54.2	12.9	0.00166	7.95	3.09E-08	1.1	9	0.83
55.7	328.85	0.1013	76.9	1592	13.33	0.44	12.02	1101	894	54.1	12.9	0.00167	7.9	3.09E-08	1.1	8.9	0.83
60	333.15	0.117	75.2	1581	15.25	0.42	12.17	1107	900	53.6	13.2	0.00168	7.55	3.06E-08	1	8.6	0.83
70	343.15	0.16	71.1	1554	20.49	0.38	12.53	1123	913	52.5	13.9	0.00171	6.75	3.01E-08	0.7	8.1	0.82
80	353.15	0.213	66.7	1528	27	0.34	12.88	1138	926	51.5	14.6	0.00174	5.97	2.96E-08	0.6	7.6	0.82

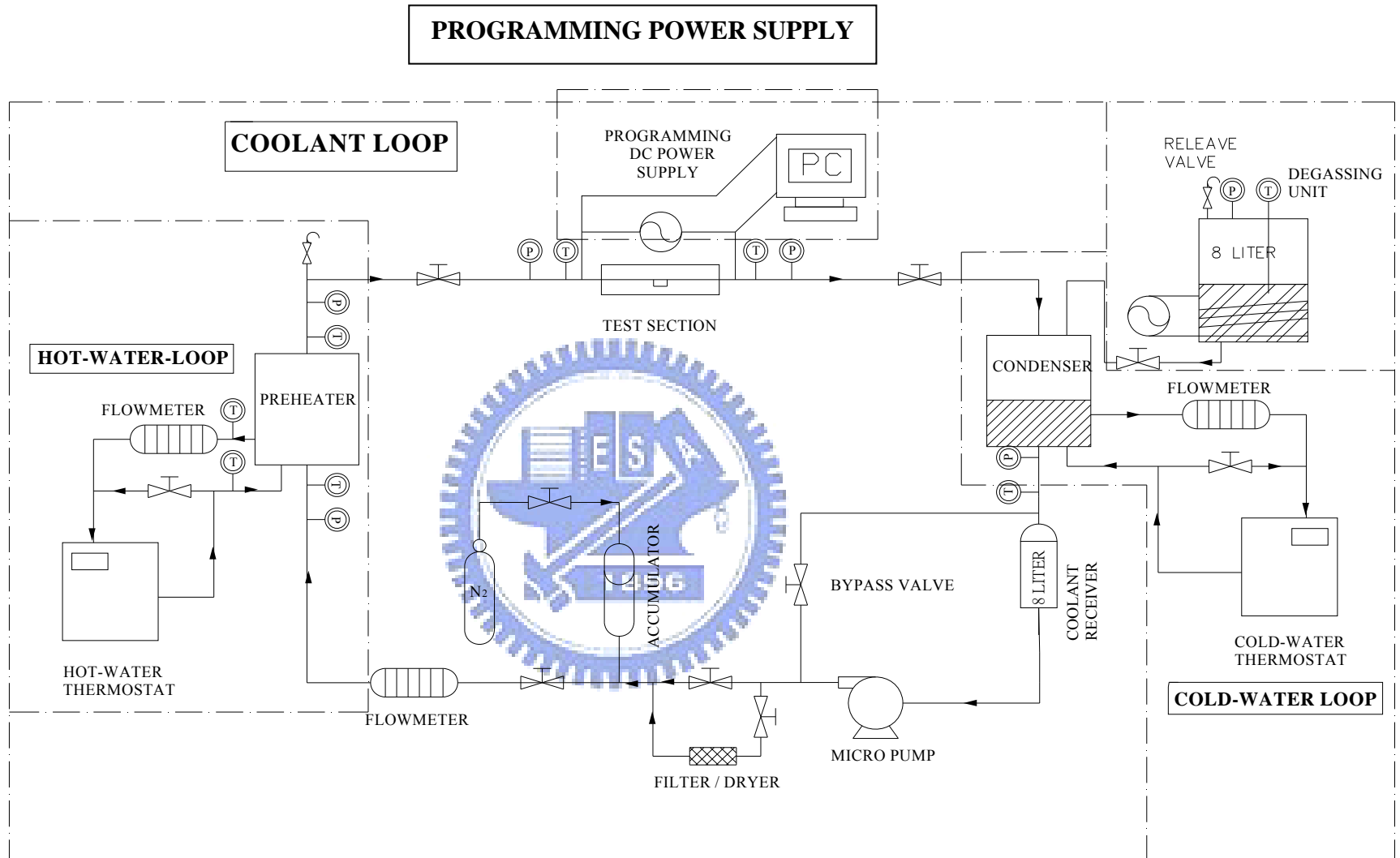


Fig. 2.1 Schematic diagram of experimental apparatus

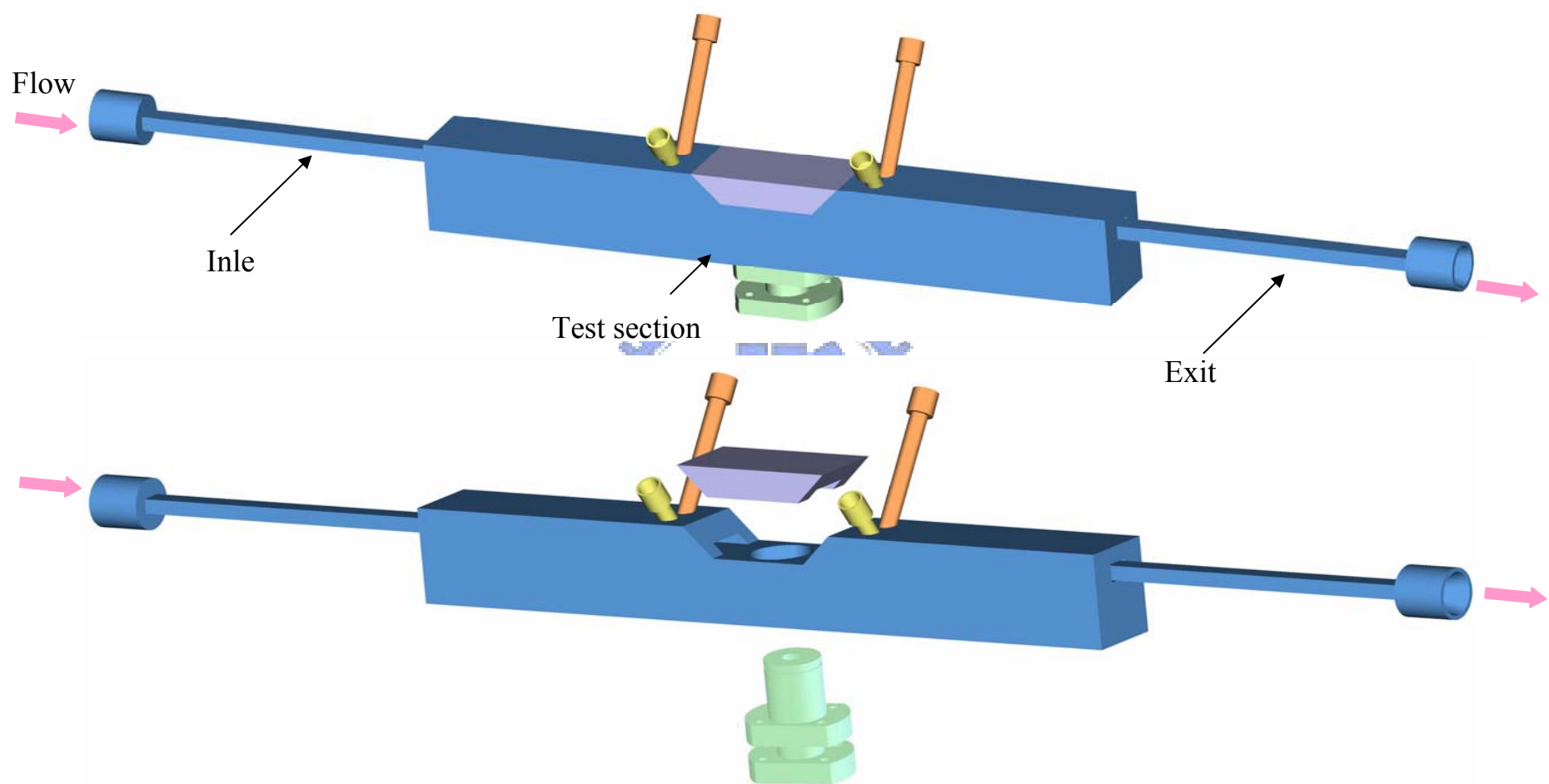


Fig. 2.2 Three-dimensional plots of test section along with inlet and outlet sections.

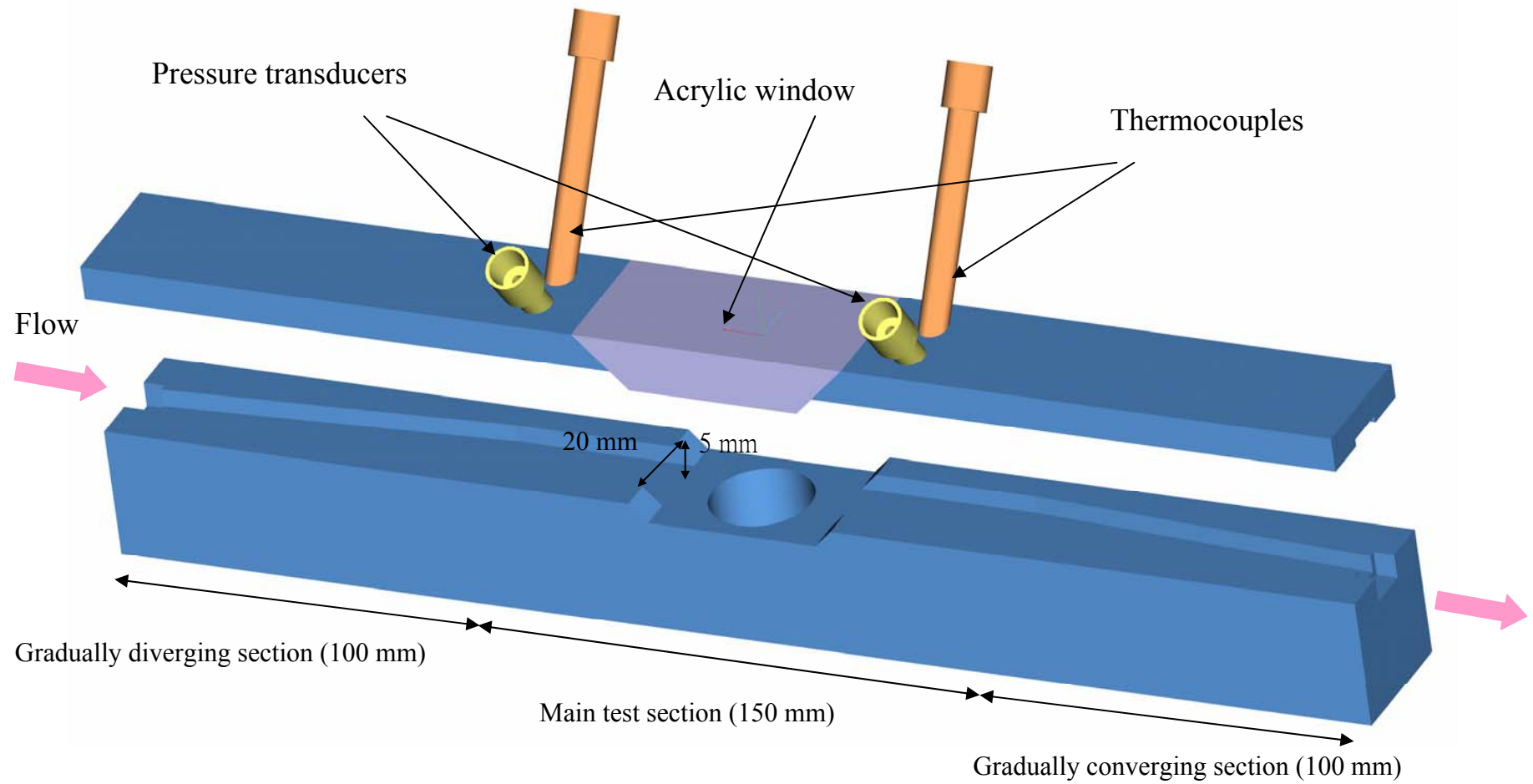


Fig. 2.3 Three-dimensional plots illustrating the test section in the rectangular flow channel.

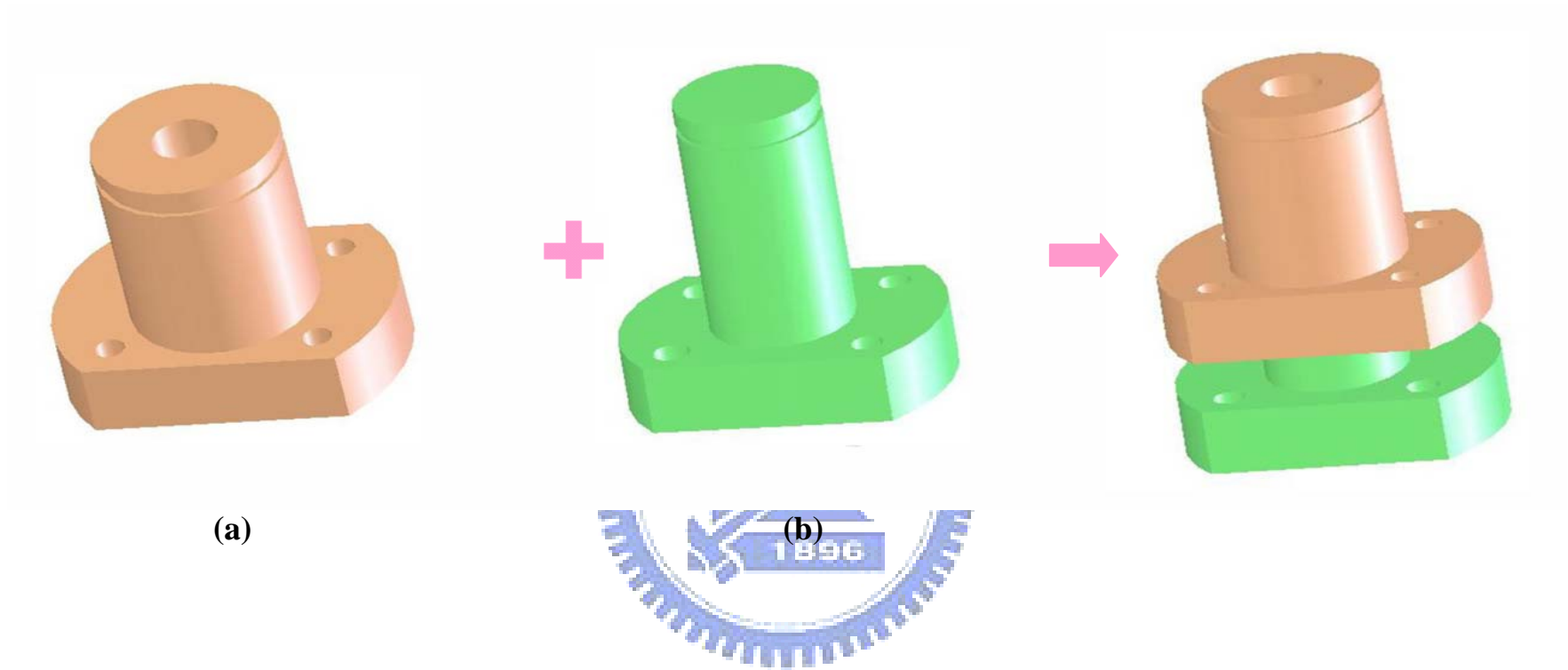
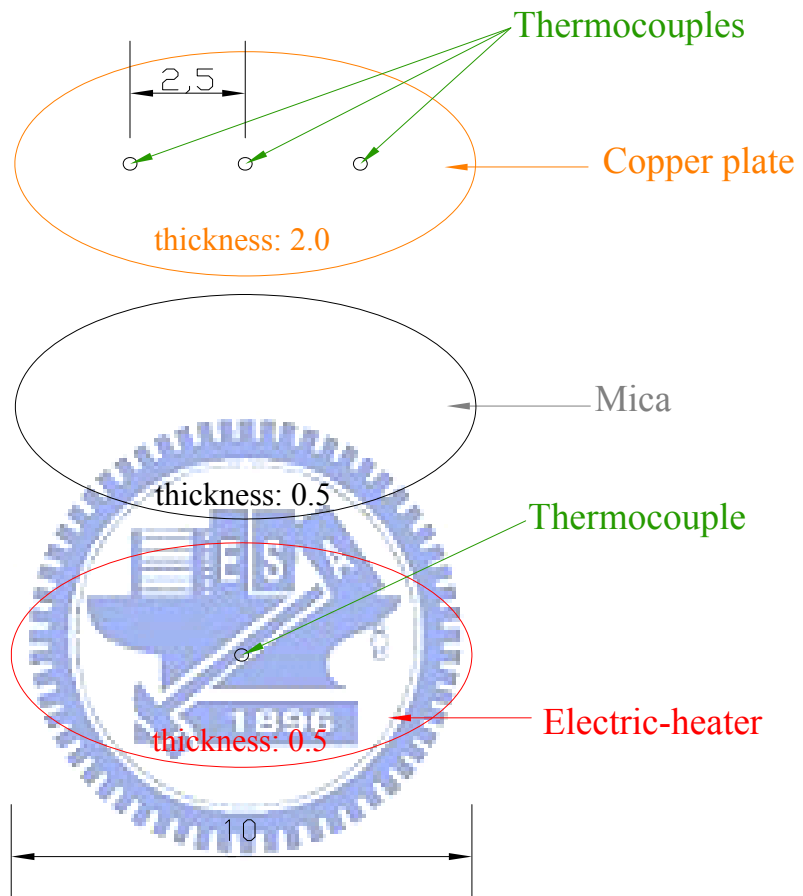


Fig. 2.4 Three-dimensional pictures showing (a) hollow cylindrical Teflon block and (b) cylindrical Teflon bolt.



(unit: mm)

Fig. 2.5 Locations of thermocouples.

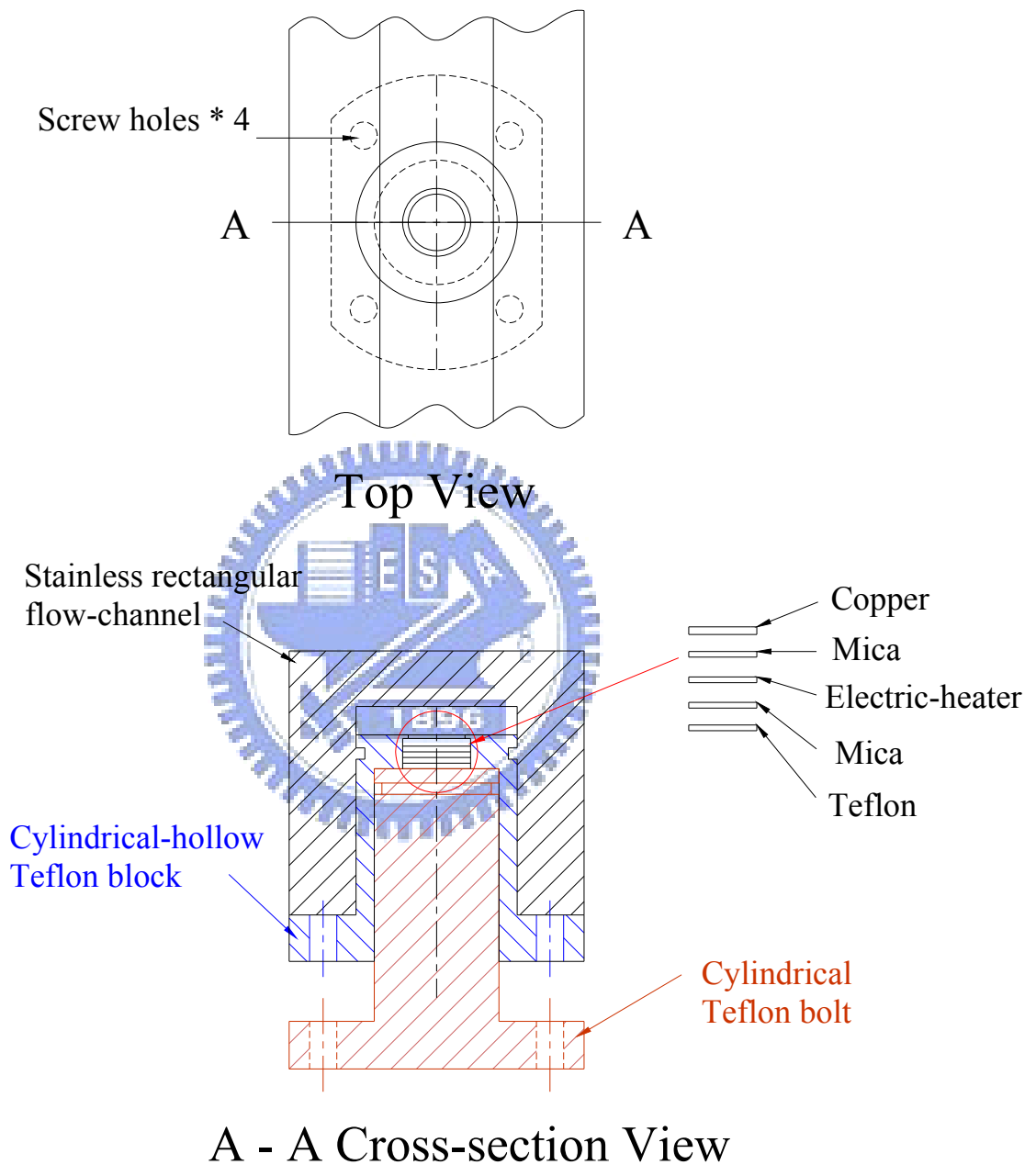


Fig. 2.6 Schematics of the copper plate module.

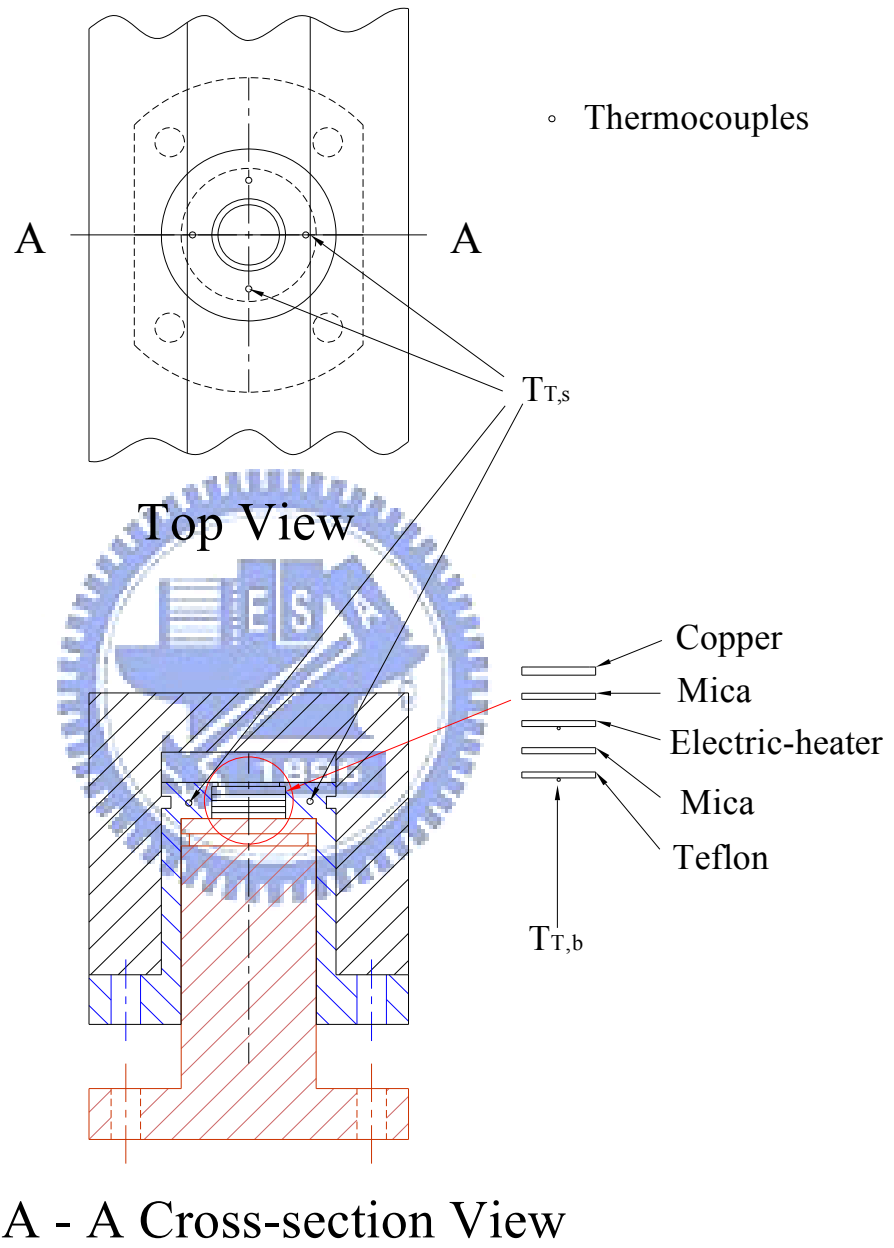


Fig. 2.7 Locations of the thermocouples inside the cylindrical-hollow Teflon block.

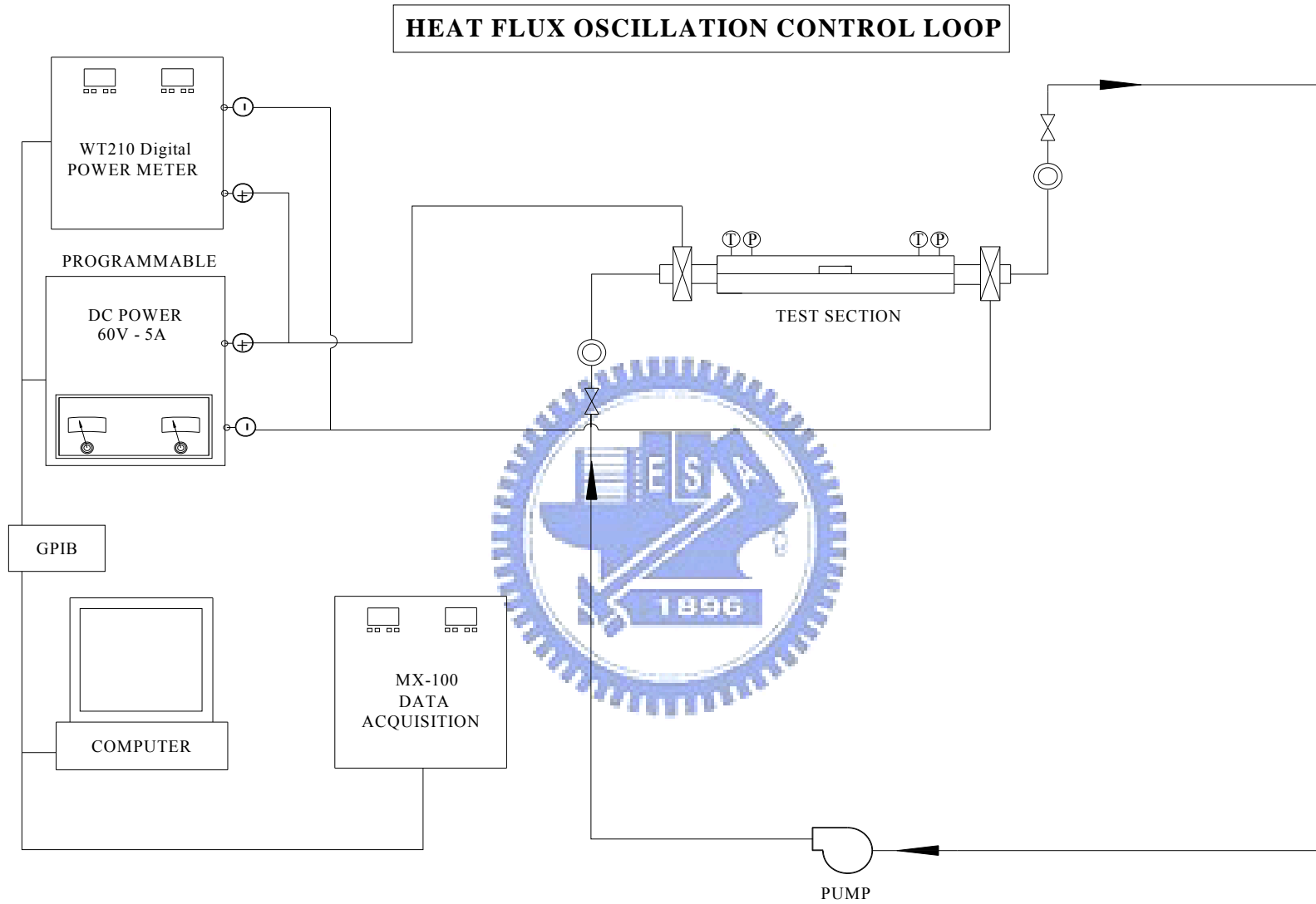


Fig. 2.8 Schematic diagram of heat flux oscillation control loop

CHAPTER 3

DATA REDUCTION

The single-phase liquid convection and two-phase flow boiling heat transfer coefficients of the coolant FC-72 flowing over the small heated copper plate flush mounted on the bottom of a horizontal rectangular-channel will be deduced from the measured raw data. The space-average heated surface temperature is calculated from the measured average temperature from the thermocouples located near the upper surface of the copper plate according to the one-dimensional steady state conduction heat transfer. Specifically,

$$T_w = T_{Cu} - \left(q \times \frac{l}{k_{Cu}} \right) \quad (3.1)$$

where T_{Cu} is the average measured temperature from the thermocouples and k_{Cu} and l are individually the thermal conductivity of copper and the vertical distance between the thermocouple tips and the upper surface of the copper plate.

3.1 Single-phase Heat Transfer

Before the two-phase experiments, the net power input Q_n to the coolant flowing over the copper plate is evaluated from the difference between the total power input Q_t to the copper plate and the total heat loss from the test section Q_{loss} . The total power input can be calculated from the measured voltage drop across the electric-heater V and the electric current passing through it I .

The total power input Q_t and the effective power input Q_n are hence evaluated respectively from the equations:

$$Q_t = V \cdot I \quad (3.2)$$

and

$$Q_n = Q_t - Q_{\text{loss}} \quad (3.3)$$

Here the total heat loss from the copper plate is approximately estimated by accounting for the radial conduction heat transfer from the copper plate to the cylindrical Teflon block and downward heat conduction from the electric heater to bottom Teflon plate as

$$Q_{\text{loss}} = \frac{2\pi L k_T (T_w - T_{T,s})}{\ln(r_{T,s}/r_w)} + \frac{(T_e - T_{T,b})}{\frac{L_{T,b}}{k_T A_{T,b}} + \frac{L_M}{k_M A_M}} \quad (3.4)$$

In the above equation k_T and k_M are the thermal conductivities of the Teflon and the mica, respectively; $A_{T,b}$ and A_M are respectively the bottom surface areas of the Teflon and mica plates; L , $L_{T,b}$ and L_M are individually the thickness of the copper, Teflon and mica plates; T_w and T_e are respectively the space-average temperature of the copper plate and the temperature at the bottom surface of the electric-heater; $T_{T,b}$ is the temperature of the bottom Teflon plate, as schematically shown in Fig. 2.7.

The net imposed heat flux at the copper plate surface is defined as

$$q = Q_n / A_{cp} \quad (3.5)$$

where A_{cp} is the surface area of the copper plate. The relative heat loss from the heated copper plate is defined as

$$\varepsilon = \frac{Q_{\text{loss}}}{Q_t} \times 100\% \quad (3.6)$$

The results from this estimation show that the relative heat losses for all cases investigated here for the single-phase flow are about 20% at $q=1\text{W}/\text{cm}^2$. The average single-phase liquid convection heat transfer coefficient over the copper plate is defined as

$$h_{1\phi} = \frac{Q_n}{A_{cp} \cdot (T_w - T_{in})} \quad (3.7)$$

where T_{in} is the coolant temperature at the inlet of the test section and T_w is the space-average temperature of the upper surface of the copper plate.

3.2 Flow Boiling Heat Transfer

In the flow boiling experiment the state of coolant FC-72 at the inlet of the rectangular flow-channel is evaluated from the energy balance for the pre-heater. The total heat transfer rate in the pre-heater is calculated from the temperature drop on the water side as

$$Q_{w,p} = \dot{m}_{w,p} \cdot c_{p,w} \cdot (T_{w,p,i} - T_{w,p,o}) \quad (3.8)$$

Where $\dot{m}_{w,p}$ is the mass flow rate of the hot water at the inlet of the pre-heater, $c_{p,w}$ is the specific heat of water, and $T_{w,p,i}$ and $T_{w,p,o}$ are respectively the temperatures of the water at the pre-heater inlet and outlet. Note that in the pre-heater the coolant FC-72 is still in liquid state. Hence on the coolant side in the pre-heater

$$Q_{w,p} = \dot{m}_r \cdot c_{p,r} \cdot (T_{r,p,o} - T_{r,p,i}) \quad (3.9)$$

where \dot{m}_r is the mass flow rate of the coolant in the pre-heater, $c_{p,r}$ is the specific heat of coolant, and $T_{r,p,o}$ and $T_{r,p,i}$ are respectively the temperatures of the coolant at the outlet and inlet of the coiled pipe immersed in the container in the pre-heater. Combining the above two equations allows us to calculate $T_{r,p,o}$, which is considered as the temperature of FC-72 at the test section inlet. On the other hand, the average two-phase boiling heat transfer coefficient for the coolant flow over the copper plate is defined as

$$h_{2\phi,sat} = \frac{Q_n}{A_{cp} \cdot (T_w - \bar{T}_{sat})} \quad \text{for saturated and subcooled flow boiling,} \quad (3.10)$$

Where \bar{T}_{sat} is the time-average saturated temperature of the coolant FC-72.

Note that the above definitions for single-phase convection and two-phase boiling heat transfer coefficients are usually adopted in steady heat transfer. They are also

employed here for the transient oscillatory boiling heat transfer investigated in the present study with Q_t and Q_n also evaluated by Equations (3.1)-(3.3) through using the measured instantaneous values for V and I and the measured instantaneous temperature data at selected locations.

3.3 Uncertainty Analysis

Uncertainties of the single-phase liquid convection and flow boiling heat transfer coefficients and other parameters are estimated by the procedures proposed by Kline and McClintock [51]. The detailed results from this uncertainty analysis are summarized in Table 3.1.



Table 3.1 Summary of the uncertainty analysis

Parameter	Uncertainty
Rectangular channel geometry	
Length, width and thickness (%)	$\pm 0.5\%$
Area (%)	$\pm 1.0\%$
Parameter measurement	
Temperature, T (°C)	± 0.2
Temperature difference, ΔT (°C)	± 0.3
Mean system pressure, P (kPa)	± 2
Mean mass flux of coolant, \bar{G} (%)	± 3
Amplitude of mass flux oscillation, $\Delta G / \bar{G}$ (%)	± 4.8
Period of mass flux oscillation, t_p (sec)	± 0.25
Mean imposed heat flux, \bar{q}	± 2.1
Amplitude of heat flux oscillation, $\Delta q / \bar{q}$ (%)	± 0.2
Period of heat flux oscillation, t_p (sec)	± 0.25
Single-phase heat transfer in rectangular channel	
Heat transfer coefficient, $h_{1\phi}$ (%)	± 12.3
Two-phase heat transfer in Rectangular channel	
Heat transfer coefficient, $h_{2\phi}$ (%)	± 12.3

CHAPTER 4

TIME PERIODIC SATURATED FLOW BOILING OF FC-72 OVER A SMALL HEATED COPPER PLATE

In the first part of the present study the coolant at the test section inlet is kept at the liquid state and its temperature is controlled at the time-average value of the saturated temperature corresponding to the inlet coolant pressure which oscillates time periodically with the coolant flow rate. This is designated as “transient oscillatory saturated flow boiling” in this study. Results obtained in the first part of the study are presented here to illustrate how the imposed simultaneous heat flux and mass flux oscillations affect the transient oscillatory saturated flow boiling heat transfer of FC-72 over a small heated circular copper flat plate flush mounted on the bottom of the horizontal rectangular channel. The present experiment is conducted for the mean FC-72 mass flux \bar{G} fixed at 300 and 400 kg/m²s with the time-average imposed heat flux \bar{q} varied from 0.1 W/cm² to 10 W/cm². Besides, the amplitude of the coolant mass flux oscillation ΔG is set at 0, 5 and 10% of the mean coolant mass flux and the amplitude of the heat flux oscillation Δq is set at 10, 30 and 50% of the average heat flux. In addition, the periods of the heat flux and mass flux oscillations t_p are chosen to be the same and are fixed at 10, 20 and 30 seconds. Initially, the coolant FC-72 in the test section is at a slightly subatmospheric pressure of 99 KPa with the saturated temperature $T_{\text{sat}}=55^\circ\text{C}$ before each test is started. In the following, the effects of the experimental parameters including the mean levels and amplitudes and periods of the heat and mass flux oscillations on the time periodic flow boiling will be explored for both in-phase and out-of-phase G and q oscillations. Note that for the limiting case of constant heat flux and mass flux ($\Delta q = 0$ and $\Delta G = 0$) we have saturated boiling of FC-72 at constant q and G in the test section, which is designated as “stable saturated flow boiling” in the present study. The heat transfer performance is mainly presented in terms of the time variations of the space-average surface temperature of the copper plate and boiling

heat transfer coefficient.

4.1 Single-phase Liquid Convective Heat Transfer

Before beginning the two-phase flow boiling experiments, steady single-phase liquid convective heat transfer experiments are conducted for constant FC-72 flow rate over the copper plate heated by a constant heat flux in the rectangular channel. The measured space-average heat transfer coefficient for single-phase convection from the heated copper surface to the coolant is compared with the correlation proposed by Gersey and Mudawar [5]. Their correlation is

$$\overline{Nu}_L = 0.362 \cdot Re_L^{0.614} \cdot Pr^{1/3} \quad (4.1)$$

where

$$Re_L = \frac{G \cdot L}{\mu_1} \quad (4.2)$$

$$\overline{h}_{1\phi} = \frac{K_L}{L} \overline{Nu}_L \quad (4.3)$$

Their correlation is based on the experimental data procured from the same liquid and same flow configuration as the present data and the comparison is shown in Fig. 4.1 for the dimensional and dimensionless heat transfer coefficients. The results indicate that our data are in good agreement with their correlation.

It should be mentioned that the working fluid properties used in reducing the data for Fig. 4.1 from Equations (4.1) – (4.3) are calculated at the coolant inlet temperature. The copper plate diameter is chosen as the characteristic length in defining the Reynolds number Re_L and average Nusselt number \overline{Nu}_L because of its significant effect on the heat transfer performance [5].

4.2 Time Periodic Saturated Flow Boiling Heat Transfer Characteristics

The temporal boiling heat transfer characteristics for the FC-72 flow over the heated copper plate resulting from the imposed temporal heat flux and mass flux oscillations are illustrated by

presenting the time variations of the space-average heated surface temperature T_w and heat transfer coefficient $h_{2\phi}$ for various \bar{G} , \bar{q} , $\Delta q/\bar{q}$, $\Delta G/\bar{G}$ and t_p . First, the measured time variations of T_w for the limiting cases of stable flow boiling at constant G and q are shown in Fig. 4.2 for $G=300$ and $400\text{kg/m}^2\text{s}$ at various q . These data indicate that the fluctuations of the space-average heated surface temperatures with time for various q are relatively small. The resulting boiling in the flow for $\Delta G=0$ and $\Delta q=0$ can be regarded essentially as at a statistically stable state. The corresponding boiling curves are shown in Fig. 4.3. The data in Fig. 4.3 show that the required heat flux and wall superheat for the onset of nucleate boiling (ONB) are higher for a higher coolant mass flux.

Next, we move further to examine the T_w data for the imposed heat flux and coolant mass flux oscillating periodically in time respectively in forms of nearly a sinusoidal wave and a triangular wave. The results are given first in Fig. 4.4 for $\bar{G}=200\text{kg/m}^2\text{s}$ and $t_p=20$ sec. for $\Delta G/\bar{G}=10\%$ and $\Delta q/\bar{q}=30\%$ at various \bar{q} . For comparison purpose the data for constant G ($\Delta G=0$) but oscillation q are also shown in the figure. Besides, the data for both in-phase and out-of-phase G and q oscillations are presented. Note that for each case the temporal oscillation of the heated surface temperature is also periodic in time and is at the same frequency as the heat flux and/or mass flux. Moreover, the T_w oscillation gets slightly stronger for a higher mean level of the heat flux oscillation irrespective of the in-phase or out-of-phase oscillations. A close inspection of these data further reveals that the heated surface temperature oscillation lags significantly behind the imposed heated flux oscillation for constant G and for both in-phase and out-of-phase G and q oscillations. This time lag in T_w results mainly from the thermal inertia of the copper plate since the time lag in T_w due to the mass flux oscillation is small [52]. We also note that in the single-phase flow prevailed only at low imposed heat flux the time lag is even longer than that for the flow boiling. Table 4.1 summarizes the quantitative data for the amplitude of the heated surface temperature oscillation ΔT_w and the relative magnitude of the time lag t_l/t_p . The results clearly

manifest that the time lag in T_w is somewhat longer when G and q are in out-of-phase oscillations than the other situations. It is of interest to note that in the single-phase flow the T_w oscillation is strongest for the out-of-phase G and q oscillations. But the opposite is true for the flow boiling which prevails at high imposed heat flux, showing the T_w oscillation is suppressed by the out-of-phase oscillations. This unusual outcome requires in-depth examination of the detailed heat transfer mechanisms in the flow subject to the simultaneous G and q oscillations. Here we provide preliminary interpretation. When only the heat flux oscillation exists, the heated surface temperature increases with the heat flux for both single- and two-phase flows after accounting for the time lag, as evident from Fig. 4.4(a). But when only the mass flux oscillation exists, our previous study[52] showed that in the two-phase boiling flow T_w decreases at decreasing mass flux due to drastic increase in the active bubble nucleation site density. The trend is reversed for the single-phase flow. This explains why an out-of-phase mass flux oscillation can reduce the T_w oscillation resulting from the heat flux oscillation in the boiling flow and can intensify the T_w oscillation in the single-phase flow.

Effects of the experimental parameters on the T_w oscillation are illustrated in Figs. 4.5-4.15. The results indicate that the heated surface temperature oscillates in a larger amplitude for higher oscillation amplitudes in the heat flux and mass flux. It is worth noting that an increase in the period of the G and q oscillations causes a much stronger T_w oscillation, are evident by comparing the data in Figs. 4.5-4.7 with that in Figs. 4.13-4.15. To be more quantitative, we summarize the present data for the amplitude and time lag of the T_w oscillation in Tables 4.2-4.6 for various \bar{G} , $\Delta G/\bar{G}$, t_p , \bar{q} and $\Delta q/\bar{q}$. It is of interest to note that the imposed out-of-phase G & q oscillations do not always weaken the T_w oscillation in the boiling flow. Similarly, in-phase G & q oscillations may not reduce the T_w oscillation in the single-phase flow especially at high $\Delta q/\bar{q}$. We also note that the relative time lag t_l/t_p varies nonmonotonically with the experimental parameters.

At this point we move further to investigate whether it is possible to completely suppress the

heated surface temperature oscillation driven by a given time periodic heat flux oscillation by choosing an appropriate in-phase or out-of-phase mass flux oscillation. It is noted in this investigation that the chosen mass flux oscillation should be at a suitable amplitude and at the same period as the heat flux oscillation. Most importantly, the time lags in the T_w oscillation due to the q and G oscillations have to be taken into consideration. The results from this investigation are illustrated in Figs. 4.16 and 4.17 for $\bar{G}=300\text{kg/m}^2\text{s}$, $\Delta G/\bar{G}=15\% \text{ \& } 20\%$ and $t_p=20\text{sec} \text{ \& } 30\text{sec}$ for several \bar{q} . Here in the single-phase flow an in-phase G oscillation is imposed. But an out-of-phase G oscillation is imposed in the two-phase flow. Note that a small time lag in the T_w oscillation also exists due to the mass flux oscillation (Figs. 4.16(b) and 4.17(b)), as already mentioned above. The results in Fig. 4.16 indicate that as the G oscillation is imposed at a time instant behind the q oscillation by the difference in the time lags respectively due to the q and G oscillations, the T_w oscillations can indeed be suppressed to be relatively small in magnitude (Fig. 4.16(c)). In fact, the resulting T_w oscillation amplitude is below 0.1°C which is smaller than the thermal disturbances in the background and the experimental uncertainty in measuring the temperature by the thermocouples. Hence the heated surface temperature can be regarded at steady state. At a high \bar{q} the T_w oscillation can only be reduced by the G oscillation to a significant degree (Fig. 4.17(c)). It cannot be completely suppressed.

The associated heat transfer coefficients for the single-phase and boiling flows affected by the imposed heat and mass flux oscillations are presented in Figs. 4.18-4.29. The results indicate that the oscillations in the heat transfer coefficient exhibit a similar trend to the heated surface temperature oscillation. Specifically, the $h_{1\phi}$ and $h_{2\phi}$ oscillations are also periodic in time and are at the same frequency as the heat flux and/or mass flux. Besides, at a higher \bar{q} the oscillations in $h_{1\phi}$ and $h_{2\phi}$ are slightly stronger. But the oscillation amplitudes in $h_{1\phi}$ and $h_{2\phi}$ depend only slightly on the in-phase or out-of-phase G and q oscillations. Moreover, $h_{1\phi}$ and $h_{2\phi}$ are in stronger oscillations for a higher amplitude and a longer period of the imposed G and q oscillations.

4.3 Bubble Characteristics

To elucidate the above time periodic flow boiling heat transfer characteristics, the data for the bubble characteristics of FC-72 obtained from the present flow visualization are examined in the following. The photos taken from the top view of the boiling flow in a small region around the geometric center of the heated surface for various coolant mass fluxes and imposed heat fluxes are shown in Figs. 4.32 - 4.49. At first, the bubble characteristics for the limiting cases of constant imposed heat and mass fluxes are illustrated by the photos in Fig. 4.32. It is noted in the flow visualization and the results in Fig. 4.32 that in the stable flow boiling the vapor bubbles begin to appear as the heated surface temperature exceeds that required for the boiling incipient superheat. In the beginning, tiny bubbles are observed in the active nucleation sites. The bubbles grow and then detach from the heated surface with certain bubble departure diameters. As the imposed heat flux increases, more bubbles are generated on more active nucleation sites and more bubbles detach from the heated surface. Besides, the detached bubbles tend to merge into larger bubbles. Note that the large bubbles become distorted and elongated as they slide on the heating surface. Moreover, at a higher mass flux the bubbles are smaller and the bubble coalescence is less significant for a given heat flux.

Next, the bubble characteristics in the time periodic flow boiling are illustrated by presenting the photos of the boiling flow at eight selected time instants in a typical periodic cycle in Figs. 4.33-4.49. In these figures the symbol “ $t=t_0$ ” signifies the time instant at which the instantaneous heat fluxes is at the lowest level and starts to increase with time and the mass flux is also at the lowest level and starts to increase with time for the in-phase G and q oscillations. But for the out-of-phase G and q oscillations at t_0 the mass flux is at the highest level and starts to decrease with time.

The results in Fig. 4.33 for an imposed heat flux oscillation at a given constant G of 200 $\text{kg/m}^2\text{s}$ qualitative indicate that in the first half of the periodic cycle in which the surface heat flux increases with time the bubbles grow with time and merge together to form big bubbles. Besides,

more bubbles nucleate from the heated surface. The bubbles are in rigorous motion and the photos become somewhat blurred as the heat flux exceeds certain level. In the second half of the cycle the opposite processes take place. It is important to point out that the bubble behavior in the boiling flow affected by the mass flux oscillation exhibits an opposite trend [52]. Specifically, at increasing mass flux in the first half of the periodic cycle the bubbles get smaller and become more disperse. Besides, less bubble nucleation occurs on the heated surface. Thus, when the G and q oscillations are in-phase, the bubble behavior is counter-balanced by two opposite effects and its change with time is rather mild (Figs. 4.34, 4.37, 4.39, 4.42, 4.45) except for some cases with large differences in the amplitudes of heat and mass flux oscillations (Figs. 4.38, 4.42). But when G and q are in out-of-phase oscillations the two effects augment each other and the bubble behavior can show drastic variation with time (Figs. 4.35, 4.38, 4.40, 4.46, and 4.49). Moreover, at higher $\Delta G/\bar{G}$ and $\Delta q/\bar{q}$ and at a longer t_p the bubble characteristics experience stronger time variations.

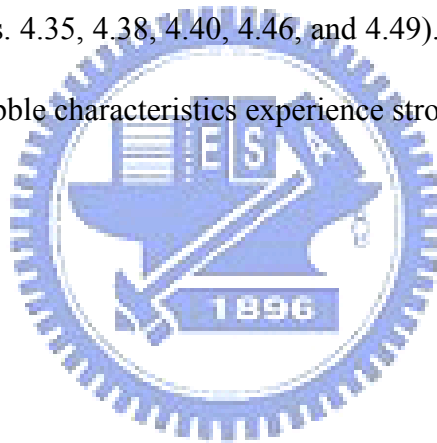


Table 4.1 Amplitudes of T_w oscillation and relative time lags in transient oscillatory saturated flow

boiling for various \bar{q} at $\Delta q/\bar{q} = 30\%$, $\Delta G/\bar{G} = 10\%$ and $t_p = 20\text{sec}$. for $\bar{G} = 200\text{kg/m}^2\text{s}$.

$\Delta G/\bar{G}$	Period $t_p(\text{sec})$	$\Delta q/\bar{q}$	$\bar{G} = 200\text{kg/m}^2\text{s}$				
			$\bar{q}(\text{W/cm}^2)$		$\Delta T_w (K)$	t_1/t_p	
10%	20	30%	1.01 (single-phase)	Heat flux oscillation only		0.24	0.375
				In-phase G & q oscillations		0.23	0.375
				Out-of-phase G & q oscillations		0.30	0.475
			2.37	Heat flux oscillation only		0.33	0.25
				In-phase G & q oscillations		0.39	0.225
				Out-of-phase G & q oscillations		0.31	0.35
			4.05	Heat flux oscillation only		0.43	0.175
				In-phase G & q oscillations		0.43	0.2
				Out-of-phase G & q oscillations		0.41	0.225
			6.02	Heat flux oscillation only		0.53	0.225
				In-phase G & q oscillations		0.58	0.225
				Out-of-phase G & q oscillations		0.51	0.25

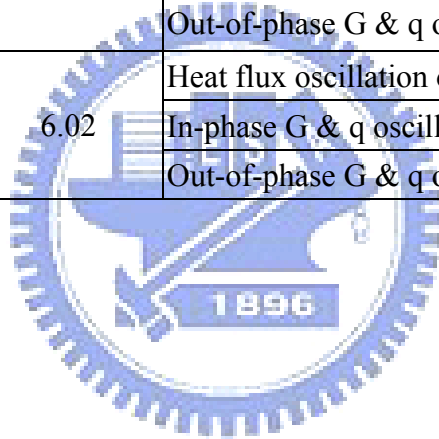


Table 4.2 Amplitudes of T_w oscillation and relative time lags in transient oscillatory saturated flow

boiling for various \bar{q} at $\Delta q/\bar{q} = 10,30,50\%$, $\Delta G/\bar{G} = 5\%$ and $t_p = 20\text{sec}$. for $\bar{G} = 300\text{kg/m}^2\text{s}$.

$\Delta G/\bar{G}$	Period $t_p(\text{sec})$	$\Delta q/\bar{q}$	$\bar{G} = 300\text{kg/m}^2\text{s}$				
			$\bar{q}(\text{W/cm}^2)$		$\Delta T_w(K)$	t_1/t_p	
5%	20	10%	1.02 (single-phase)	Heat flux oscillation only		0.11	0.4
				In-phase G & q oscillations		0.11	0.4
				Out-of-phase G & q oscillations		0.11	0.4
			1.90	Heat flux oscillation only		0.18	0.375
				In-phase G & q oscillations		0.23	0.2
				Out-of-phase G & q oscillations		0.17	0.3
			4.10	Heat flux oscillation only		0.20	0.2
				In-phase G & q oscillations		0.31	0.05
				Out-of-phase G & q oscillations		0.24	0.35
		5.08	Heat flux oscillation only		0.20	0.15	
			In-phase G & q oscillations		0.25	0.075	
			Out-of-phase G & q oscillations		0.21	0.25	
		30%	1.02 (single-phase)	Heat flux oscillation only		0.28	0.375
				In-phase G & q oscillations		0.27	0.35
				Out-of-phase G & q oscillations		0.26	0.425
			1.94	Heat flux oscillation only		0.35	0.2
				In-phase G & q oscillations		0.42	0.175
				Out-of-phase G & q oscillations		0.35	0.2
			4.10	Heat flux oscillation only		0.47	0.15
				In-phase G & q oscillations		0.49	0.1
				Out-of-phase G & q oscillations		0.48	0.225
		5.10	Heat flux oscillation only		0.54	0.2	
			In-phase G & q oscillations		0.56	0.175	
			Out-of-phase G & q oscillations		0.57	0.225	
		50%	1.02 (single-phase)	Heat flux oscillation only		0.42	0.4
				In-phase G & q oscillations		0.41	0.375
				Out-of-phase G & q oscillations		0.43	0.3
			1.94	Heat flux oscillation only		0.59	0.2
				In-phase G & q oscillations		0.71	0.2
				Out-of-phase G & q oscillations		0.62	0.25
			4.10	Heat flux oscillation only		0.81	0.175
				In-phase G & q oscillations		0.85	0.125
				Out-of-phase G & q oscillations		0.77	0.15
		5.10	Heat flux oscillation only		0.91	0.2	
			In-phase G & q oscillations		0.89	0.15	
			Out-of-phase G & q oscillations		0.83	0.175	

Table 4.3 Amplitudes of T_w oscillation and relative time lags in transient oscillatory saturated flow

boiling for various \bar{q} at $\Delta q/\bar{q} = 10, 30, 50\%$, $\Delta G/\bar{G} = 10\%$ and $t_p = 20$ sec. for $\bar{G} = 300 \text{ kg/m}^2\text{s}$.

$\Delta G/\bar{G}$	Period t_p (sec)	$\Delta q/\bar{q}$	$\bar{G} = 300 \text{ kg/m}^2\text{s}$			
			\bar{q} (W/cm^2)		ΔT_w (K)	t_1/t_p
10%	20	10%	1.03 (single-phase)	Heat flux oscillation only	0.10	0.275
				In-phase G & q oscillations	0.14	0.425
				Out-of-phase G & q oscillations	0.16	0.225
			2.67	Heat flux oscillation only	0.14	0.325
				In-phase G & q oscillations	0.27	0.075
				Out-of-phase G & q oscillations	0.26	0.475
			4.03	Heat flux oscillation only	0.15	0.225
				In-phase G & q oscillations	0.34	0.025
				Out-of-phase G & q oscillations	0.34	0.4
		6.12	Heat flux oscillation only	0.19	0.2	
			In-phase G & q oscillations	0.33	0.05	
			Out-of-phase G & q oscillations	0.34	0.475	
		30%	1.02 (single-phase)	Heat flux oscillation only	0.23	0.45
				In-phase G & q oscillations	0.22	0.575
				Out-of-phase G & q oscillations	0.30	0.35
			2.35	Heat flux oscillation only	0.38	0.3
				In-phase G & q oscillations	0.44	0.225
				Out-of-phase G & q oscillations	0.38	0.3
			5.04	Heat flux oscillation only	0.51	0.275
				In-phase G & q oscillations	0.59	0.15
				Out-of-phase G & q oscillations	0.49	0.3
		6.11	Heat flux oscillation only	0.56	0.25	
			In-phase G & q oscillations	0.66	0.2	
			Out-of-phase G & q oscillations	0.57	0.3	
		50%	1.02 (single-phase)	Heat flux oscillation only	0.42	0.375
				In-phase G & q oscillations	0.38	0.425
				Out-of-phase G & q oscillations	0.47	0.4
			2.16	Heat flux oscillation only	0.64	0.3
				In-phase G & q oscillations	0.68	0.25
				Out-of-phase G & q oscillations	0.63	0.3
			4.07	Heat flux oscillation only	0.77	0.25
				In-phase G & q oscillations	0.85	0.25
				Out-of-phase G & q oscillations	0.70	0.25
		6.09	Heat flux oscillation only	0.94	0.275	
			In-phase G & q oscillations	1.04	0.225	
			Out-of-phase G & q oscillations	0.85	0.3	

Table 4.4 Amplitudes of T_w oscillation and relative time lags in transient oscillatory saturated flow

boiling for various \bar{q} at $\Delta q/\bar{q} = 30\%$, $\Delta G/\bar{G} = 15\%$ and $t_p = 20$ sec. for $\bar{G} = 300 \text{ kg/m}^2\text{s}$.

$\Delta G/\bar{G}$	Period t_p (sec)	$\Delta q/\bar{q}$	$\bar{G} = 300 \text{ kg/m}^2\text{s}$				
			$\bar{q}(\text{W/cm}^2)$		$\Delta T_w (K)$	t_1/t_p	
15%	20	30%	1.01 (single-phase)	Heat flux oscillation only		0.26	0.375
				In-phase G & q oscillations		0.24	0.475
				Out-of-phase G & q oscillations		0.30	0.375
			2.53	Heat flux oscillation only		0.41	0.25
				In-phase G & q oscillations		0.48	0.225
				Out-of-phase G & q oscillations		0.37	0.3
			4.13	Heat flux oscillation only		0.43	0.2
				In-phase G & q oscillations		0.59	0.175
				Out-of-phase G & q oscillations		0.42	0.325
			6.19	Heat flux oscillation only		0.54	0.225
				In-phase G & q oscillations		0.68	0.175
				Out-of-phase G & q oscillations		0.50	0.25

Table 4.5 Amplitudes of T_w oscillation and relative time lags in transient oscillatory saturated flow

boiling for various \bar{q} at $\Delta q/\bar{q} = 30\%$, $\Delta G/\bar{G} = 10\%$ and $t_p = 20$ sec. for $\bar{G} = 400 \text{ kg/m}^2\text{s}$.

$\Delta G/\bar{G}$	Period t_p (sec)	$\Delta q/\bar{q}$	$\bar{G} = 400 \text{ kg/m}^2\text{s}$				
			$\bar{q}(\text{W/cm}^2)$		$\Delta T_w (K)$	t_1/t_p	
10%	20	30%	1.02 (single-phase)	Heat flux oscillation only		0.27	0.275
				In-phase G & q oscillations		0.24	0.275
				Out-of-phase G & q oscillations		0.28	0.35
			3.03	Heat flux oscillation only		0.45	0.225
				In-phase G & q oscillations		0.63	0.225
				Out-of-phase G & q oscillations		0.40	0.325
			4.12	Heat flux oscillation only		0.48	0.2
				In-phase G & q oscillations		0.68	0.175
				Out-of-phase G & q oscillations		0.42	0.375
			6.13	Heat flux oscillation only		0.55	0.2
				In-phase G & q oscillations		0.69	0.175
				Out-of-phase G & q oscillations		0.55	0.375

Table 4.6 Amplitudes of T_w oscillation and relative time lags in transient oscillatory saturated flow

boiling for various \bar{q} at $\Delta q/\bar{q} = 10,30,50\%$, $\Delta G/\bar{G} = 5\%$ and $t_p = 30\text{sec}$. for $\bar{G} = 300\text{kg/m}^2\text{s}$.

$\Delta G/\bar{G}$	Period $t_p(\text{sec})$	$\Delta q/\bar{q}$	$\bar{G} = 300\text{kg/m}^2\text{s}$				
			$\bar{q}(\text{W/cm}^2)$		$\Delta T_w(K)$	t_1/t_p	
5%	30	10%	1.04 (single-phase)	Heat flux oscillation only		0.16	0.233
				In-phase G & q oscillations		0.12	0.433
				Out-of-phase G & q oscillations		0.19	0.283
			2.35	Heat flux oscillation only		0.19	0.217
				In-phase G & q oscillations		0.21	0.2
				Out-of-phase G & q oscillations		0.16	0.233
			4.07	Heat flux oscillation only		0.21	0.217
				In-phase G & q oscillations		0.27	0.183
				Out-of-phase G & q oscillations		0.18	0.267
		6.04	Heat flux oscillation only		0.25	0.2	
			In-phase G & q oscillations		0.32	0.167	
			Out-of-phase G & q oscillations		0.22	0.233	
		30%	1.02 (single-phase)	Heat flux oscillation only		0.41	0.3
				In-phase G & q oscillations		0.37	0.367
				Out-of-phase G & q oscillations		0.45	0.317
			2.34	Heat flux oscillation only		0.53	0.233
				In-phase G & q oscillations		0.52	0.25
				Out-of-phase G & q oscillations		0.46	0.233
			4.98	Heat flux oscillation only		0.64	0.217
				In-phase G & q oscillations		0.67	0.217
				Out-of-phase G & q oscillations		0.59	0.217
		6.01	Heat flux oscillation only		0.69	0.2	
			In-phase G & q oscillations		0.73	0.183	
			Out-of-phase G & q oscillations		0.67	0.233	
		50%	1.01 (single-phase)	Heat flux oscillation only		0.68	0.35
				In-phase G & q oscillations		0.69	0.35
				Out-of-phase G & q oscillations		0.69	0.333
			1.6	Heat flux oscillation only		0.93	0.25
				In-phase G & q oscillations		0.91	0.3
				Out-of-phase G & q oscillations		0.88	0.283
			4.06	Heat flux oscillation only		0.99	0.233
				In-phase G & q oscillations		1.02	0.2
				Out-of-phase G & q oscillations		0.88	0.183
		6.01	Heat flux oscillation only		1.25	0.2	
			In-phase G & q oscillations		1.29	0.183	
			Out-of-phase G & q oscillations		1.20	0.183	

Table 4.7 Amplitudes of T_w oscillation and relative time lags in transient oscillatory saturated flow boiling for various \bar{q} at $\Delta q/\bar{q} = 10, 20\%$, $\Delta G/\bar{G} = 15\%$ and $t_p = 20$ sec. for $\bar{G} = 300 \text{ kg/m}^2\text{s}$.

$\Delta G/\bar{G}$	Period t_p (sec)	$\Delta q/\bar{q}$	$\bar{G} = 300 \text{ kg/m}^2\text{s}$			
			\bar{q} (W/cm^2)		ΔT_w (K)	t_l/t_p
15%	20	10%	1.09 (single-phase)	Heat flux oscillation only	0.11	0.375
				Mass flux oscillation only	0.11	0.175
				In-phase G & q oscillations	0.04	x
		20%	4.13	Heat flux oscillation only	0.15	0.3
				Mass flux oscillation only	0.14	0.075
				Out-of-phase G & q oscillations	0.06	x
		20%	4.13	Heat flux oscillation only	0.29	0.225
				Mass flux oscillation only	0.30	0.025
				Out-of-phase G & q oscillations	0.08	x

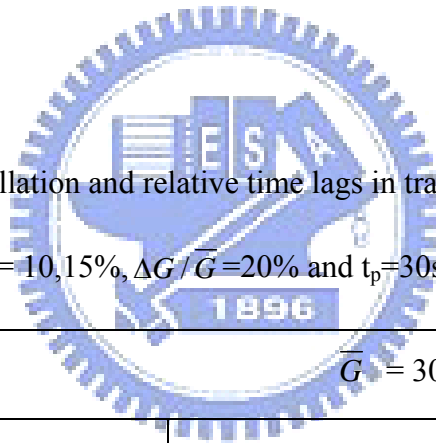


Table 4.8 Amplitudes of T_w oscillation and relative time lags in transient oscillatory saturated flow boiling for various \bar{q} at $\Delta q/\bar{q} = 10, 15\%$, $\Delta G/\bar{G} = 20\%$ and $t_p = 30$ sec. for $\bar{G} = 300 \text{ kg/m}^2\text{s}$.

$\Delta G/\bar{G}$	Period t_p (sec)	$\Delta q/\bar{q}$	$\bar{G} = 300 \text{ kg/m}^2\text{s}$			
			\bar{q} (W/cm^2)		ΔT_w (K)	t_l/t_p
20%	30	10%	1.03 (single-phase)	Heat flux oscillation only	0.18	0.250
				Mass flux oscillation only	0.18	0.130
				In-phase G & q oscillations	0.05	x
		15%	8.08	Heat flux oscillation only	0.43	0.183
				Mass flux oscillation only	0.42	0.017
				Out-of-phase G & q oscillations	0.14	x

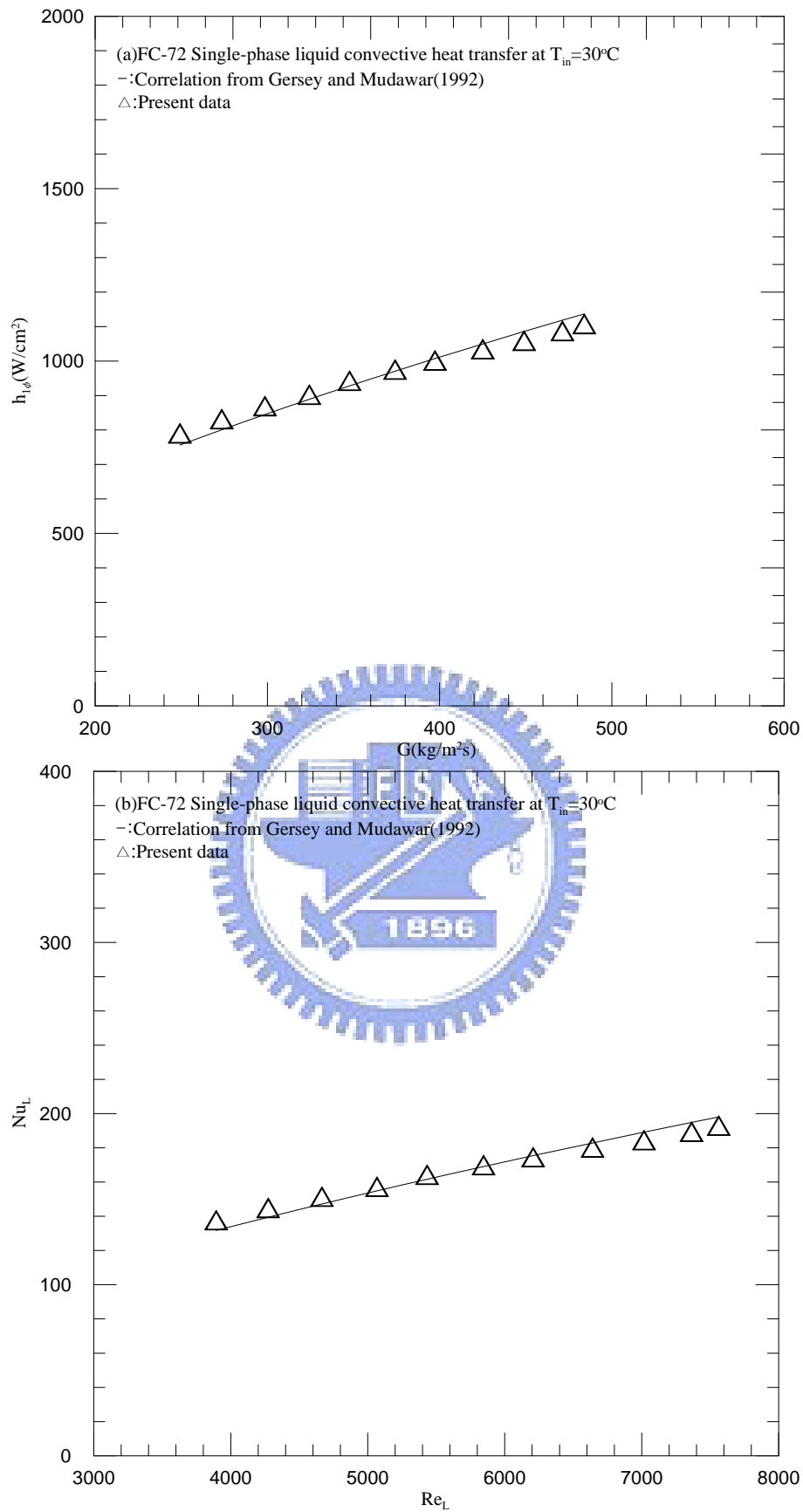


Fig. 4.1 Comparison of the present steady single-phase liquid convection heat transfer data with the correlation of Gersey and Mudawar (1992) for (a) $h_{1\phi}$ vs. G and (b) Nu_L vs. Re_L .

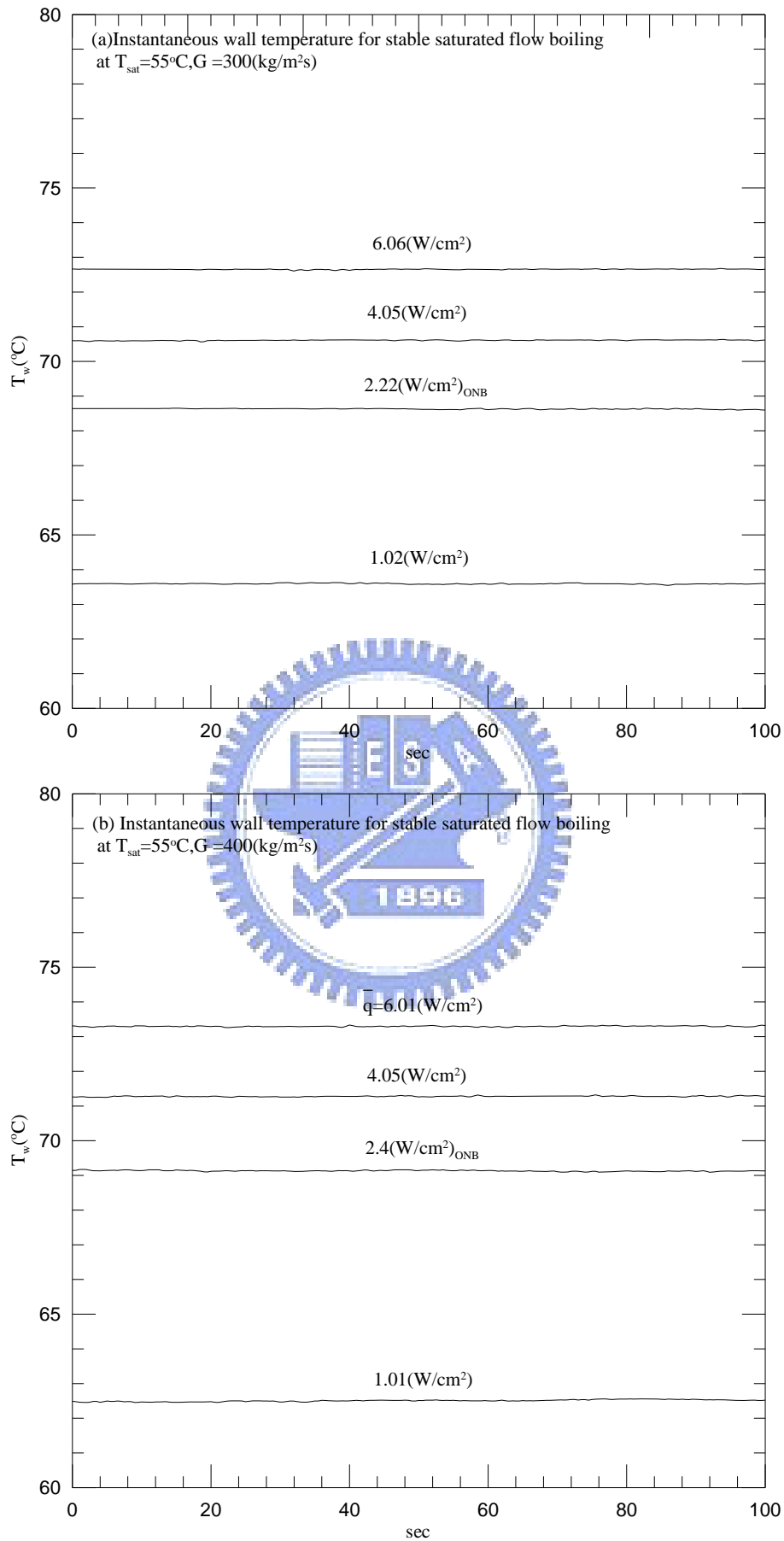


Fig. 4.2 Time variations of the copper plate temperature in stable saturated flow boiling for various imposed heat fluxes at (a) $G=300\text{kg}/\text{m}^2\text{s}$ and (b) $G=400\text{kg}/\text{m}^2\text{s}$

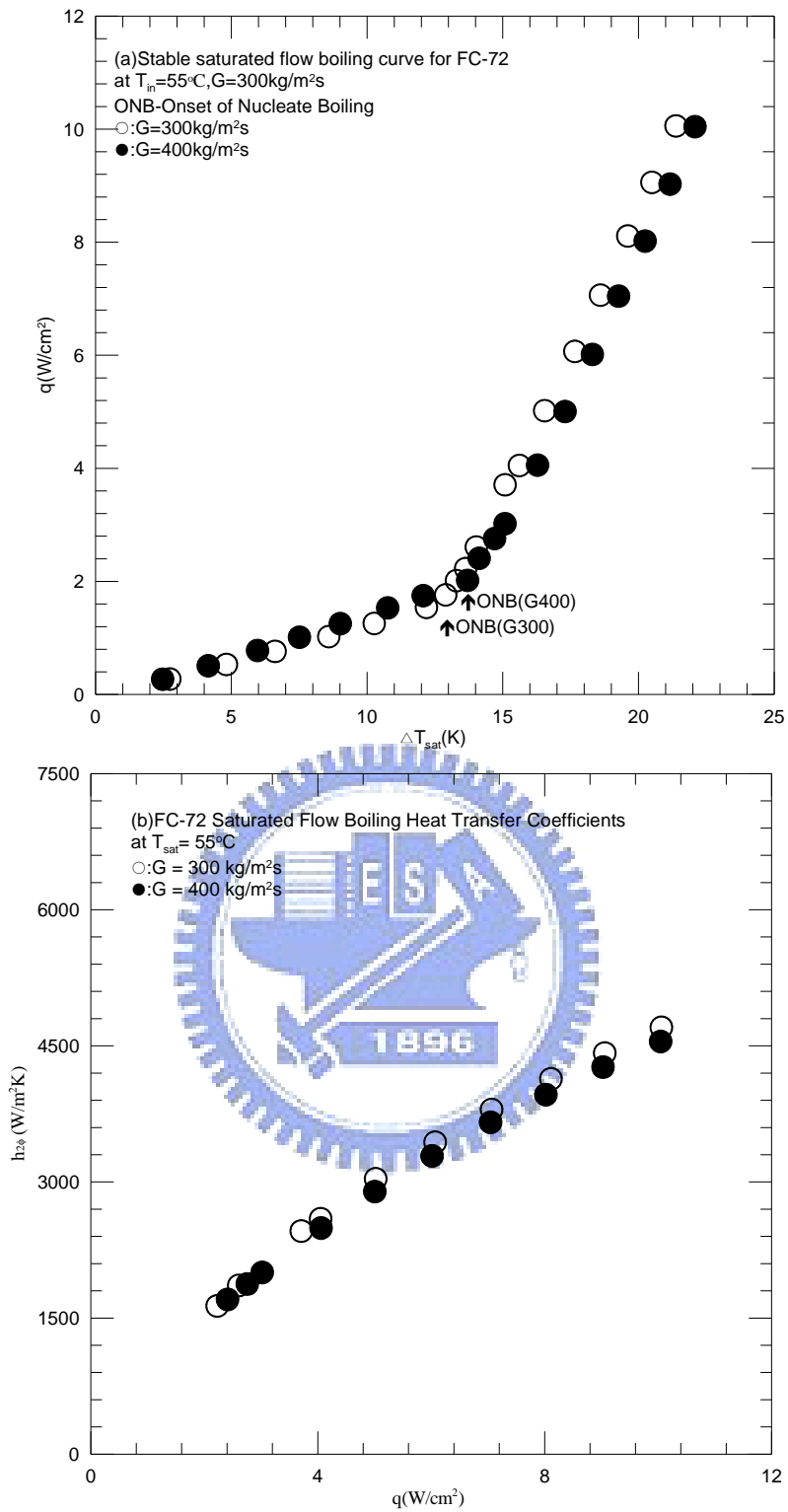


Fig. 4.3 (a) Stable saturated flow boiling curve and (b) stable saturated flow boiling heat transfer coefficients.

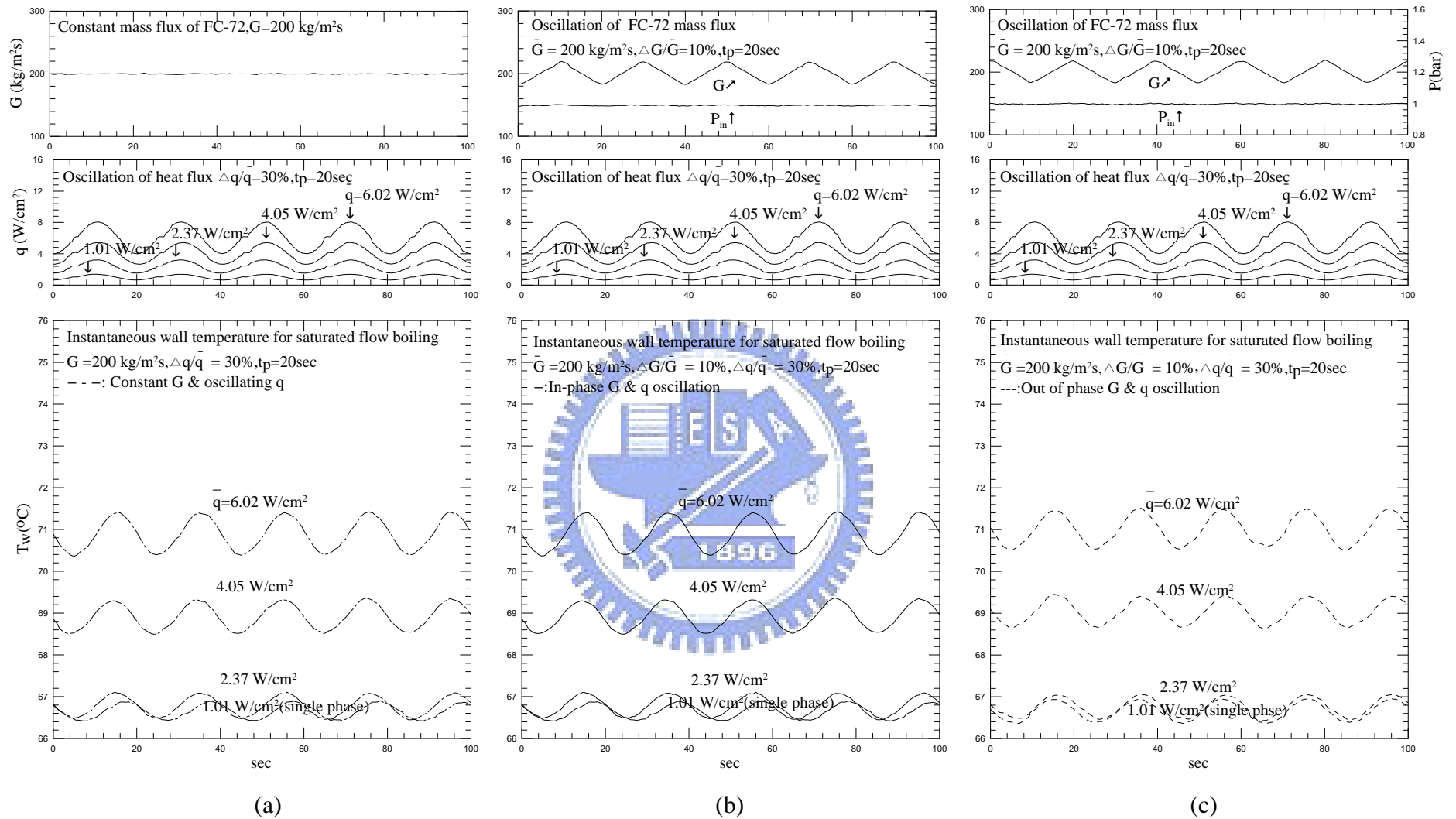


Fig.4.4 Time variations of the measured instantaneous heated surface temperature for (a) imposed heat flux oscillation only, (b) in-phase G and q oscillations and (c) out-of-phase G and q oscillations at $\bar{G} = 200$ kg/m²s and $\Delta G/\bar{G} = 10\%$ for $\Delta q/\bar{q} = 30\%$ and $t_p = 20$ sec.

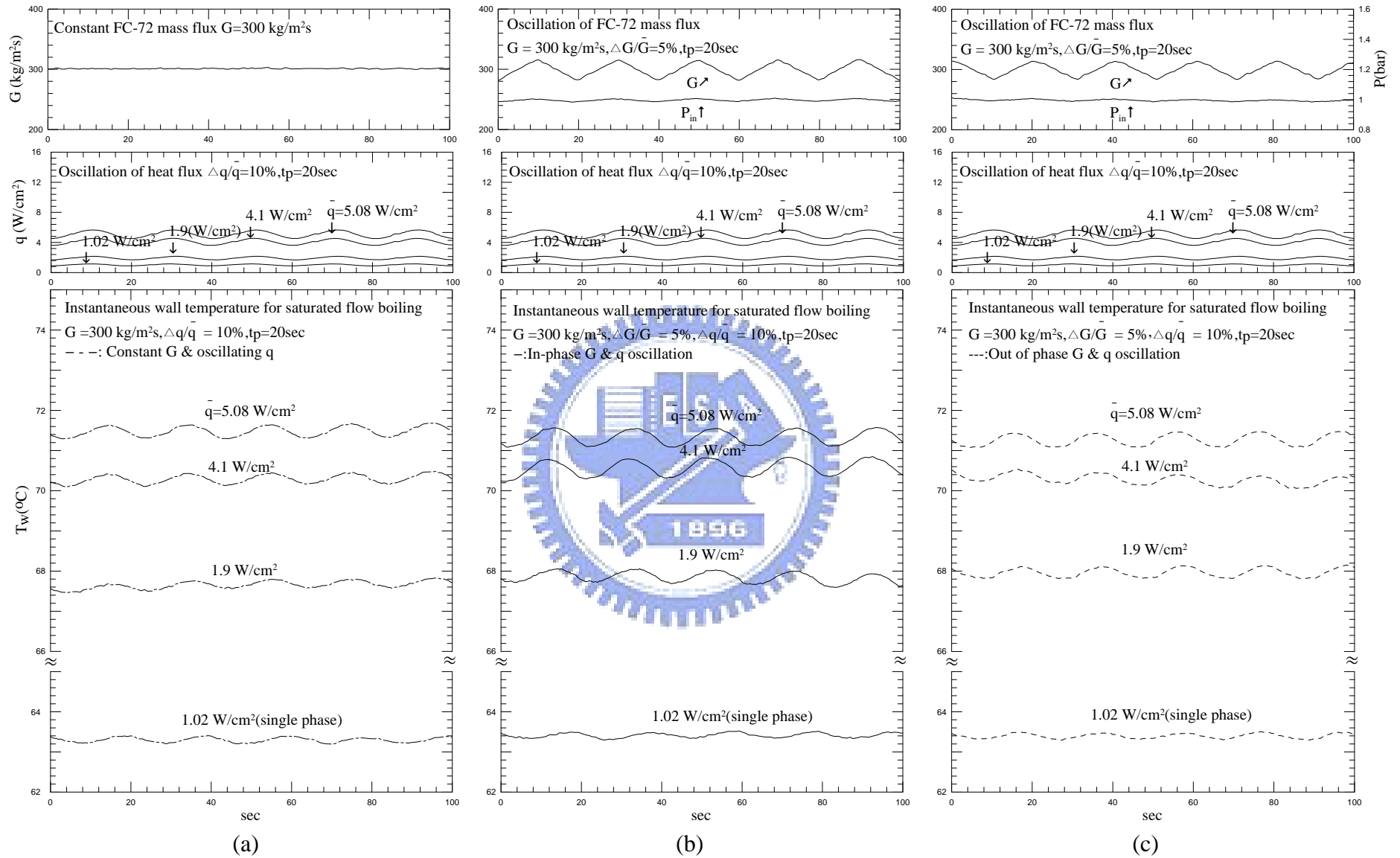


Fig.4.5 Time variations of the measured instantaneous heated surface temperature for (a) imposed heat flux oscillation only, (b) in-phase G and q oscillations and (c) out-of-phase G and q oscillations at $\bar{G} = 300 \text{ kg/m}^2\text{s}$ and $\Delta G/\bar{G} = 5\%$ for $\Delta q/\bar{q} = 10\%$ and $t_p = 20 \text{ sec}$.

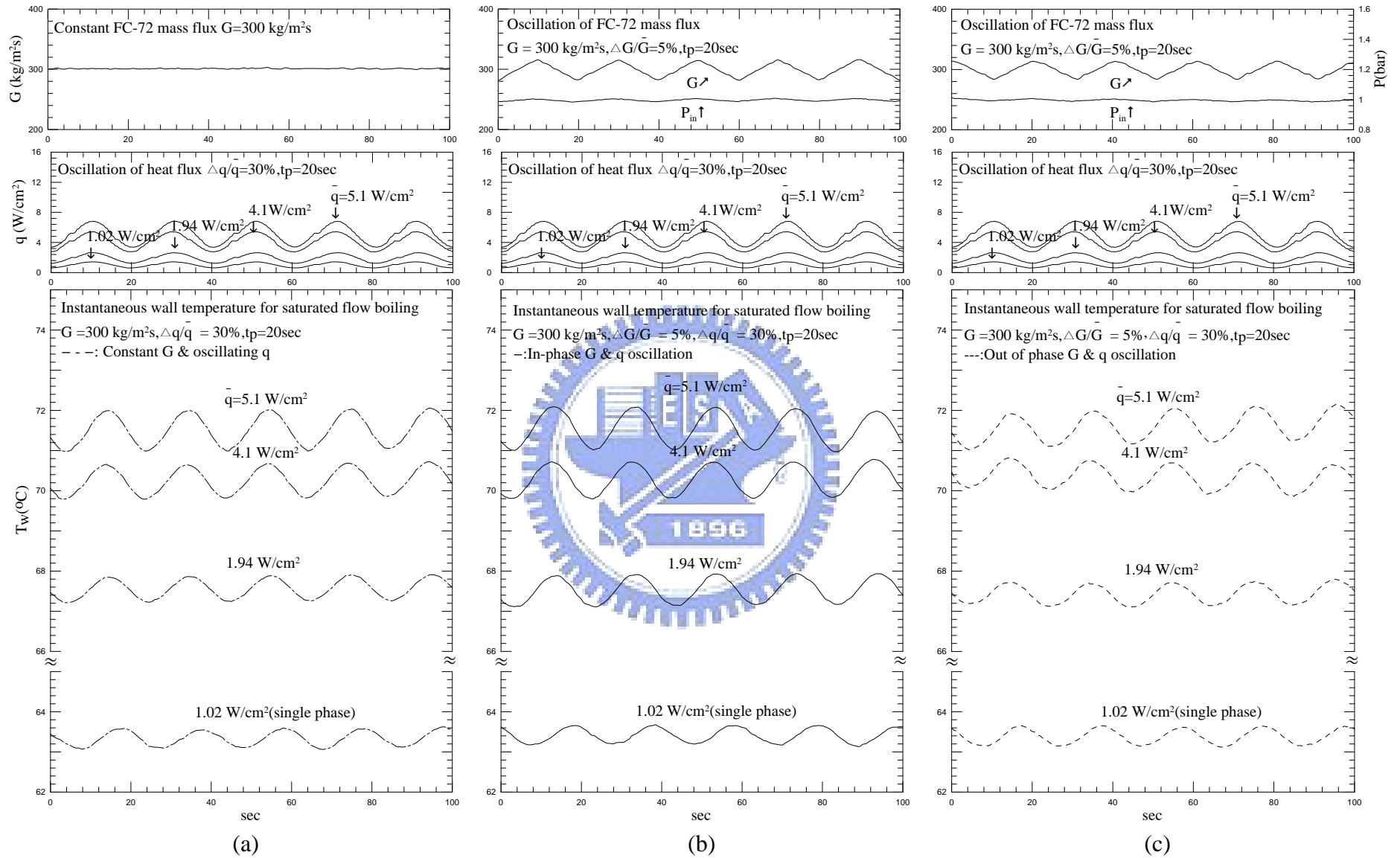


Fig.4.6 Time variations of the measured instantaneous heated surface temperature for (a) imposed heat flux oscillation only, (b) in-phase G and q oscillations and (c) out-of-phase G and q oscillations at $\bar{G} = 300 \text{ kg/m}^2\text{s}$ and $\Delta G/\bar{G} = 5\%$ for $\Delta q/\bar{q} = 30\%$ and $t_p = 20 \text{ sec}$.

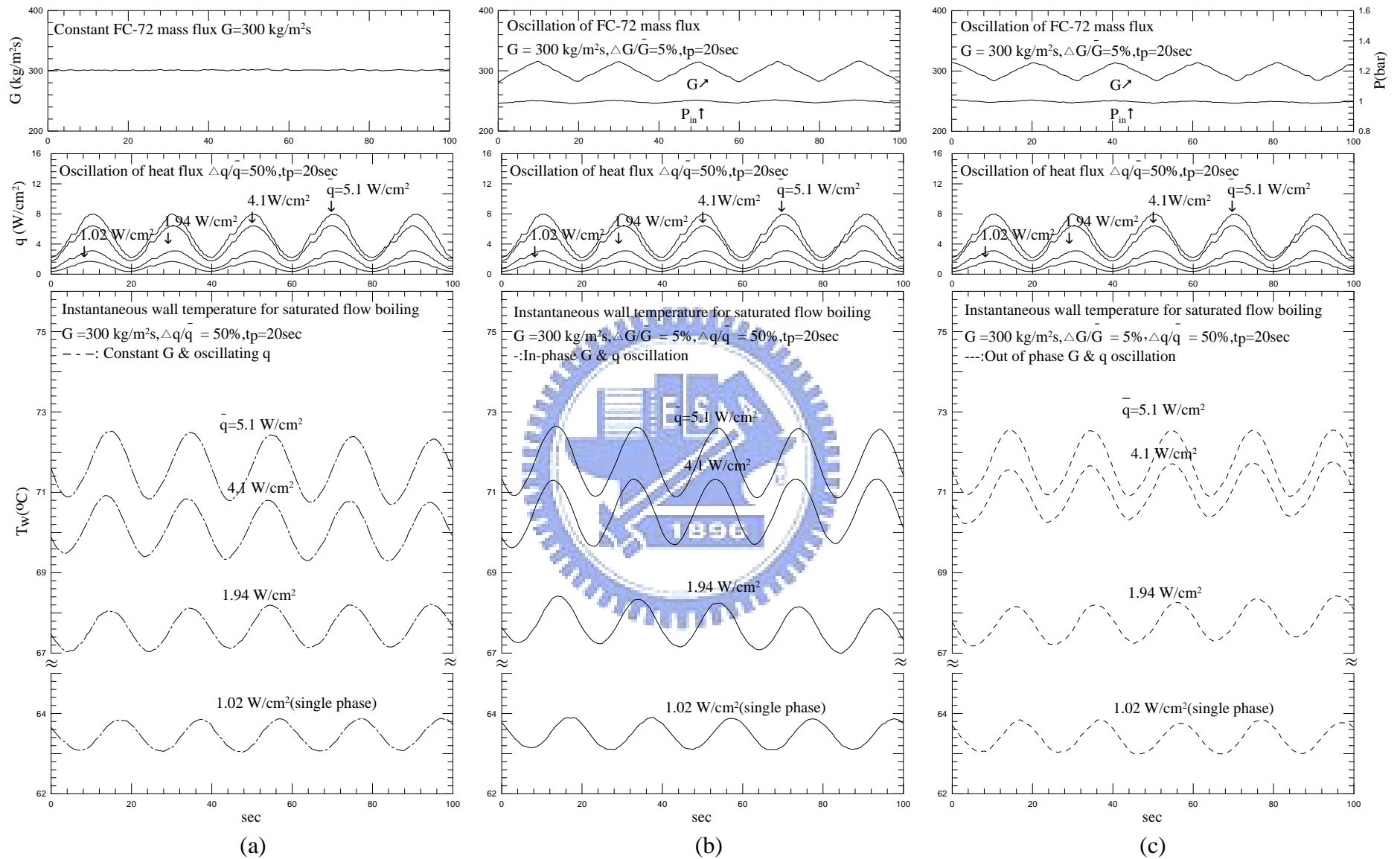


Fig.4.7 Time variations of the measured instantaneous heated surface temperature for (a) imposed heat flux oscillation only, (b) in-phase G and q oscillations and (c) out-of-phase G and q oscillations at $\bar{G} = 300 \text{ kg/m}^2\text{s}$ and $\Delta G/\bar{G} = 5\%$ for $\Delta q/\bar{q} = 50\%$ and $t_p = 20 \text{ sec}$.

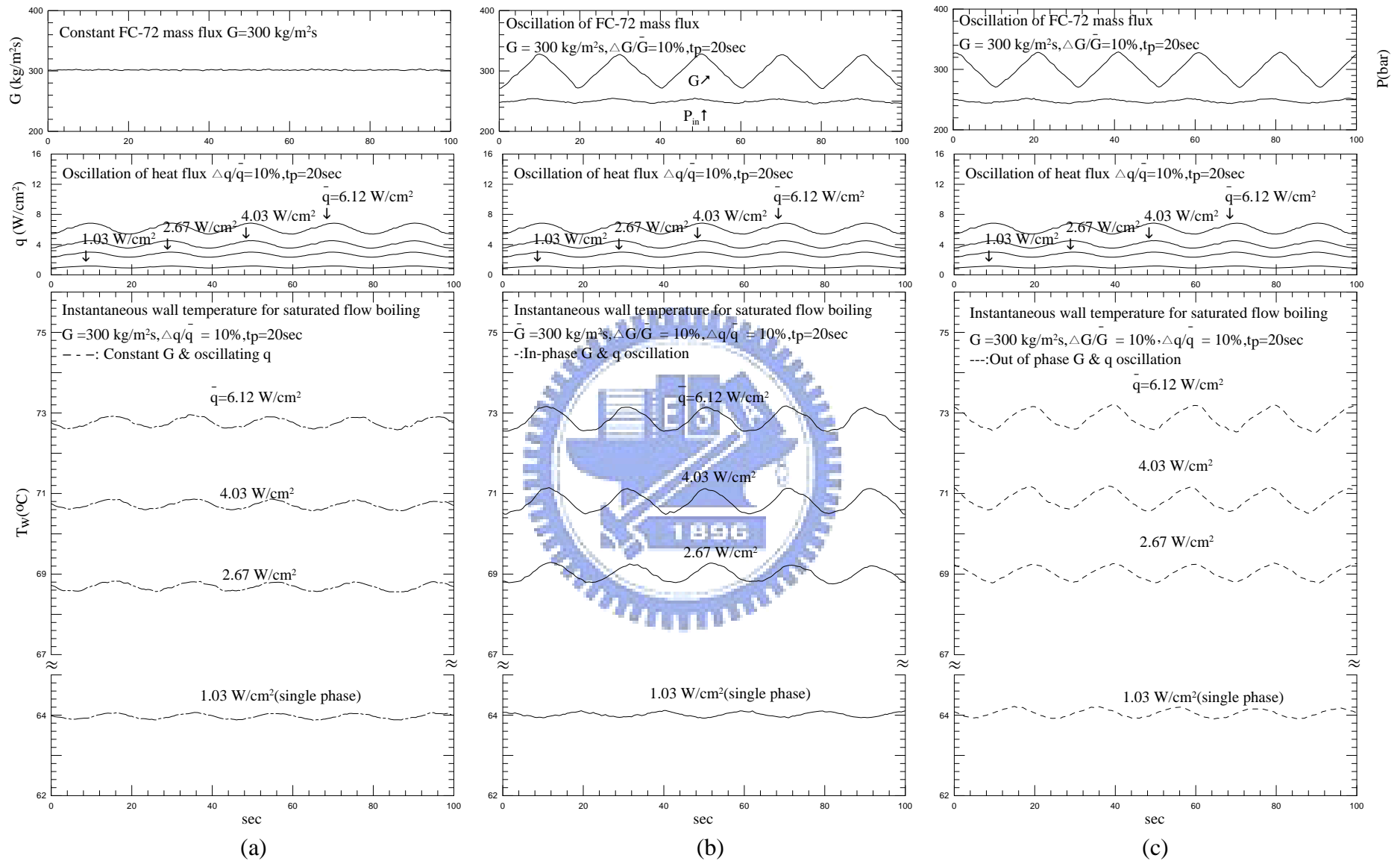


Fig.4.8 Time variations of the measured instantaneous heated surface temperature for (a) imposed heat flux oscillation only, (b) in-phase G and q oscillations and (c) out-of-phase G and q oscillations at $\bar{G} = 300 \text{ kg/m}^2 \text{ s}$ and $\Delta G/\bar{G} = 10\%$ for $\Delta q/\bar{q} = 10\%$ and $t_p = 20 \text{ sec}$.

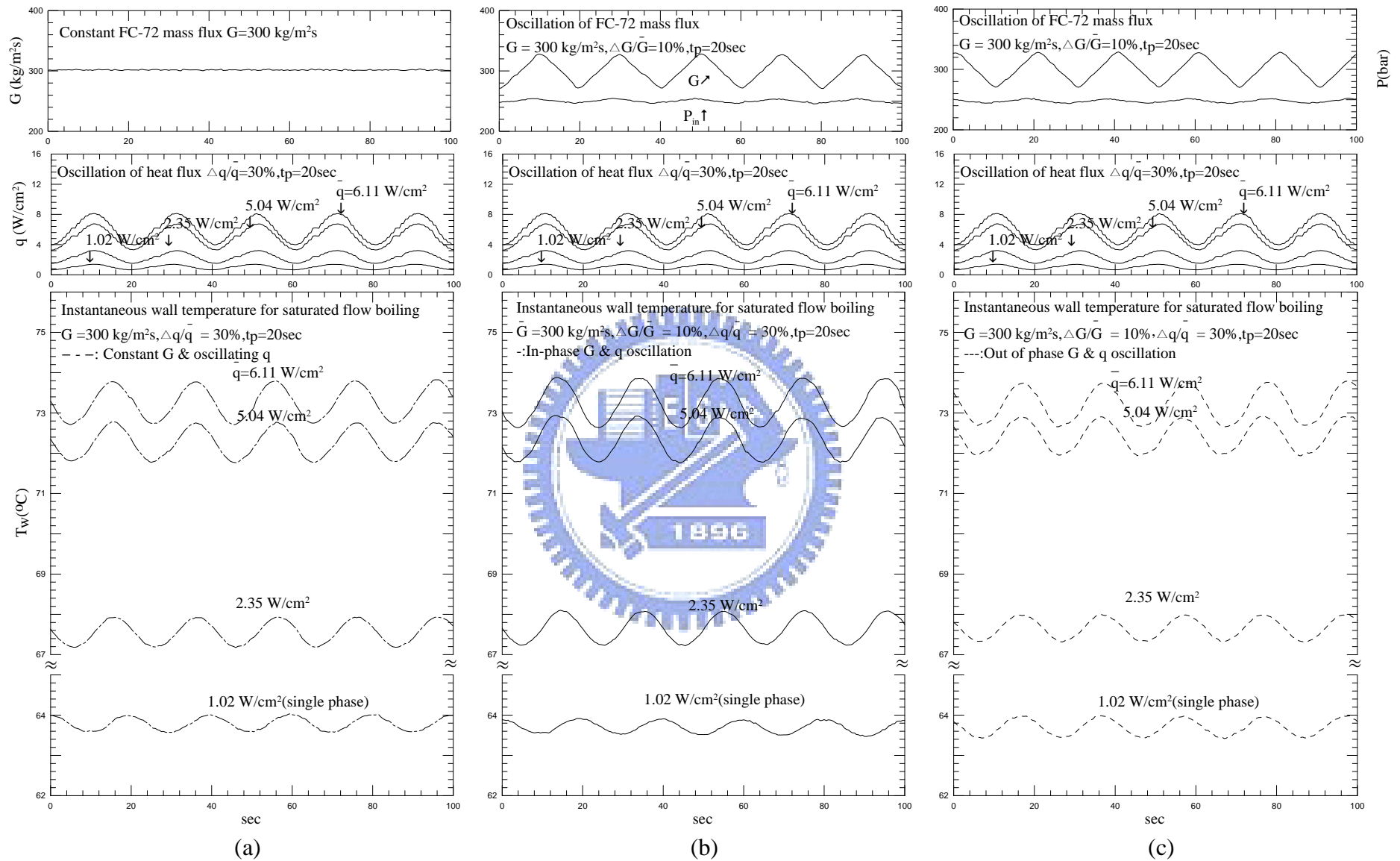


Fig.4.9 Time variations of the measured instantaneous heated surface temperature for (a) imposed heat flux oscillation only, (b) in-phase G and q oscillations and (c) out-of-phase G and q oscillations at $\bar{G} = 300 \text{ kg/m}^2 \text{ s}$ and $\Delta G/\bar{G} = 10\%$ for $\Delta q/\bar{q} = 30\%$ and $t_p = 20 \text{ sec}$.

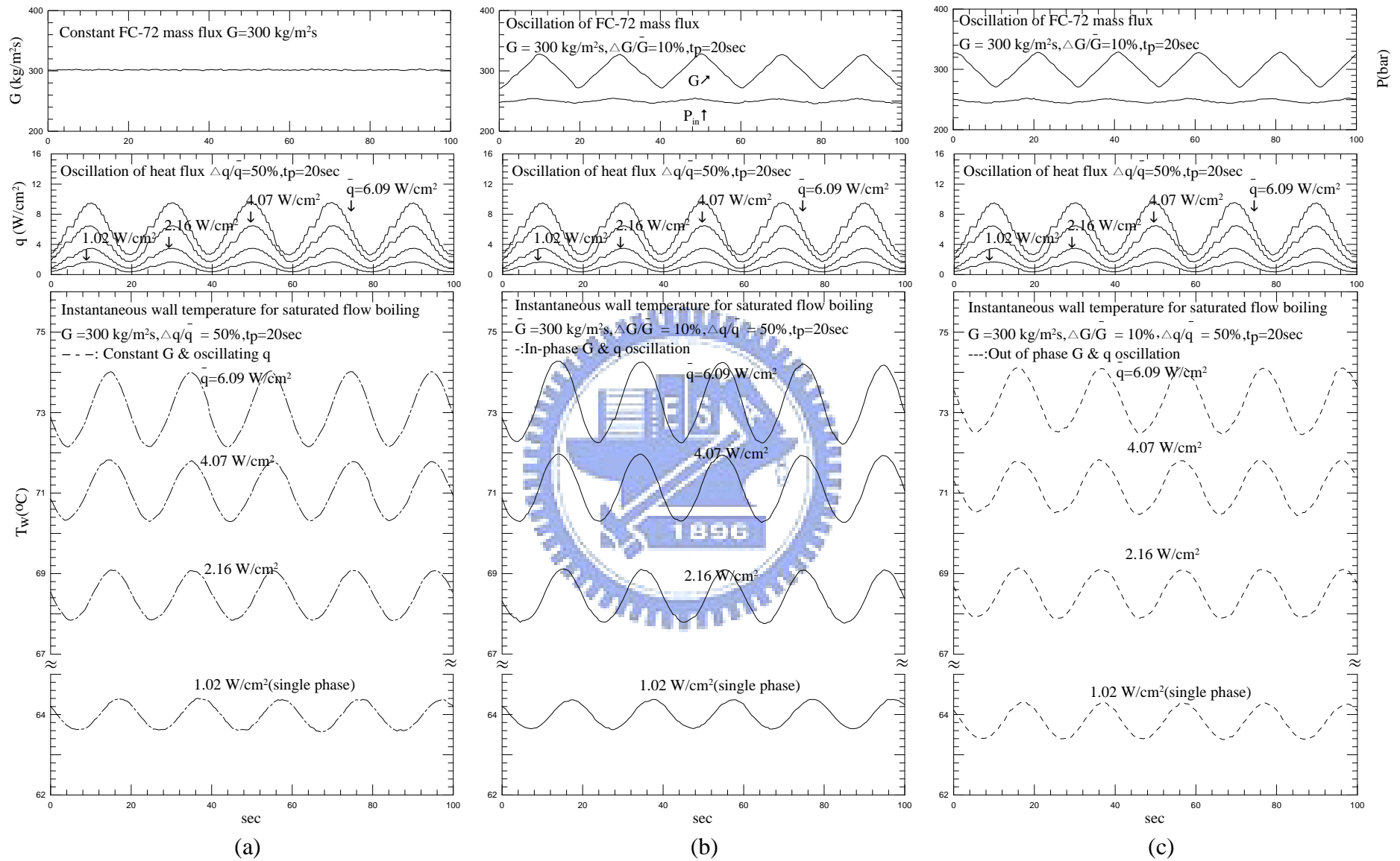


Fig.4.10 Time variations of the measured instantaneous heated surface temperature for (a) imposed heat flux oscillation only, (b) in-phase G and q oscillations and (c) out-of-phase G and q oscillations at $\bar{G} = 300 \text{ kg/m}^2\text{s}$ and $\Delta G/\bar{G} = 10\%$ for $\Delta q/\bar{q} = 50\%$ and $t_p = 20 \text{ sec}$.

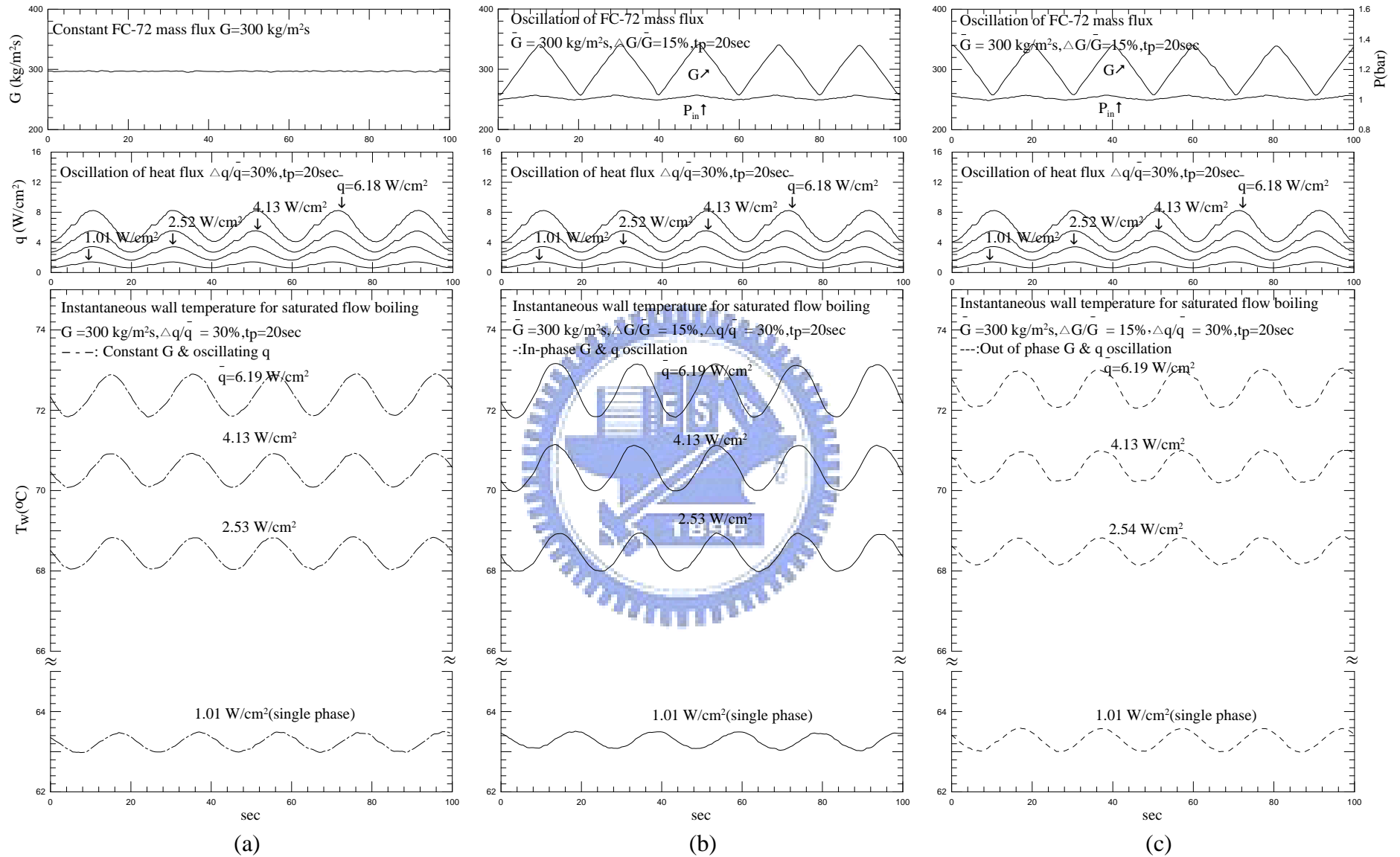


Fig.4.11 Time variations of the measured instantaneous heated surface temperature for (a) imposed heat flux oscillation only, (b) in-phase G and q oscillations and (c) out-of-phase G and q oscillations at $\bar{G} = 300 \text{ kg/m}^2\text{s}$ and $\Delta G/\bar{G} = 15\%$ for $\Delta q/\bar{q} = 30\%$ and $t_p = 20 \text{ sec}$.

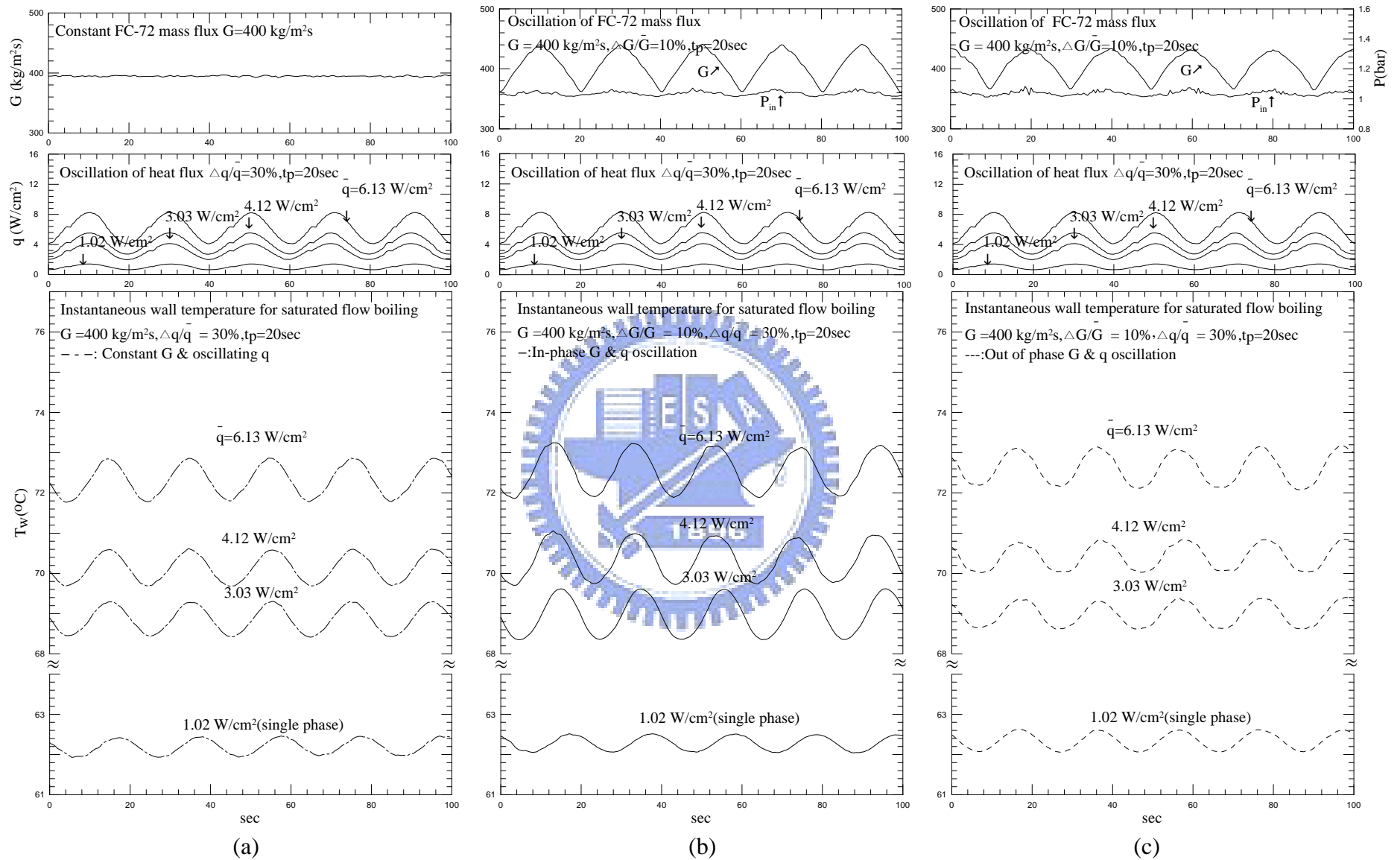


Fig.4.12 Time variations of the measured instantaneous heated surface temperature for (a) imposed heat flux oscillation only, (b) in-phase G and q oscillations and (c) out-of-phase G and q oscillations at $\bar{G} = 400 \text{ kg/m}^2 \text{ s}$ and $\Delta G/\bar{G} = 10\%$ for $\Delta q/\bar{q} = 30\%$ and $t_p = 20 \text{ sec}$.

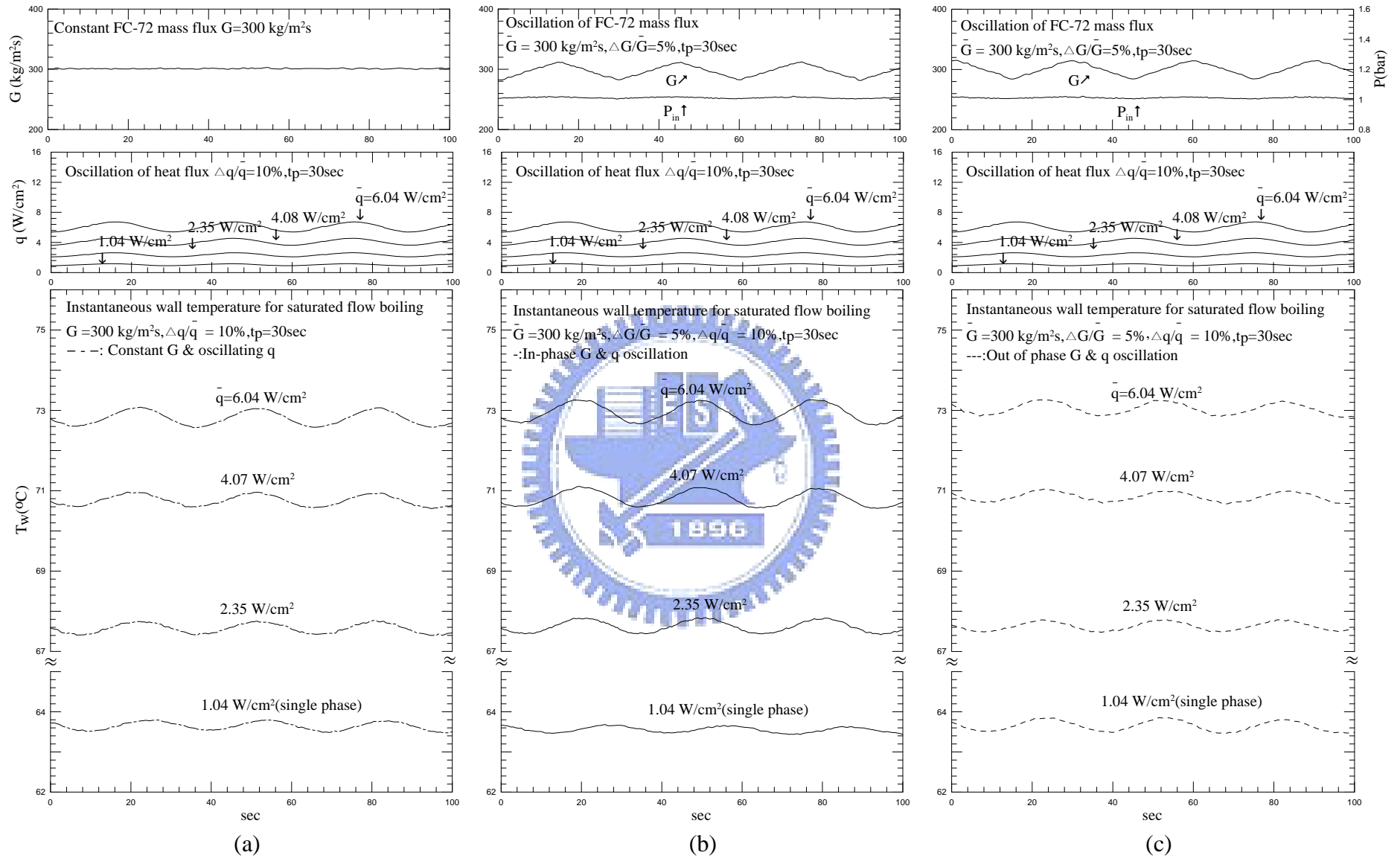


Fig.4.13 Time variations of the measured instantaneous heated surface temperature for (a) imposed heat flux oscillation only, (b) in-phase G and q oscillations and (c) out-of-phase G and q oscillations at $\bar{G} = 300 \text{ kg/m}^2 \text{ s}$ and $\Delta G/\bar{G} = 5\%$ for $\Delta q/\bar{q} = 10\%$ and $t_p = 30 \text{ sec}$.

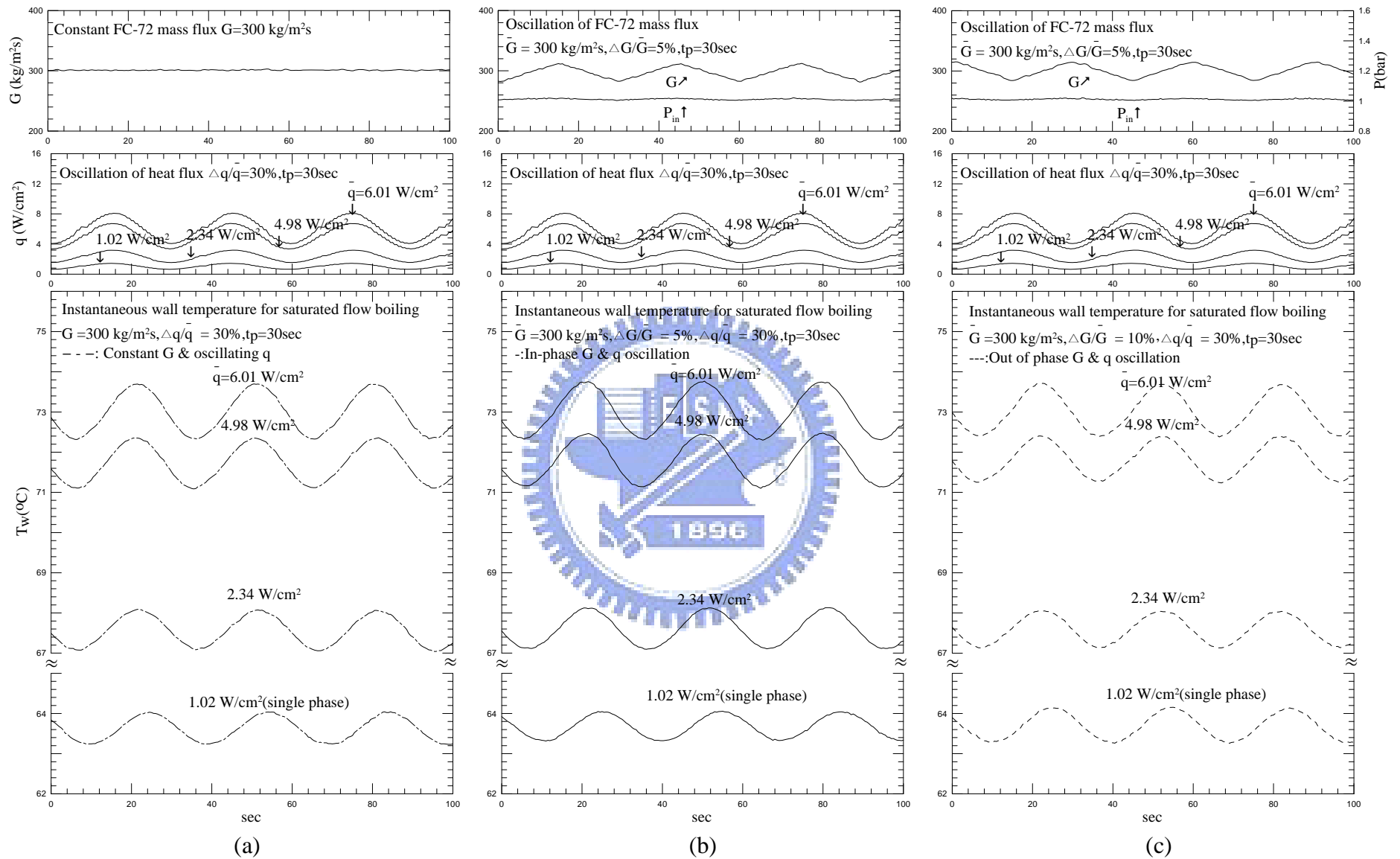


Fig.4.14 Time variations of the measured instantaneous heated surface temperature for (a) imposed heat flux oscillation only, (b) in-phase G and q oscillations and (c) out-of-phase G and q oscillations at $\bar{G} = 300$ kg/m²s and $\Delta G/\bar{G} = 5\%$ for $\Delta q/\bar{q} = 30\%$ and $t_p = 30$ sec.

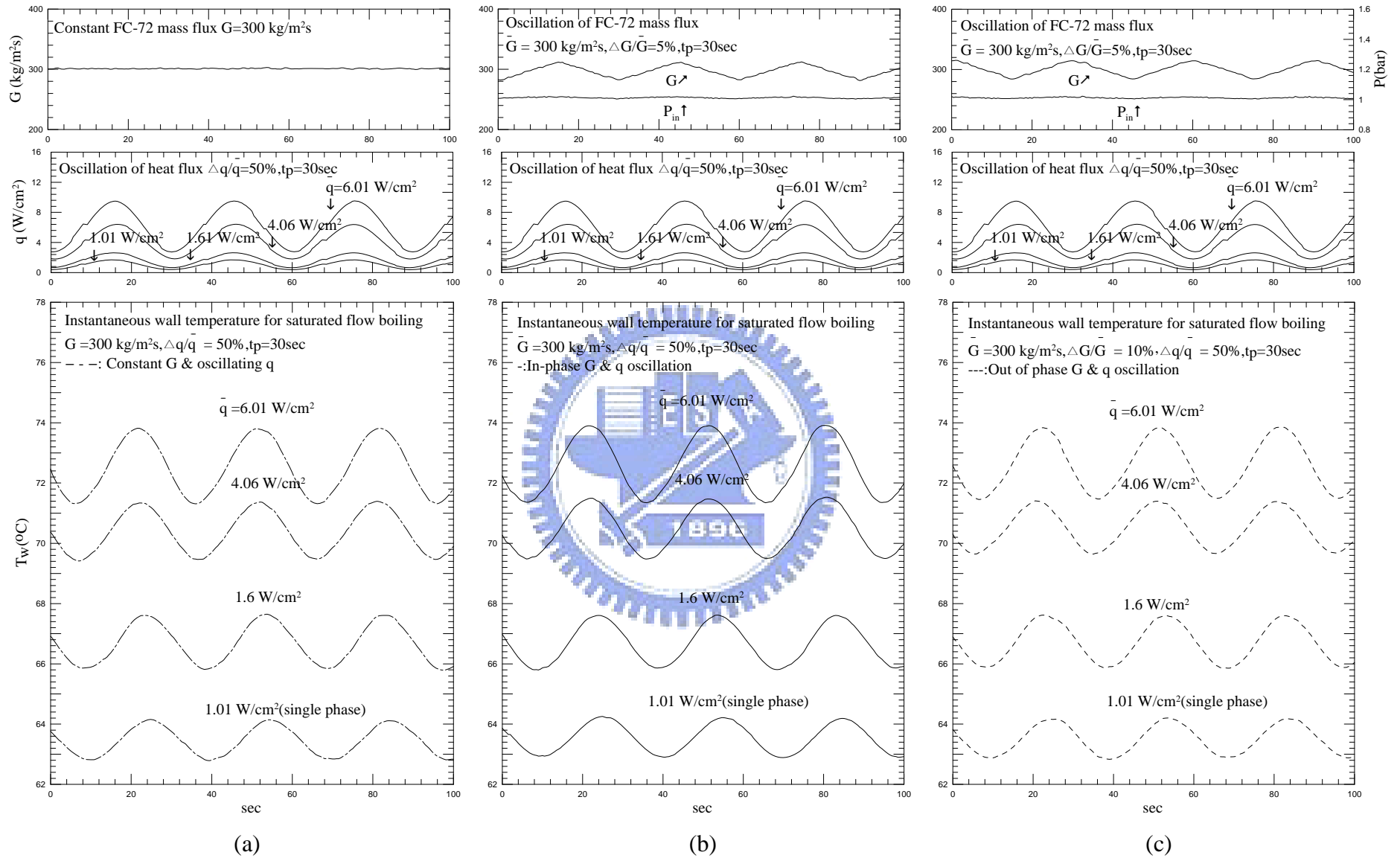


Fig.4.15 Time variations of the measured instantaneous heated surface temperature for (a) imposed heat flux oscillation only, (b) in-phase G and q oscillations and (c) out-of-phase G and q oscillations at $\bar{G} = 300 \text{ kg/m}^2\text{s}$ and $\Delta G/\bar{G} = 5\%$ for $\Delta q/\bar{q} = 50\%$ and $t_p = 30 \text{ sec}$.

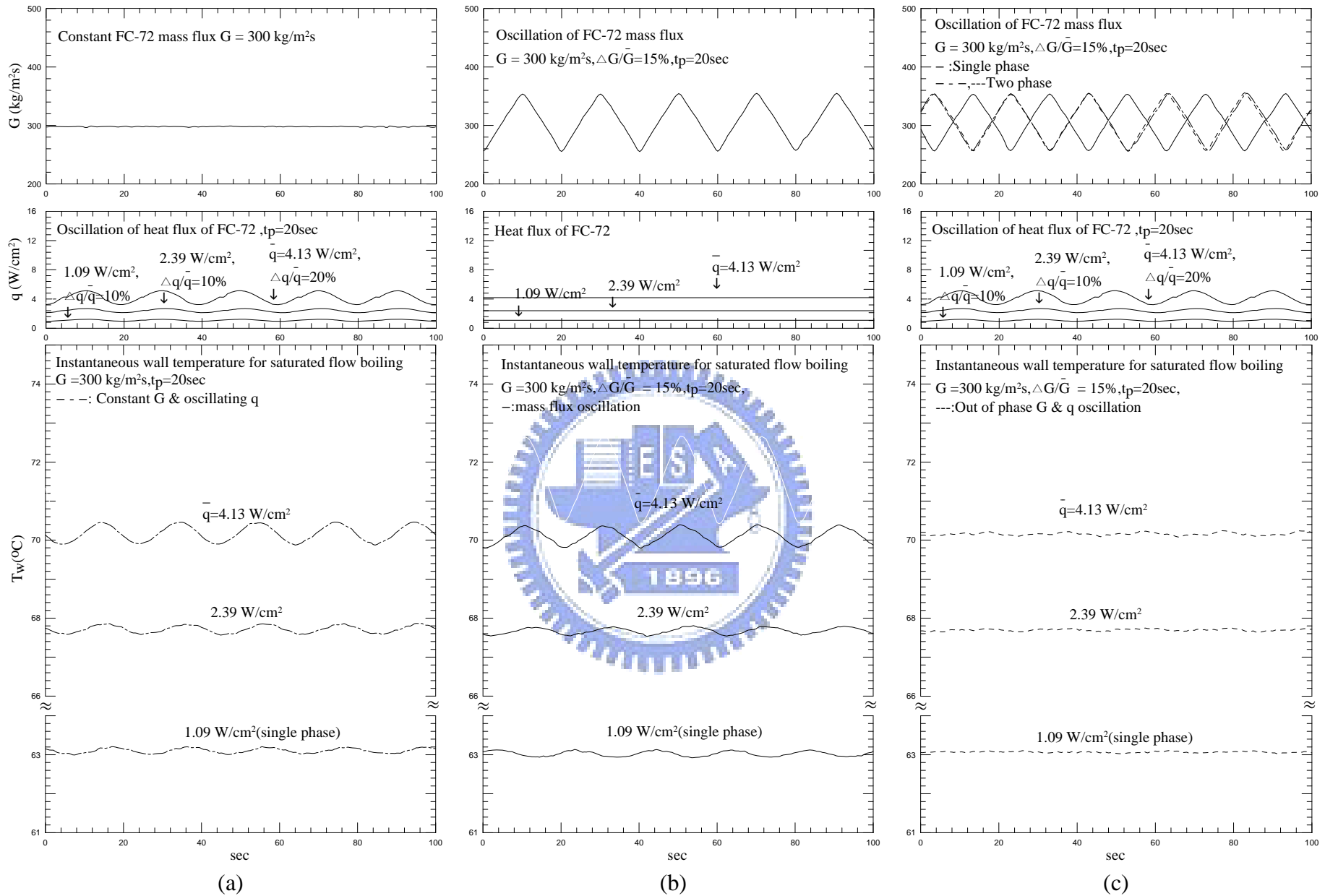


Fig.4.16 Time variations of the measured instantaneous heated surface temperature for (a) imposed heat flux oscillation only, (b) imposed mass flux oscillation only, and (c) in-phase or out-of-phase G and q oscillations at $\bar{G} = 300 \text{ kg/m}^2\text{s}$ and $\Delta G/\bar{G} = 15\%$ for various \bar{q} at $t_p = 20 \text{ sec}$.

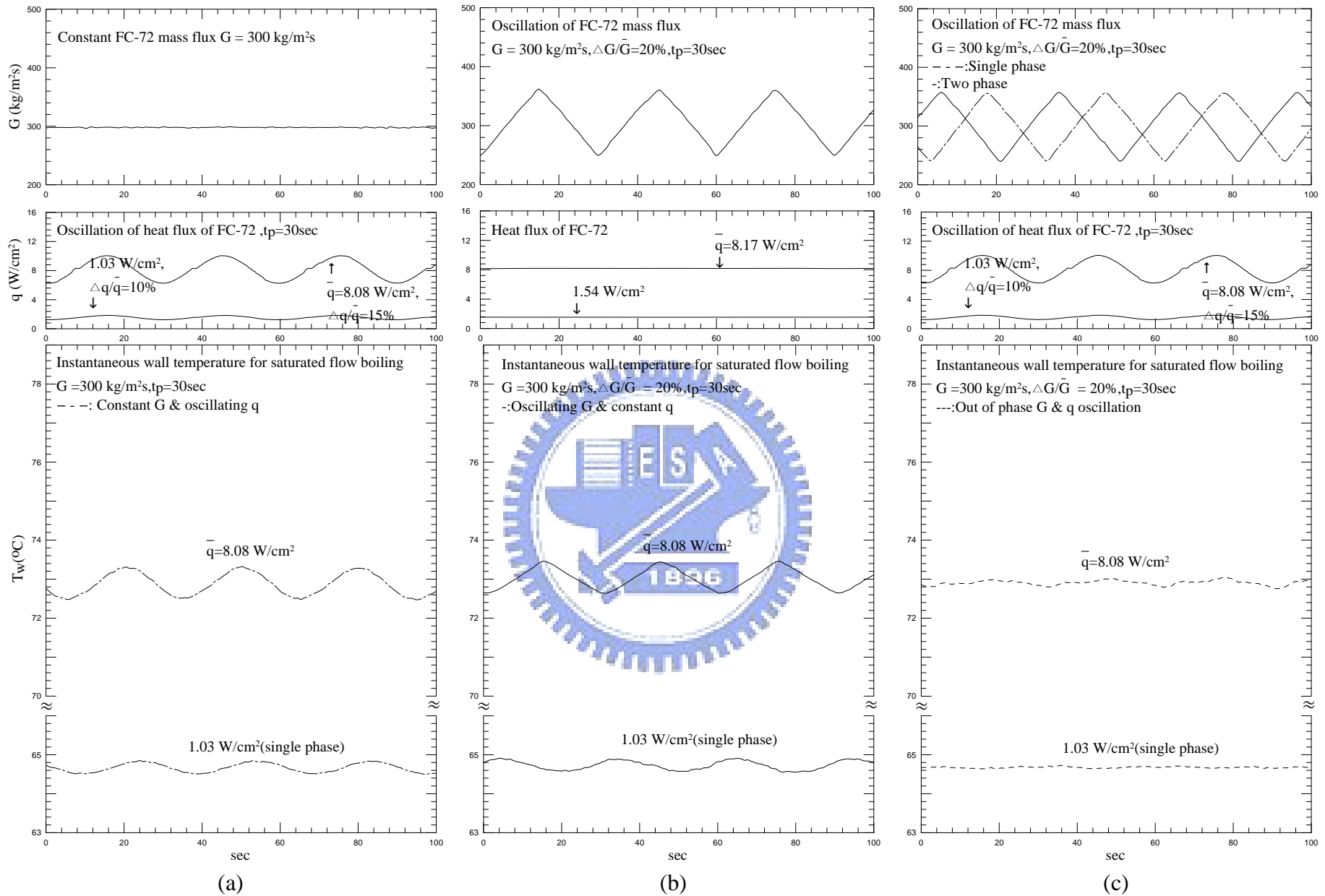


Fig.4.17 Time variations of the measured instantaneous heated surface temperature for (a) imposed heat flux oscillation only, (b) imposed mass flux oscillation only, and (c) in-phase or out-of-phase G and q oscillations at $\bar{G} = 300 \text{ kg/m}^2\text{s}$ and $\Delta G/\bar{G} = 20\%$ for various \bar{q} at $t_p = 30 \text{ sec}$.

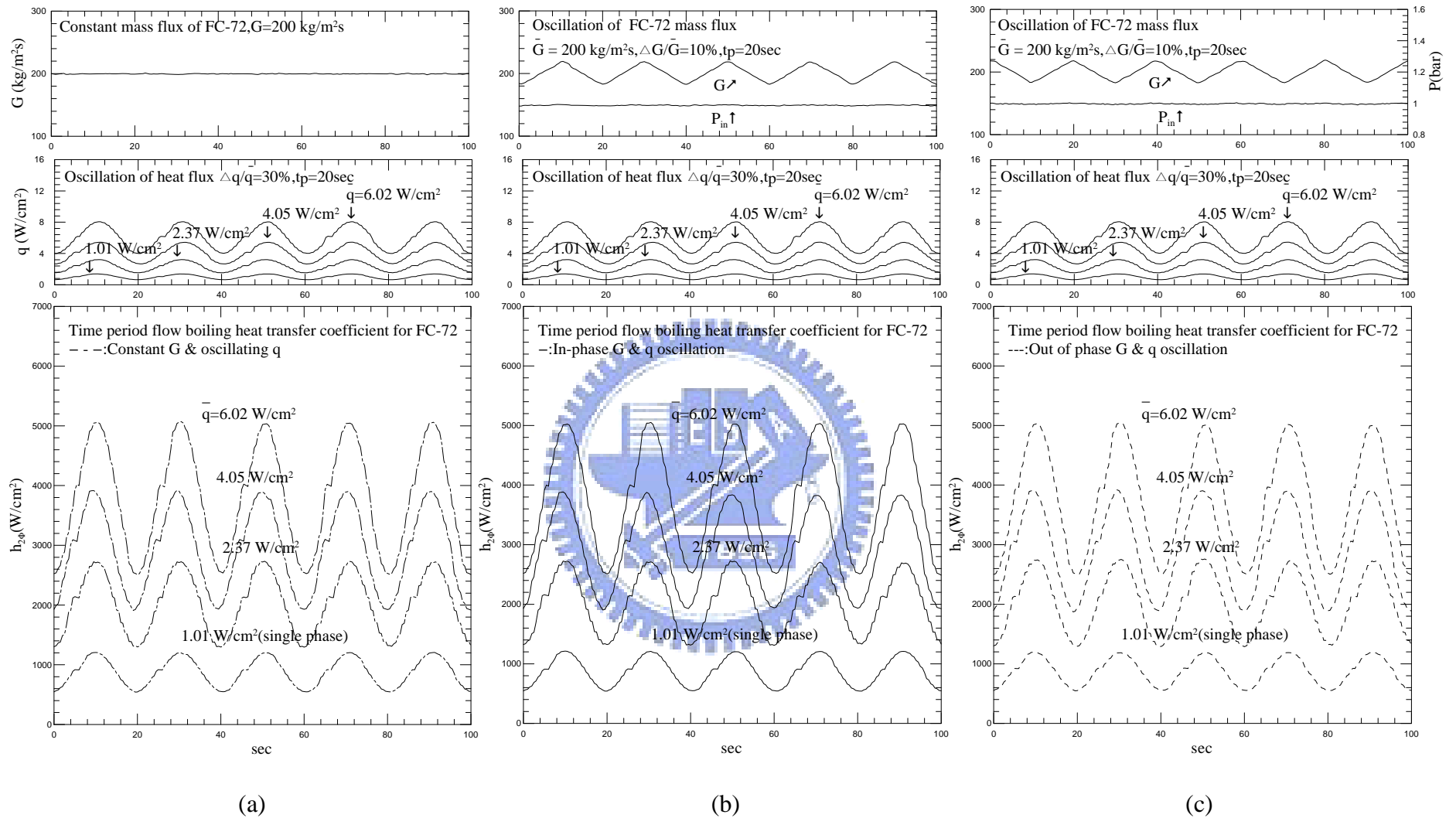


Fig. 4.18 Time variations of the heat transfer coefficient for (a) imposed heat flux oscillation only, (b) in-phase G and q oscillations and (c) out-of-phase G and q oscillations at $\bar{G} = 200 \text{ kg/m}^2 \text{ s}$ and $\Delta G/\bar{G} = 10\%$ for $\Delta q/\bar{q} = 30\%$ and $t_p = 20 \text{ sec}$.

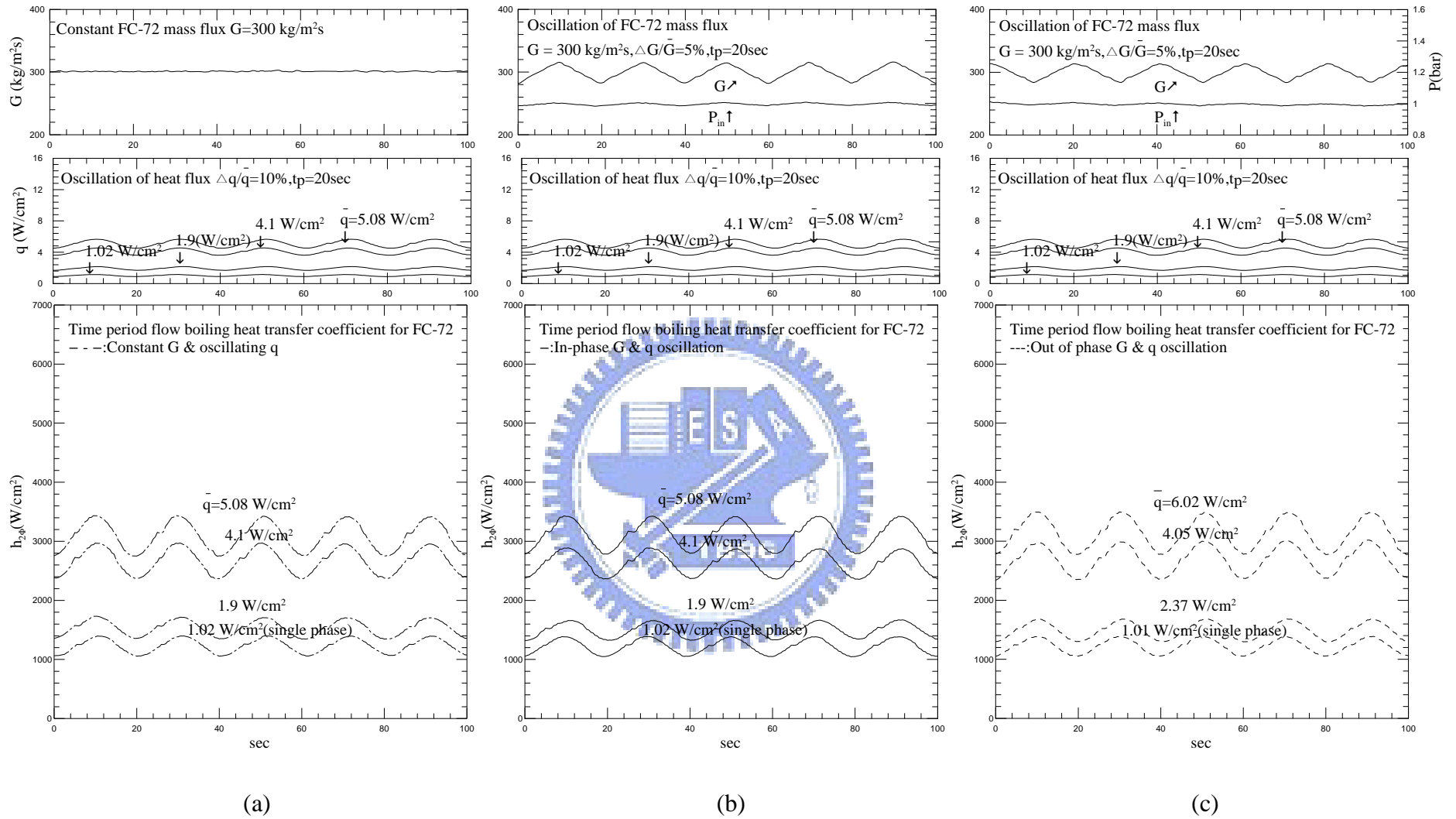


Fig. 4.19 Time variations of the heat transfer coefficient for (a) imposed heat flux oscillation only, (b) in-phase G and q oscillations and (c) out-of-phase G and q oscillations at $\bar{G} = 300 \text{ kg/m}^2\text{s}$ and $\Delta G/\bar{G} = 5\%$ for $\Delta q/\bar{q} = 10\%$ and $t_p = 20 \text{ sec}$.

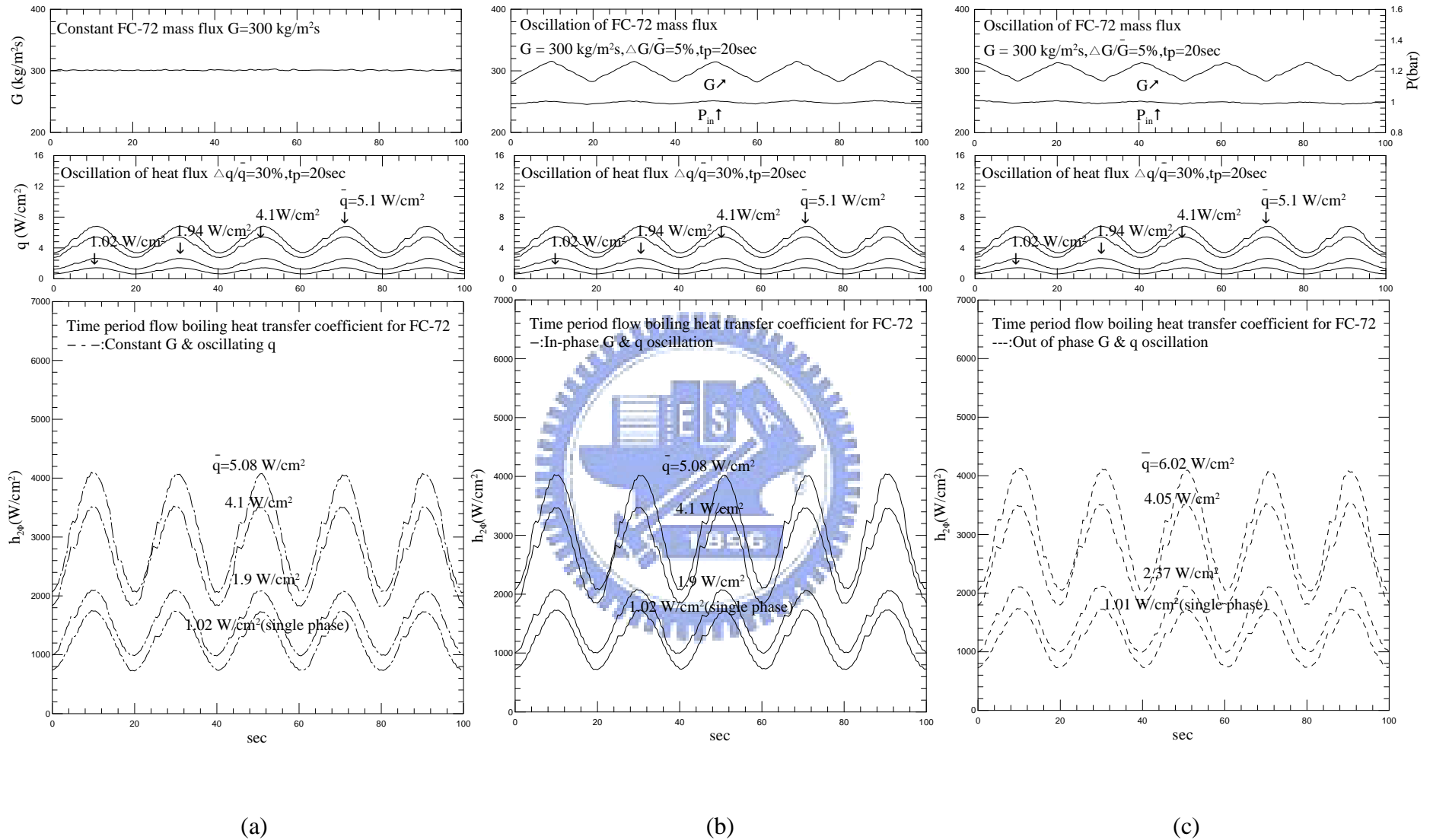


Fig. 4.20 Time variations of the heat transfer coefficient for (a) imposed heat flux oscillation only, (b) in-phase G and q oscillations and (c) out-of-phase G and q oscillations at $\bar{G} = 300 \text{ kg/m}^2\text{s}$ and $\Delta G/\bar{G} = 5\%$ for $\Delta q/\bar{q} = 30\%$ and $t_p = 20 \text{ sec}$.

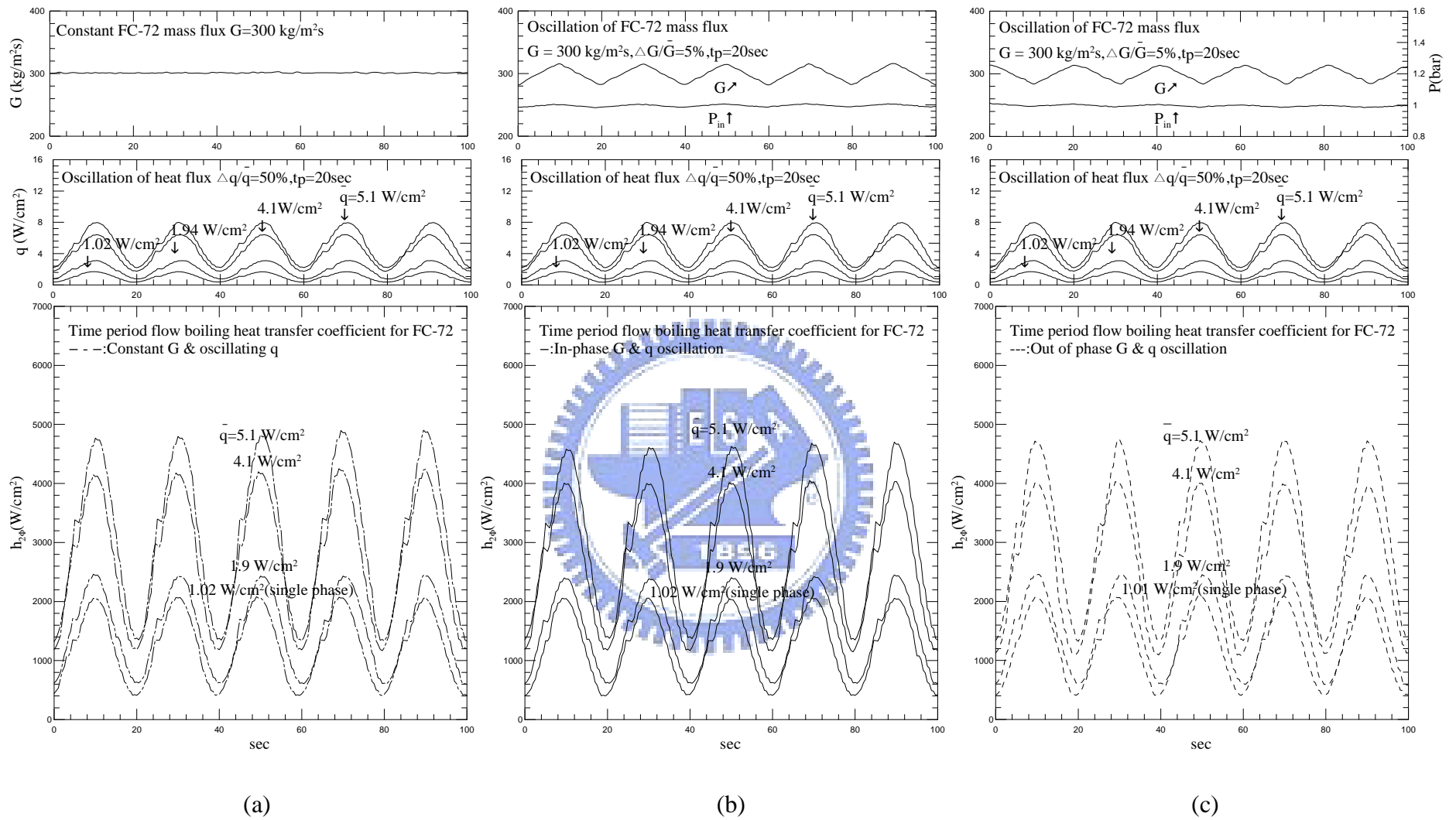


Fig. 4.21 Time variations of the heat transfer coefficient for (a) imposed heat flux oscillation only, (b) in-phase G and q oscillations and (c) out-of-phase G and q oscillations at $\bar{G} = 300$ kg/m²s and $\Delta G/\bar{G} = 5\%$ for $\Delta q/\bar{q} = 50\%$ and $t_p = 20$ sec.

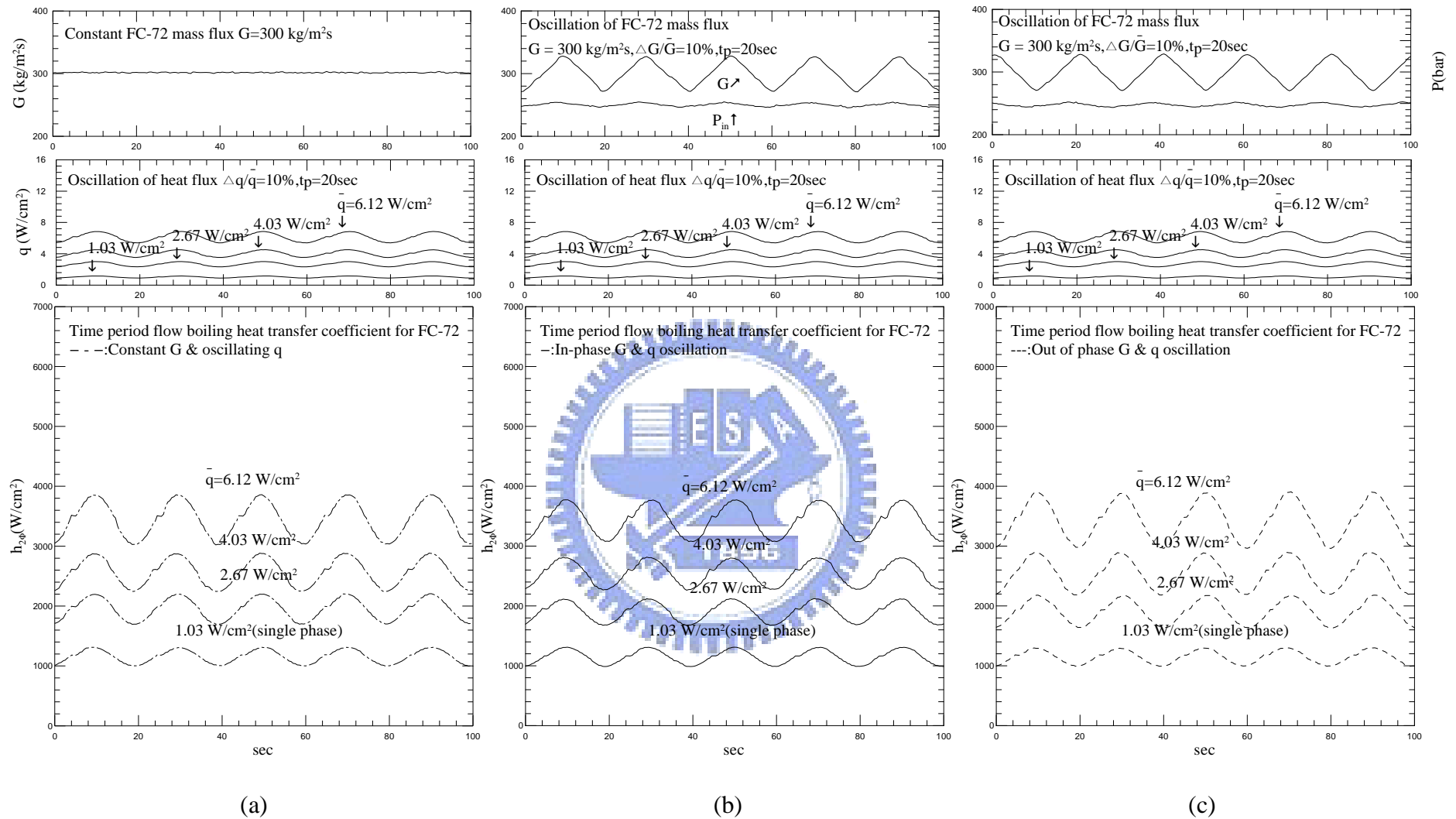


Fig. 4.22 Time variations of the heat transfer coefficient for (a) imposed heat flux oscillation only, (b) in-phase G and q oscillations and (c) out-of-phase G and q oscillations at $\bar{G} = 300 \text{ kg/m}^2\text{s}$ and $\Delta G/\bar{G} = 10\%$ for $\Delta q/\bar{q} = 10\%$ and $t_p = 20 \text{ sec}$.

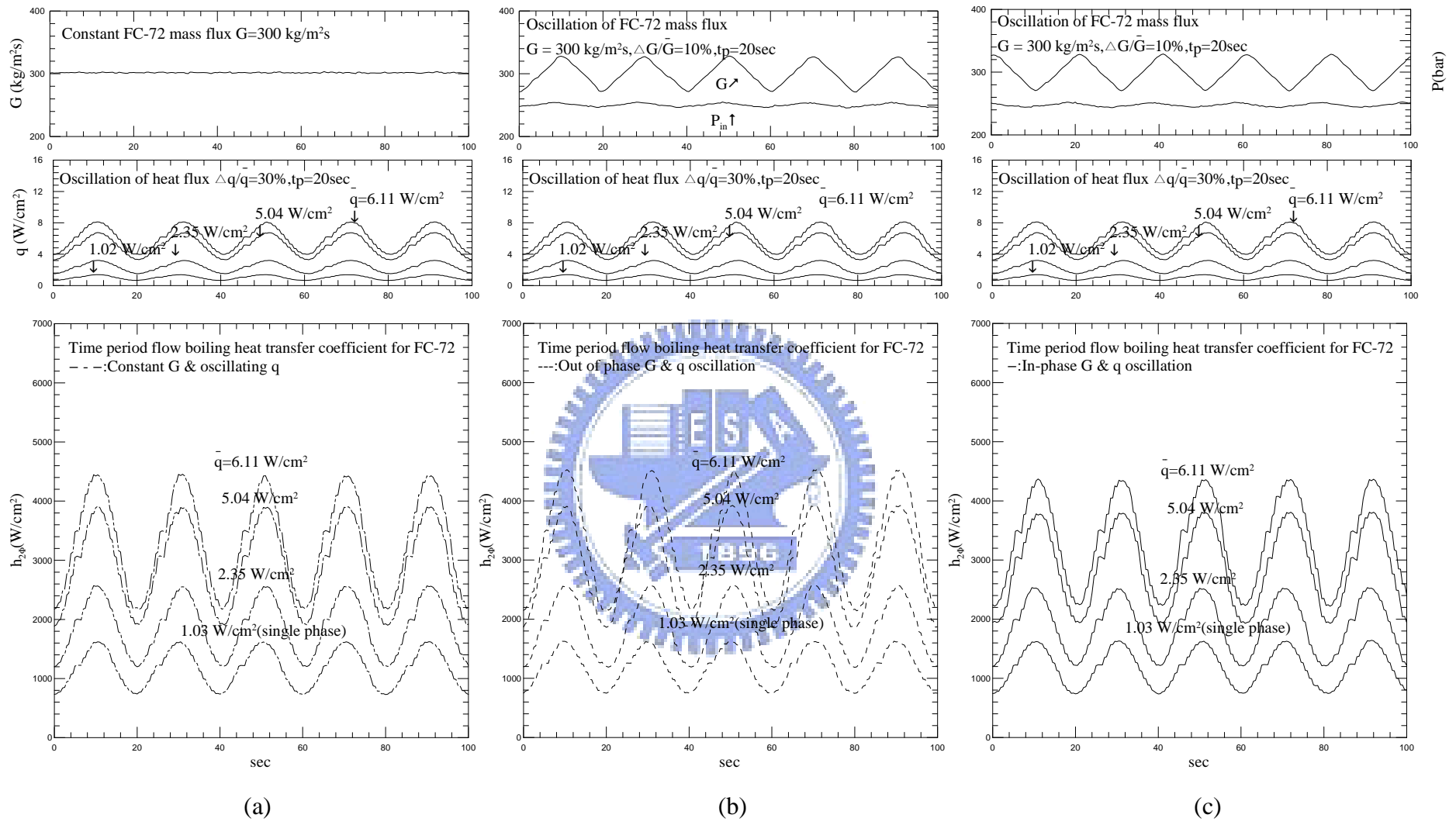


Fig. 4.23 Time variations of the heat transfer coefficient for (a) imposed heat flux oscillation only, (b) in-phase G and q oscillations and (c) out-of-phase G and q oscillations at $\bar{G} = 300$ kg/m²s and $\Delta G/\bar{G} = 10\%$ for $\Delta q/\bar{q} = 30\%$ and $t_p = 20$ sec.

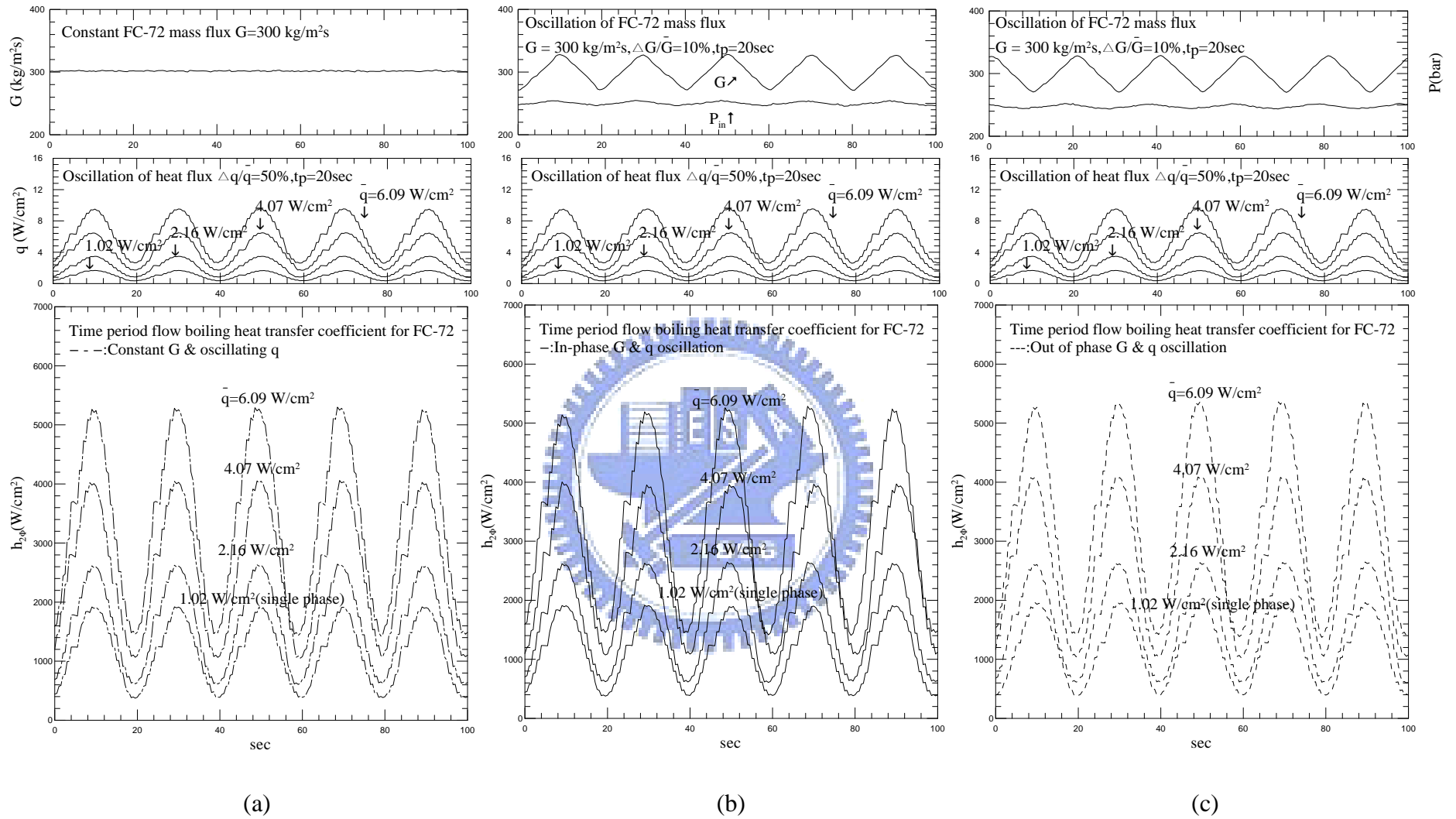


Fig. 4.24 Time variations of the heat transfer coefficient for (a) imposed heat flux oscillation only, (b) in-phase G and q oscillations and (c) out-of-phase G and q oscillations at $\bar{G} = 300$ kg/m²s and $\Delta G/\bar{G} = 10\%$ for $\Delta q/\bar{q} = 50\%$ and $t_p = 20$ sec.

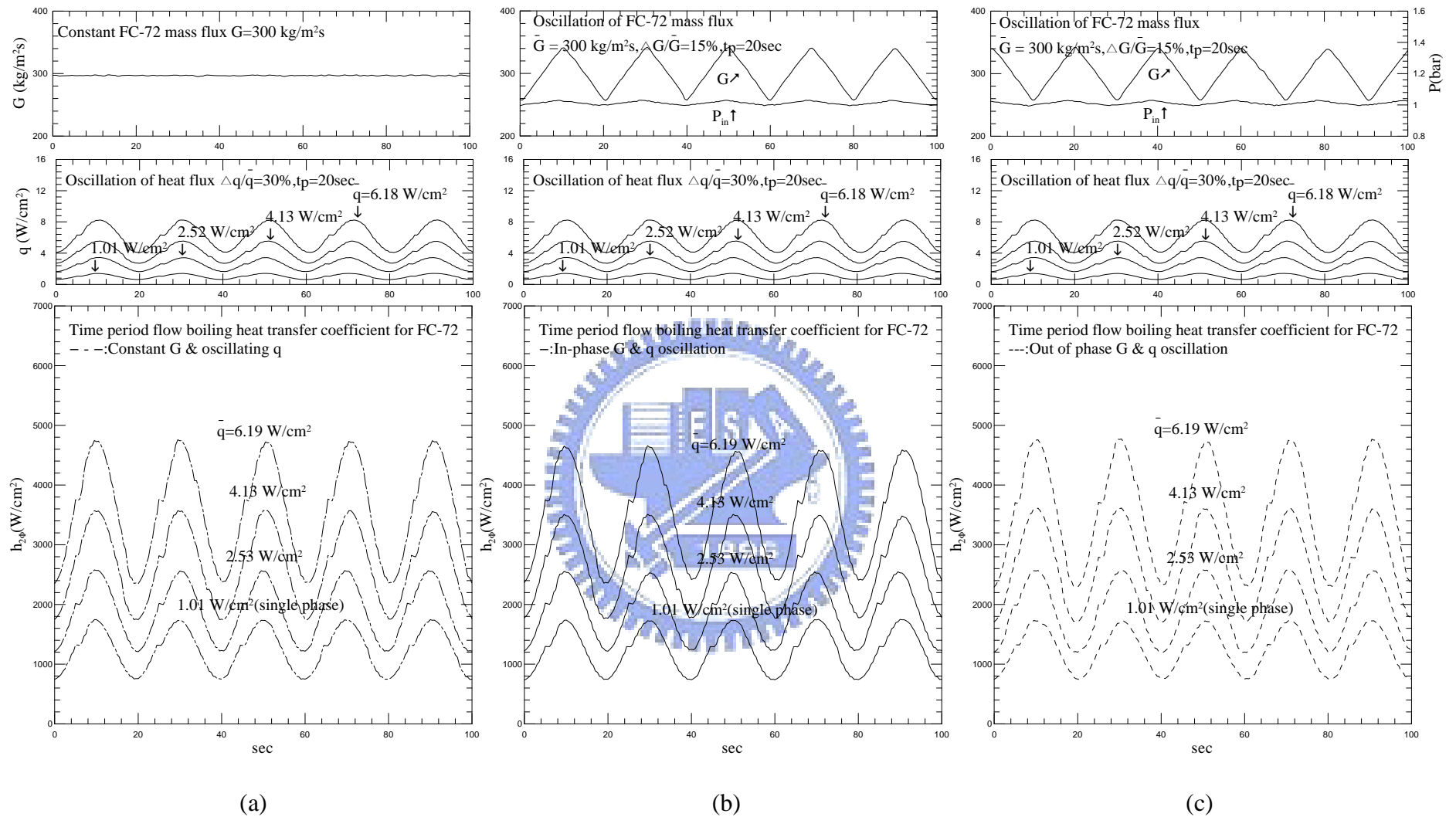


Fig. 4.25 Time variations of the heat transfer coefficient for (a) imposed heat flux oscillation only, (b) in-phase G and q oscillations and (c) out-of-phase G and q oscillations at $\bar{G} = 300 \text{ kg/m}^2\text{s}$ and $\Delta G/\bar{G} = 15\%$ for $\Delta q/\bar{q} = 30\%$ and $t_p = 20 \text{ sec}$.

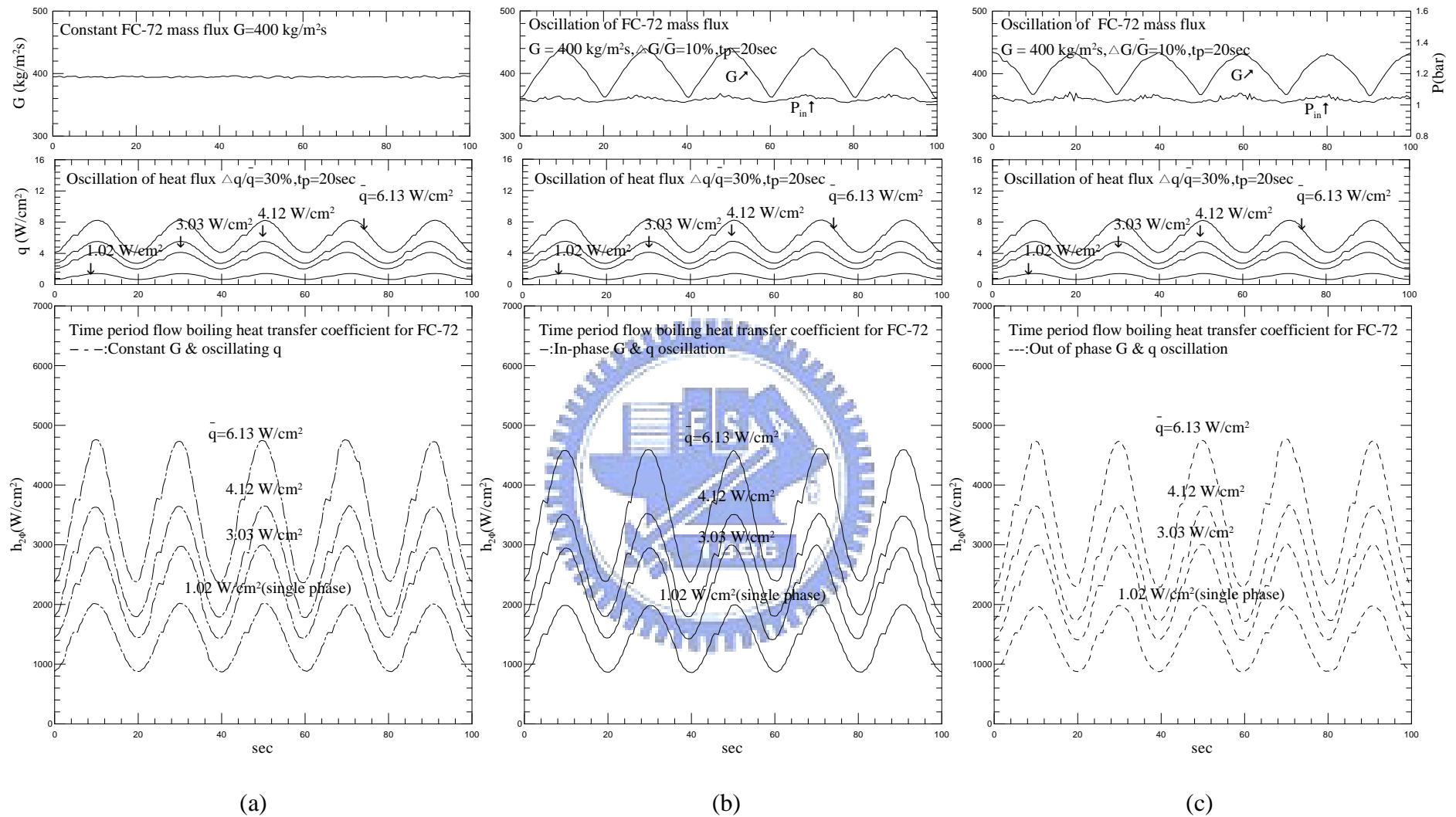


Fig. 4.26 Time variations of the heat transfer coefficient for (a) imposed heat flux oscillation only, (b) in-phase G and q oscillations and (c) out-of-phase G and q oscillations at $\bar{G} = 400 \text{ kg/m}^2\text{s}$ and $\Delta G/\bar{G} = 10\%$ for $\Delta q/\bar{q} = 30\%$ and $t_p = 20 \text{ sec}$.

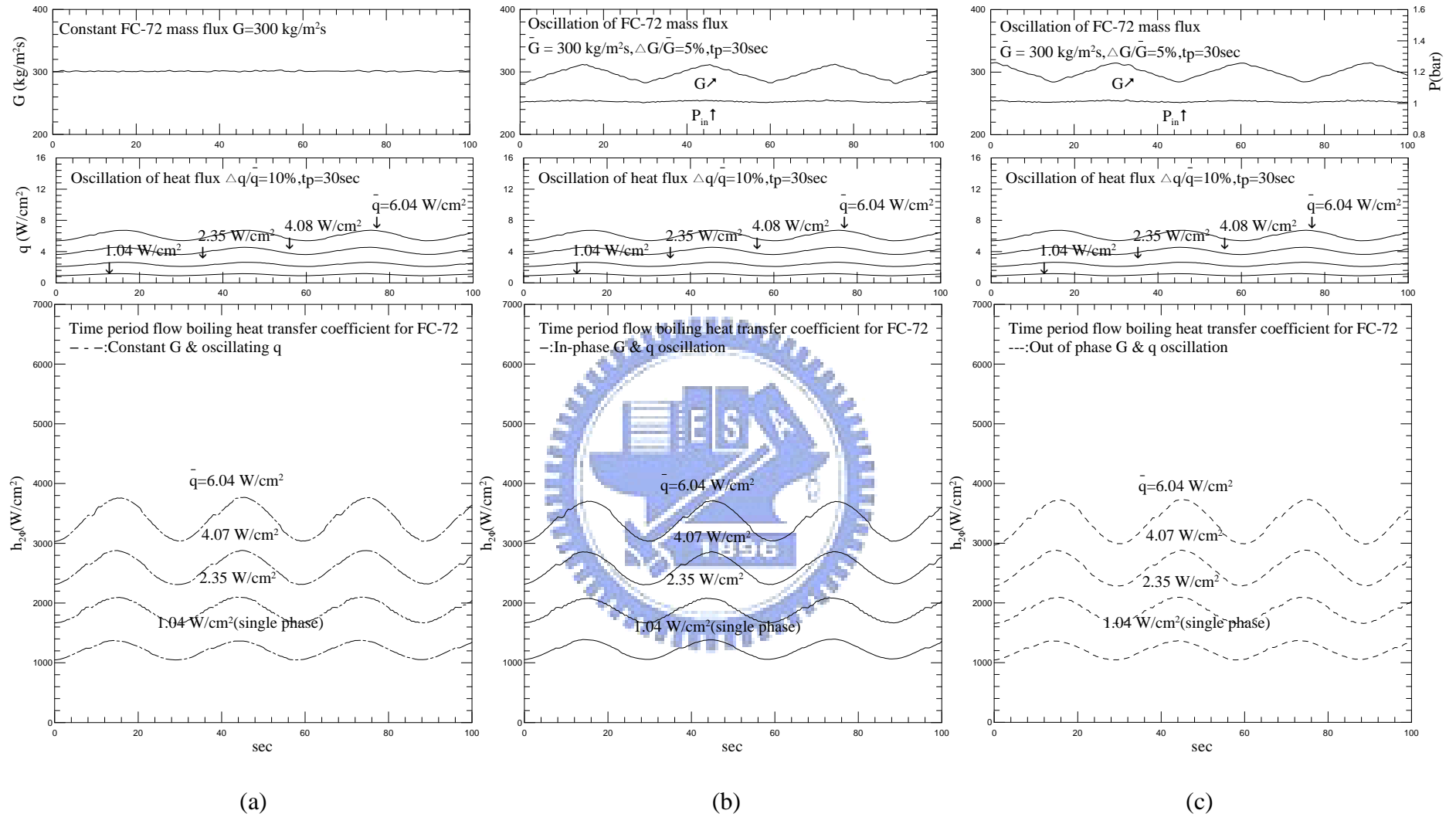


Fig. 4.27 Time variations of the heat transfer coefficient for (a) imposed heat flux oscillation only, (b) in-phase G and q oscillations and (c) out-of-phase G and q oscillations at $\bar{G} = 300 \text{ kg/m}^2 \text{ s}$ and $\Delta G/\bar{G} = 5\%$ for $\Delta q/\bar{q} = 10\%$ and $t_p = 30 \text{ sec}$.

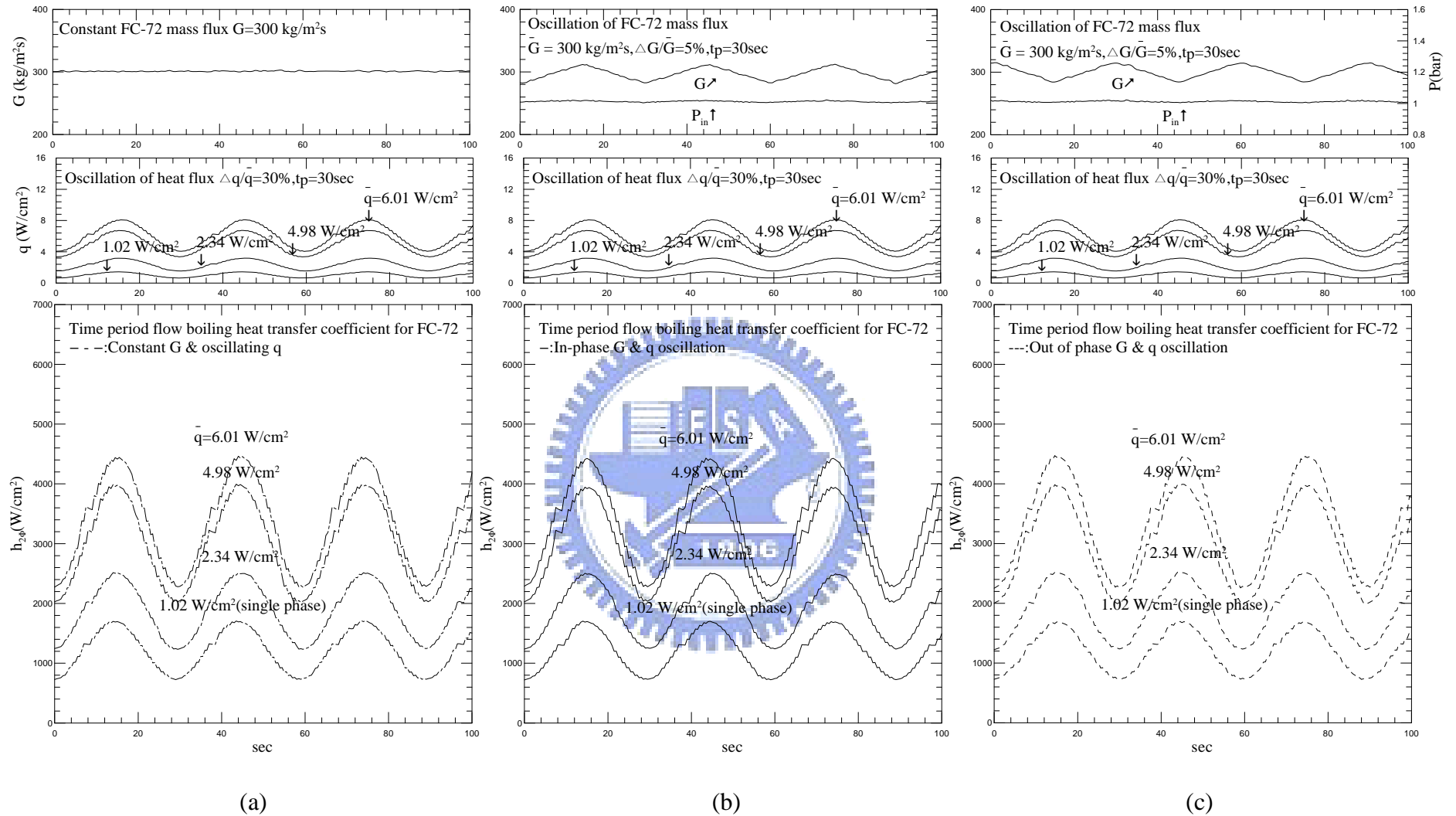


Fig. 4.28 Time variations of the heat transfer coefficient for (a) imposed heat flux oscillation only, (b) in-phase G and q oscillations and (c) out-of-phase G and q oscillations at $\bar{G} = 300 \text{ kg/m}^2 \text{ s}$ and $\Delta G/\bar{G} = 5\%$ for $\Delta q/\bar{q} = 30\%$ and $t_p = 30 \text{ sec}$.

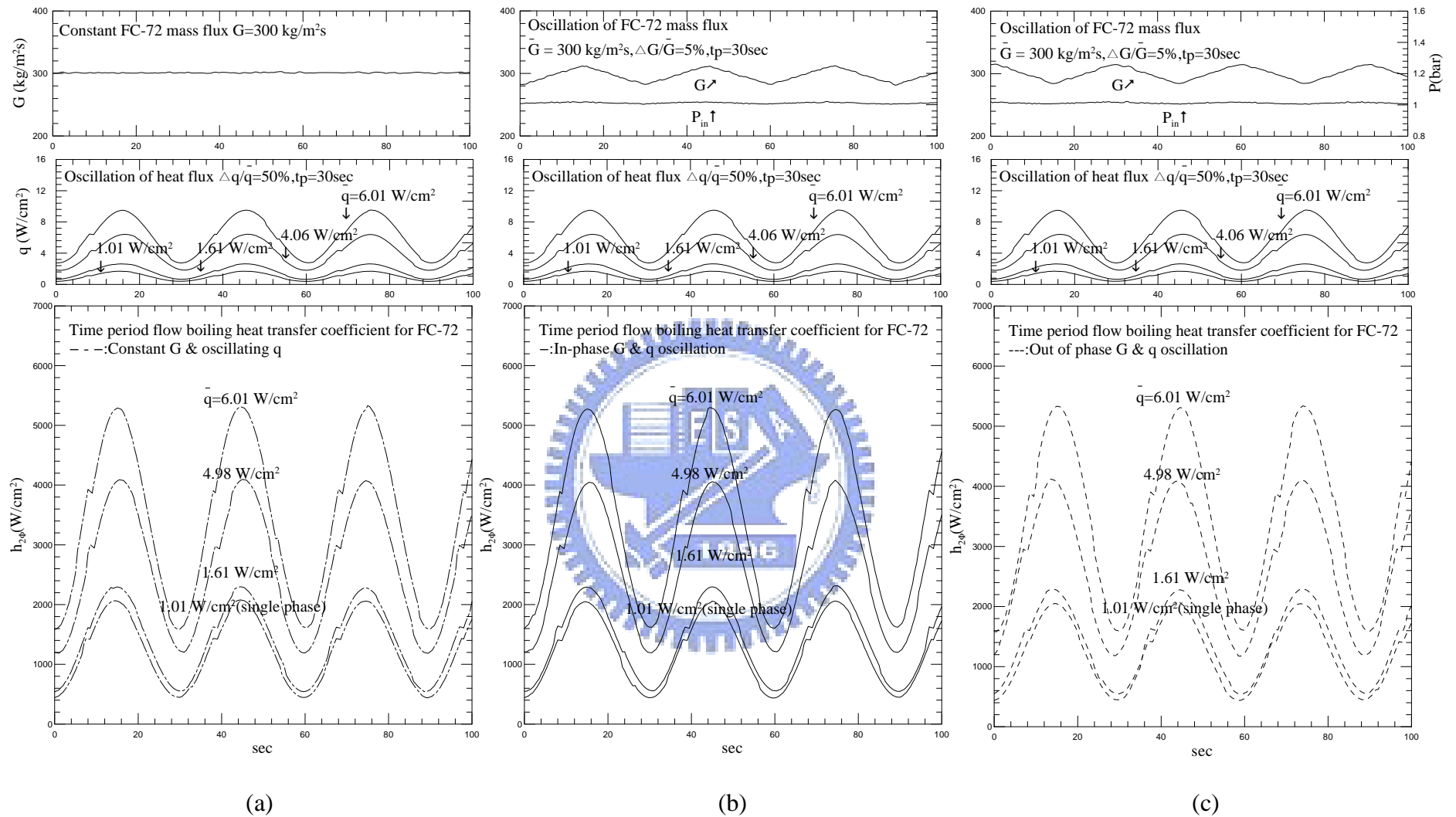


Fig. 4.29 Time variations of the heat transfer coefficient for (a) imposed heat flux oscillation only, (b) in-phase G and q oscillations and (c) out-of-phase G and q oscillations at $\bar{G} = 300 \text{ kg/m}^2 \text{ s}$ and $\Delta G/\bar{G} = 5\%$ for $\Delta q/\bar{q} = 50\%$ and $t_p = 30 \text{ sec}$.

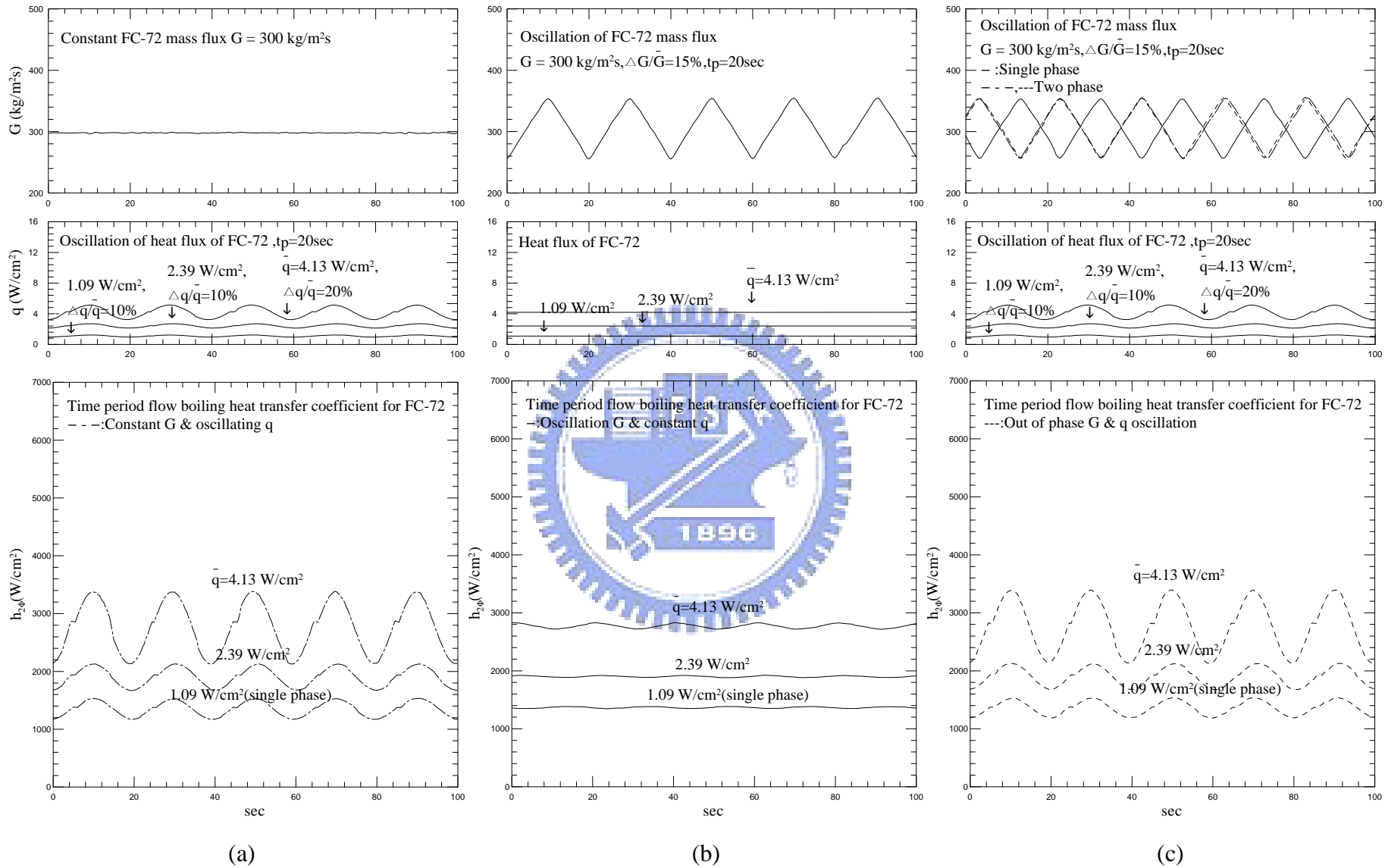


Fig. 4.30 Time variations of the heat transfer coefficient for (a) imposed heat flux oscillation only, (b) imposed mass flux oscillation only and (c) out-of-phase G and q oscillations at $\bar{G} = 300 \text{ kg/m}^2 \text{ s}$ and $\Delta G/\bar{G} = 15\%$ for $\Delta q/\bar{q} = 10, 20\%$ and $t_p = 20 \text{ sec}$.

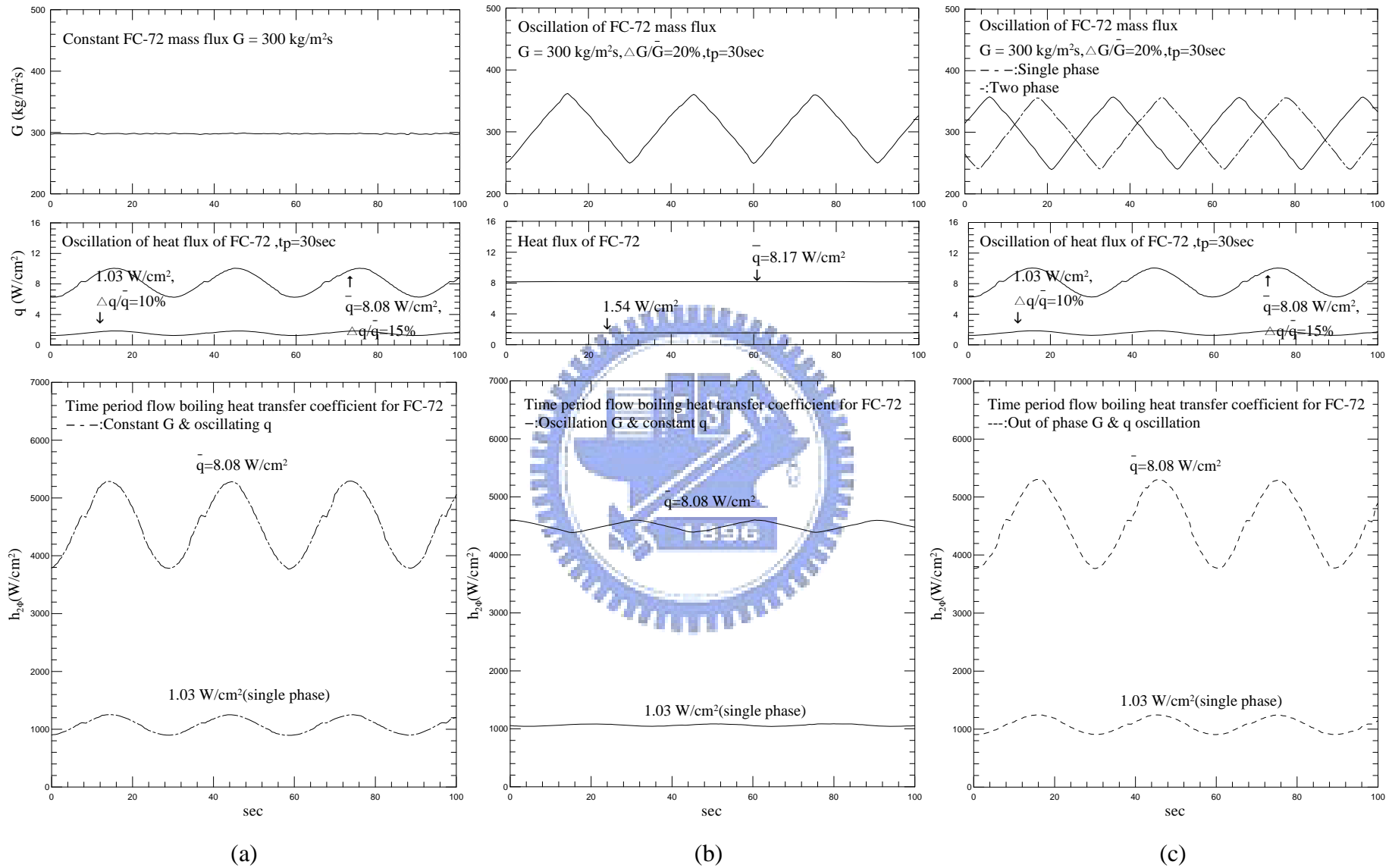


Fig. 4.31 Time variations of the heat transfer coefficient for (a) imposed heat flux oscillation only, (b) imposed mass flux oscillation only and (c) out-of-phase G and q oscillations at $\bar{G} = 300 \text{ kg/m}^2 \text{ s}$ and $\Delta G/\bar{G} = 20\%$ for $\Delta q/\bar{q} = 10, 15\%$ and $t_p = 20$ sec.

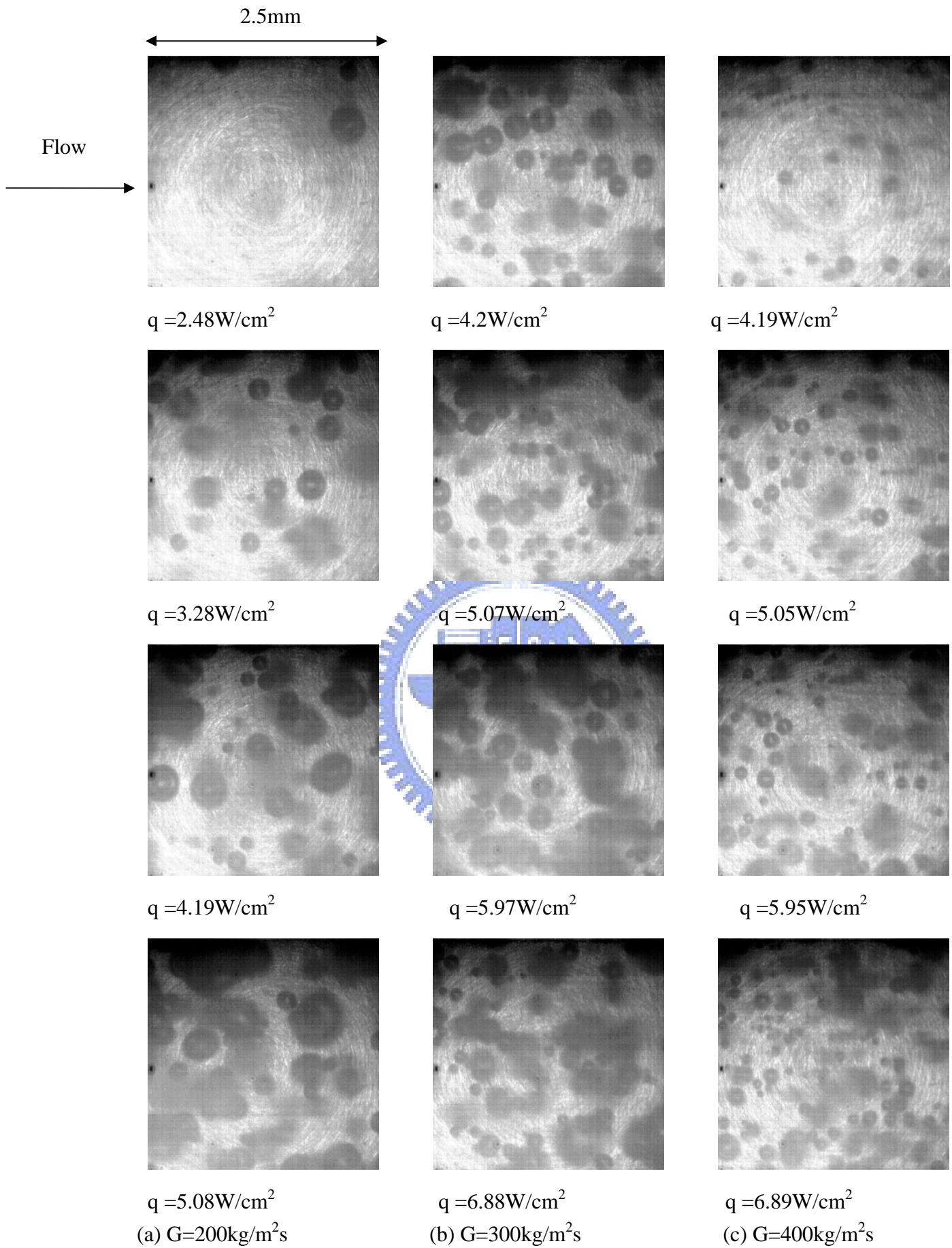


Fig. 4.32 Photos of stable saturated flow boiling at certain time instants in statistical state for various imposed heat fluxes for (a) $G = 200 \text{ kg/m}^2\text{s}$, (b) $G = 300 \text{ kg/m}^2\text{s}$ and (c) $G = 400 \text{ kg/m}^2\text{s}$.

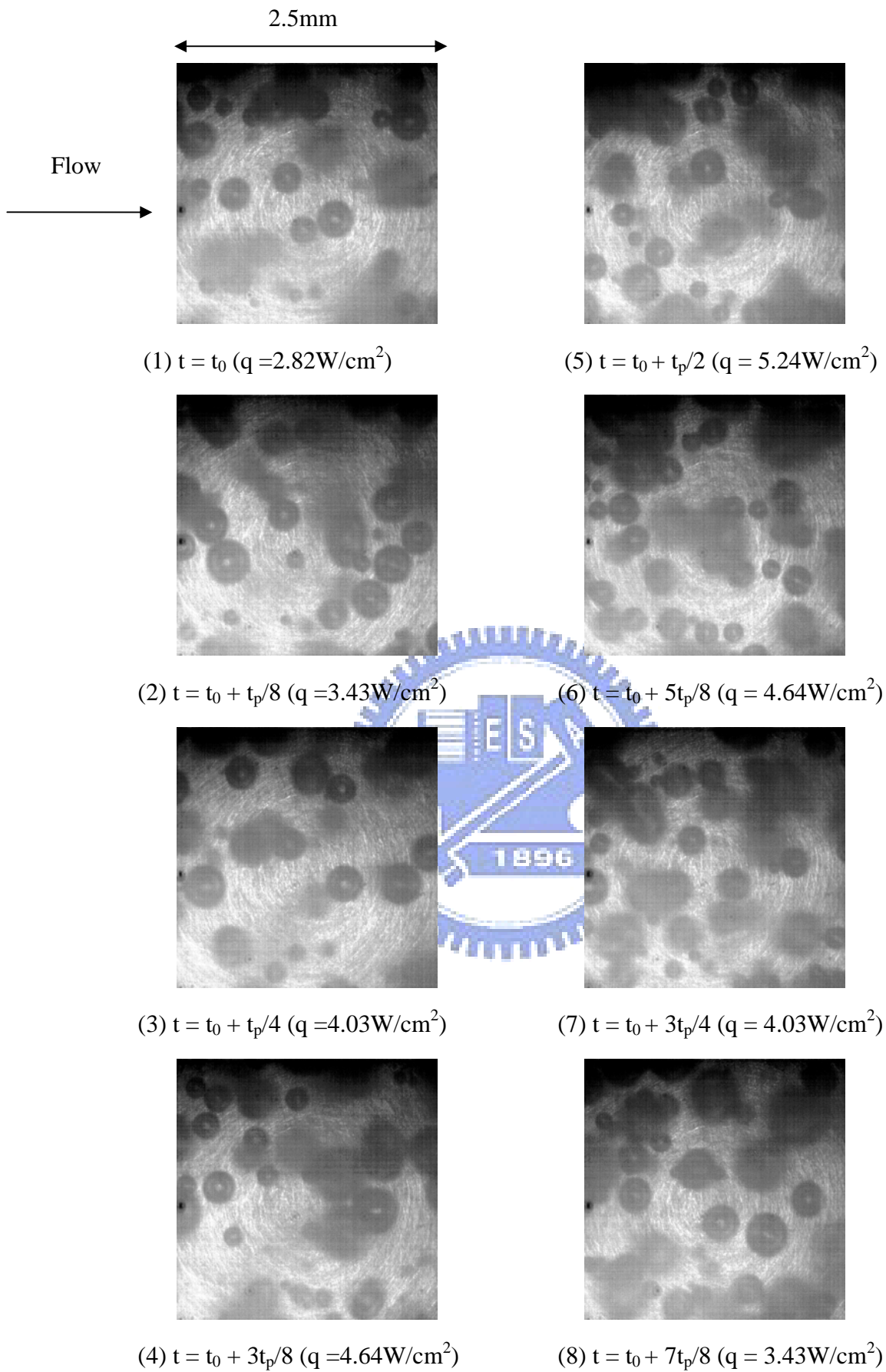


Fig. 4.33 Photos of saturated flow boiling at certain time instants in a typical time periodic cycle for an imposed constant mass flux at $\bar{q} = 4.03 \text{W/cm}^2$, $\Delta q / \bar{q} = 30\%$, $G = 200 \text{kg/m}^2\text{s}$ and $t_p = 20 \text{sec}$.

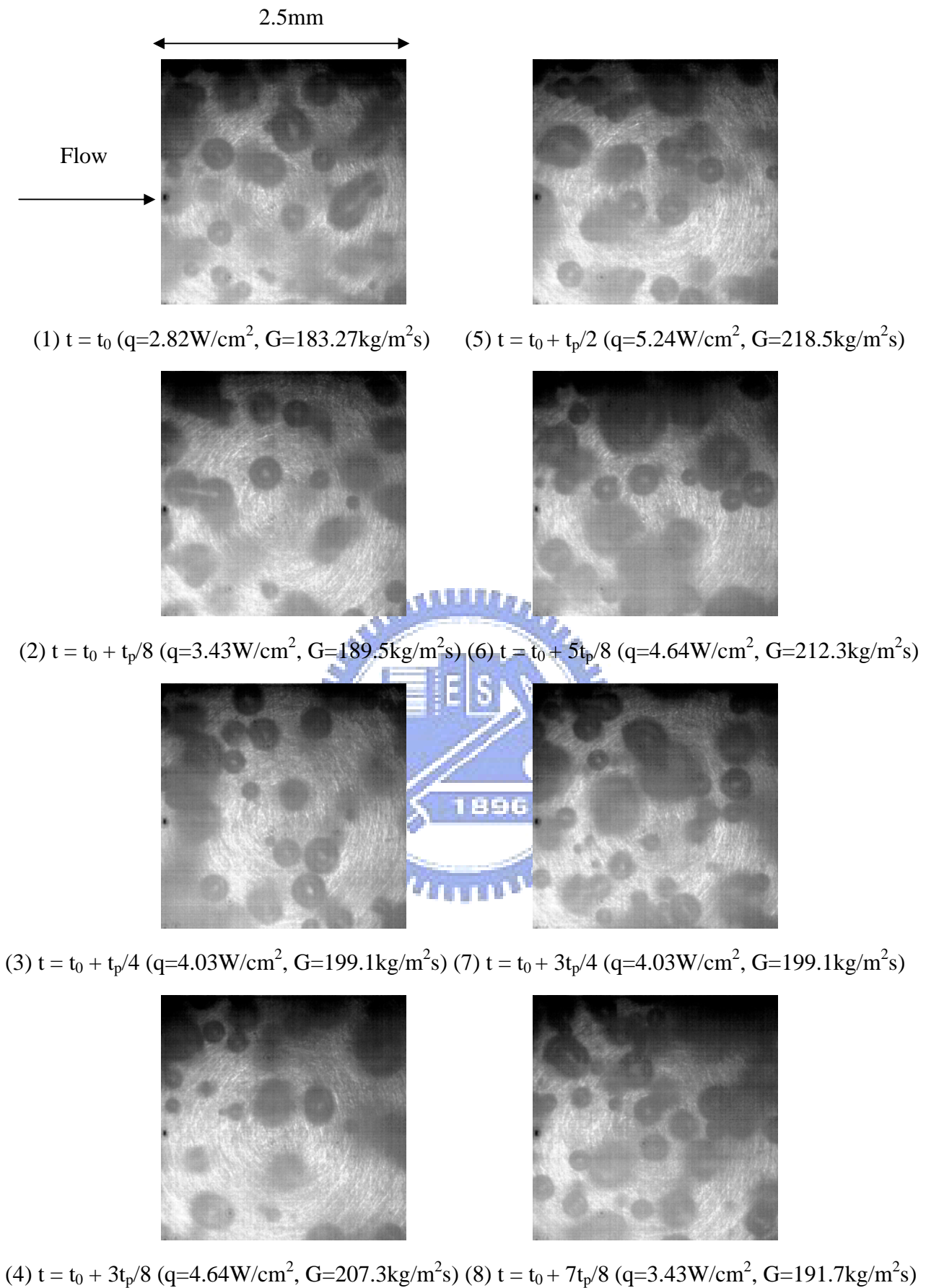


Fig. 4.34 Photos of saturated flow boiling at certain time instants in a typical time periodic cycle for imposed in-phase G & q oscillations at $\bar{G} = 200\text{kg/m}^2\text{s}$, $\Delta G/\bar{G} = 10\%$, $\bar{q} = 4.03\text{W/cm}^2$ and $\Delta q/\bar{q} = 30\%$ with $t_p = 20\text{sec}$.

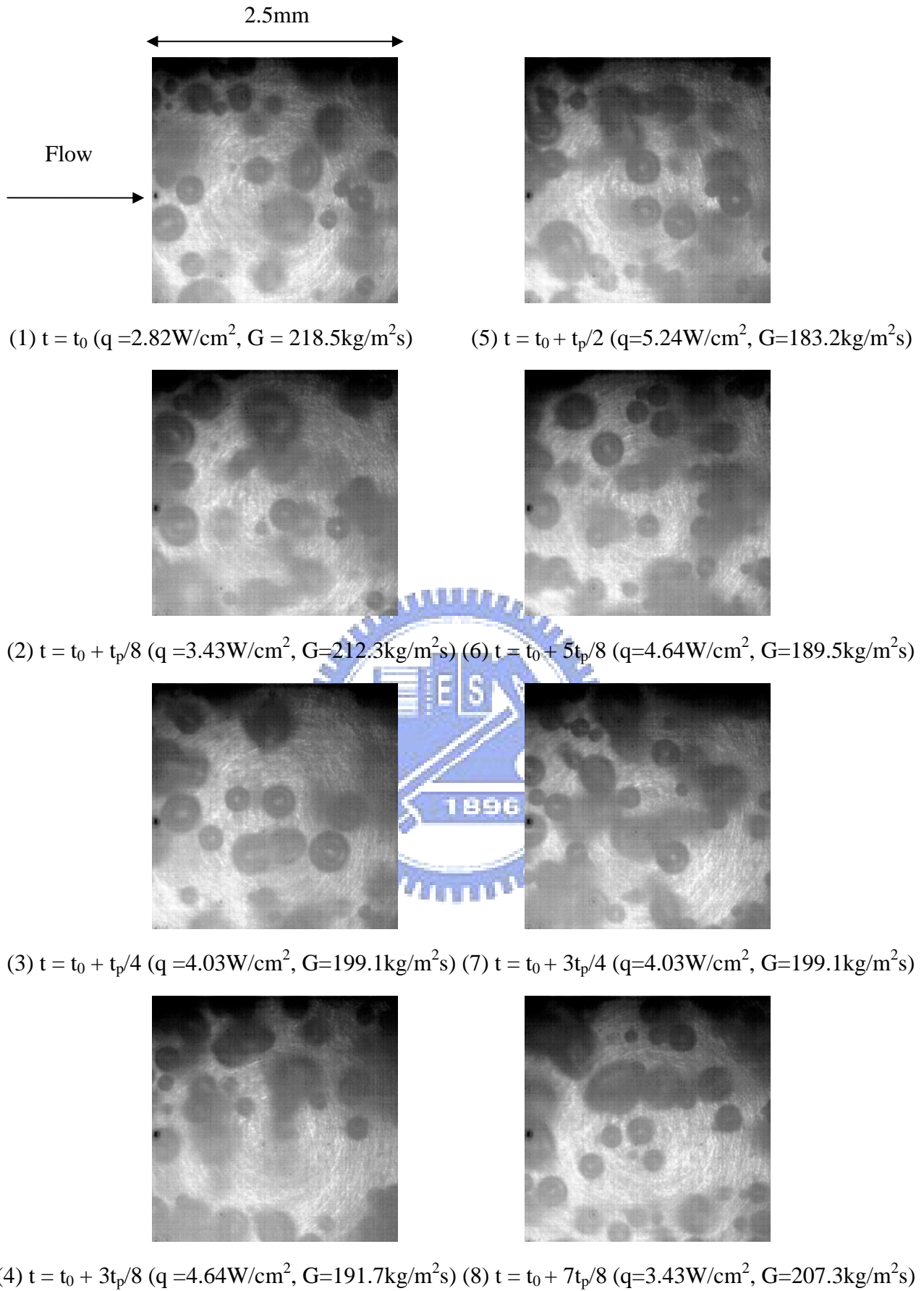


Fig. 4.35 Photos of saturated flow boiling at certain time instants in a typical time periodic cycle for imposed out-of-phase G & q oscillations at $\bar{G} = 200\text{kg/m}^2\text{s}$, $\Delta G/\bar{G} = 10\%$, $\bar{q} = 4.03\text{W/cm}^2$ and $\Delta q/\bar{q} = 30\%$ with $t_p = 20\text{sec}$.

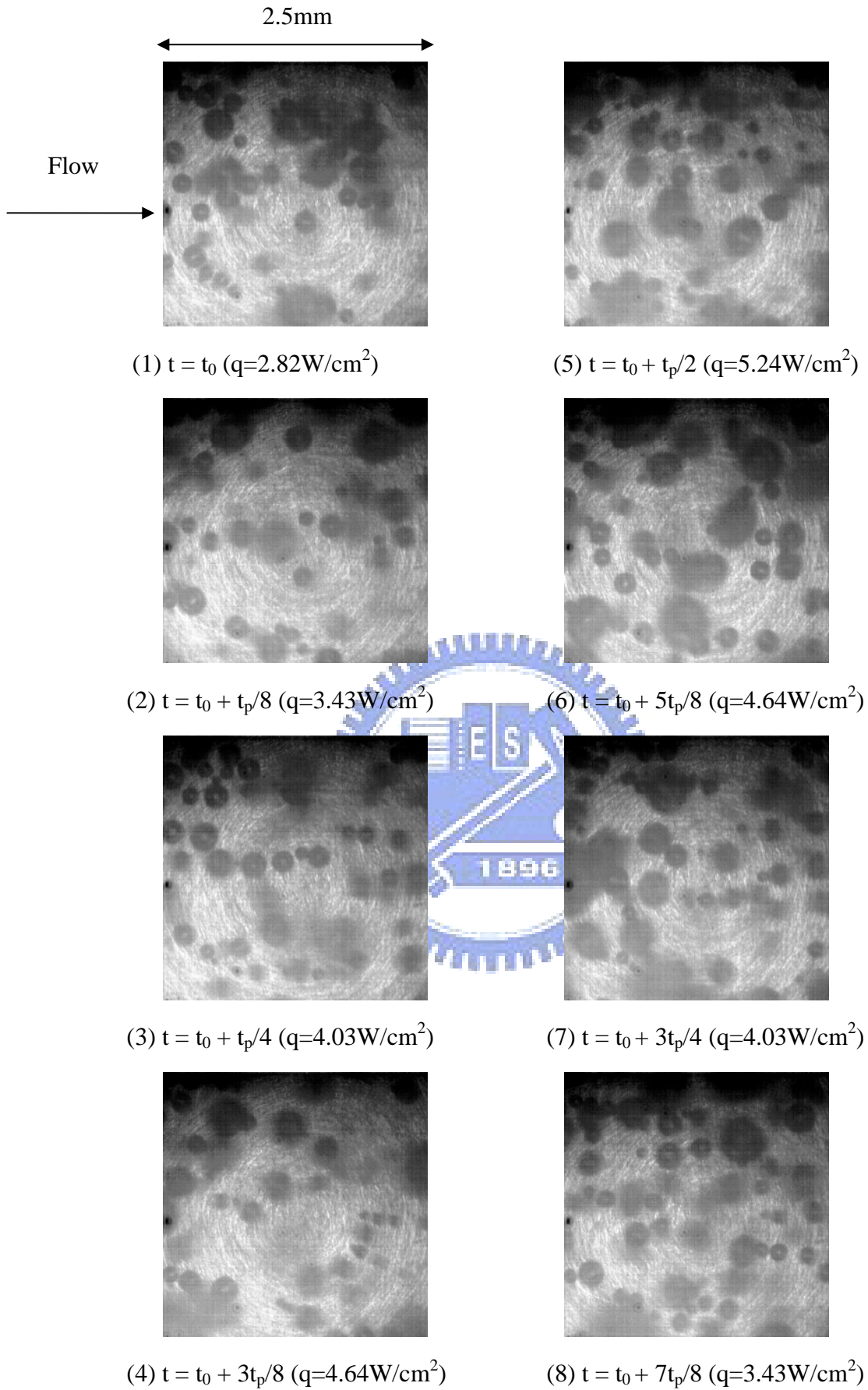


Fig. 4.36 Photos of saturated flow boiling at certain time instants in a typical time periodic cycle for an imposed constant mass flux at $\bar{q}=4.03\text{W/cm}^2$, $\Delta q/\bar{q}=30\%$, $G = 300\text{kg/m}^2\text{s}$ and $t_p = 20\text{sec}$.

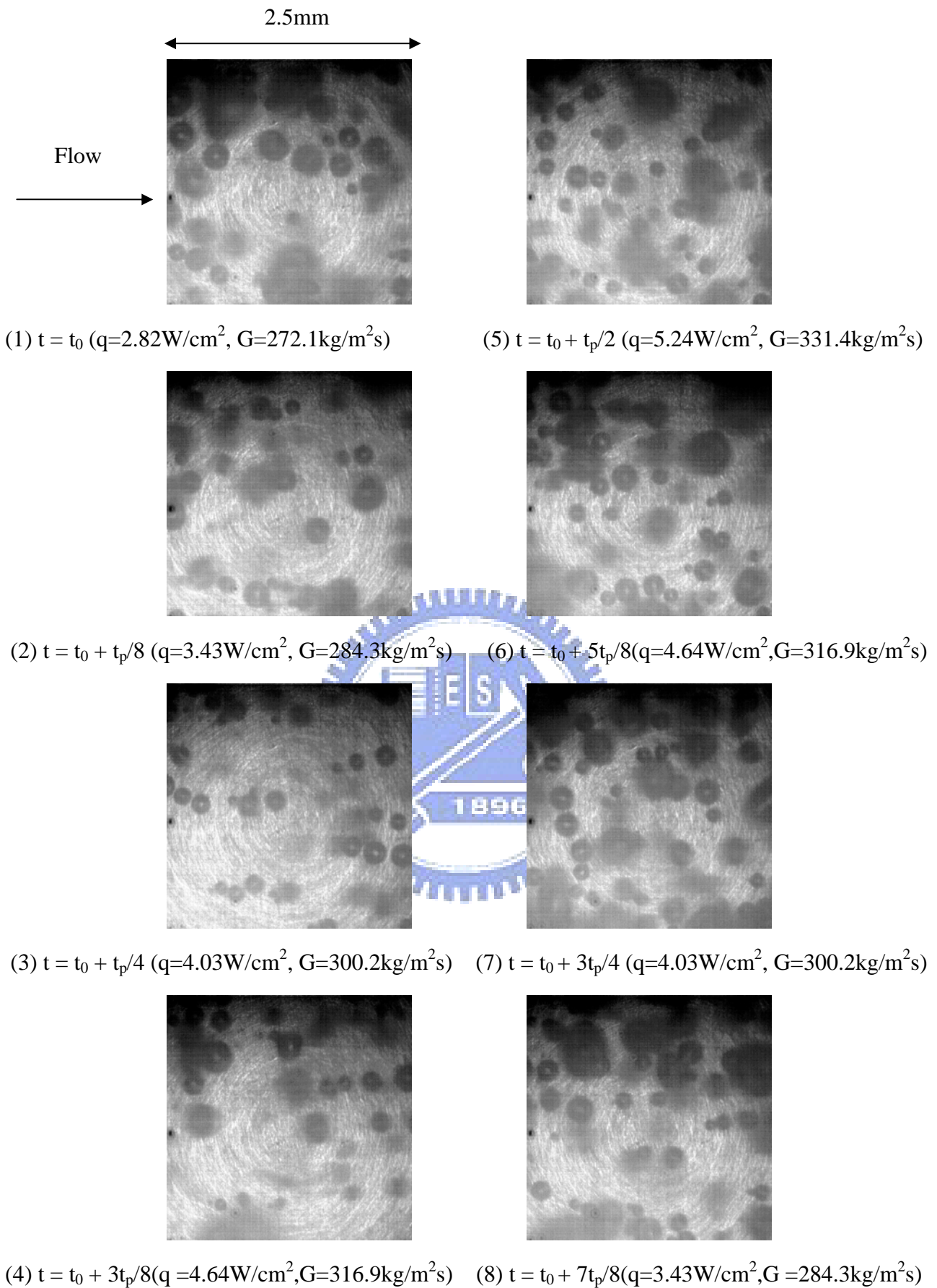


Fig. 4.37 Photos of saturated flow boiling at certain time instants in a typical time periodic cycle for imposed in-phase G & q oscillations at $\bar{G} = 300\text{kg/m}^2\text{s}$, $\Delta G/\bar{G} = 10\%$, $\bar{q} = 4.03\text{W/cm}^2$ and $\Delta q/\bar{q} = 30\%$ with $t_p = 20\text{sec}$.

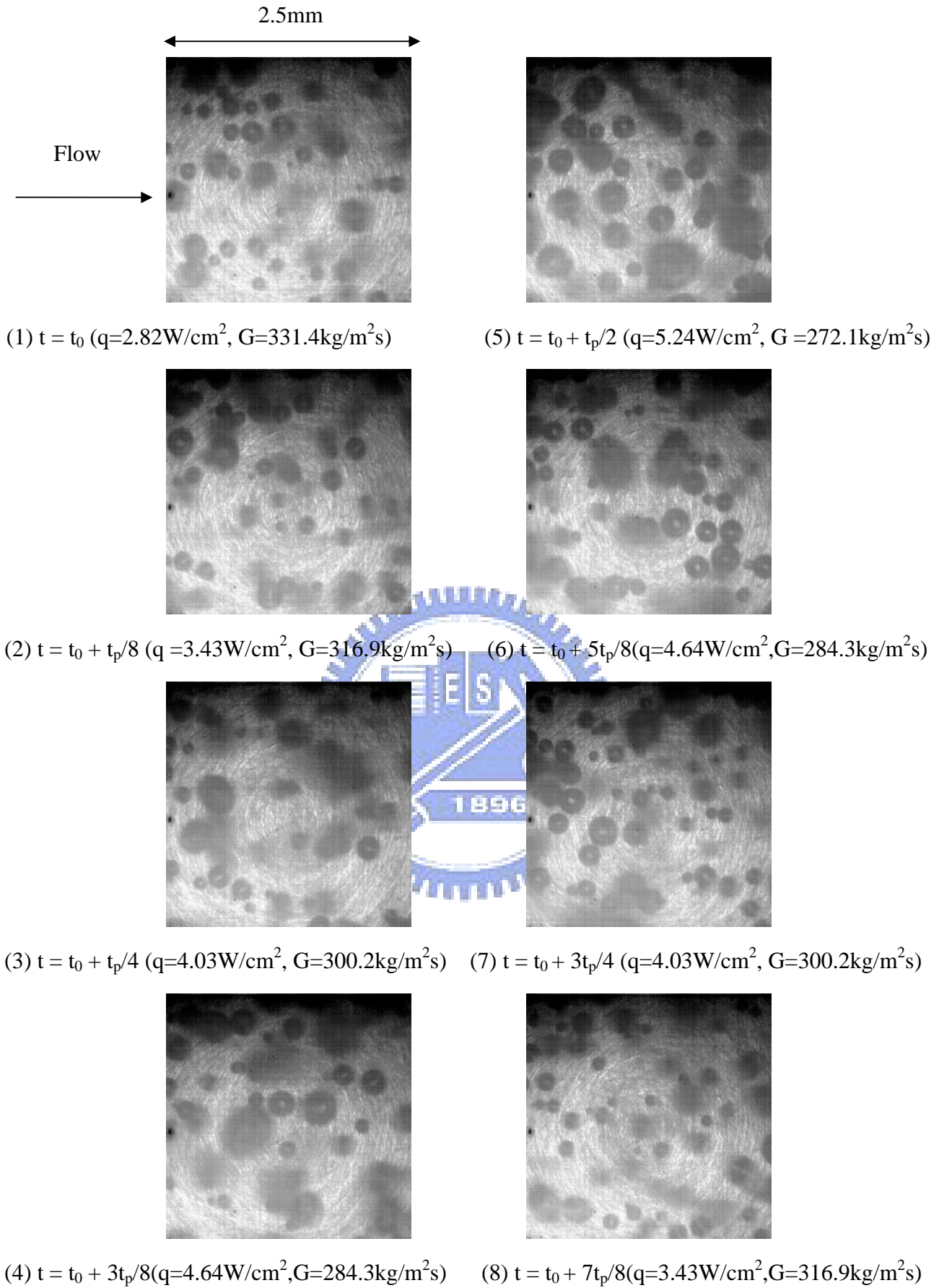


Fig. 4.38 Photos of saturated flow boiling at certain time instants in a typical time periodic cycle for imposed out-of-phase G & q oscillations at $\bar{G} = 300\text{kg/m}^2\text{s}$, $\Delta G/\bar{G} = 10\%$, $\bar{q} = 4.03\text{W/cm}^2$ and $\Delta q/\bar{q} = 30\%$ with $t_p = 20\text{sec}$.

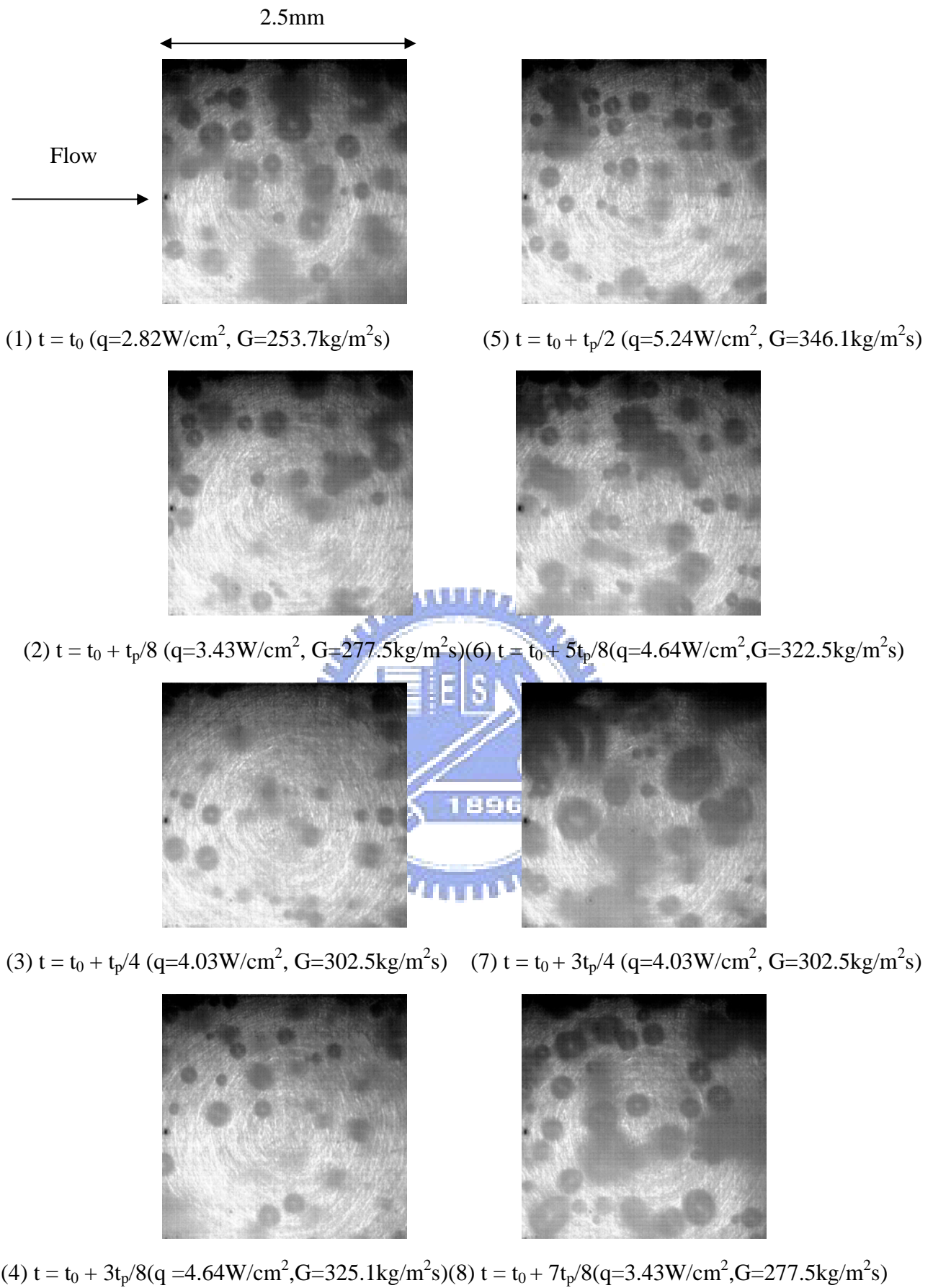


Fig. 4.39 Photos of saturated flow boiling at certain time instants in a typical time periodic cycle for imposed in-phase G & q oscillations at $\bar{G} = 300\text{kg/m}^2\text{s}$, $\Delta G/\bar{G} = 15\%$, $\bar{q} = 4.03\text{W/cm}^2$ and $\Delta q/\bar{q} = 30\%$ with $t_p = 20\text{sec}$.

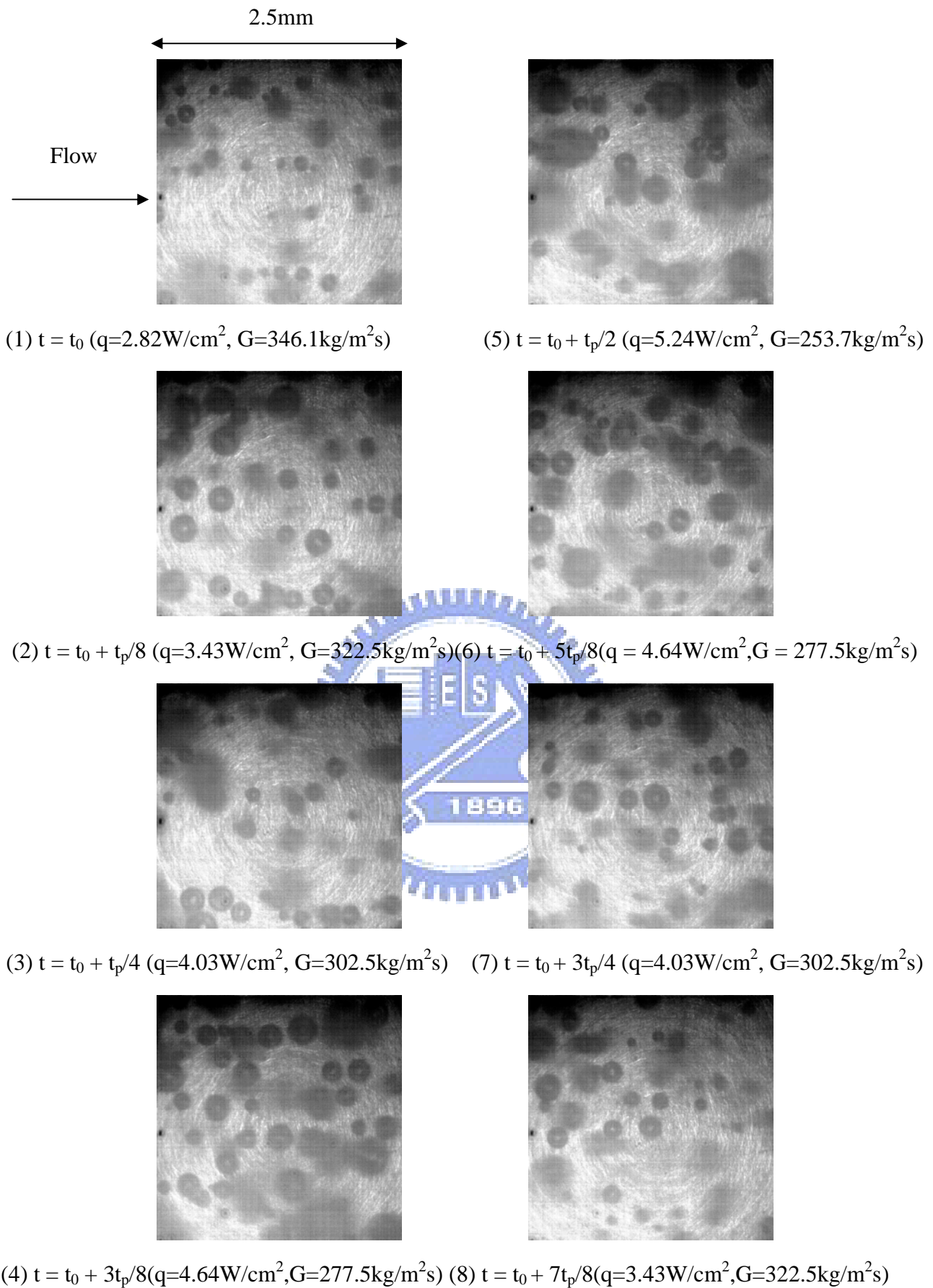


Fig. 4.40 Photos of saturated flow boiling at certain time instants in a typical time periodic cycle for imposed out-of-phase G & q oscillations at $\bar{G} = 300\text{kg/m}^2\text{s}$, $\Delta G/\bar{G} = 15\%$, $\bar{q} = 4.03\text{W/cm}^2$ and $\Delta q/\bar{q} = 30\%$ with $t_p = 20\text{sec}$.

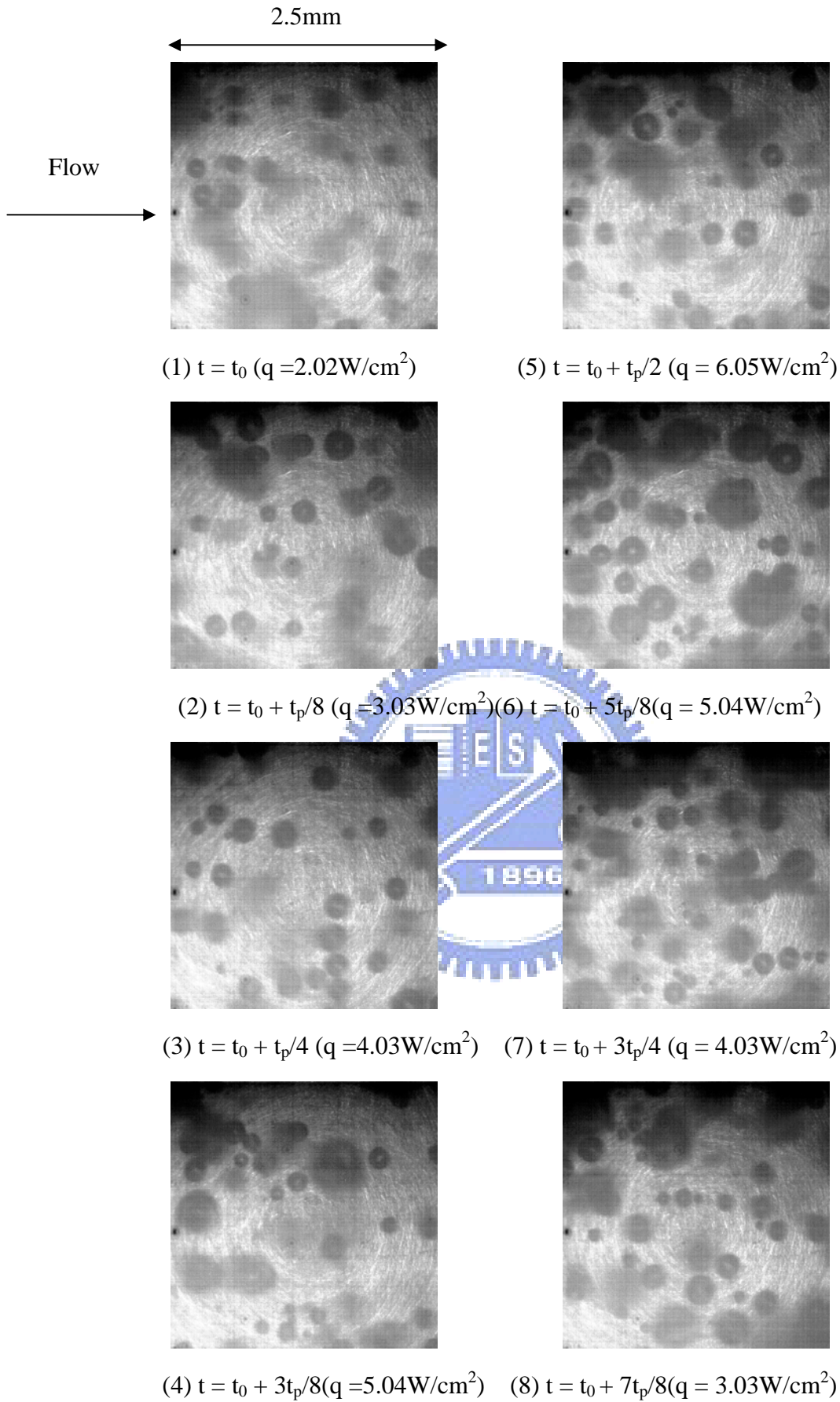


Fig. 4.41 Photos of saturated flow boiling at certain time instants in a typical time periodic cycle for an imposed constant mass flux at $\bar{q} = 4.03 \text{ W/cm}^2$, $\Delta q / \bar{q} = 50\%$, $G = 300 \text{ kg/m}^2\text{s}$ and $t_p = 20 \text{ sec}$.

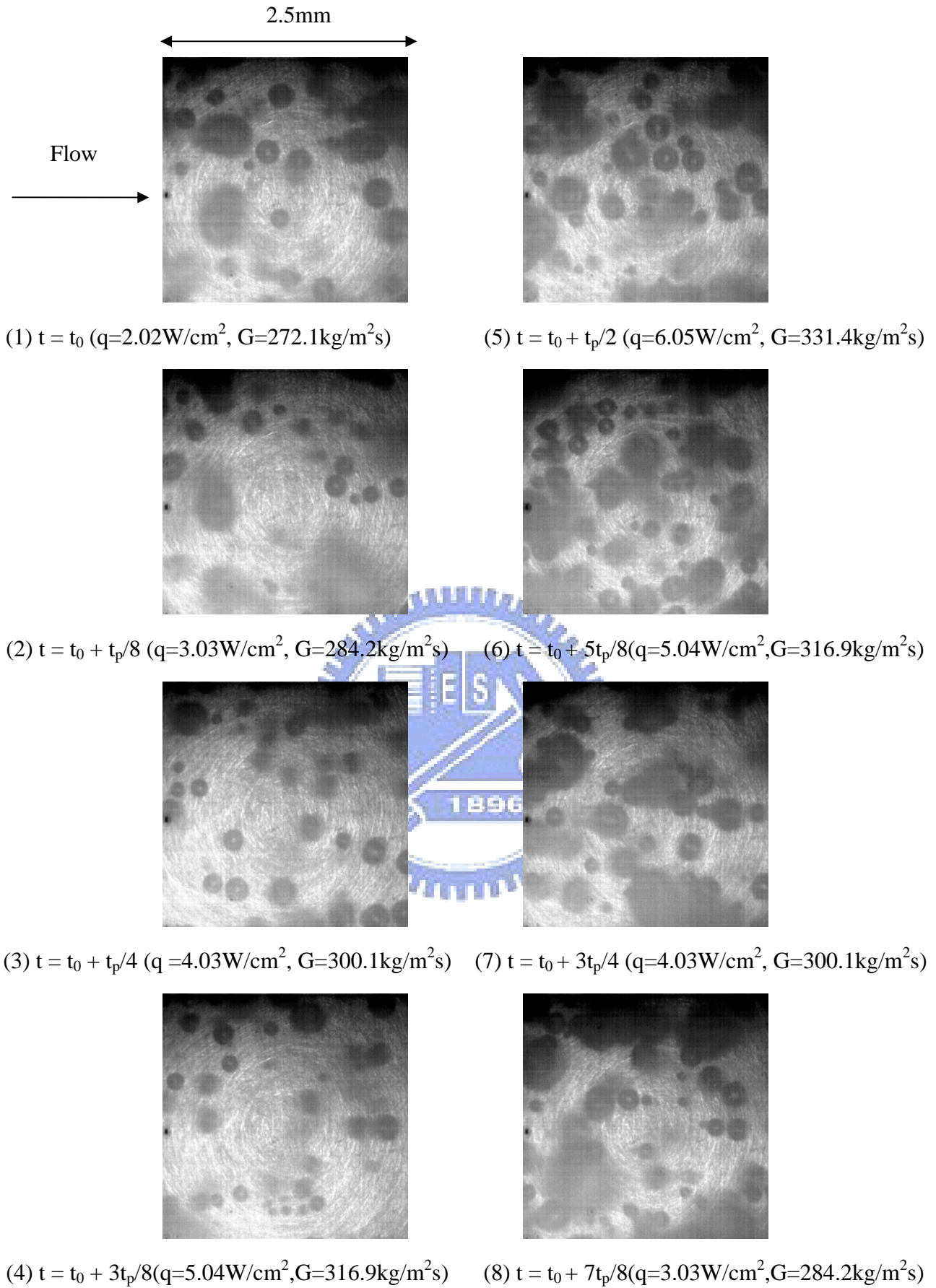


Fig. 4.42 Photos of saturated flow boiling at certain time instants in a typical time periodic cycle for imposed in-phase G & q oscillations at $\bar{G} = 300\text{kg/m}^2\text{s}$, $\Delta G/\bar{G} = 10\%$, $\bar{q} = 4.03\text{W/cm}^2$ and $\Delta q/\bar{q} = 50\%$ with $t_p = 20\text{sec}$.

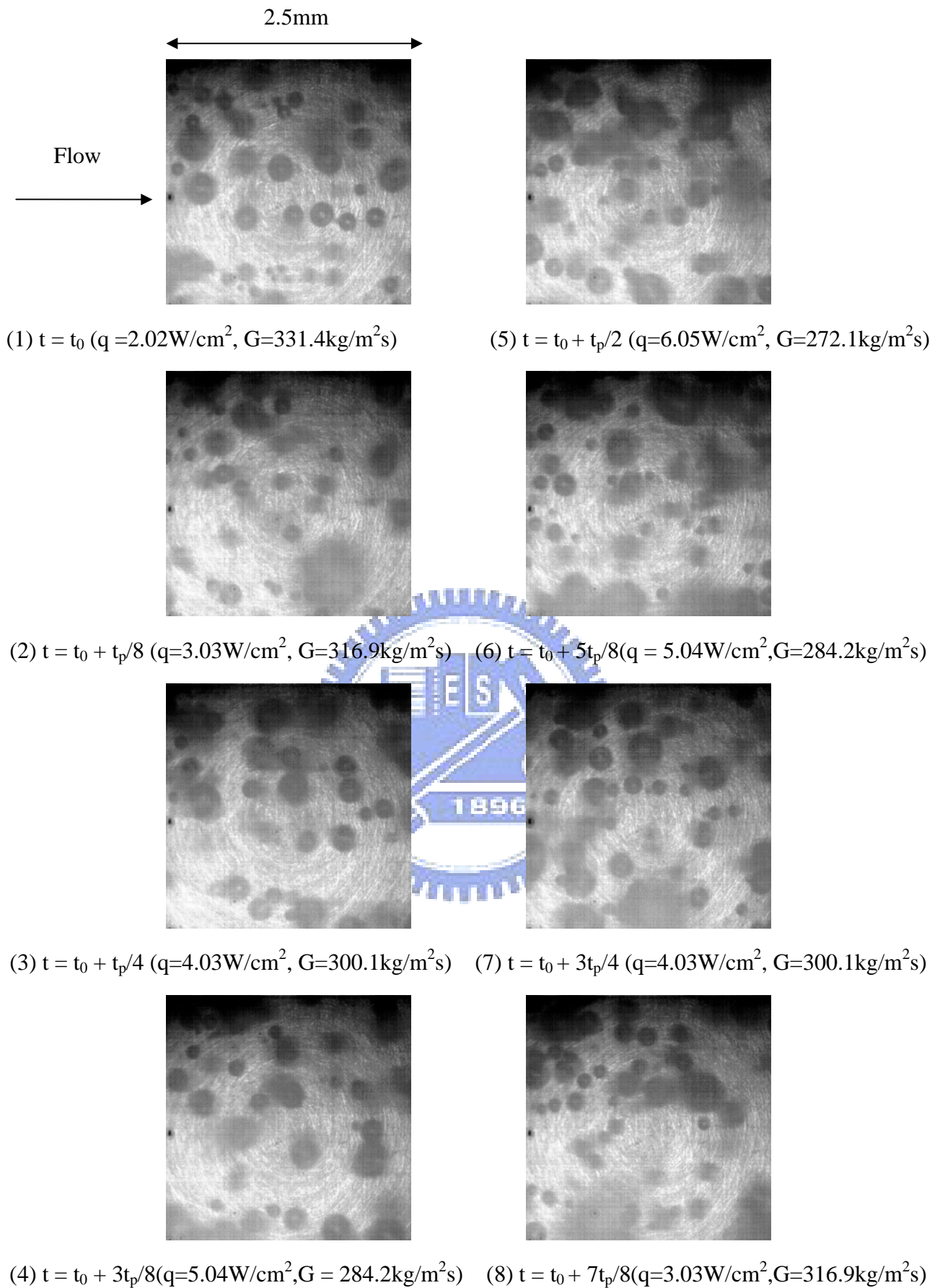


Fig. 4.43 Photos of saturated flow boiling at certain time instants in a typical time periodic cycle for imposed out-of-phase G & q oscillations at $\bar{G} = 300 \text{ kg/m}^2\text{s}$, $\Delta G/\bar{G} = 10\%$, $\bar{q} = 4.03 \text{ W/cm}^2$ and $\Delta q/\bar{q} = 50\%$ with $t_p = 20 \text{ sec}$.

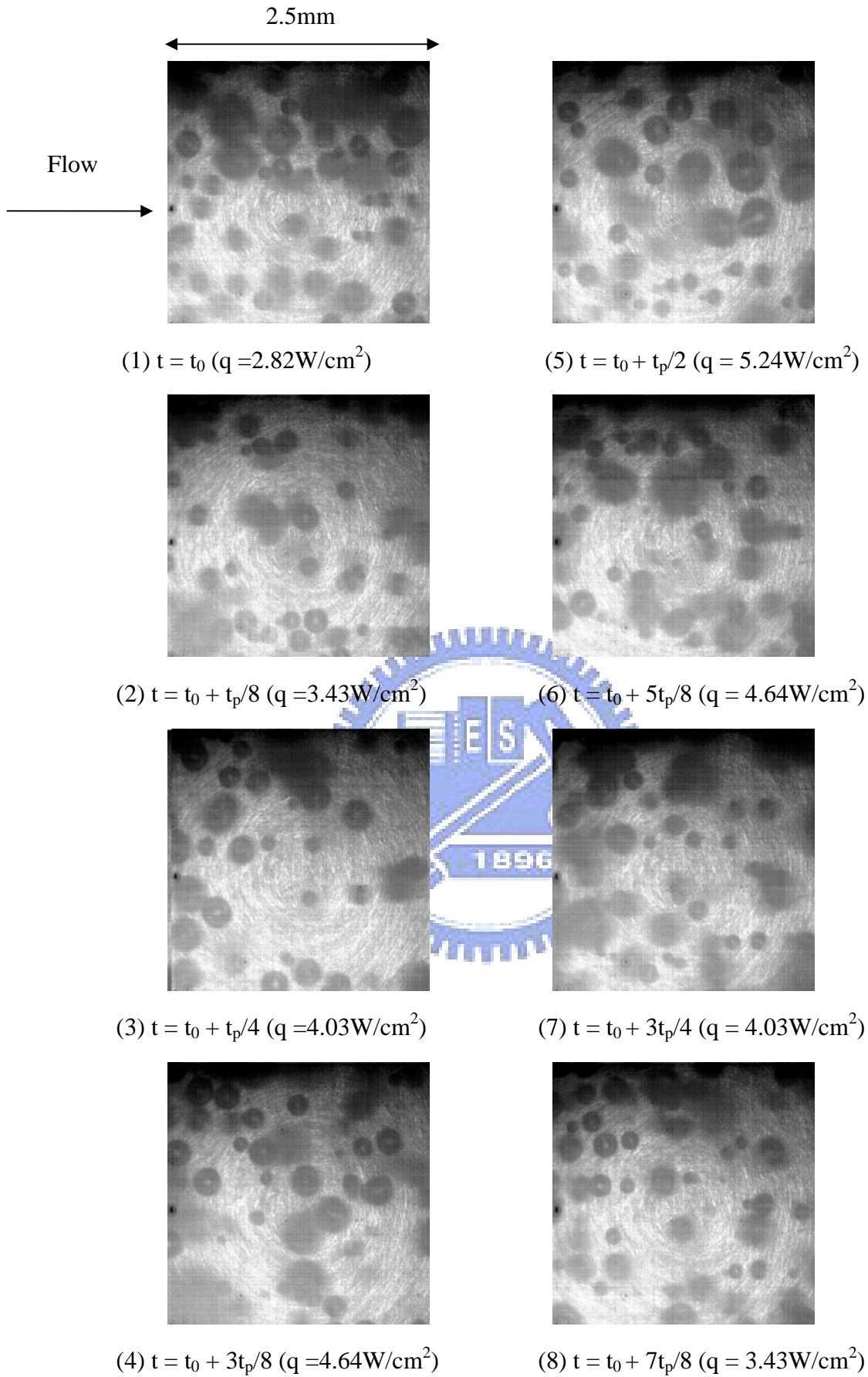


Fig. 4.44 Photos of saturated flow boiling at certain time instants in a typical time periodic cycle for an imposed constant mass flux at $\bar{q} = 4.03\text{W/cm}^2$, $\Delta q/\bar{q} = 30\%$, $G = 300\text{kg/m}^2\text{s}$ and $t_p = 30\text{sec}$.

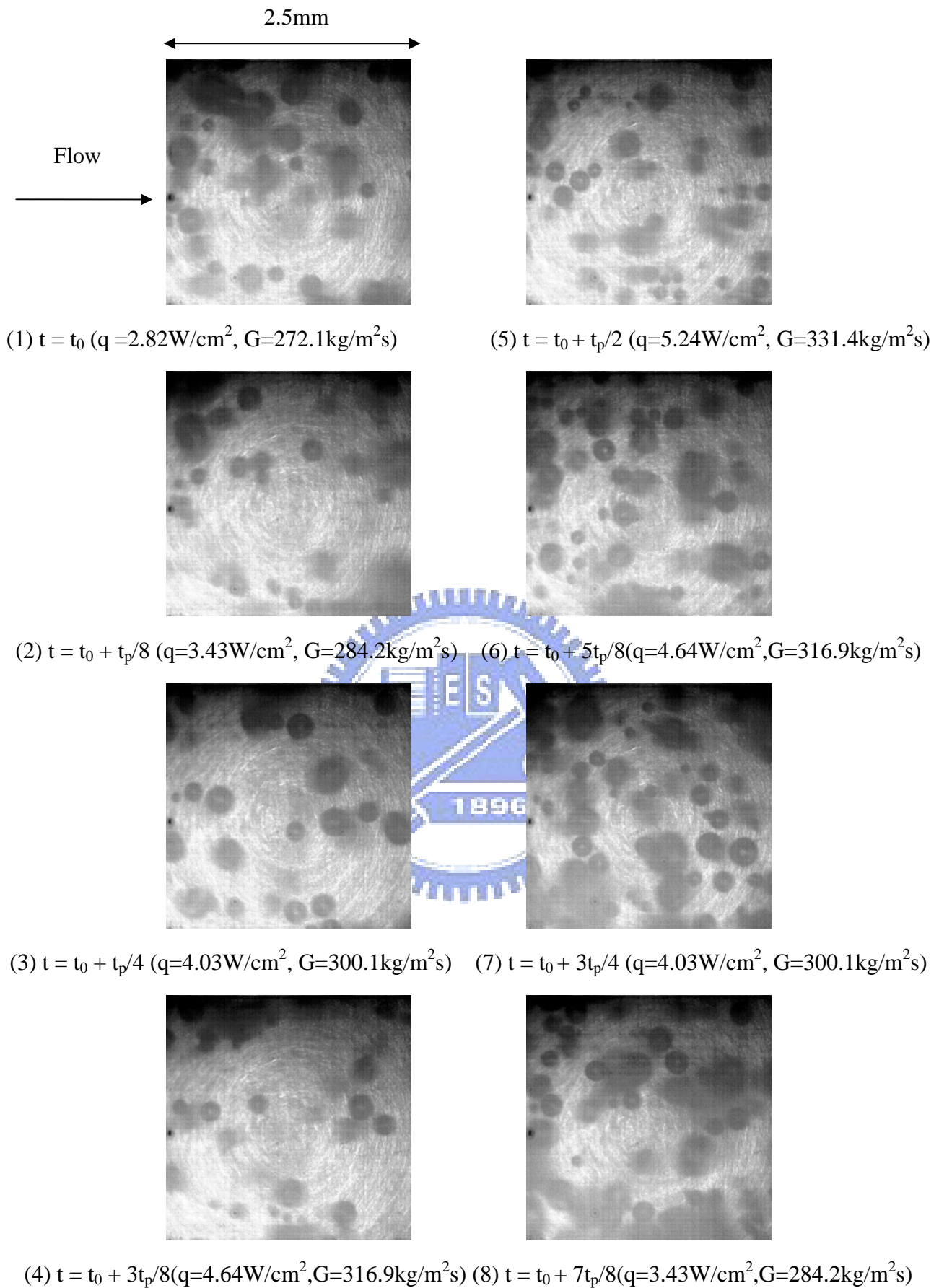


Fig. 4.45 Photos of saturated flow boiling at certain time instants in a typical time periodic cycle for imposed in-phase G & q oscillations at $\bar{G} = 300 \text{ kg/m}^2\text{s}$, $\Delta G/\bar{G} = 10\%$, $\bar{q} = 4.03 \text{ W/cm}^2$ and $\Delta q/\bar{q} = 30\%$ with $t_p = 30 \text{ sec}$.

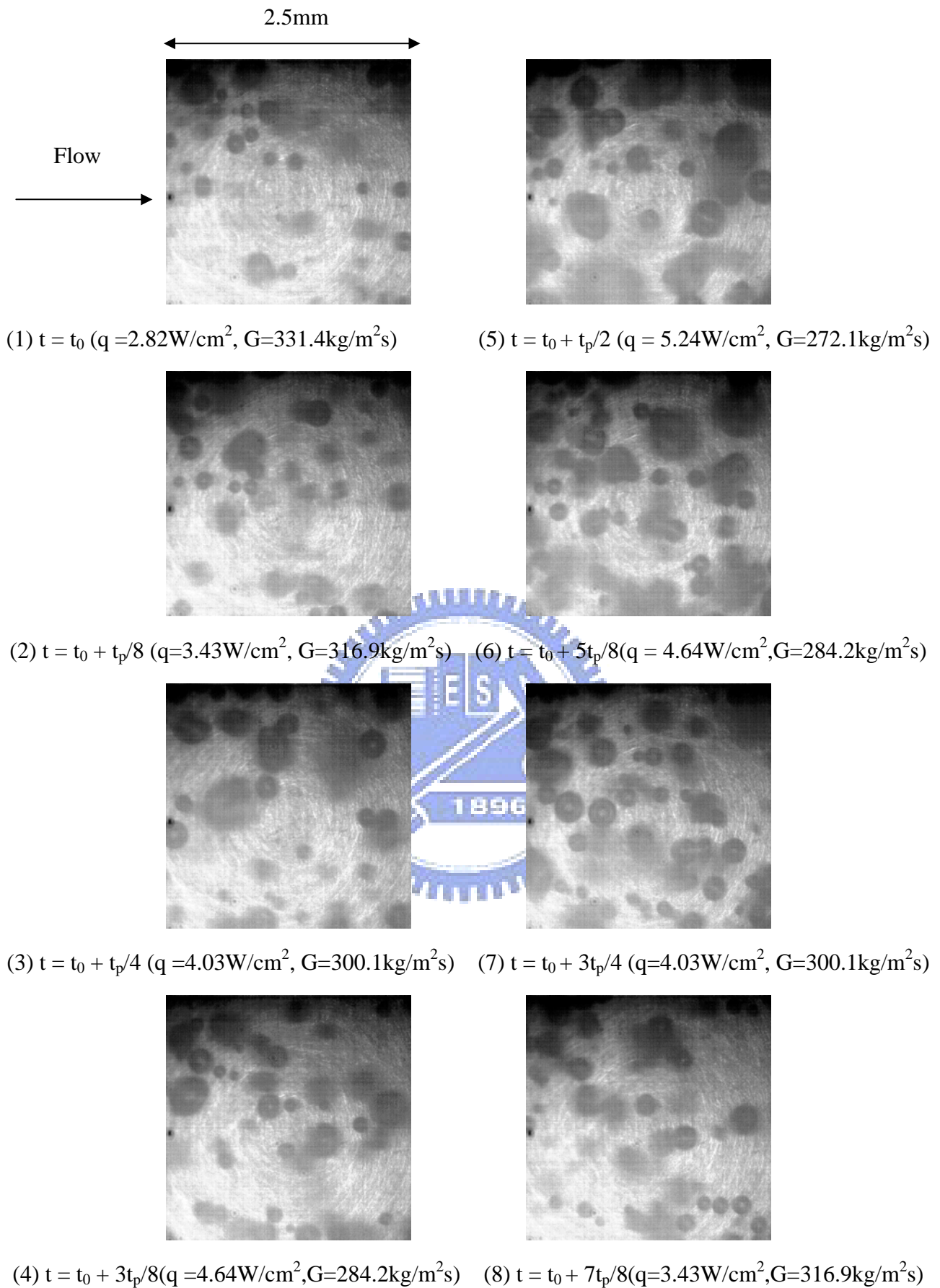


Fig. 4.46 Photos of saturated flow boiling at certain time instants in a typical time periodic cycle for imposed out-of-phase G & q oscillations at $\bar{G} = 300 \text{kg/m}^2\text{s}$, $\Delta G/\bar{G} = 10\%$, $\bar{q} = 4.03 \text{W/cm}^2$ and $\Delta q/\bar{q} = 30\%$ with $t_p = 30 \text{sec}$.

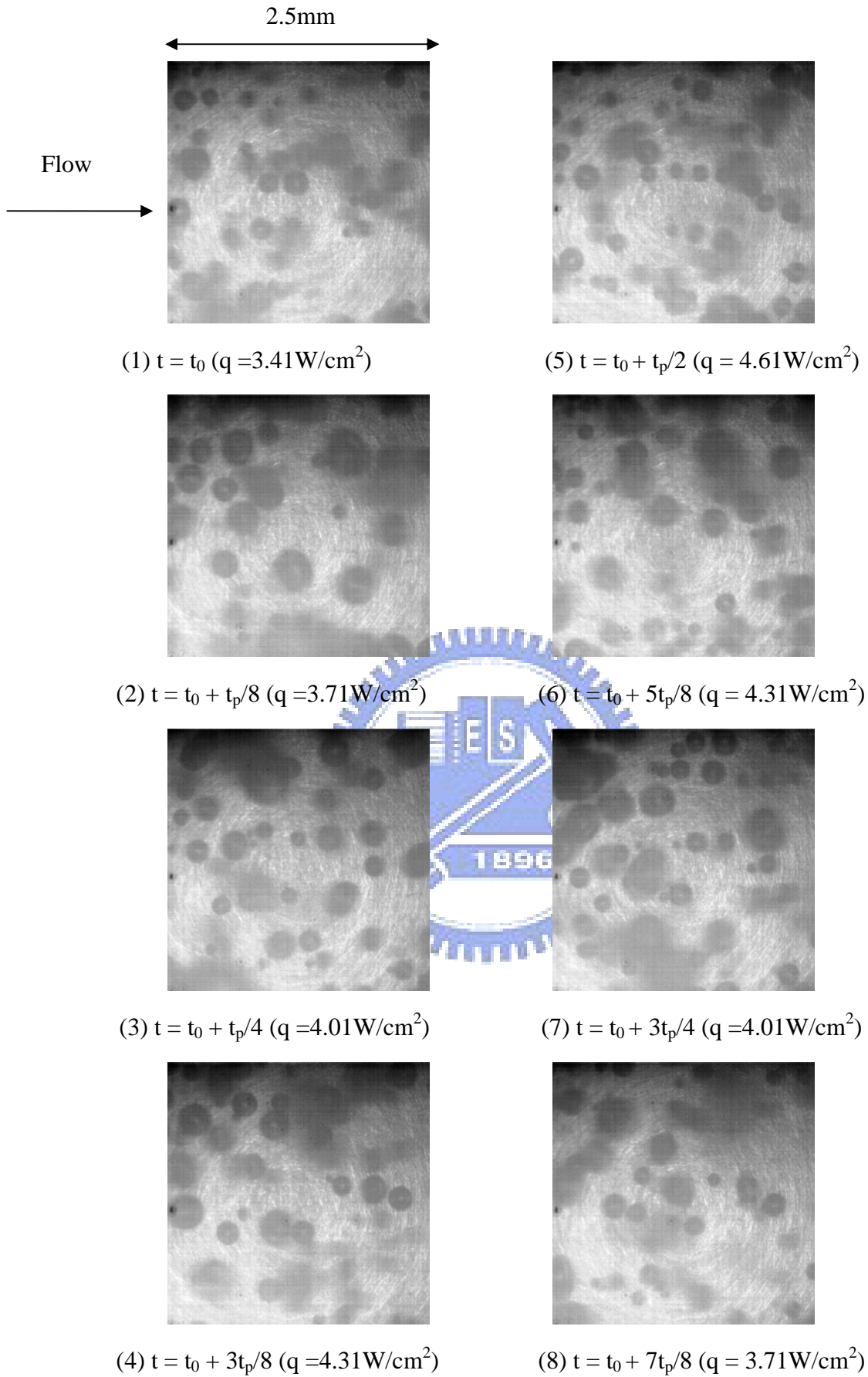


Fig. 4.47 Photos of subcooled flow boiling at certain time instants in a typical time periodic cycle for an imposed constant mass flux at $\bar{q} = 4.01 \text{ W/cm}^2$, $\Delta q / \bar{q} = 15\%$, $G = 300 \text{ kg/m}^2\text{s}$ with $t_p = 20 \text{ sec}$.

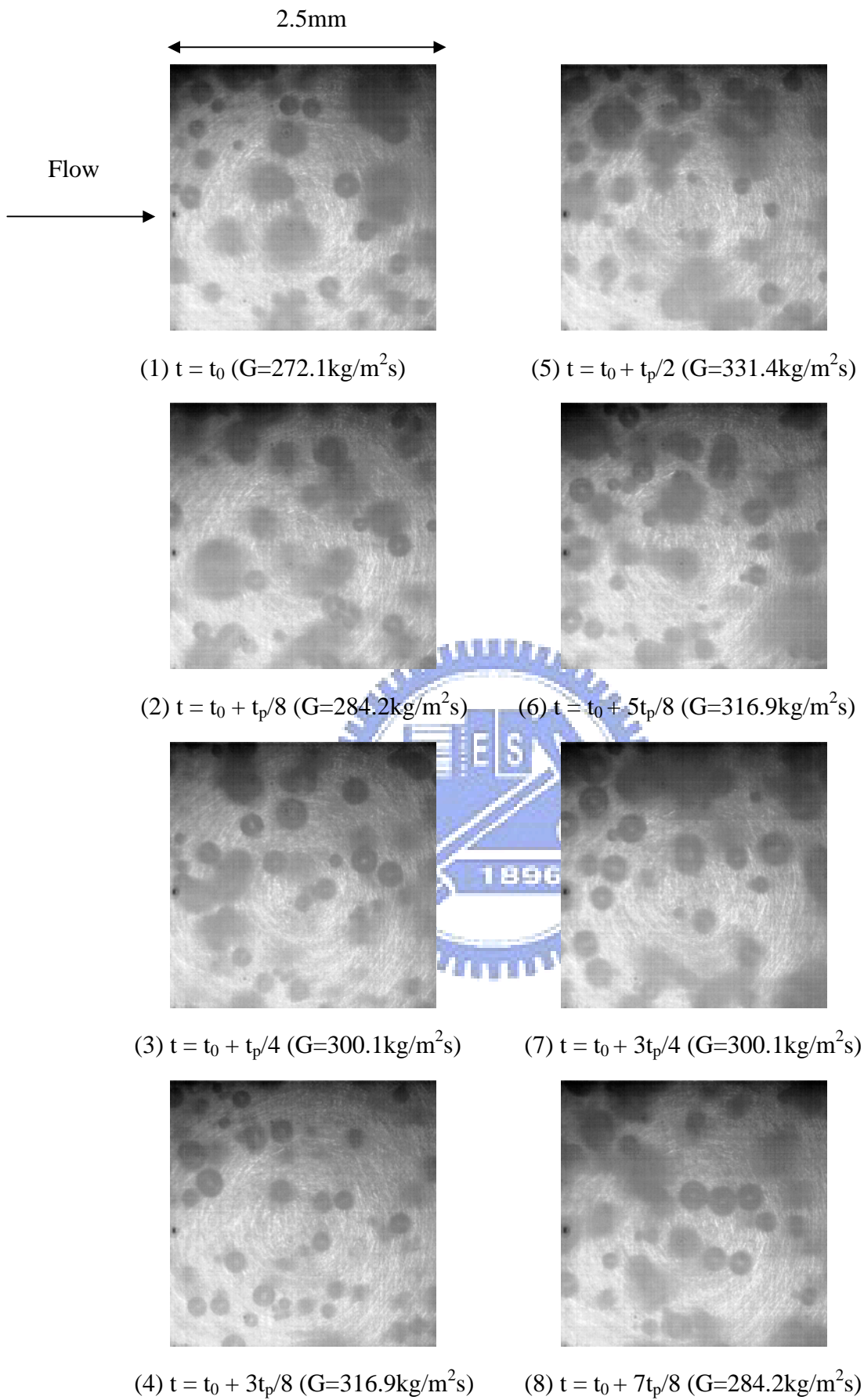


Fig. 4.48 Photos of subcooled flow boiling at certain time instants in a typical time periodic cycle for an imposed constant heat flux at $\bar{q}=4.01\text{W/cm}^2$, $G = 300\text{kg/m}^2\text{s}$, $\Delta G/\bar{G}=10\%$ with $t_p = 20\text{sec}$.

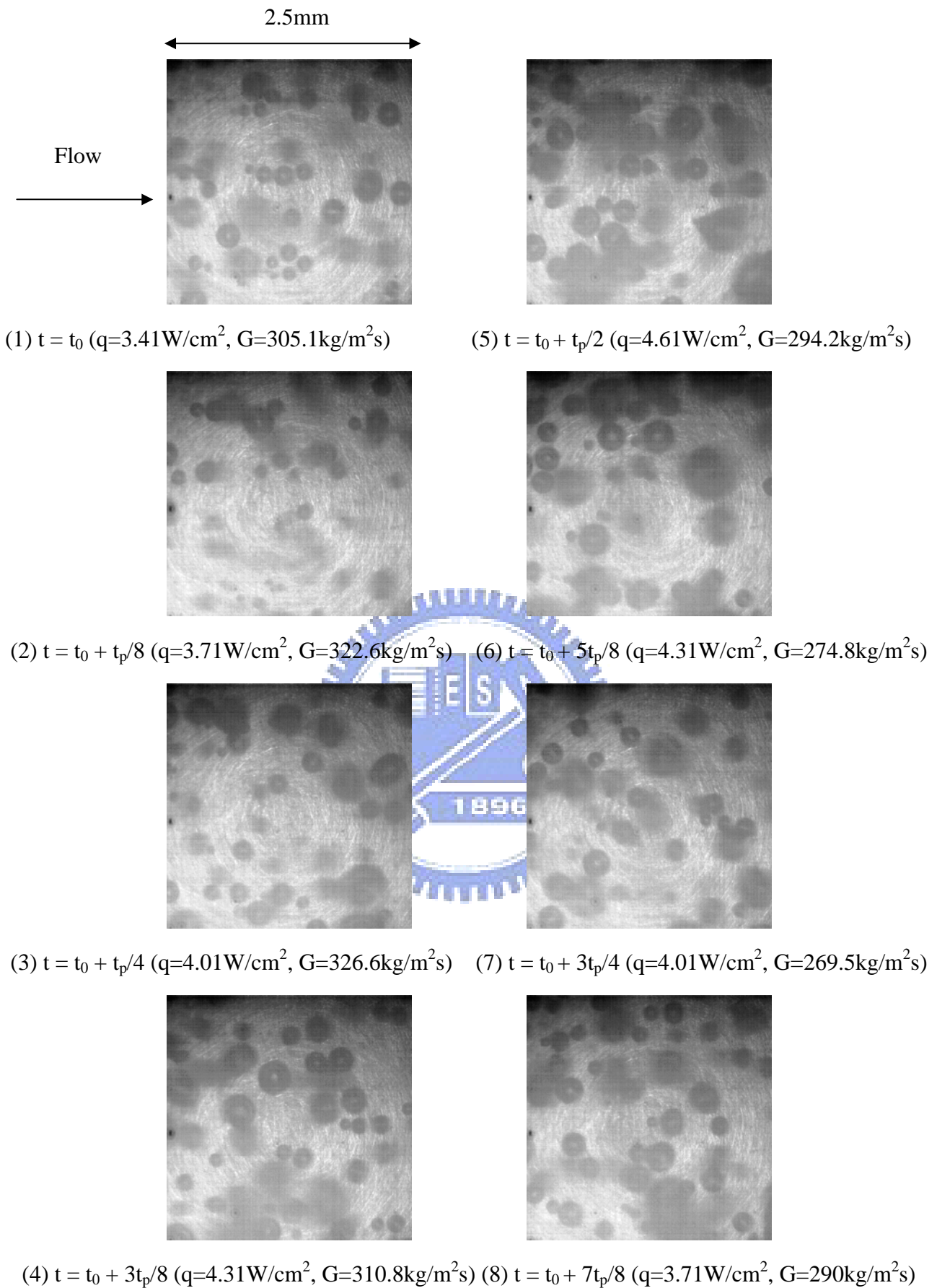


Fig. 4.49 Photos of subcooled flow boiling at certain time instants in a typical time periodic cycle for imposed out-of-phase G & q oscillations at $\bar{G}=300\text{kg/m}^2\text{s}$, $\Delta G/\bar{G}=10\%$, $\bar{q}=4.01\text{W/cm}^2$ and $\Delta q/\bar{q}=15\%$ with $t_p = 20\text{sec}$.

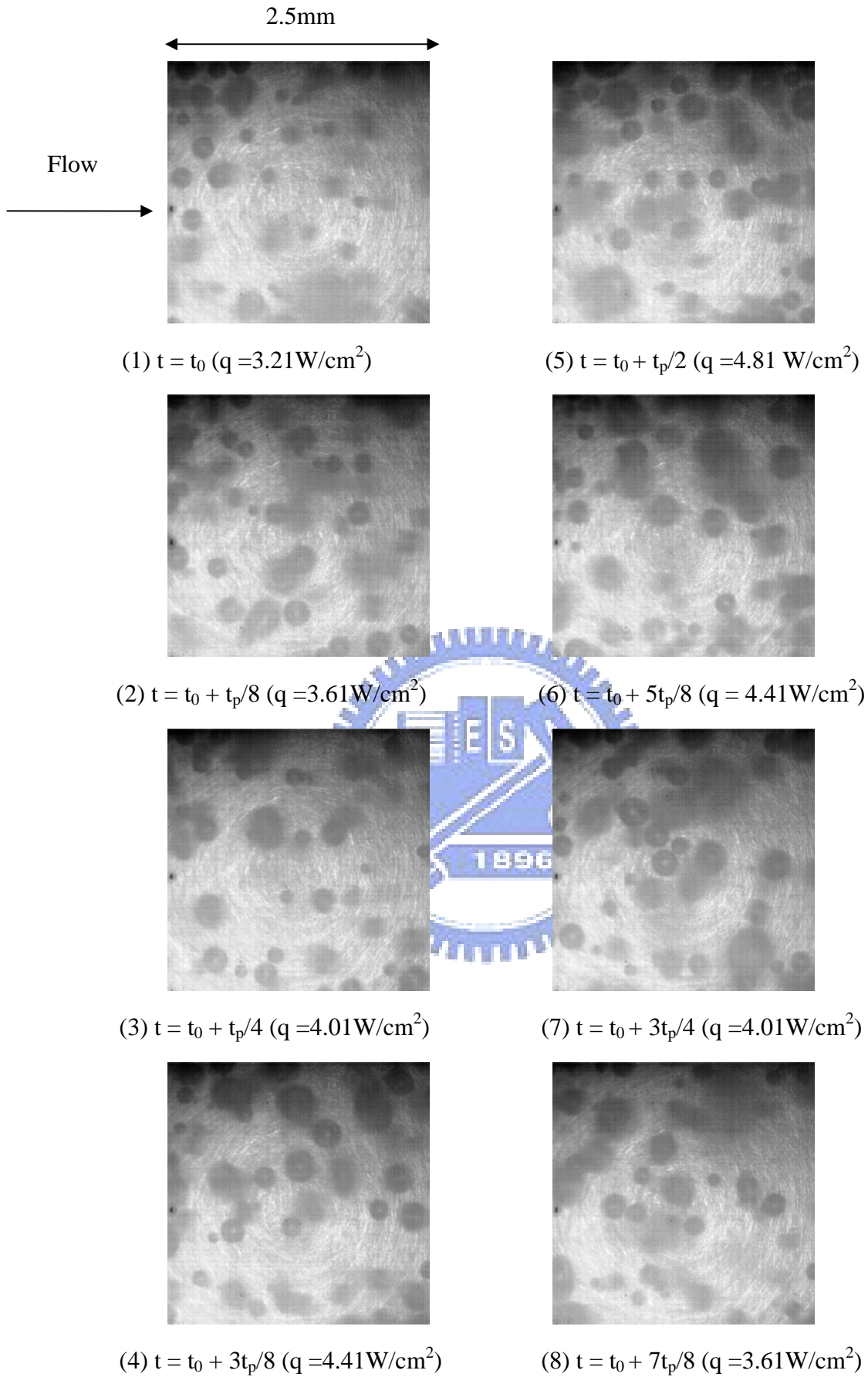


Fig. 4.50 Photos of subcooled flow boiling at certain time instants in a typical time periodic cycle for an imposed constant mass flux at $\bar{q} = 4.01 \text{ W/cm}^2$, $\Delta q/\bar{q} = 20\%$, $G = 300 \text{ kg/m}^2\text{s}$ with $t_p = 20 \text{ sec}$.

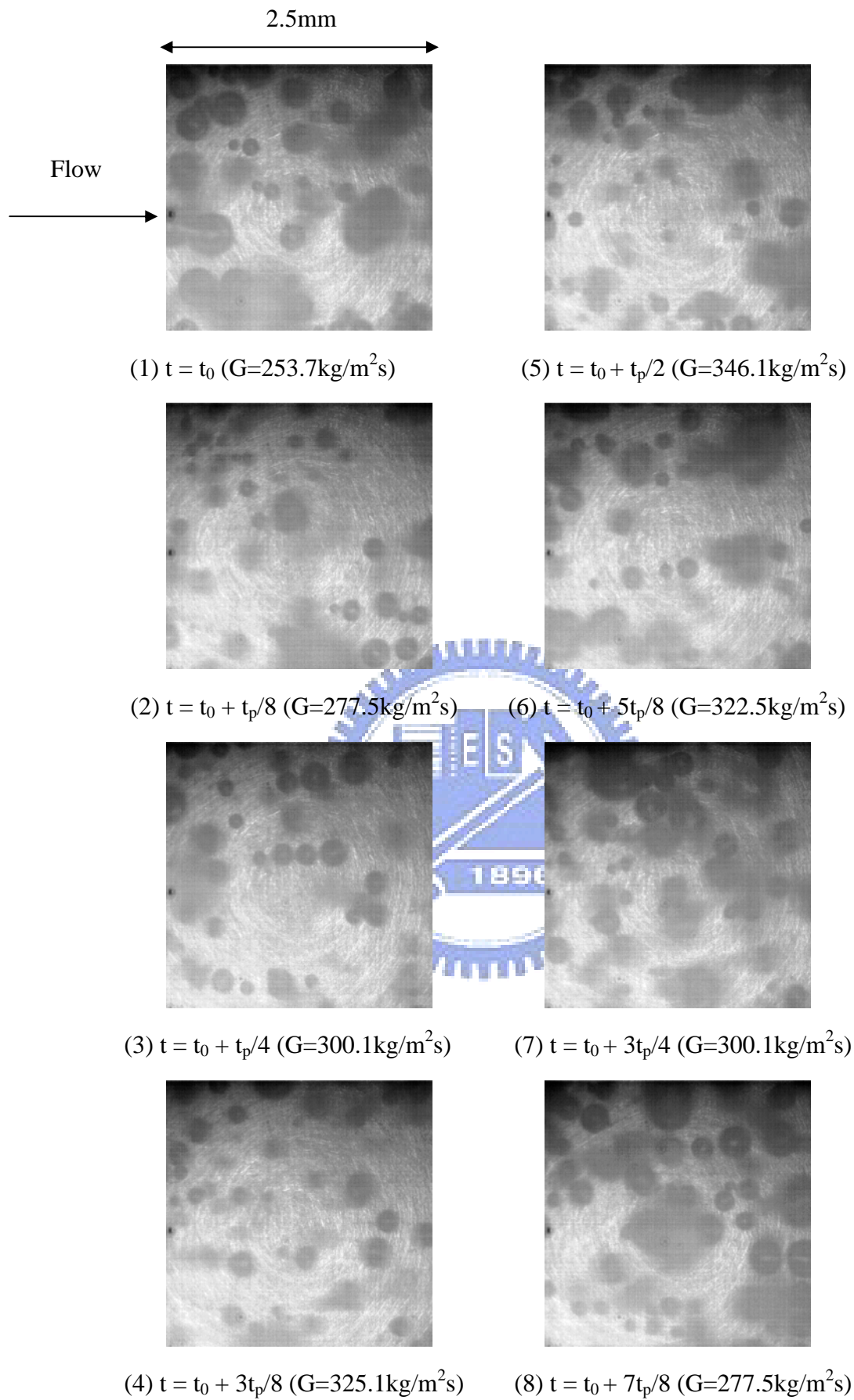


Fig. 4.51 Photos of subcooled flow boiling at certain time instants in a typical time periodic cycle for an imposed constant heat flux at $\bar{q}=4.01\text{W/cm}^2$, $G = 300\text{kg/m}^2\text{s}$, $\Delta G/\bar{G}=15\%$ with $t_p = 20\text{sec}$.

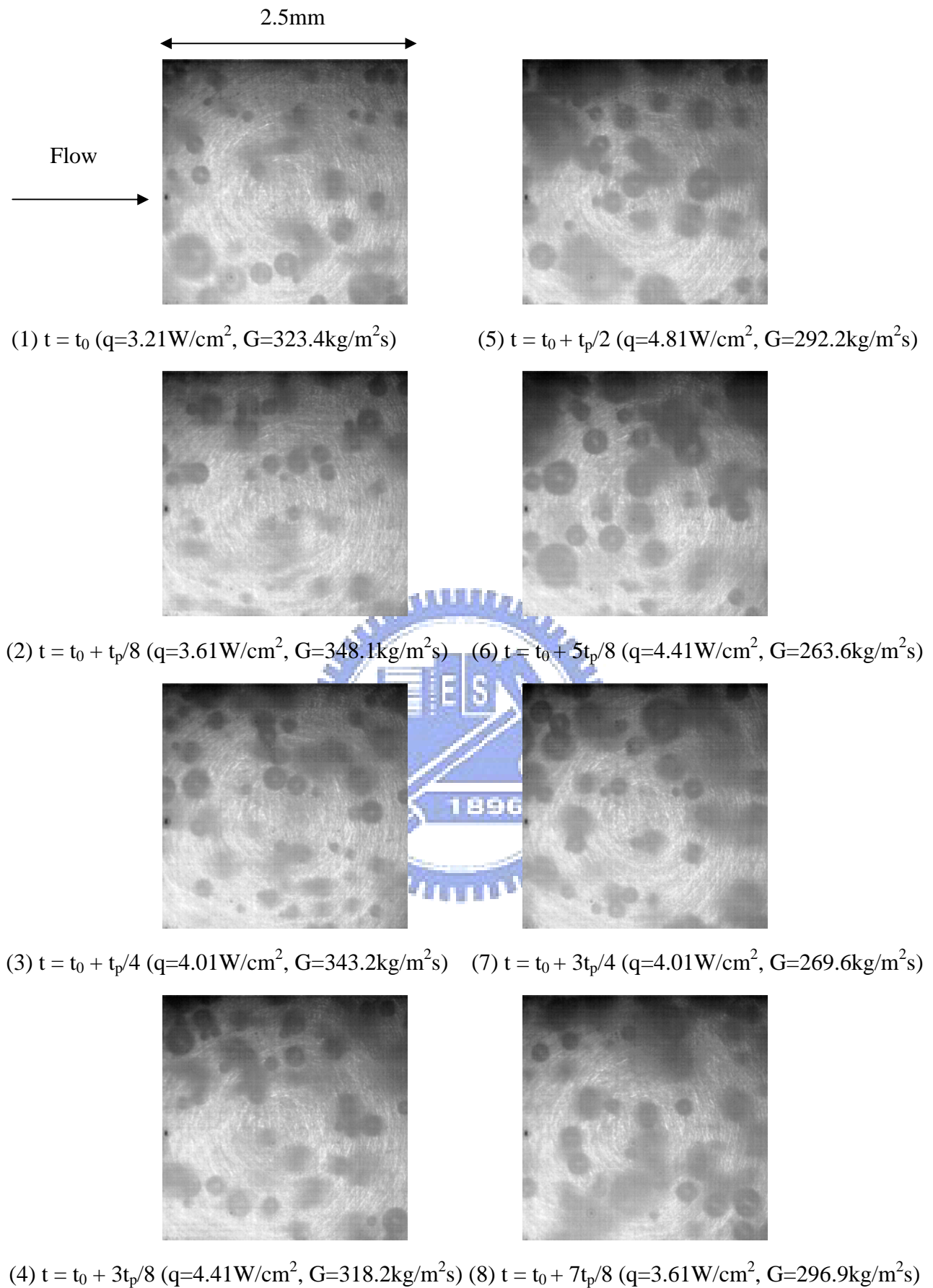


Fig. 4.52 Photos of subcooled flow boiling at certain time instants in a typical time periodic cycle for imposed out-of-phase G & q oscillations at $\bar{G}=300\text{kg/m}^2\text{s}$, $\Delta G/\bar{G}=15\%$, $\bar{q}=4.01\text{W/cm}^2$ and $\Delta q/\bar{q}=20\%$ with $t_p = 20\text{sec}$.

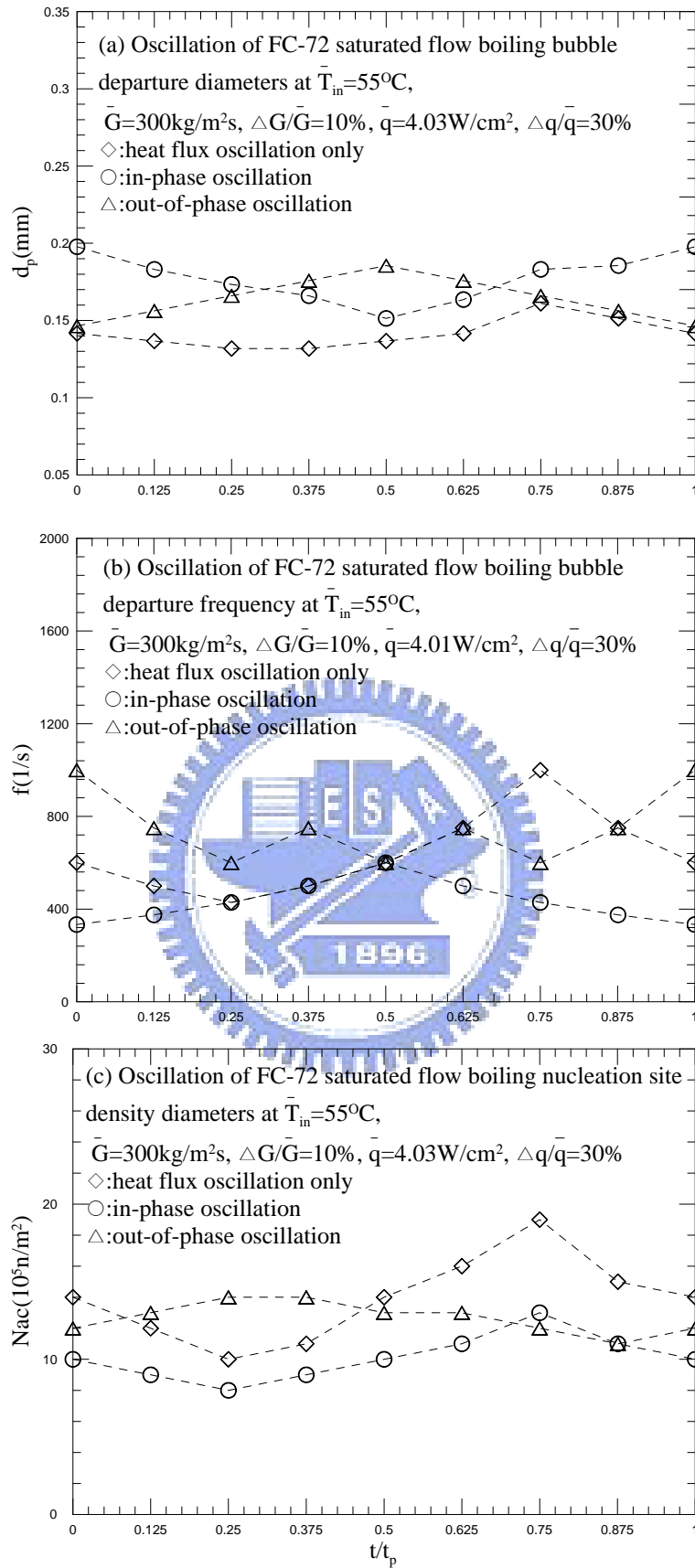


Fig. 4.53 Time period oscillatory saturated flow boiling of FC-72 with $\bar{q} = 4.03\text{W/cm}^2$, $\Delta q/\bar{q} = 30\%$, $G=300\text{kg/m}^2\text{s}$, $\Delta G/\bar{G} = 10\%$ and $t_p=20\text{sec}$. for the time variations of bubble characteristics: (a) bubble departure diameter (b) bubble departure frequency (c) active nucleation site density.

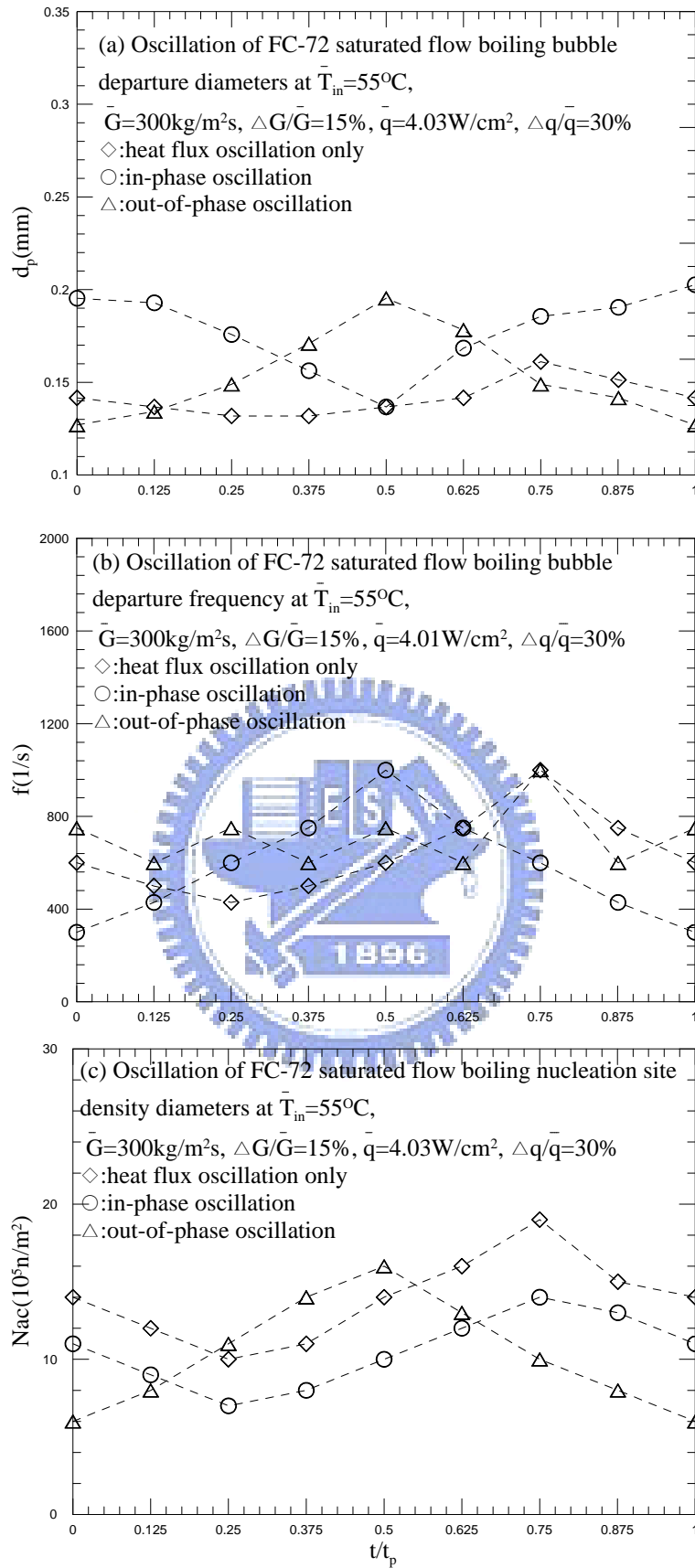


Fig. 4.54 Time period oscillatory saturated flow boiling of FC-72 with $\bar{q} = 4.03\text{W/cm}^2$, $\Delta q/\bar{q} = 30\%$, $G=300\text{kg/m}^2\text{s}$, $\Delta G/\bar{G} = 15\%$ and $t_p=20\text{sec}$. for the time variations of bubble characteristics: (a) bubble departure diameter (b) bubble departure frequency (c) active nucleation site density.

CHAPTER 5

TIME PERIODIC SUBCOOLED FLOW BOILING OF FC-72 OVER A SMALL HEATED COPPER PLATE

In the second part of the present study the coolant at the test section inlet is also kept at the liquid state and its temperature is controlled at a constant level below the time-average value of the refrigerated saturated temperature corresponding to the inlet pressure which oscillates time periodically with the coolant mass flux oscillation. Results obtained in the second part of the study are presented here to illustrate how the imposed simultaneous heat flux and mass flux oscillations affect the time periodic subcooled flow boiling heat transfer of FC-72 over a small heated circular copper flat plate flush mounted on the bottom of the horizontal rectangular channel. The present experiment is carried out for the mean FC-72 mass flux \bar{G} fixed at 200, 300 and 400 kg/m²s for the average inlet liquid subcooling $\Delta\bar{T}_{sub}$ of 5K, 10K and 15K with the time-average imposed heat flux \bar{q} varied from 0.1 W/cm² to 10 W/cm². Besides, the amplitude of the coolant mass flux oscillation ΔG is set at 0, 5, 10 and 15% of the mean coolant mass flux and the amplitude of the heat flux oscillation Δq is set at 10, 30 and 50% of the time-average heat flux. In addition, the period of the heat flux and mass flux oscillations t_p is fixed at 10, 20 and 30 seconds. Initially, the coolant FC-72 in the test section is at a slightly subatmospheric pressure of 99 KPa with the saturated temperature $T_{sat}=55^\circ\text{C}$ before each test is started. In the following, the effects of the experimental parameters including the mean levels and amplitudes and period of the heat and mass flux oscillations on the time periodic subcooled flow boiling will be explored for both in-phase and out-of-phase G and q oscillations. Note that for the limiting case of constant heat and mass fluxes ($\Delta q = 0$ and $\Delta G = 0$) we have subcooled boiling of FC-72 at constant q and G in the test section, which is designated as “stable subcooled flow boiling” in the present study. The heat transfer performance is mainly presented in terms of the time variations of the space-average surface temperature of the copper plate and boiling heat transfer coefficient.

5.1 Time Periodic Subcooled Flow Boiling Heat Transfer Characteristics

The time periodic boiling heat transfer characteristics for the subcooled FC-72 flow over the heated copper plate resulting from the imposed temporal heat flux and mass flux oscillations are illustrated by presenting the time variations of the space-average heated surface temperature T_w and heat transfer coefficient $h_{2\phi}$ for various $\Delta\bar{T}_{sub}$, \bar{G} , \bar{q} , $\Delta q/\bar{q}$, $\Delta G/\bar{G}$ and t_p . First, the measured time variations of T_w for the limiting cases of constant G and q are shown in Fig. 5.1 for $G=300$ and $400\text{kg/m}^2\text{s}$ at various q . These data indicate that the fluctuations in the space-average heated surface temperature with time for various q are relatively small. The resulting subcooled boiling in the flow for $\Delta G=0$ and $\Delta q=0$ can be regarded as at a statistically stable state. The corresponding boiling curves are shown in Fig. 5.2. The data in Fig. 5.2 show that the required heat flux and wall surperheat for the onset of nucleate boiling (ONB) are both higher for a higher coolant mass flux.

Next, we move further to examine the T_w data for the heat flux and coolant mass flux oscillating periodically in time respectively in forms of nearly a sinusoidal wave and a triangular wave. The results are given first in Fig. 5.3 for $\bar{G}=300\text{ kg/m}^2\text{s}$ and $t_p=20\text{ sec.}$ for $\Delta G/\bar{G}=10\%$ and $\Delta q/\bar{q}=30\%$ at various \bar{q} with $\Delta\bar{T}_{sub}=5\text{K}$. For comparison purpose the data for $\Delta G=0$ but $\Delta q>0$ are also shown in the figure. Besides, the data for both in-phase and out-of-phase G and q oscillations are presented. Note that for each case the temporal oscillation of the heated surface temperature is also periodic in time and is at the same frequency as the heat flux and/or mass flux. Moreover, the T_w oscillation gets slightly stronger for a higher mean level of the heat flux oscillation. A close inspection of these data further reveals that the heated surface temperature oscillation lags significantly behind the imposed heated flux oscillation for constant G and for both in-phase and out-of-phase G and q oscillations. This time lag in T_w results mainly from the thermal inertia of the copper plate since the time lag in T_w due to the mass flux oscillation is small[52]. We also note that in the single-phase flow prevailed only at low imposed heat flux the time lag can be even longer than that for the flow boiling. Table 5.1 summarizes the quantitative data for the

amplitude of the heated surface temperature oscillation T_w and the relative magnitude of the time lag t_l/t_p . The results clearly manifest that for the temporal subcooled flow boiling the time lag in T_w is somewhat longer when G and q are in out-of-phase oscillations than the other situations. It is of interest to note that in the single-phase flow the T_w oscillation is strongest for the out-of-phase G and q oscillations. But the T_w oscillation is weakened for the out-of-phase G and q oscillations than that for the in-phase G and q oscillations in the flow boiling which prevails at high imposed heat flux, showing that the T_w oscillation is suppressed by the out-of-phase oscillations. This unusual outcome requires in-depth examination of the detailed heat transfer mechanisms in the boiling flow subject to the simultaneous G and q oscillations. Here we provide preliminary interpretation. When only the heat flux oscillation exists, the heated surface temperature increases with the heat flux for both single- and two-phase flows after accounting for the time lag, as evident from Fig. 5.3(a). But when only the mass flux oscillation exists, our previous study[52] showed that in the two-phase boiling flow T_w decreases at decreasing mass flux due to drastic increase in the active bubble nucleation site density. The trend is reversed for the single-phase flow. This explains why an out-of-phase mass flux oscillation can reduce the T_w oscillation in the boiling flow and can intensify the T_w oscillation in the single-phase flow.

Effects of the experimental parameters on the T_w oscillation are illustrated in Figs. 5.4-5.12. The results indicate that the heated surface temperature oscillates in a larger amplitude for higher oscillation amplitudes in the heat flux and mass flux. It is worth noting that an increase in the period of the G and q oscillations also causes a much stronger T_w oscillation, as evident by comparing the data in Fig. 5.7 with that in Figs. 5.12. Besides, comparing the data in Figs. 5.3, 5.7 and 5.11 reveals that a raise in the inlet liquid subcooling results in a stronger T_w oscillation. To be more quantitative, we summarize the present data for the amplitude and time lag of the T_w oscillation in Tables 5.2-5.8 for various \bar{G} , $\Delta G/\bar{G}$, t_p , \bar{q} , $\Delta q/\bar{q}$ and ΔT_{sub} . It is of interest to note that out-of-phase G & q oscillations do not always weaken the T_w oscillation in the boiling flow. Similarly, in-phase G & q oscillations may not reduce the T_w oscillation in the single-phase flow especially at high $\Delta q/\bar{q}$. We

also note that the relative time lag t_l/t_p varies nonmonotonically with the experimental parameters.

At this point we move further to investigate whether it is possible to completely suppress the heated surface temperature oscillation driven by a given time periodic heat flux oscillation by choosing an appropriate in-phase or out-of-phase mass flux oscillation in the single-phase flow and the subcooled flow boiling. It is noted in this investigation that the chosen mass flux oscillation should be at a suitable amplitude and at the same period as the heat flux oscillation. Most importantly, the time lags in the T_w oscillation due to the q and G oscillations have to be taken into consideration. The results from this investigation are illustrated in Figs. 5.13, 5.14 and 5.15 for $\bar{G}=300\text{kg/m}^2\text{s}$, $\Delta G/\bar{G}=5\%$, 10% & 15% and $t_p=20\text{sec}$ for several \bar{q} . Here in the single-phase flow an in-phase G oscillation is imposed. But an out-of-phase G oscillation is imposed in the two-phase boiling flow. Note that a small time lag in the T_w oscillation also exists due to the mass flux oscillation(Figs. 5.13(b), 5.14(b) and 5.15(b)), as already mentioned above. The results in Fig. 5.13 indicate that as the G oscillation is imposed at a time instant behind the q oscillation by the difference in the time lags respectively due to the q and G oscillations, the T_w oscillations can indeed be suppressed to be relatively small in magnitude (Fig. 5.13(c)) for the case with $\bar{q}=4.08$ and 2.08W/cm^2 . In fact, the resulting T_w oscillation amplitude is below 0.1°C which is smaller than the thermal disturbances in the background and the experimental uncertainty in measuring the temperature by the thermocouples. Hence the heated surface temperature can be regarded at steady state. At higher \bar{q} the T_w oscillation can only be suppressed to a significant degree.

The associated heat transfer coefficients for the single-phase and boiling flows affected by the imposed heat and mass flux oscillations are presented in Figs. 5.16-5.25. The results indicate that the oscillation in the heat transfer coefficient exhibits a similar trend to the heated surface temperature oscillation. Specifically, the $h_{1\phi}$ and $h_{2\phi}$ oscillations are also periodic in time and are at the same frequency as the heat flux and/or mass flux. Besides, at a higher \bar{q} the oscillations in $h_{1\phi}$ and $h_{2\phi}$ are slightly stronger. But the oscillation amplitudes in $h_{1\phi}$ and $h_{2\phi}$ depend only slightly on the in-phase or out-of-phase G and q oscillations. Moreover, $h_{1\phi}$ and $h_{2\phi}$ are in stronger oscillations

for a higher amplitude and a longer period of the imposed G and q oscillations.

5.2 Bubble Characteristics

To elucidate the above time periodic subcooled flow boiling heat transfer characteristics, the data for the bubble characteristics of FC-72 obtained from the present flow visualization are examined in the following. The photos taken from the top view of the boiling flow in a small region around the geometric center of the heated surface for various coolant mass fluxes and imposed heat fluxes are shown in Figs. 5.29 - 5.49. At first, the bubble characteristics for the limiting cases of constant imposed heat and mass fluxes are illustrated by the photos in Fig. 5.29. It is noted in the flow visualization and the results in Fig. 5.29 that in the stable flow boiling the vapor bubbles begin to appear as the heated surface temperature exceeds that required for the boiling incipient superheat. In the beginning, tiny bubbles are observed in the active nucleation sites. The bubbles grow and then detach from the heated surface with certain bubble departure diameters. As the imposed heat flux increases, more bubbles are generated on more active nucleation sites and more bubbles detach from the heated surface. Besides, the detached bubbles tend to merge into larger bubbles. Note that the large bubbles become distorted and elongated as they slide on the heating surface. Moreover, at a higher mass flux the bubbles are smaller and the bubble coalescence is less significant for a given heat flux.

Next, the bubble characteristics in the time periodic subcooled flow boiling are illustrated by presenting the photos of the boiling flow at eight selected time instants in a typical periodic cycle in Figs. 5.30-5.49. In these figures the symbol “ $t=t_0$ ” signifies the time instant at which the instantaneous heat flux is at the lowest levels and starts to increase with time and the mass flux is also at the lowest level and starts to increase with time for the in-phase G and q oscillations. But for the out-of-phase G and q oscillations at t_0 the mass flux is at the highest level and starts to decrease with time.

The results in Fig. 5.30 for an imposed heat flux oscillation at a given constant G of 200 $\text{kg/m}^2\text{s}$ qualitatively indicate that in the first half of the periodic cycle in which the surface heat flux

increases with time the bubbles grow with time and merge together to form big bubbles. Besides, more bubbles nucleate from the heated surface. The bubbles are in rigorous motion and the photos become somewhat blurred as the heat flux exceeds certain level. In the second half of the cycle the opposite processes take place. It is important to point out that the bubble behavior in the boiling flow affected by the mass flux oscillation exhibits an opposite trend [52]. Specifically, at increasing mass flux in the first half of the periodic cycle the bubbles get smaller and become more disperse. Besides, less bubble nucleation occurs on the heated surface. Thus, when the G and q oscillations are in-phase, the bubble behavior is counter-balanced by two opposite effects and its change with time is rather mild (Figs. 5.31, 5.34, 5.36, 5.39, 5.42, 5.45) except for some cases with large differences in the amplitudes of heat and mass flux oscillations (Figs. 5.34, 5.35). But when G and q are in out-of-phase oscillations the two effects augment each other and the bubble behavior can show drastic variation with time (Figs. 5.32, 5.35, 5.37, 5.40, and 5.43). Moreover, at higher $\Delta G/\bar{G}$ and $\Delta q/\bar{q}$ and at a longer t_p , the bubble characteristics experience stronger time variations.

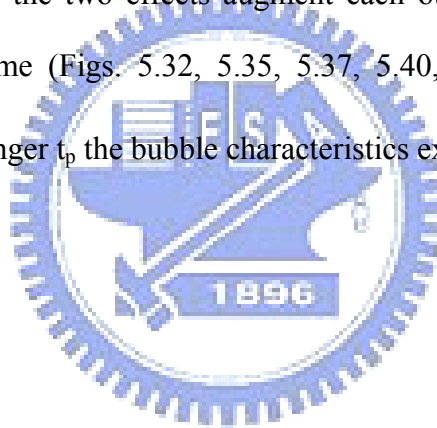


Table 5.1 Amplitudes of T_w oscillation and relative time lags in transient oscillatory subcooled flow boiling for various \bar{q} for $\Delta q/\bar{q}=30\%$, $\Delta G/\bar{G}=10\%$ and $t_p=20\text{sec}$. at $\bar{G}=300\text{kg/m}^2\text{s}$ and $\Delta T_{sub}=5\text{K}$.

$\Delta G/\bar{G}$	Period $t_p(\text{sec})$	$\Delta q/\bar{q}$	$G = 300\text{kg/m}^2\text{s}$			
			$\bar{q}(\text{W/cm}^2)$	$\Delta T_{sub}=5\text{K}$	$\Delta T_w(K)$	t_1/t_p
10%	20	30%	1.11 (single phase)	Heat flux oscillation only	0.27	0.35
				In-phase G & q oscillations	0.25	0.375
				Out-of-phase G & q oscillations	0.3	0.35
			3.88	Heat flux oscillation only	0.55	0.25
				In-phase G & q oscillations	0.81	0.175
				Out-of-phase G & q oscillations	0.59	0.45
			5.13	Heat flux oscillation only	0.57	0.25
				In-phase G & q oscillations	0.94	0.15
				Out-of-phase G & q oscillations	0.77	0.475
			6.08	Heat flux oscillation only	1.69	0.225
				In-phase G & q oscillations	0.99	0.125
				Out-of-phase G & q oscillations	0.74	0.45

Table 5.2 Amplitudes of T_w oscillation and relative time lags in transient oscillatory subcooled flow boiling for various \bar{q} for $\Delta q/\bar{q}=30\%$, $\Delta G/\bar{G}=10\%$ and $t_p=20\text{sec}$. at $\bar{G}=200\text{kg/m}^2\text{s}$ and $\Delta T_{sub}=10\text{K}$.

$\Delta G/\bar{G}$	Period $t_p(\text{sec})$	$\Delta q/\bar{q}$	$G = 200\text{kg/m}^2\text{s}$			
			$\bar{q}(\text{W/cm}^2)$	$\Delta T_{sub}=10\text{K}$	$\Delta T_w(K)$	t_1/t_p
10%	20	30%	2.01 (single phase)	Heat flux oscillation only	0.46	0.35
				In-phase G & q oscillations	0.41	0.425
				Out-of-phase G & q oscillations	0.57	0.325
			2.88	Heat flux oscillation only	0.55	0.3
				In-phase G & q oscillations	0.80	0.2
				Out-of-phase G & q oscillations	0.55	0.5
			4.01	Heat flux oscillation only	0.60	0.275
				In-phase G & q oscillations	0.81	0.075
				Out-of-phase G & q oscillations	0.80	0.525
			6.18	Heat flux oscillation only	0.64	0.25
				In-phase G & q oscillations	1.37	0.075
				Out-of-phase G & q oscillations	1.13	0.5

Table 5.3 Amplitudes of T_w oscillation and relative time lags in transient oscillatory subcooled flow boiling for various \bar{q} for $\Delta q/\bar{q}=30\%$, $\Delta G/\bar{G}=5\%$ and $t_p=20\text{sec}$. at $\bar{G}=300\text{kg/m}^2\text{s}$ and $\Delta T_{sub}=10\text{K}$.

$\Delta G/\bar{G}$	Period $t_p(\text{sec})$	$\Delta q/\bar{q}$	$G = 300\text{kg/m}^2\text{s}$			
			$\bar{q}(\text{W/cm}^2)$	$\Delta T_{sub}=10\text{K}$	$\Delta T_w(K)$	t_1/t_p
5%	20	30%	2.08 (single phase)	Heat flux oscillation only	0.46	0.35
				In-phase G & q oscillations	0.46	0.375
				Out-of-phase G & q oscillations	0.5	0.225
			3.94	Heat flux oscillation only	0.67	0.275
				In-phase G & q oscillations	0.81	0.225
				Out-of-phase G & q oscillations	0.55	0.35
			6.08	Heat flux oscillation only	0.71	0.25
				In-phase G & q oscillations	1.04	0.175
				Out-of-phase G & q oscillations	0.72	0.425
			7.08	Heat flux oscillation only	0.71	0.225
				In-phase G & q oscillations	1.00	0.125
				Out-of-phase G & q oscillations	0.76	0.4

Table 5.4 Amplitudes of T_w oscillation and relative time lags in transient oscillatory subcooled flow boiling for various \bar{q} for $\Delta q/\bar{q}=30\%$, $\Delta G/\bar{G}=15\%$ and $t_p=20\text{sec}$. at $\bar{G}=300\text{kg/m}^2\text{s}$ and $\Delta T_{sub}=10\text{K}$.

$\Delta G/\bar{G}$	Period $t_p(\text{sec})$	$\Delta q/\bar{q}$	$G = 300\text{kg/m}^2\text{s}$			
			$\bar{q}(\text{W/cm}^2)$	$\Delta T_{sub}=10\text{K}$	$\Delta T_w(K)$	t_1/t_p
15%	20	30%	2.08 (single phase)	Heat flux oscillation only	0.46	0.35
				In-phase G & q oscillations	0.34	0.425
				Out-of-phase G & q oscillations	0.59	0.3
			3.94	Heat flux oscillation only	0.67	0.275
				In-phase G & q oscillations	1.19	0.15
				Out-of-phase G & q oscillations	0.79	0.525
			6.08	Heat flux oscillation only	0.71	0.25
				In-phase G & q oscillations	1.85	0.075
				Out-of-phase G & q oscillations	1.62	0.525
			7.08	Heat flux oscillation only	0.70	0.225
				In-phase G & q oscillations	2.07	0.05
				Out-of-phase G & q oscillations	1.76	0.525

Table 5.5 Amplitudes of T_w oscillation and relative time lags in transient oscillatory subcooled flow boiling for various \bar{q} for $\Delta q/\bar{q}=10,30,50\%$, $\Delta G/\bar{G}=10\%$ and $t_p=20\text{sec}$ at $\bar{G}=300\text{kg/m}^2\text{s}$ and $\Delta\bar{T}_{sub}=10\text{K}$.

$\Delta G/\bar{G}$	Period $t_p(\text{sec})$	$\Delta q/\bar{q}$	$G = 300\text{kg/m}^2\text{s}$			
			$\bar{q}(\text{W/cm}^2)$	$\Delta\bar{T}_{sub}=10\text{K}$	$\Delta T_w(K)$	t_1/t_p
10%	20	10%	2.04 (single phase)	Heat flux oscillation only	0.16	0.4
				In-phase G & q oscillations	0.15	0.525
				Out-of-phase G & q oscillations	0.23	0.25
			4.4	Heat flux oscillation only	0.23	0.3
				In-phase G & q oscillations	0.72	0.125
				Out-of-phase G & q oscillations	0.54	0.575
			6.05	Heat flux oscillation only	0.24	0.325
				In-phase G & q oscillations	1.09	0.05
				Out-of-phase G & q oscillations	0.96	0.55
		7.09	Heat flux oscillation only	0.24	0.25	
			In-phase G & q oscillations	1.23	0.05	
			Out-of-phase G & q oscillations	1.13	0.5	
		30%	2.04 (single phase)	Heat flux oscillation only	0.46	0.375
				In-phase G & q oscillations	0.41	0.4
				Out-of-phase G & q oscillations	0.51	0.35
			4.4	Heat flux oscillation only	0.68	0.3
				In-phase G & q oscillations	1.05	0.2
				Out-of-phase G & q oscillations	0.75	0.5
			6.05	Heat flux oscillation only	0.69	0.25
				In-phase G & q oscillations	1.24	0.1
				Out-of-phase G & q oscillations	1.07	0.525
		7.09	Heat flux oscillation only	0.70	0.3	
			In-phase G & q oscillations	1.34	0.1	
			Out-of-phase G & q oscillations	1.14	0.525	
		50%	2.04 (single phase)	Heat flux oscillation only	0.74	0.35
				In-phase G & q oscillations	0.70	0.35
				Out-of-phase G & q oscillations	0.79	0.35
4.4	Heat flux oscillation only		1.13	0.25		
	In-phase G & q oscillations		1.46	0.225		
	Out-of-phase G & q oscillations		0.98	0.375		
6.05	Heat flux oscillation only		1.16	0.25		
	In-phase G & q oscillations		1.77	0.15		
	Out-of-phase G & q oscillations		1.30	0.425		
7.09	Heat flux oscillation only	1.18	0.25			
	In-phase G & q oscillations	1.73	0.175			
	Out-of-phase G & q oscillations	1.34	0.425			

Table 5.6 Amplitudes of T_w oscillation and relative time lags in transient oscillatory subcooled flow boiling for various \bar{q} for $\Delta q/\bar{q} = 30\%$, $\Delta G/\bar{G} = 10\%$ and $t_p = 20\text{sec}$ at $\bar{G} = 400\text{kg/m}^2\text{s}$ and $\Delta\bar{T}_{sub} = 10\text{K}$.

$\Delta G/\bar{G}$	Period $t_p(\text{sec})$	$\Delta q/\bar{q}$	$G = 400\text{kg/m}^2\text{s}$			
			$\bar{q}(\text{W/cm}^2)$	$\Delta\bar{T}_{sub} = 10\text{K}$	$\Delta T_w (K)$	t_1/t_p
10%	20	30%	2.03 (single phase)	Heat flux oscillation only	0.44	0.375
				In-phase G & q oscillations	0.41	0.425
				Out-of-phase G & q oscillations	0.50	0.35
			4.57	Heat flux oscillation only	0.73	0.3
				In-phase G & q oscillations	1.02	0.2
				Out-of-phase G & q oscillations	0.78	0.5
			6.11	Heat flux oscillation only	0.79	0.275
				In-phase G & q oscillations	1.29	0.125
				Out-of-phase G & q oscillations	1.07	0.5
			7.11	Heat flux oscillation only	0.80	0.225
				In-phase G & q oscillations	1.42	0.125
				Out-of-phase G & q oscillations	1.32	0.5

Table 5.7 Amplitudes of T_w oscillation and relative time lags in transient oscillatory subcooled flow boiling for various \bar{q} for $\Delta q/\bar{q} = 30\%$, $\Delta G/\bar{G} = 10\%$ and $t_p = 20\text{sec}$ at $\bar{G} = 300\text{kg/m}^2\text{s}$ and $\Delta\bar{T}_{sub} = 15\text{K}$.

$\Delta G/\bar{G}$	Period $t_p(\text{sec})$	$\Delta q/\bar{q}$	$G = 300\text{kg/m}^2\text{s}$			
			$\bar{q}(\text{W/cm}^2)$	$\Delta\bar{T}_{sub} = 15\text{K}$	$\Delta T_w (K)$	t_1/t_p
10%	20	30%	3.04 (single phase)	Heat flux oscillation only	0.63	0.375
				In-phase G & q oscillations	0.59	0.4
				Out-of-phase G & q oscillations	0.71	0.35
			7.38	Heat flux oscillation only	0.85	0.275
				In-phase G & q oscillations	2.05	0.125
				Out-of-phase G & q oscillations	1.69	0.525
			8.06	Heat flux oscillation only	0.83	0.25
				In-phase G & q oscillations	2.12	0.1
				Out-of-phase G & q oscillations	1.97	0.525
			9.07	Heat flux oscillation only	0.78	0.25
				In-phase G & q oscillations	2.05	0.1
				Out-of-phase G & q oscillations	1.81	0.525

Table 5.8 Amplitudes of T_w oscillation and relative time lags in transient oscillatory subcooled flow boiling for various \bar{q} for $\Delta q/\bar{q}=30\%$, $\Delta G/\bar{G}=10\%$ and $t_p=30\text{sec}$ at $\bar{G}=300\text{kg/m}^2\text{s}$ and $\Delta\bar{T}_{sub}=10\text{K}$.

$\Delta G/\bar{G}$	Period $t_p(\text{sec})$	$\Delta q/\bar{q}$	$G = 300\text{kg/m}^2\text{s}$			
			$\bar{q}(\text{W/cm}^2)$	$\Delta\bar{T}_{sub}=10\text{K}$	$\Delta T_w(K)$	t_1/t_p
10%	30	30%	2.06 (single phase)	Heat flux oscillation only	0.72	0.3
				In-phase G & q oscillations	0.61	0.32
				Out-of-phase G & q oscillations	0.85	0.3
			4.42	Heat flux oscillation only	0.94	0.23
				In-phase G & q oscillations	1.39	0.15
				Out-of-phase G & q oscillations	0.89	0.38
			6.03	Heat flux oscillation only	0.92	0.2
				In-phase G & q oscillations	1.64	0.07
				Out-of-phase G & q oscillations	1.15	0.47
			7.03	Heat flux oscillation only	0.93	0.2
				In-phase G & q oscillations	1.72	0.07
				Out-of-phase G & q oscillations	1.21	0.47

Table 5.9 Amplitudes of T_w oscillation and relative time lags in transient oscillatory subcooled flow boiling for various \bar{q} for $\Delta q/\bar{q}=5,10,23\%$, $\Delta G/\bar{G}=5\%$ and $t_p=20\text{sec}$ at $\bar{G}=300\text{kg/m}^2\text{s}$ and $\Delta\bar{T}_{sub}=10\text{K}$.

$\Delta G/\bar{G}$	Period $t_p(\text{sec})$	$\Delta q/\bar{q}$	$G = 300\text{kg/m}^2\text{s}$			
			$\bar{q}(\text{W/cm}^2)$	$\Delta\bar{T}_{sub}=10\text{K}$	$\Delta T_w(K)$	t_1/t_p
5%	20	5%	2.08 (single phase)	Heat flux oscillation only	0.10	0.375
				Mass flux oscillation only	0.08	0.15
				In-phase G & q oscillations	0.04	x
		10%	4.08	Heat flux oscillation only	0.24	0.3
				Mass flux oscillation only	0.23	0.125
				Out-of-phase G & q oscillations	0.08	x
		23%	6.07	Heat flux oscillation only	0.56	0.2
				Mass flux oscillation only	0.56	0.075
				Out-of-phase G & q oscillations	0.14	x

Table 5.10 Amplitudes of T_w oscillation and relative time lags in transient oscillatory subcooled flow boiling for various \bar{q} for $\Delta q/\bar{q}=8,30,32,45\%$, $\Delta G/\bar{G}=10\%$ and $t_p=20\text{sec}$ at $\bar{G}=300\text{kg/m}^2\text{s}$ and $\Delta\bar{T}_{sub}=10\text{K}$.

$\Delta G/\bar{G}$	Period $t_p(\text{sec})$	$\Delta q/\bar{q}$	$G = 300\text{kg/m}^2\text{s}$			
			$\bar{q}(\text{W/cm}^2)$	$\Delta\bar{T}_{sub}=10\text{K}$	$\Delta T_w(K)$	t_1/t_p
10%	20	8%	2.05 (single phase)	Heat flux oscillation only	0.17	0.35
				Mass flux oscillation only	0.13	0.175
				In-phase G & q oscillations	0.07	x
		30%	4.61	Heat flux oscillation only	0.69	0.275
				Mass flux oscillation only	0.67	0.025
				Out-of-phase G & q oscillations	0.18	x
		32%	6.05	Heat flux oscillation only	0.76	0.25
				Mass flux oscillation only	0.98	0.025
				Out-of-phase G & q oscillations	0.31	x
		45%	7.09	Heat flux oscillation only	1.08	0.25
				Mass flux oscillation only	1.14	0.025
				Out-of-phase G & q oscillations	0.28	x

Table 5.11 Amplitudes of T_w oscillation and relative time lags in transient oscillatory subcooled flow boiling for various \bar{q} for $\Delta q/\bar{q}=15,35,50\%$, $\Delta G/\bar{G}=15\%$ and $t_p=20\text{sec}$ at $\bar{G}=300\text{kg/m}^2\text{s}$ and $\Delta\bar{T}_{sub}=10\text{K}$.

$\Delta G/\bar{G}$	Period $t_p(\text{sec})$	$\Delta q/\bar{q}$	$G = 300\text{kg/m}^2\text{s}$			
			$\bar{q}(\text{W/cm}^2)$	$\Delta\bar{T}_{sub}=10\text{K}$	$\Delta T_w(K)$	t_1/t_p
15%	20	15%	2.08 (single phase)	Heat flux oscillation only	0.25	0.4
				Mass flux oscillation only	0.21	0.125
				In-phase G & q oscillations	0.06	x
		35%	4.08	Heat flux oscillation only	0.80	0.275
				Mass flux oscillation only	0.80	0.075
				Out-of-phase G & q oscillations	0.29	x
		50%	6.07	Heat flux oscillation only	1.22	0.25
				Mass flux oscillation only	1.60	0.025
				Out-of-phase G & q oscillations	0.38	x

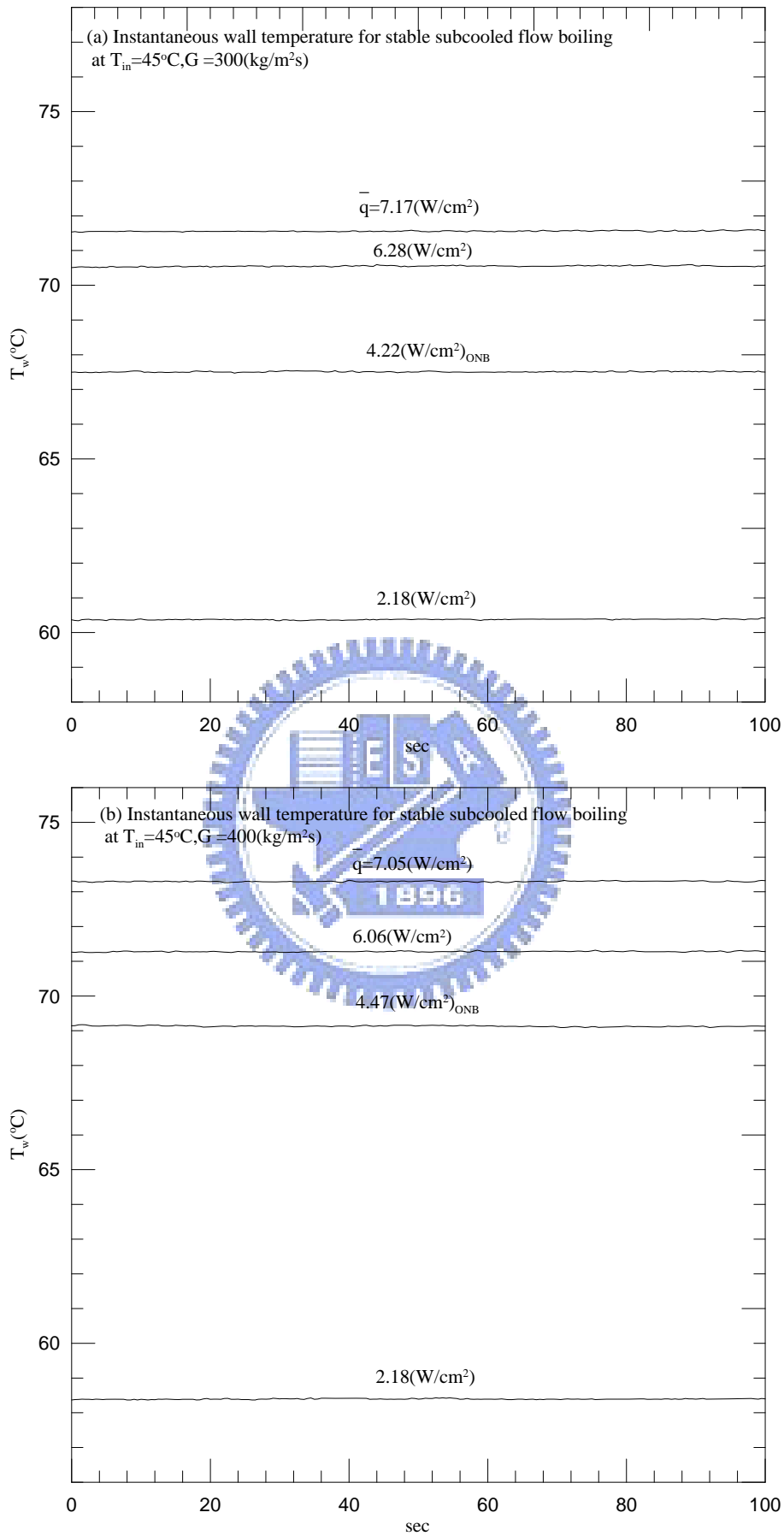


Fig. 5.1 Time variations of the copper plate temperature in stable subcooled flow boiling for various imposed heat fluxes at (a) $G=300\text{kg}/\text{m}^2\text{s}$ and (b) $G=400\text{kg}/\text{m}^2\text{s}$

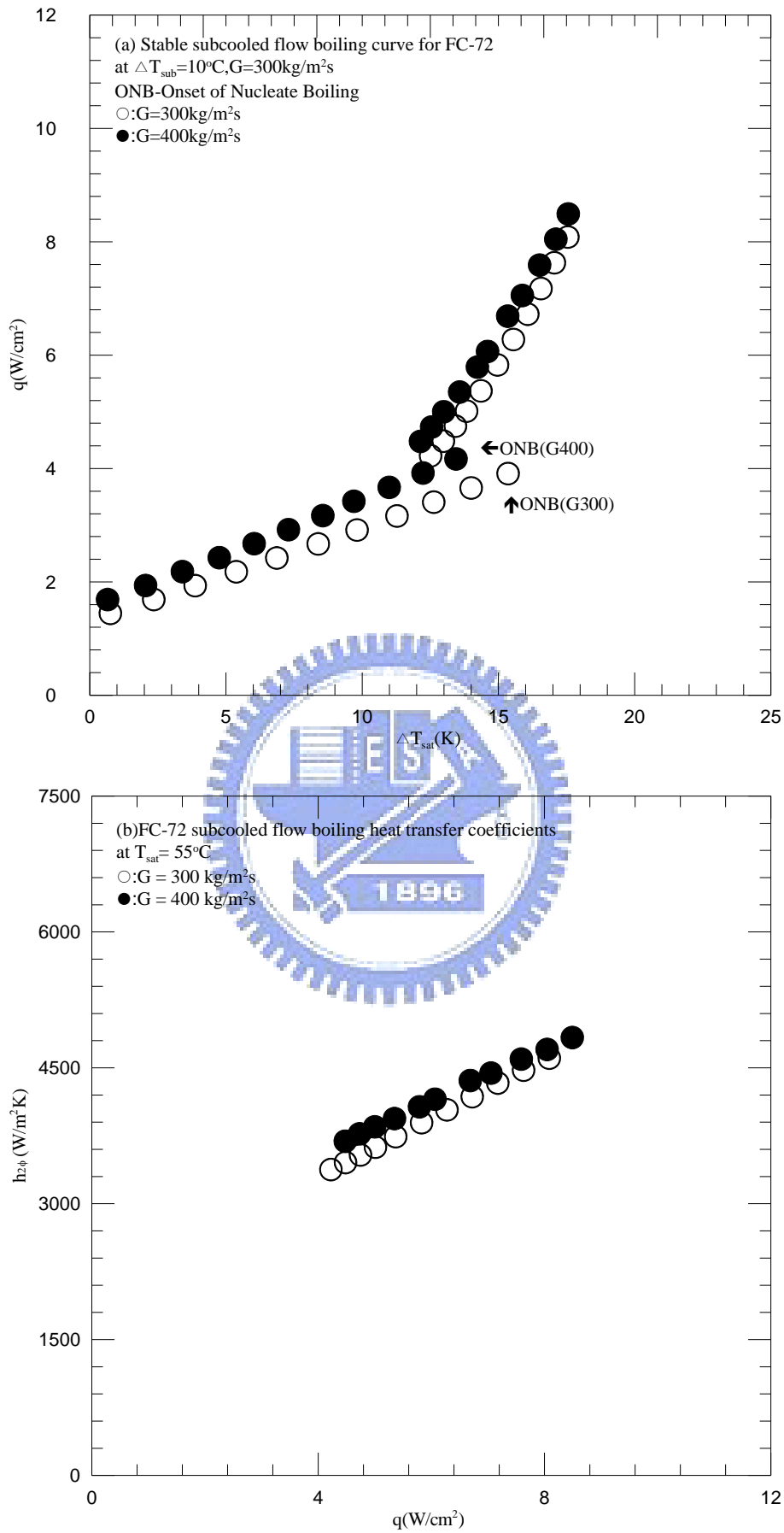


Fig. 5.2 (a) Stable subcooled flow boiling curve and (b) stable subcooled flow boiling heat transfer coefficient.

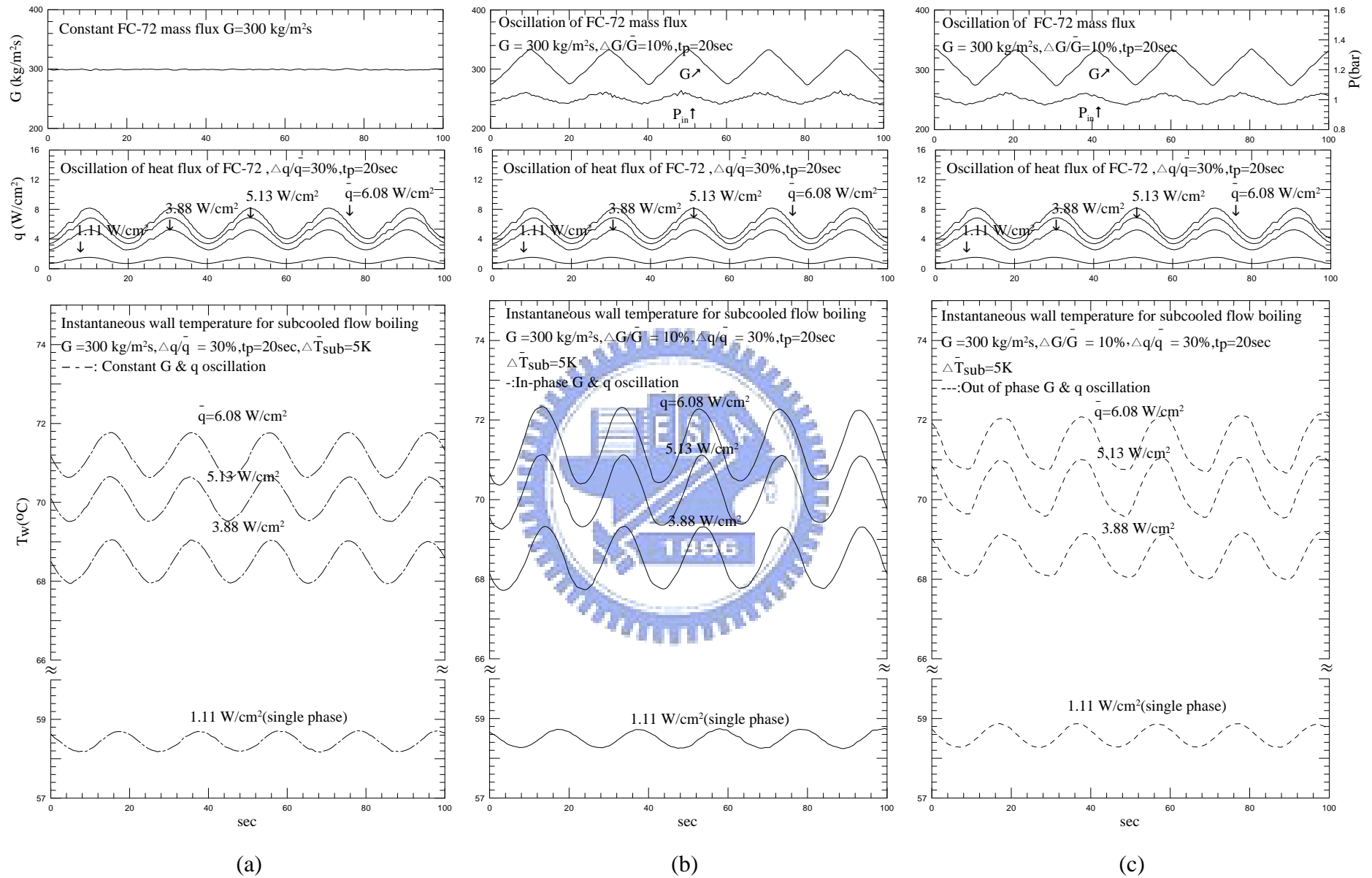


Fig. 5.3 Time variations of the measured instantaneous heated surface temperature for (a) imposed heat flux oscillation only, (b) in-phase G and q oscillations and (c) out-of-phase G and q oscillations at $\bar{G} = 300 \text{ kg/m}^2\text{s}$ and $\Delta G/\bar{G} = 10\%$ for $\Delta q/\bar{q} = 30\%$ and $t_p = 20 \text{ sec}$. for $\Delta \bar{T}_{sub} = 5 \text{ K}$.

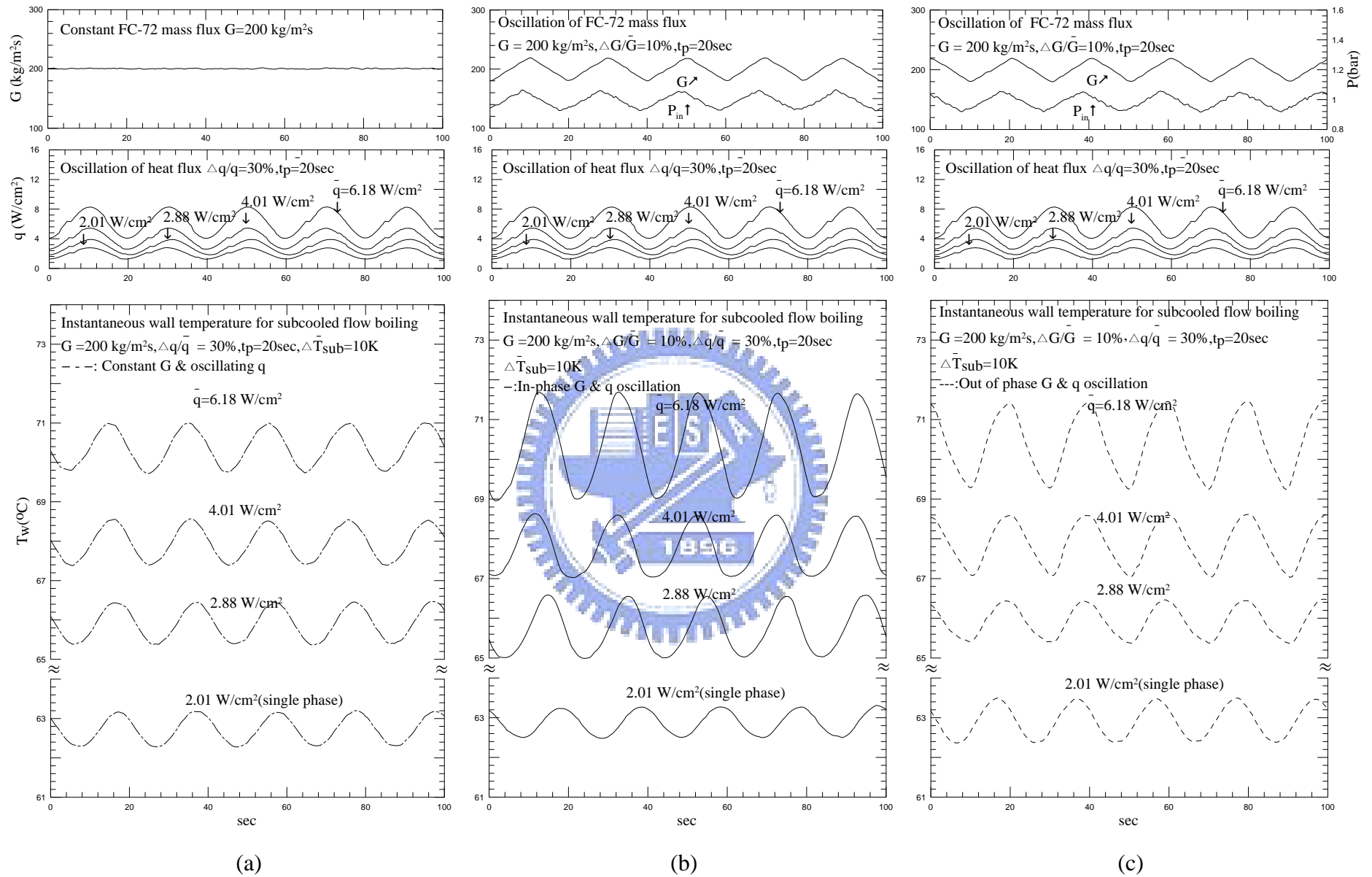


Fig. 5.4 Time variations of the measured instantaneous heated surface temperature for (a) imposed heat flux oscillation only, (b) in-phase G and q oscillations and (c) out-of-phase G and q oscillations at $\bar{G} = 200 \text{ kg/m}^2 \text{ s}$ and $\Delta G/\bar{G} = 10\%$ for $\Delta q/\bar{q} = 30\%$ and $t_p = 20 \text{ sec}$. for $\Delta \bar{T}_{sub} = 10 \text{ K}$.

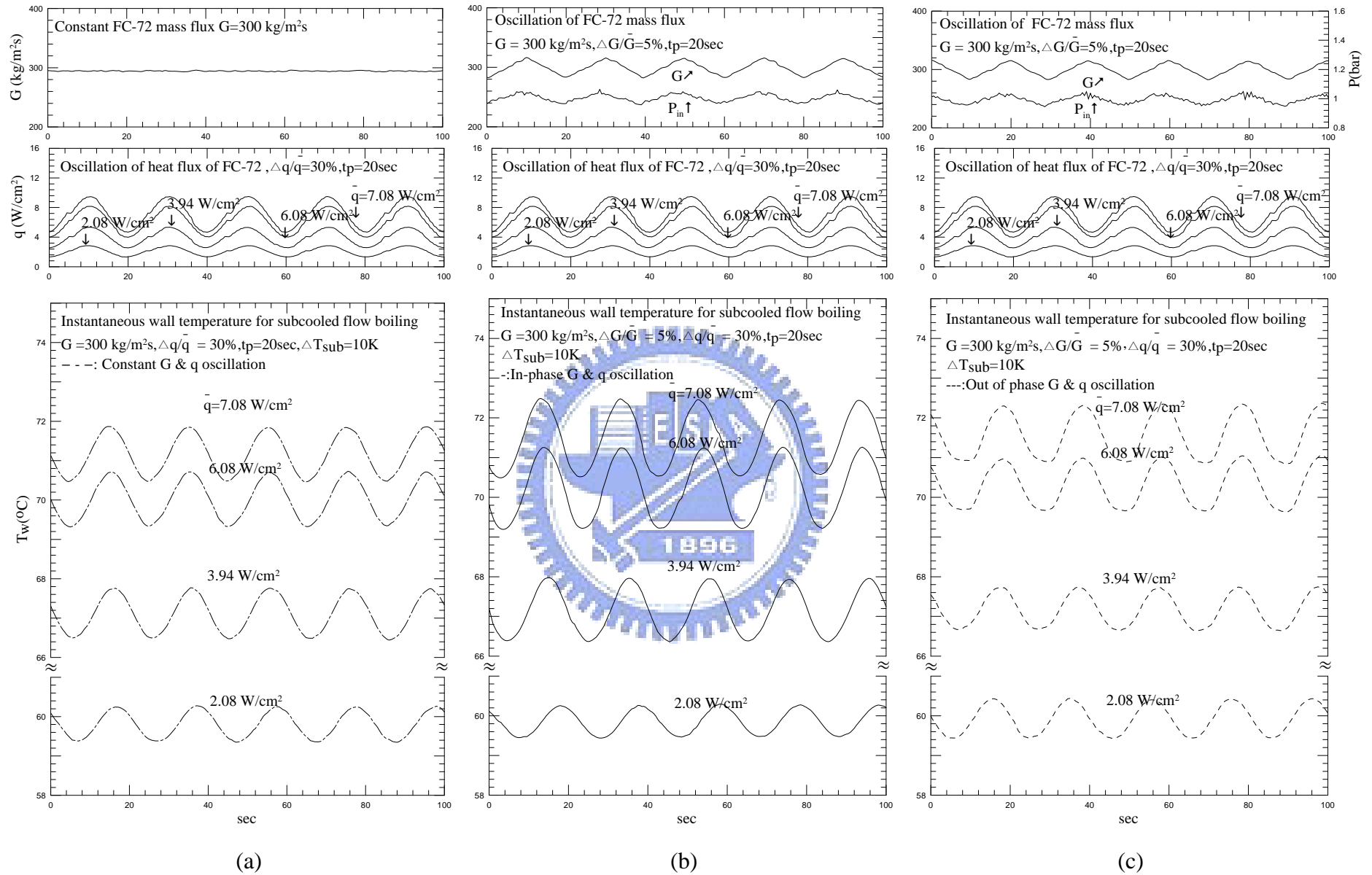
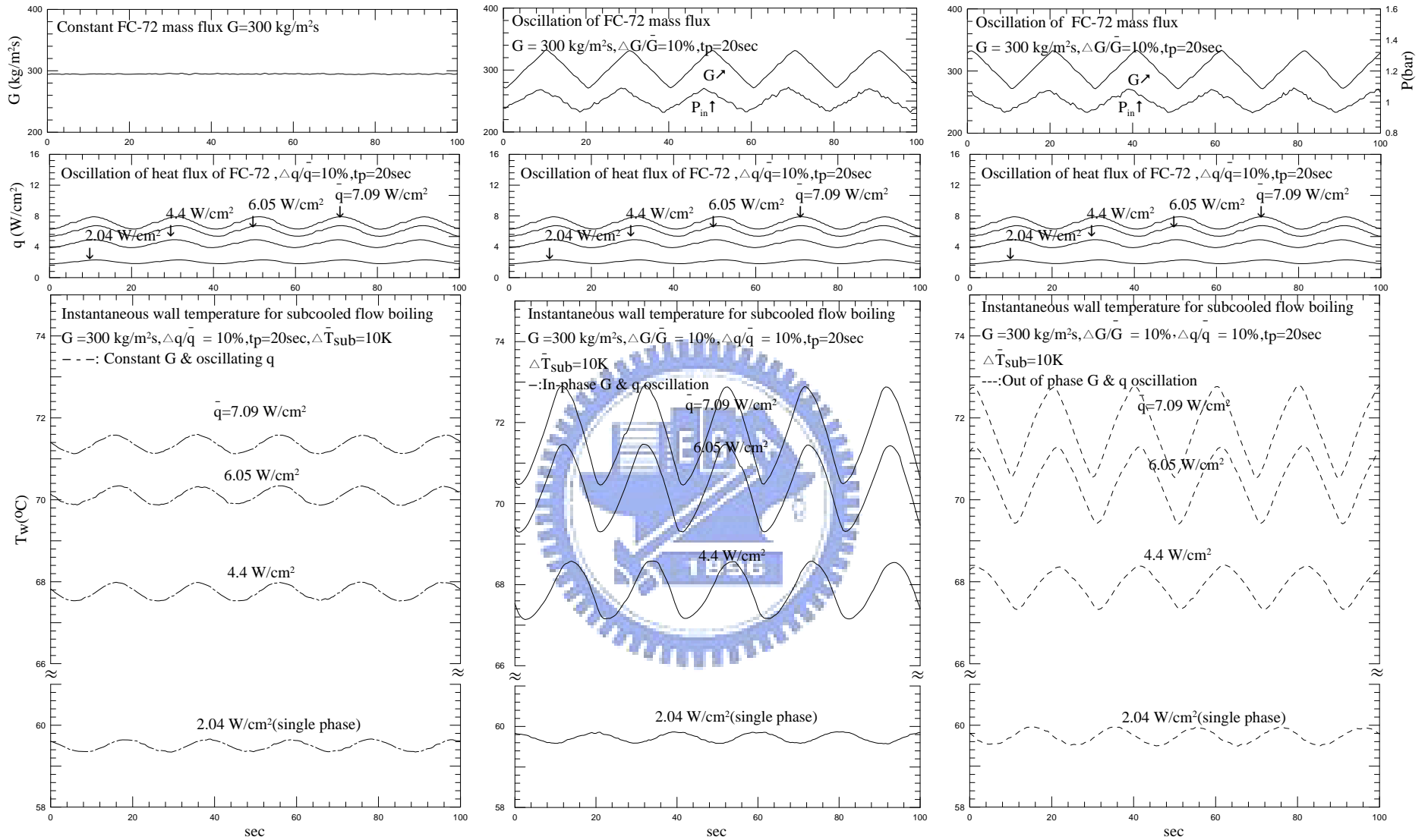


Fig. 5.5 Time variations of the measured instantaneous heated surface temperature for (a) imposed heat flux oscillation only, (b) in-phase G and q oscillations and (c) out-of-phase G and q oscillations at $\bar{G} = 300 \text{ kg/m}^2\text{s}$ and $\Delta G/\bar{G} = 5\%$ for $\Delta q/\bar{q} = 30\%$ and $t_p = 20 \text{ sec}$. for $\Delta T_{\text{sub}} = 10 \text{ K}$.



(a)

(b)

(c)

Fig. 5.6 Time variations of the measured instantaneous heated surface temperature for (a) imposed heat flux oscillation only, (b) in-phase G and q oscillations and (c) out-of-phase G and q oscillations at $\bar{G} = 300 \text{ kg/m}^2\text{s}$ and $\Delta G/\bar{G} = 10\%$ for $\Delta q/\bar{q} = 10\%$ and $t_p = 20 \text{ sec}$. for $\Delta \bar{T}_{sub} = 10 \text{ K}$.

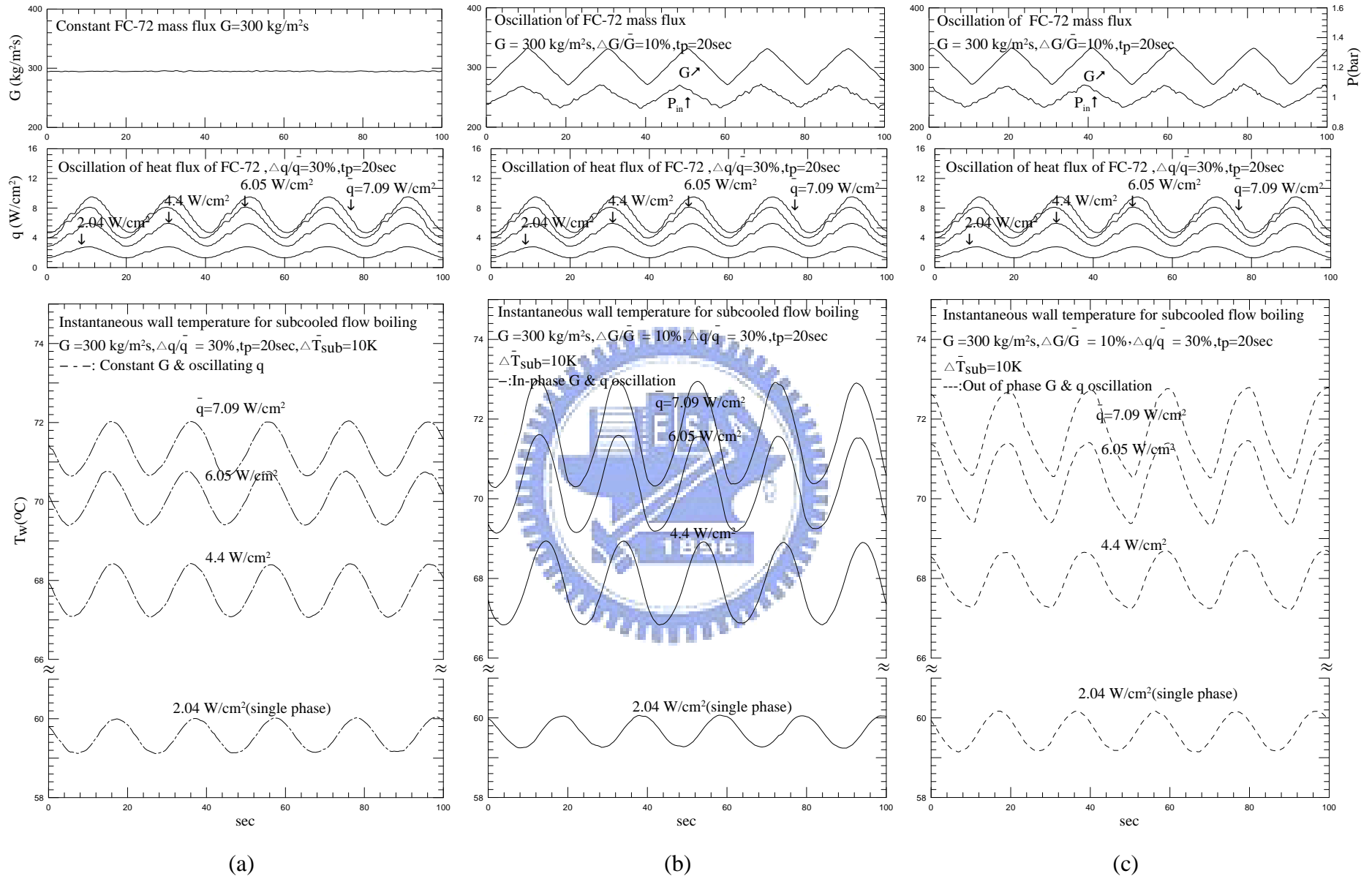
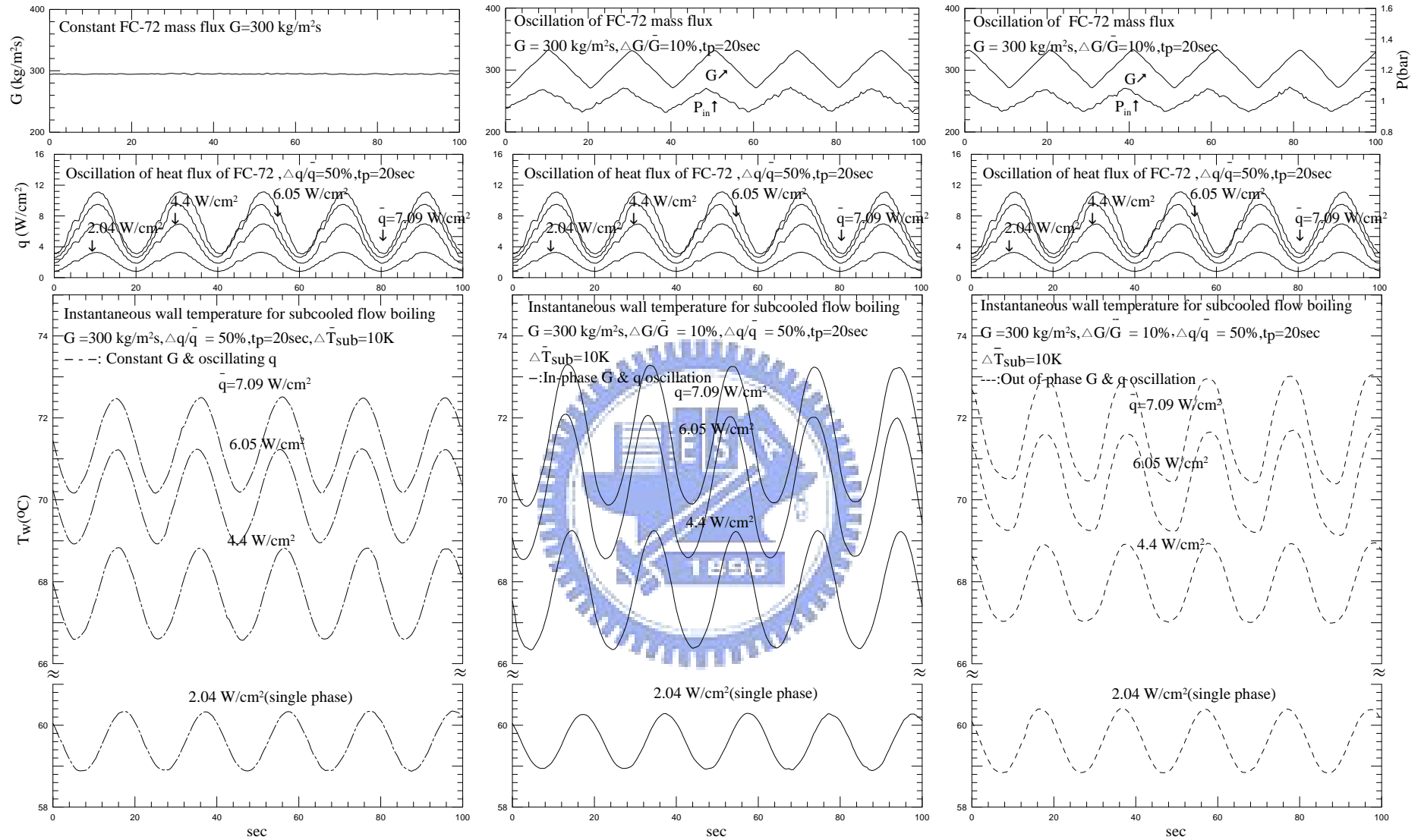


Fig. 5.7 Time variations of the measured instantaneous heated surface temperature for (a) imposed heat flux oscillation only, (b) in-phase G and q oscillations and (c) out-of-phase G and q oscillations at $\bar{G} = 300 \text{ kg/m}^2\text{s}$ and $\Delta G/\bar{G} = 10\%$ for $\Delta q/\bar{q} = 30\%$ and $t_p = 20 \text{ sec}$. for $\Delta T_{sub} = 10 \text{ K}$.



(a)

(b)

(c)

Fig. 5.8 Time variations of the measured instantaneous heated surface temperature for (a) imposed heat flux oscillation only, (b) in-phase G and q oscillations and (c) out-of-phase G and q oscillations at $\bar{G} = 300 \text{ kg/m}^2\text{s}$ and $\Delta G/\bar{G} = 10\%$ for $\Delta q/\bar{q} = 50\%$ and $t_p = 20 \text{ sec}$. for $\Delta T_{sub} = 10 \text{ K}$.

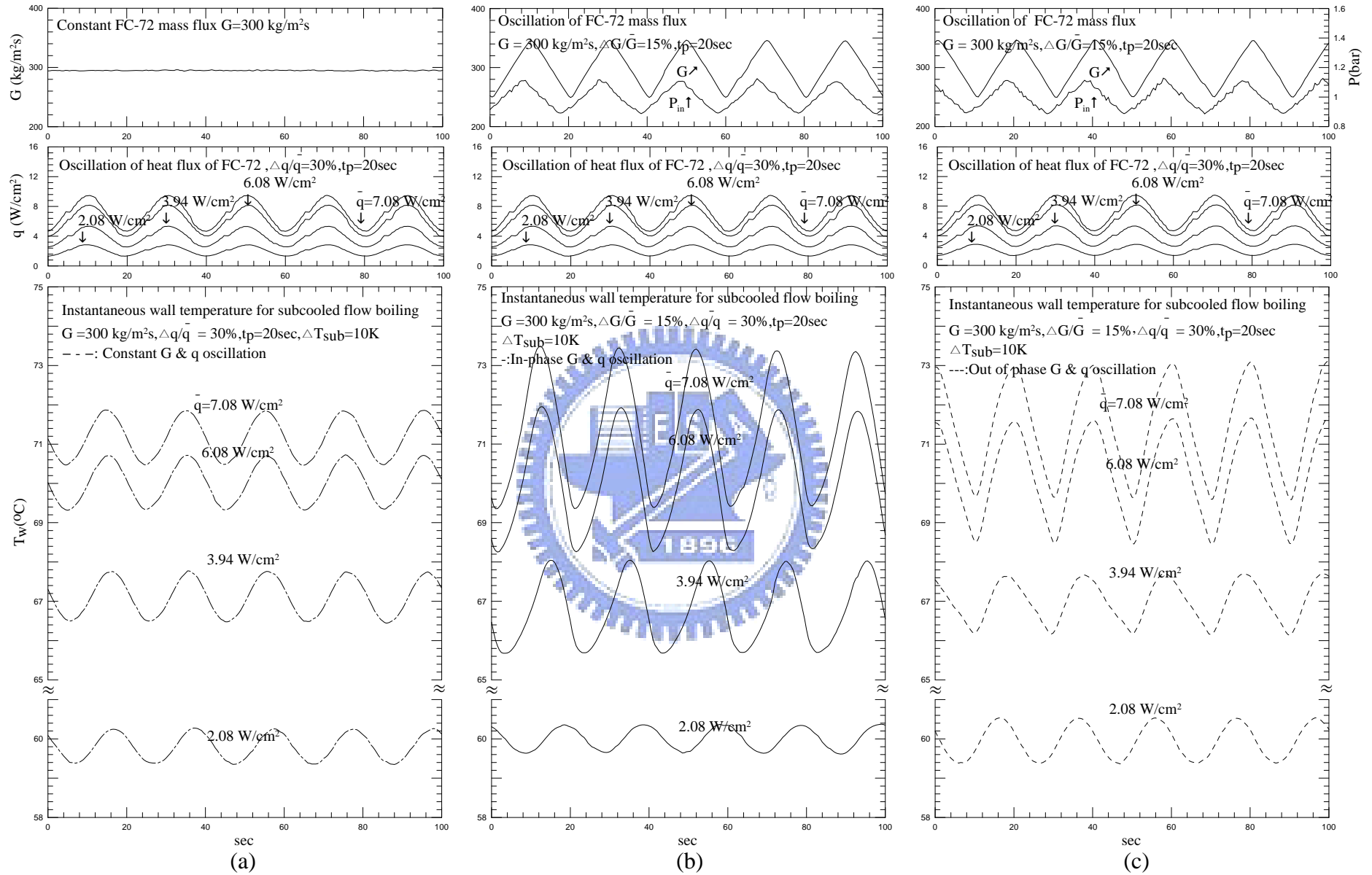


Fig. 5.9 Time variations of the measured instantaneous heated surface temperature for (a) imposed heat flux oscillation only, (b) in-phase G and q oscillations and (c) out-of-phase G and q oscillations at $\bar{G} = 300 \text{ kg/m}^2\text{s}$ and $\Delta G/\bar{G} = 15\%$ for $\Delta q/\bar{q} = 30\%$ and $t_p = 20 \text{ sec}$. for $\Delta T_{\text{sub}} = 10 \text{ K}$.

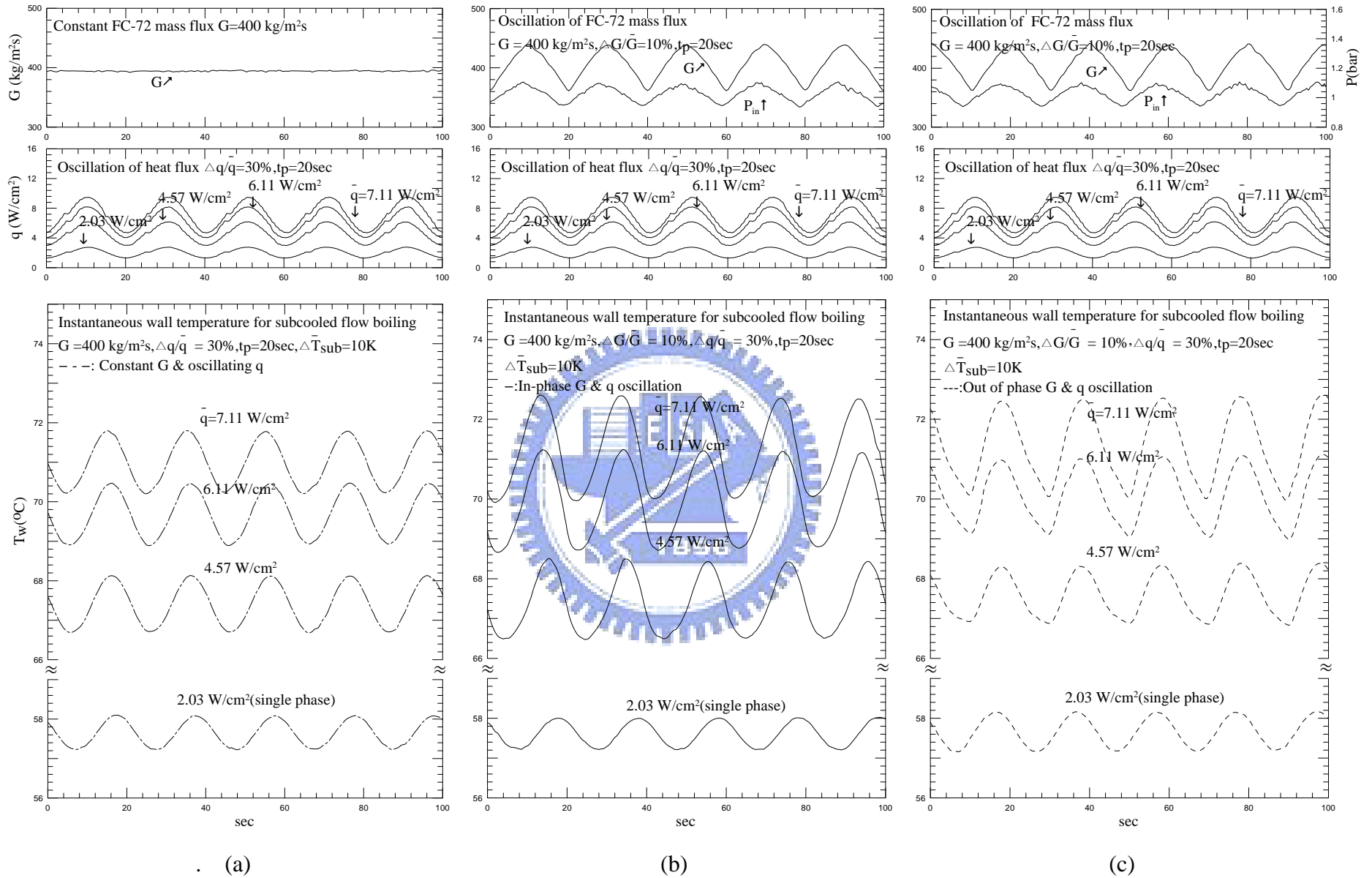


Fig. 5.10 Time variations of the measured instantaneous heated surface temperature for (a) imposed heat flux oscillation only, (b) in-phase G and q oscillations and (c) out-of-phase G and q oscillations at $\bar{G} = 400 \text{ kg/m}^2 \text{ s}$ and $\Delta \bar{G}/\bar{G} = 10\%$ for $\Delta \bar{q}/\bar{q} = 30\%$ and $t_p = 20 \text{ sec}$. for $\Delta \bar{T}_{sub} = 10 \text{ K}$.

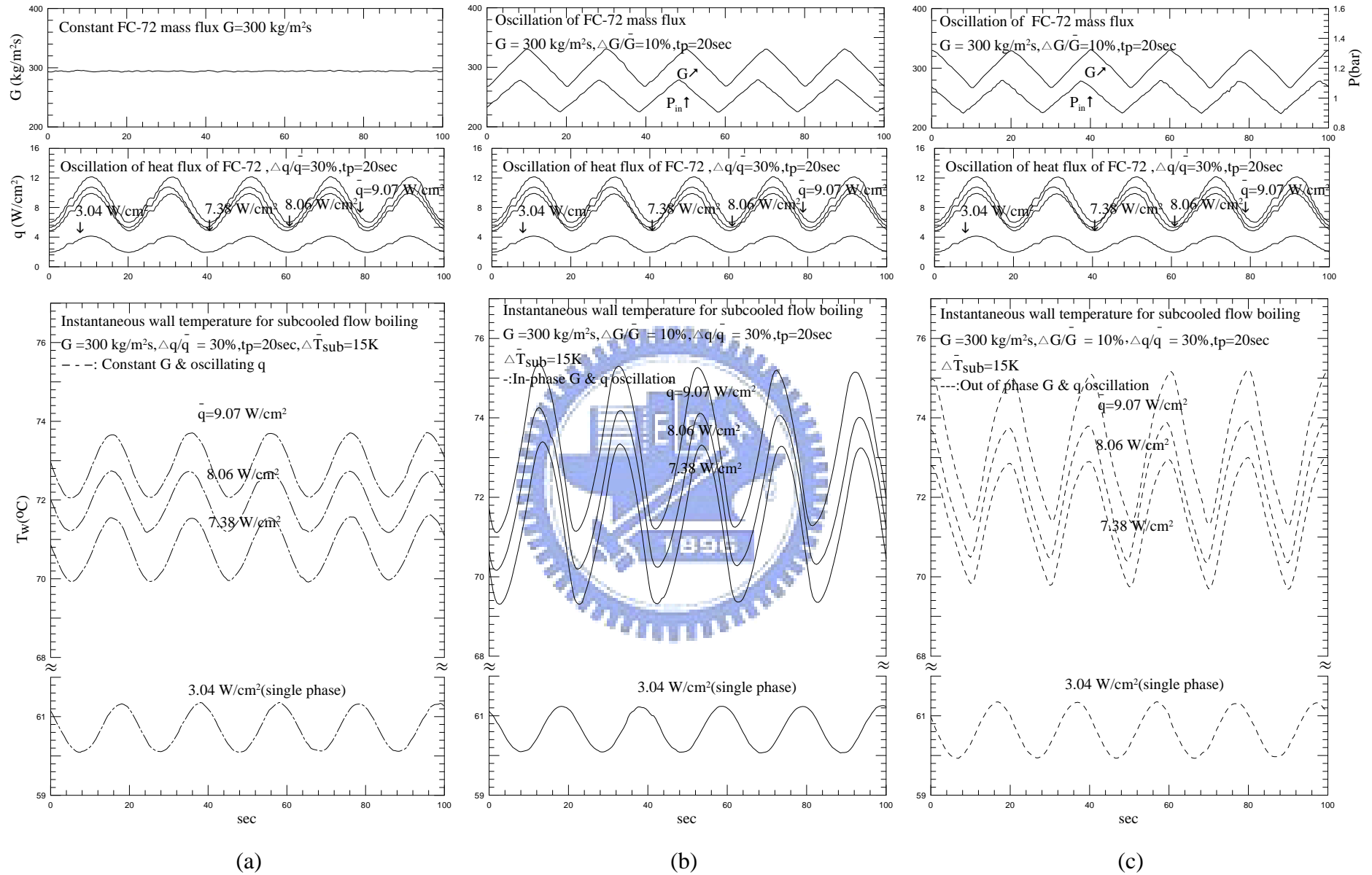


Fig. 5.11 Time variations of the measured instantaneous heated surface temperature for (a) imposed heat flux oscillation only, (b) in-phase G and q oscillations and (c) out-of-phase G and q oscillations at $\bar{G} = 300 \text{ kg/m}^2\text{s}$ and $\Delta G/\bar{G} = 10\%$ for $\Delta q/\bar{q} = 30\%$ and $t_p = 20 \text{ sec}$. for $\Delta T_{sub} = 15 \text{ K}$.

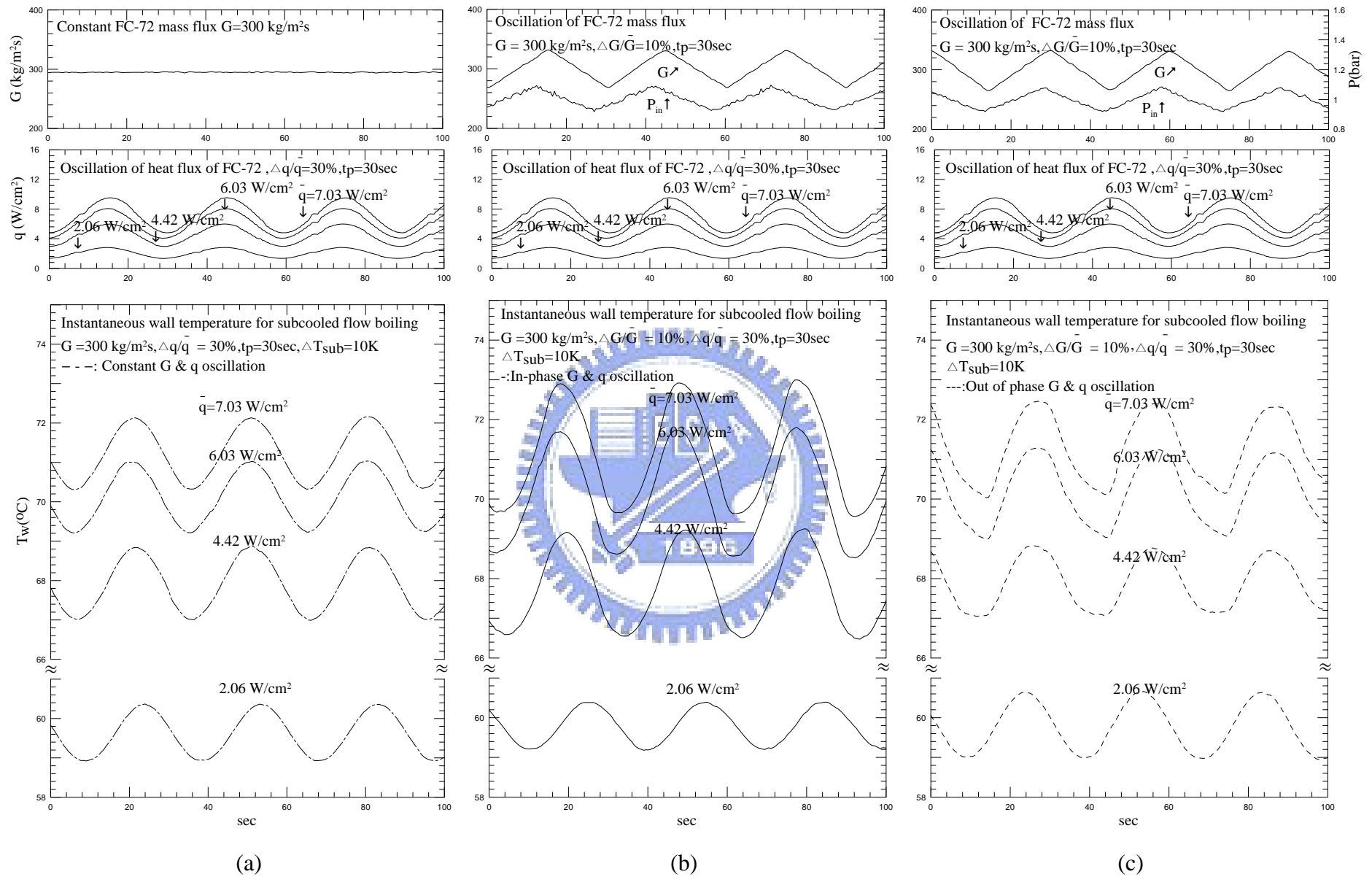


Fig. 5.12 Time variations of the measured instantaneous heated surface temperature for (a) imposed heat flux oscillation only, (b) in-phase G and q oscillations and (c) out-of-phase G and q oscillations at $\bar{G} = 300 \text{ kg/m}^2\text{s}$ and $\Delta G/\bar{G} = 10\%$ for $\Delta q/\bar{q} = 30\%$ and $t_p = 30 \text{ sec}$. for $\Delta \bar{T}_{sub} = 10 \text{ K}$.

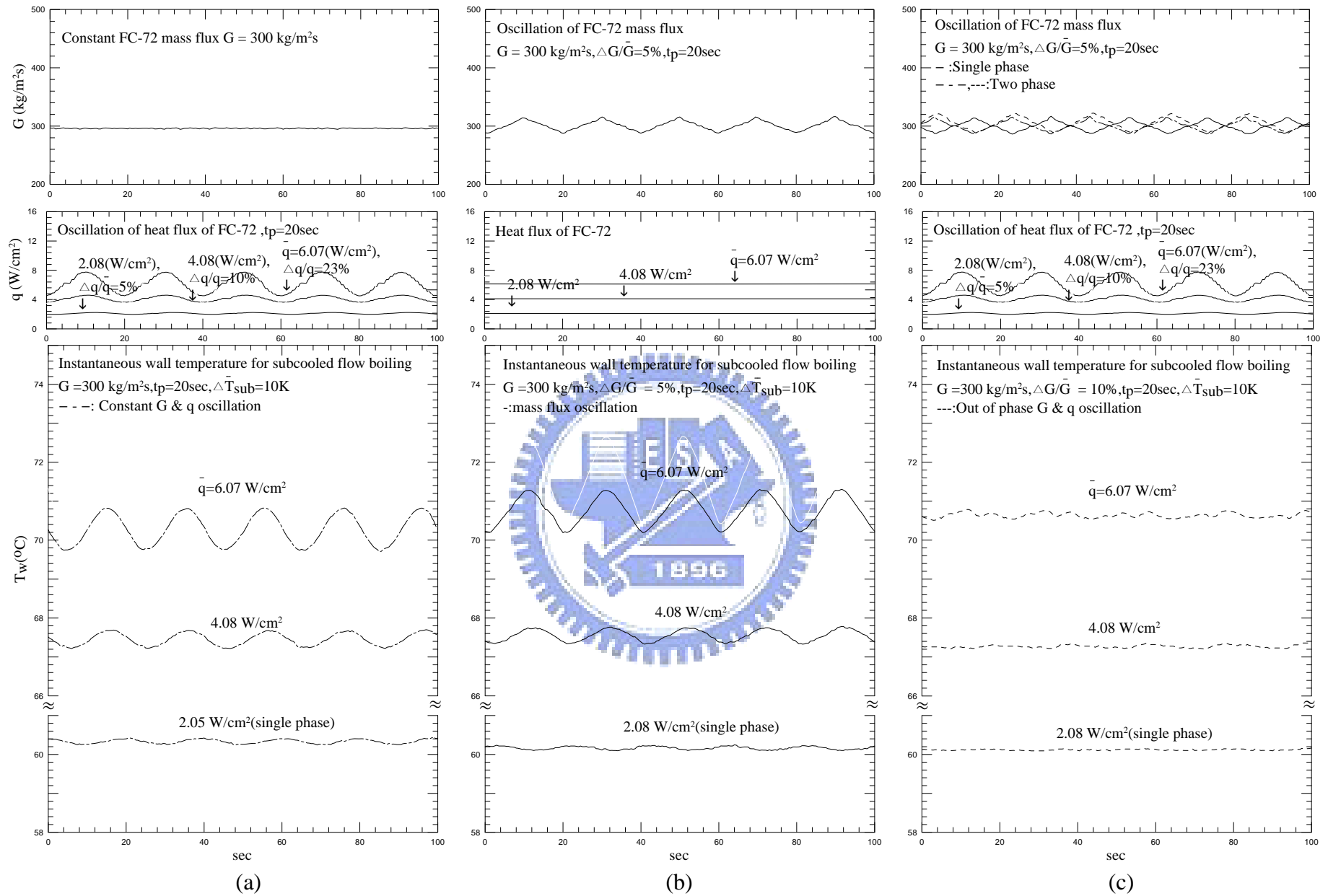


Fig. 5.13 Time variations of the measured instantaneous heated surface temperature for (a) imposed heat flux oscillation only, (b) imposed mass flux oscillation only, and (c) in-phase or out-of-phase G and q oscillations at $\bar{G} = 300 \text{ kg/m}^2\text{s}$ and $\Delta G/\bar{G} = 5\%$ for various \bar{q} at $t_p = 20 \text{ sec}$. for $\Delta \bar{T}_{sub} = 10 \text{ K}$.

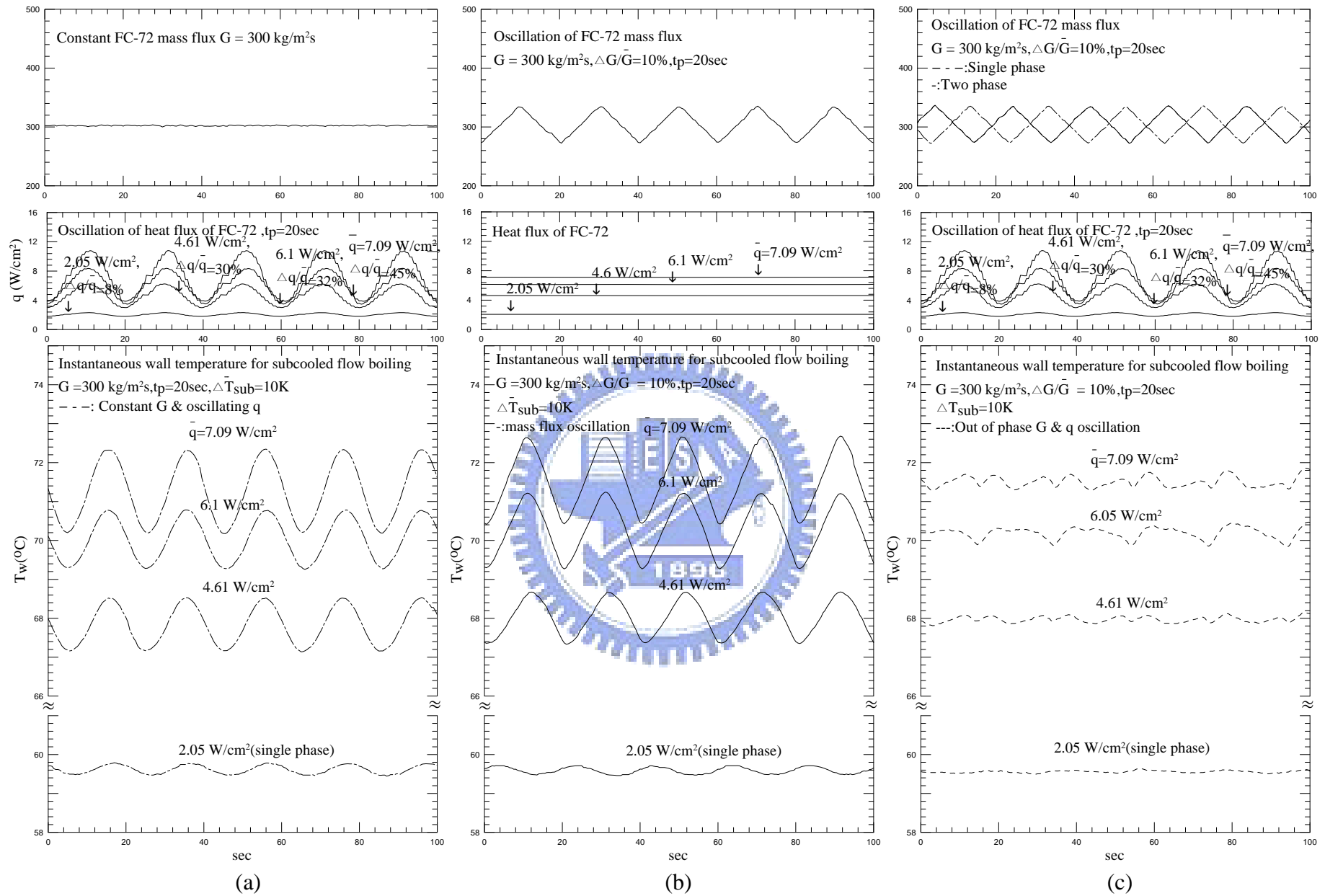


Fig. 5.14 Time variations of the measured instantaneous heated surface temperature for (a) imposed heat flux oscillation only, (b) imposed mass flux oscillation only, and (c) in-phase or out-of-phase G and q oscillations at $\bar{G} = 300 \text{ kg/m}^2\text{s}$ and $\Delta G/\bar{G} = 10\%$ for various \bar{q} at $t_p = 20 \text{ sec}$. for $\Delta \bar{T}_{sub} = 10 \text{ K}$.

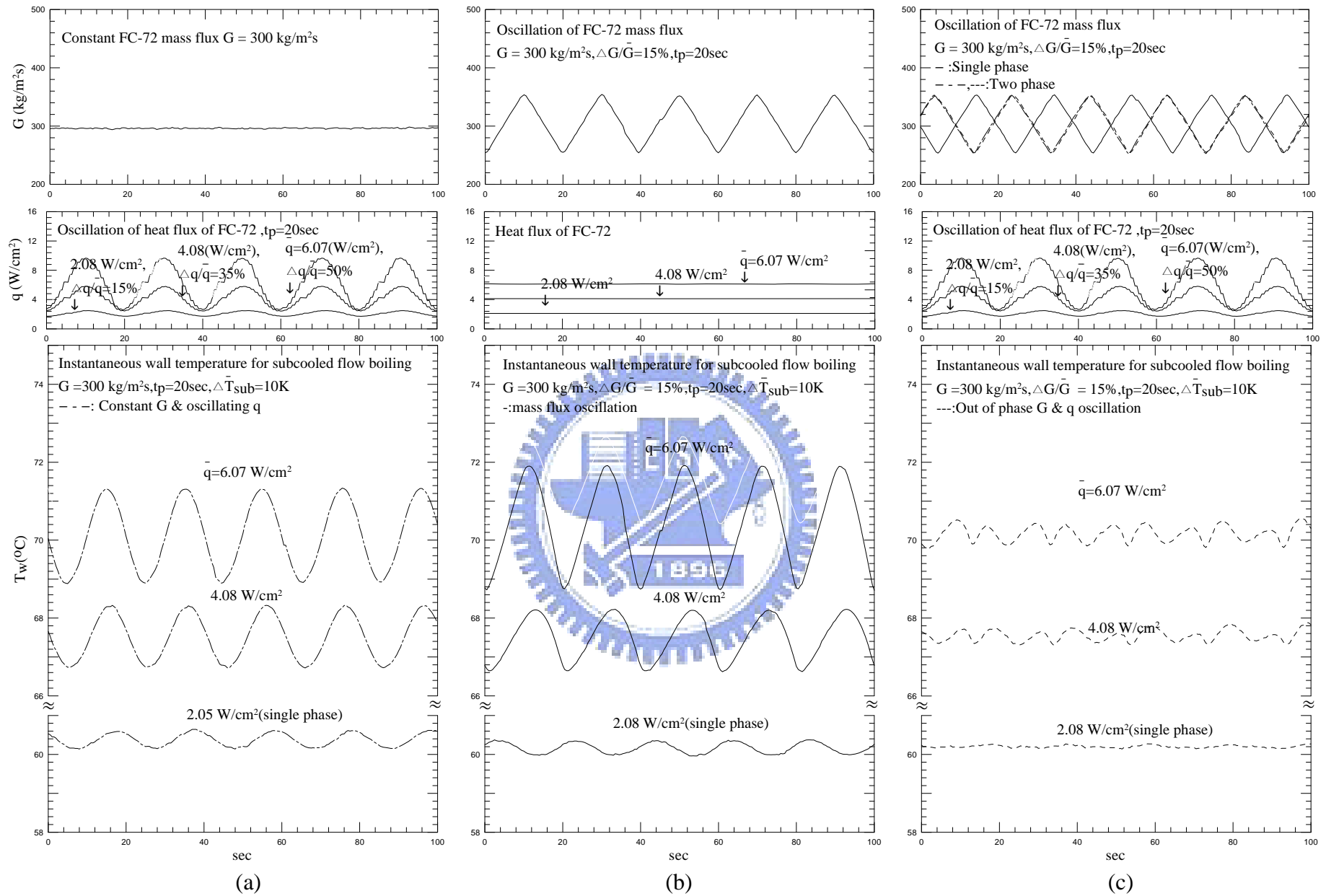


Fig. 5.15 Time variations of the measured instantaneous heated surface temperature for (a) imposed heat flux oscillation only, (b) imposed mass flux oscillation only, and (c) in-phase or out-of-phase G and q oscillations at $\bar{G} = 300$ kg/m²s and $\Delta G/\bar{G} = 15\%$ for various \bar{q} at $t_p = 20$ sec. for $\Delta \bar{T}_{sub} = 10$ K.

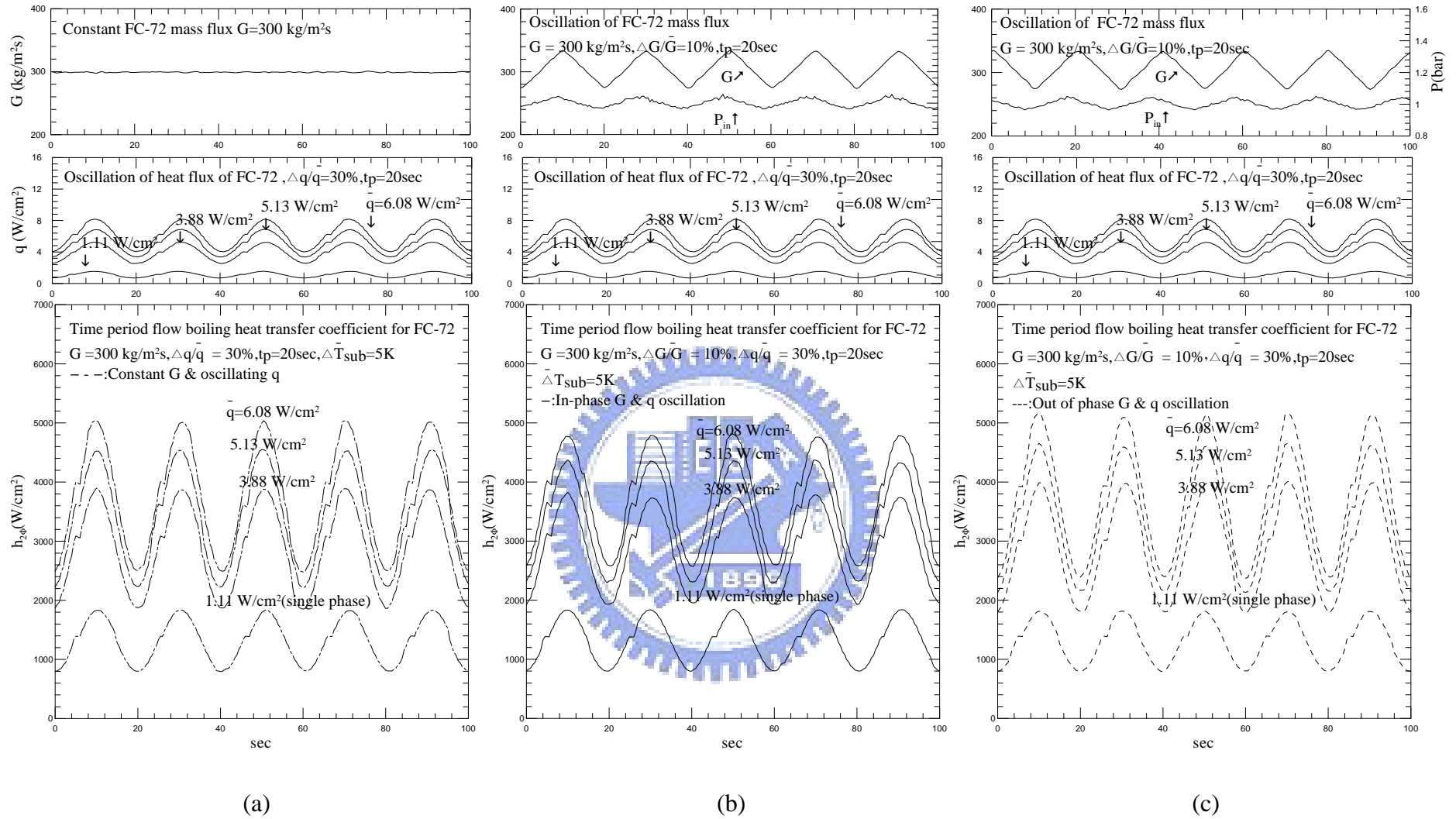


Fig. 5.16 Time variations of the heat transfer coefficient for (a) imposed heat flux oscillation only, (b) in-phase G and q oscillations and (c) out-of-phase G and q oscillations at $\bar{G} = 300 \text{ kg/m}^2\text{s}$ and $\Delta G/\bar{G} = 10\%$ for $\Delta q/\bar{q} = 30\%$ and $t_p = 20 \text{ sec}$. for $\Delta T_{sub} = 5 \text{ K}$.

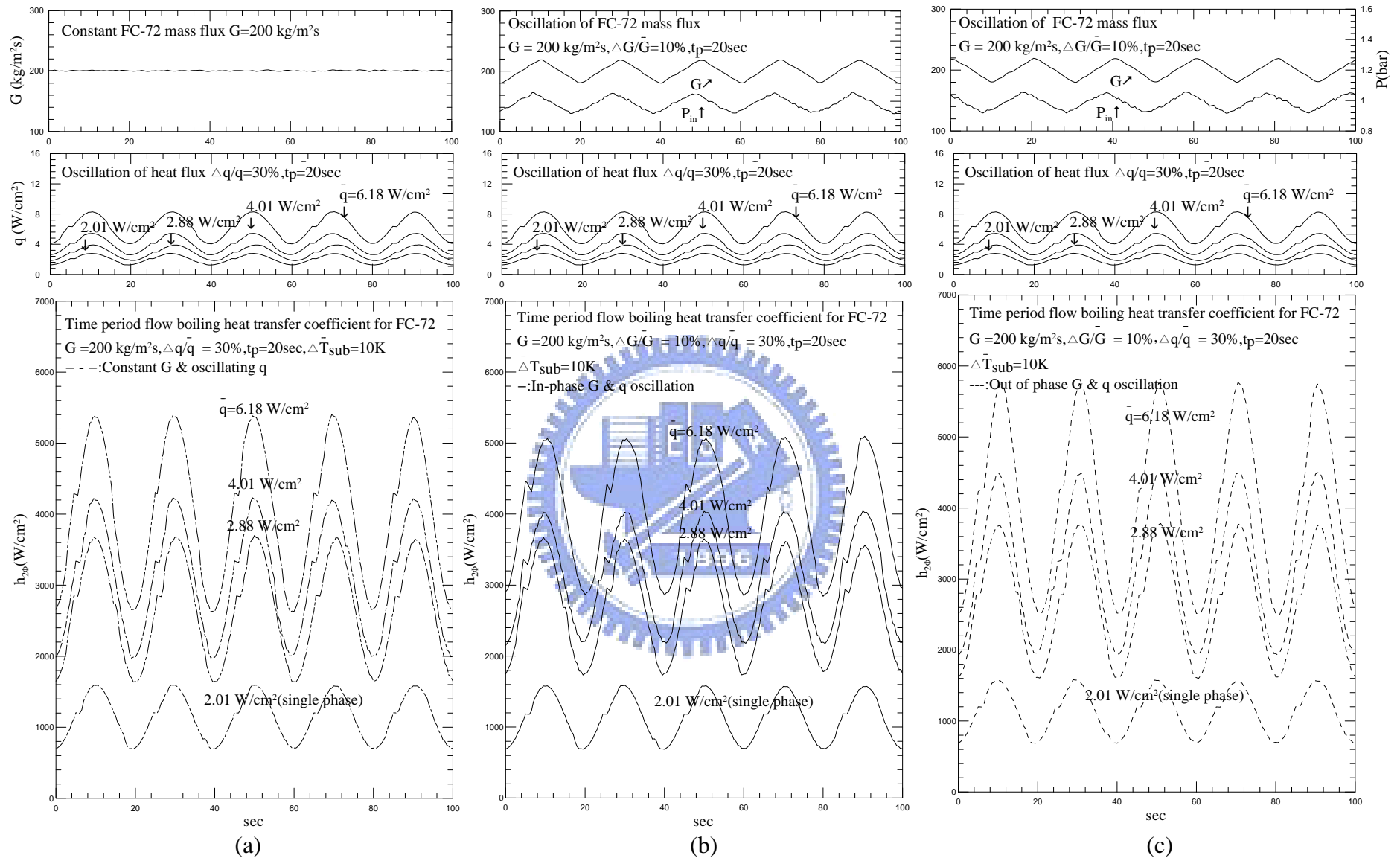


Fig. 5.17 Time variations of the heat transfer coefficient for (a) imposed heat flux oscillation only, (b) in-phase G and q oscillations and (c) out-of-phase G and q oscillations at $\bar{G} = 200$ kg/m²s and $\Delta G/\bar{G} = 10\%$ for $\Delta q/\bar{q} = 30\%$ and $t_p = 20$ sec. for $\Delta T_{sub} = 10$ K.

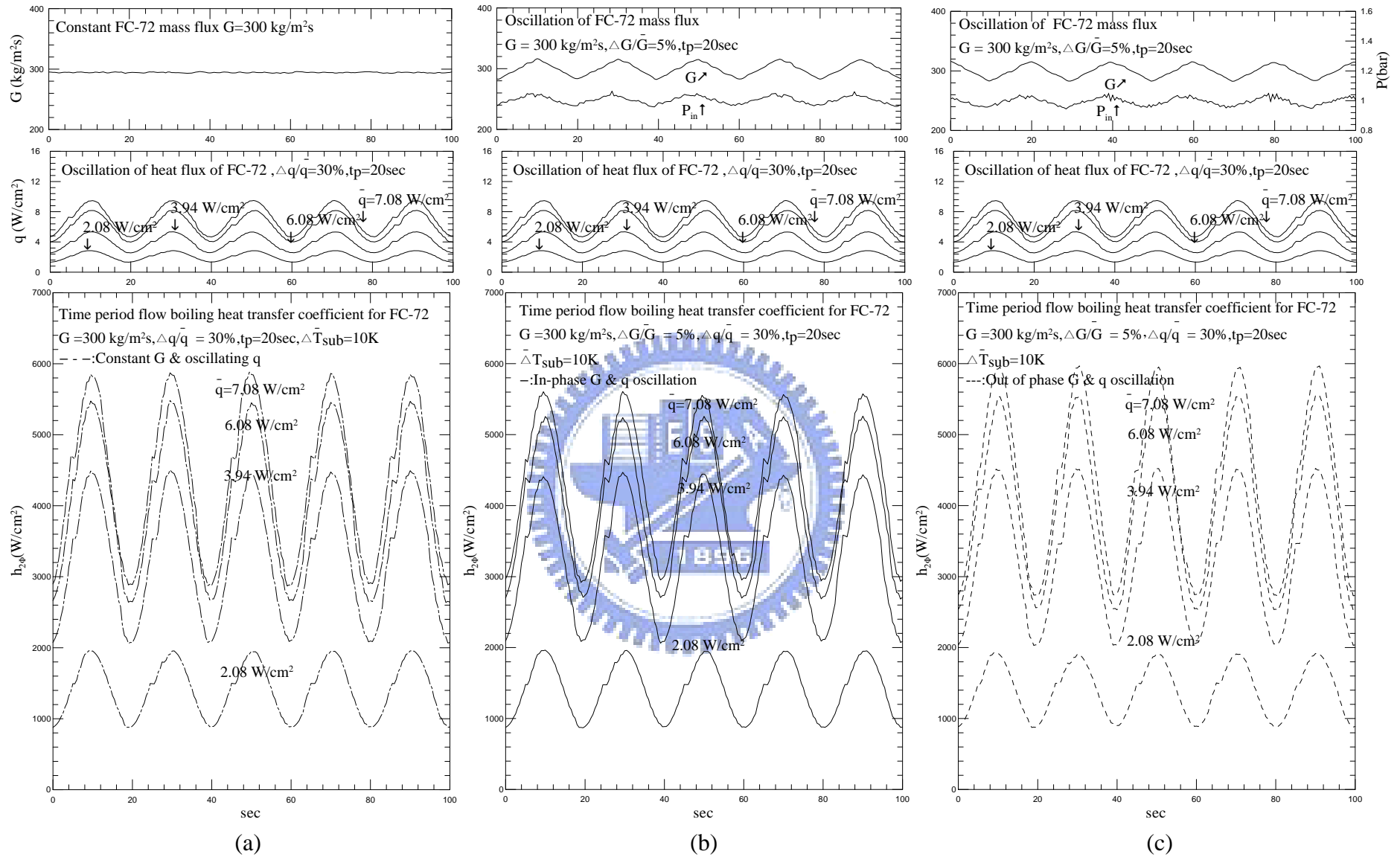


Fig. 5.18 Time variations of the heat transfer coefficient for (a) imposed heat flux oscillation only, (b) in-phase G and q oscillations and (c) out-of-phase G and q oscillations at $\bar{G} = 300 \text{ kg/m}^2\text{s}$ and $\Delta G/\bar{G} = 5\%$ for $\Delta q/\bar{q} = 30\%$ and $t_p = 20 \text{ sec}$. for $\Delta T_{\text{sub}} = 10 \text{ K}$.

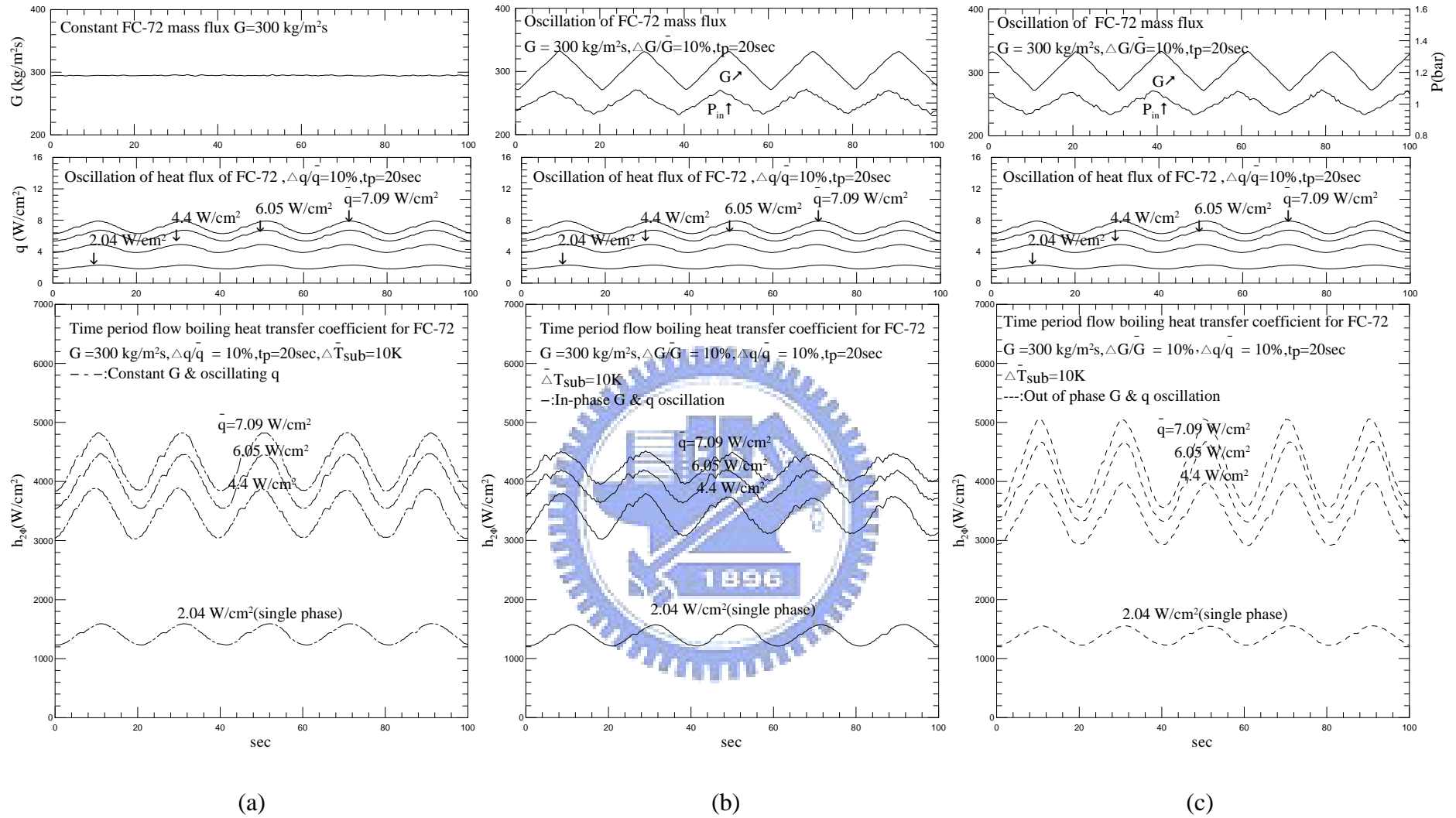


Fig. 5.19 Time variations of the heat transfer coefficient for (a) imposed heat flux oscillation only, (b) in-phase G and q oscillations and (c) out-of-phase G and q oscillations at $\bar{G} = 300 \text{ kg/m}^2\text{s}$ and $\Delta G/\bar{G} = 10\%$ for $\Delta q/\bar{q} = 10\%$ and $t_p = 20 \text{ sec}$. for $\Delta \bar{T}_{sub} = 10 \text{ K}$.

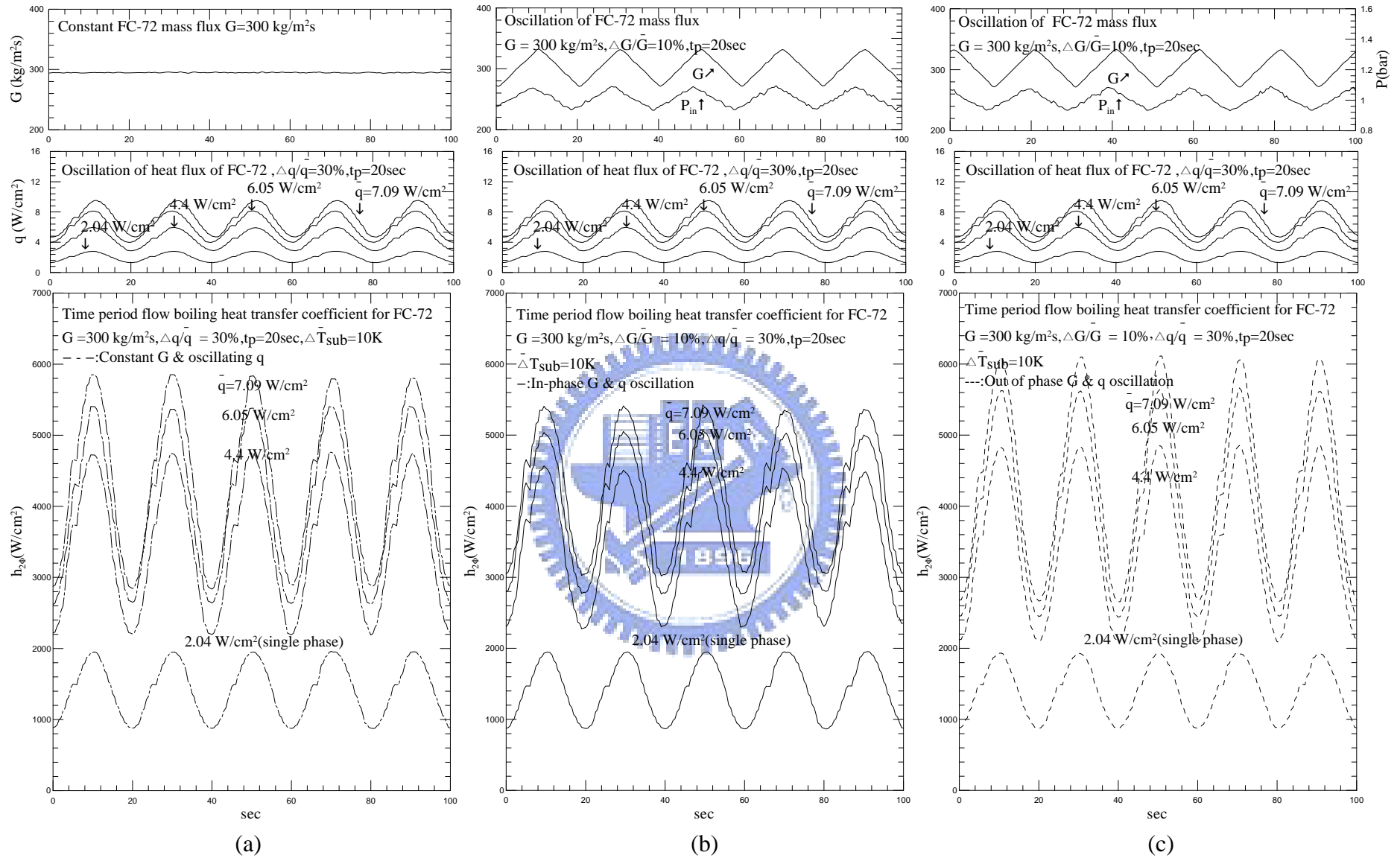


Fig. 5.20 Time variations of the heat transfer coefficient for (a) imposed heat flux oscillation only, (b) in-phase G and q oscillations and (c) out-of-phase G and q oscillations at $\bar{G} = 300 \text{ kg/m}^2\text{s}$ and $\Delta G/\bar{G} = 10\%$ for $\Delta q/\bar{q} = 30\%$ and $t_p = 20 \text{ sec}$. for $\Delta T_{sub} = 10 \text{ K}$.

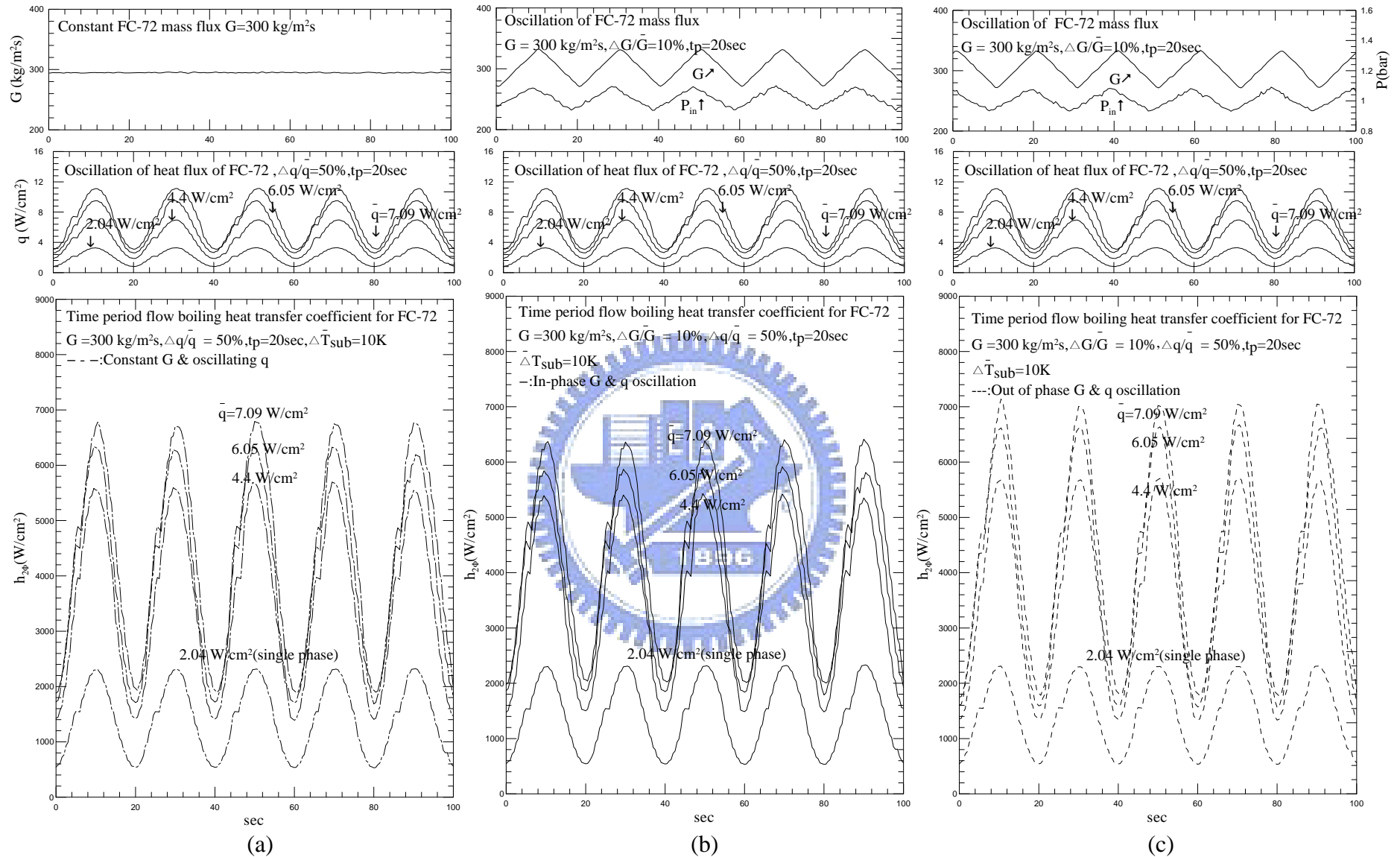


Fig. 5.21 Time variations of the heat transfer coefficient for (a) imposed heat flux oscillation only, (b) in-phase G and q oscillations and (c) out-of-phase G and q oscillations at $\bar{G} = 300 \text{ kg/m}^2\text{s}$ and $\Delta G/\bar{G} = 10\%$ for $\Delta q/\bar{q} = 50\%$ and $t_p = 20 \text{ sec}$. for $\Delta \bar{T}_{sub} = 10 \text{ K}$.

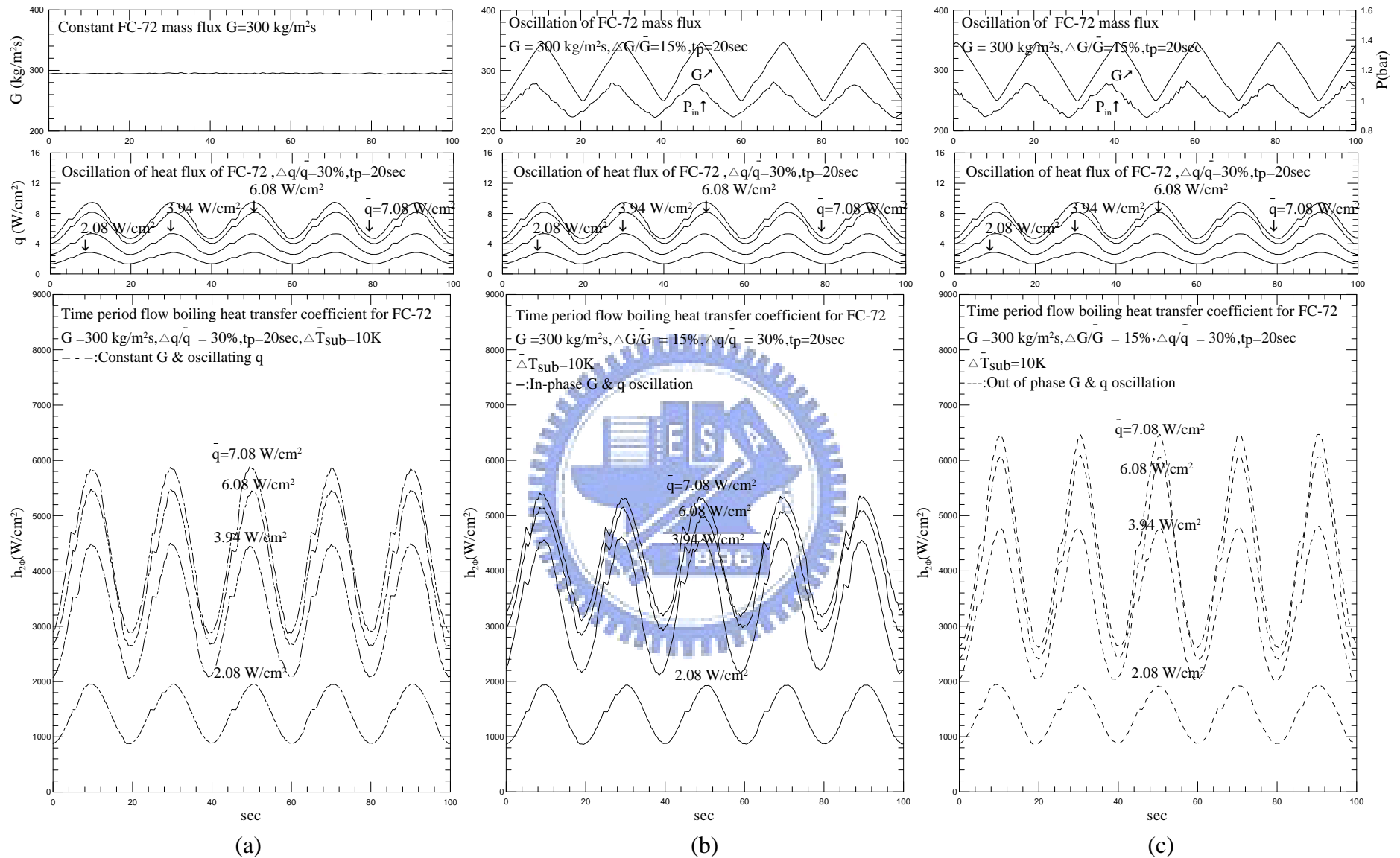


Fig. 5.22 Time variations of the heat transfer coefficient for (a) imposed heat flux oscillation only, (b) in-phase G and q oscillations and (c) out-of-phase G and q oscillations at $\bar{G} = 300 \text{ kg/m}^2\text{s}$ and $\Delta G/\bar{G} = 15\%$ for $\Delta q/\bar{q} = 30\%$ and $t_p = 20 \text{ sec}$. for $\Delta \bar{T}_{sub} = 10 \text{ K}$.

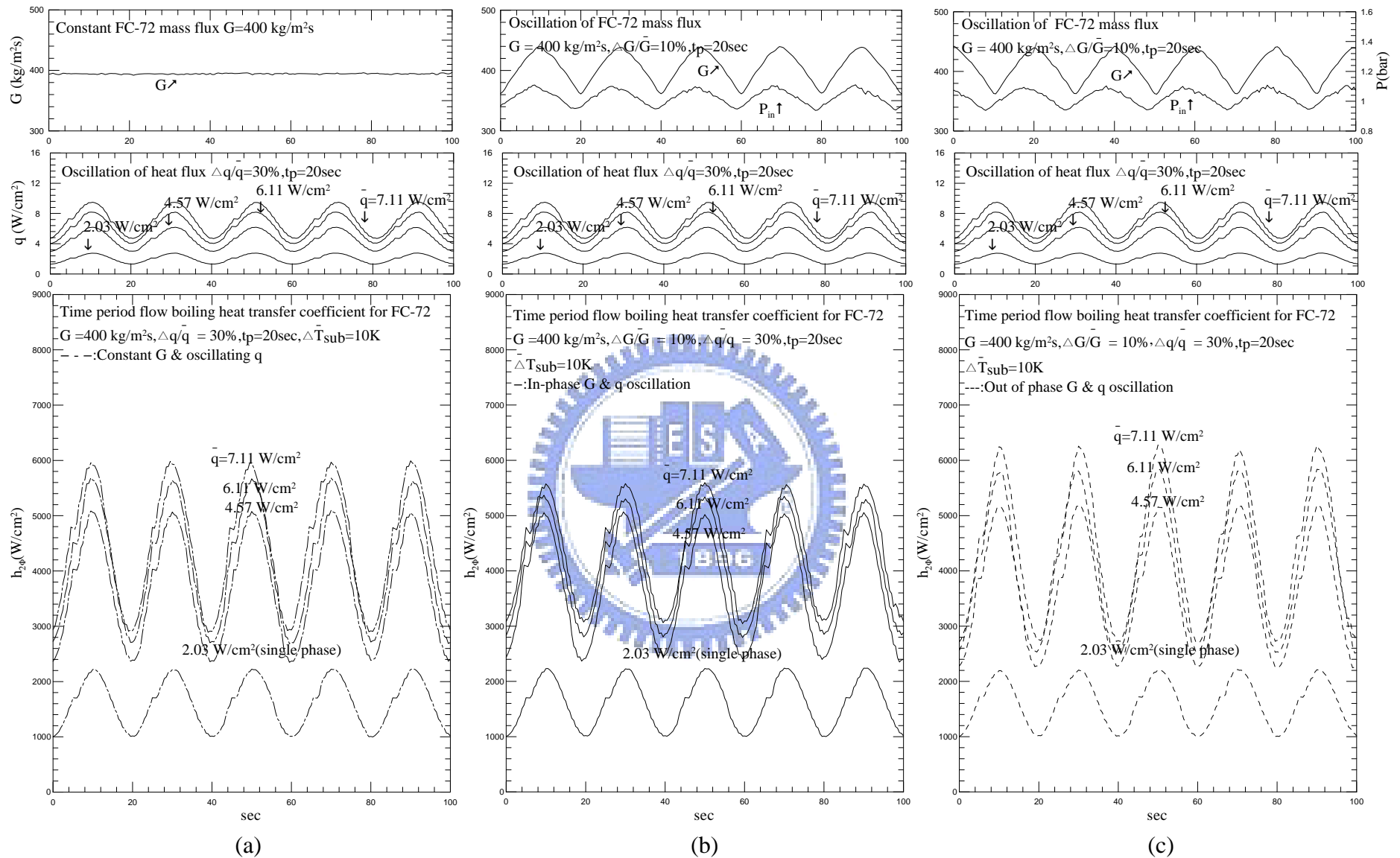


Fig. 5.23 Time variations of the heat transfer coefficient for (a) imposed heat flux oscillation only, (b) in-phase G and q oscillations and (c) out-of-phase G and q oscillations at $\bar{G} = 400 \text{ kg/m}^2 \text{ s}$ and $\Delta G/\bar{G} = 10\%$ for $\Delta q/\bar{q} = 30\%$ and $t_p = 20 \text{ sec}$. for $\Delta \bar{T}_{sub} = 10 \text{ K}$.

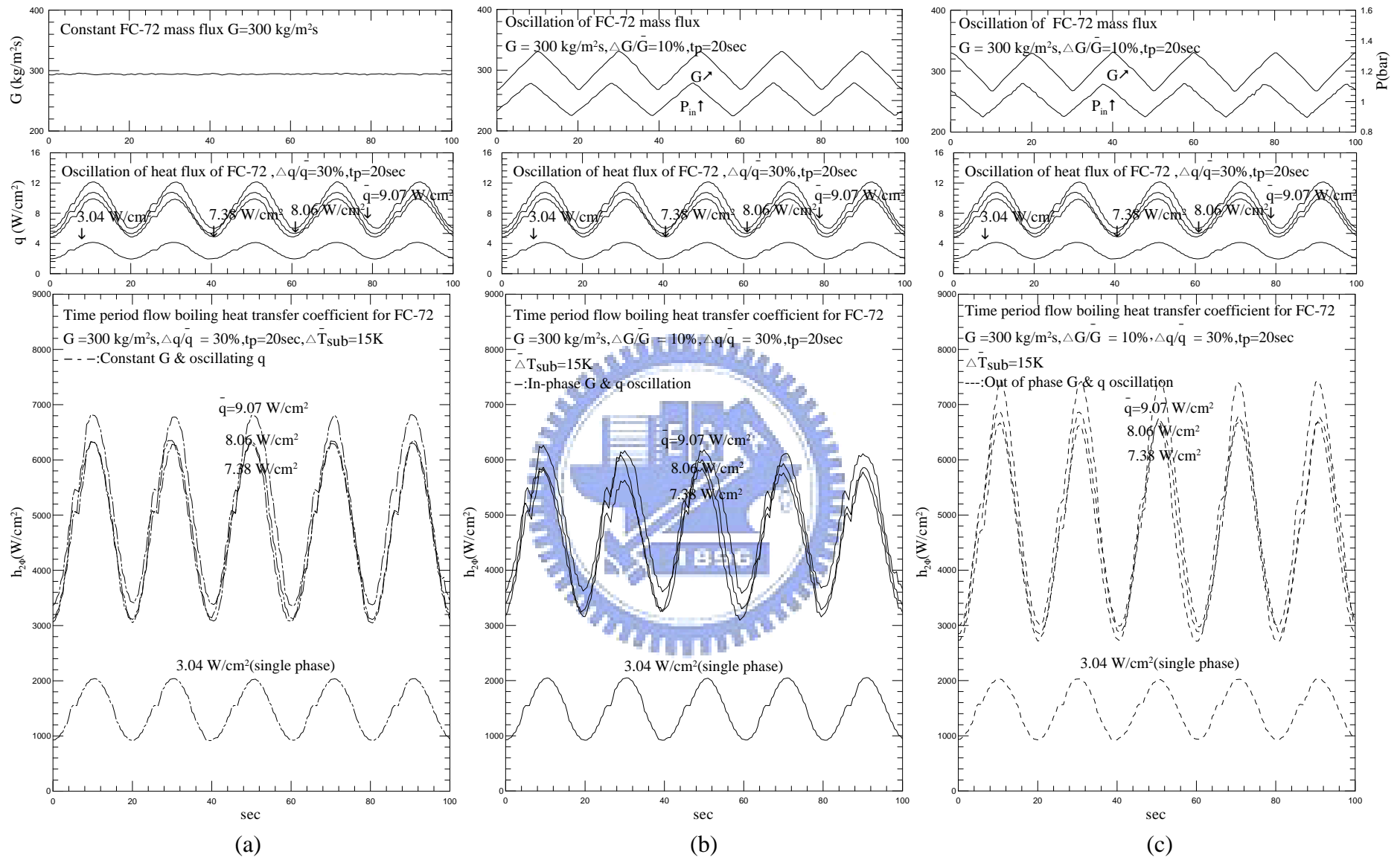


Fig. 5.24 Time variations of the heat transfer coefficient for (a) imposed heat flux oscillation only, (b) in-phase G and q oscillations and (c) out-of-phase G and q oscillations at $\bar{G} = 300 \text{ kg/m}^2\text{s}$ and $\Delta G/\bar{G} = 10\%$ for $\Delta q/\bar{q} = 30\%$ and $t_p = 20$ sec. for $\Delta \bar{T}_{sub} = 15 \text{ K}$.

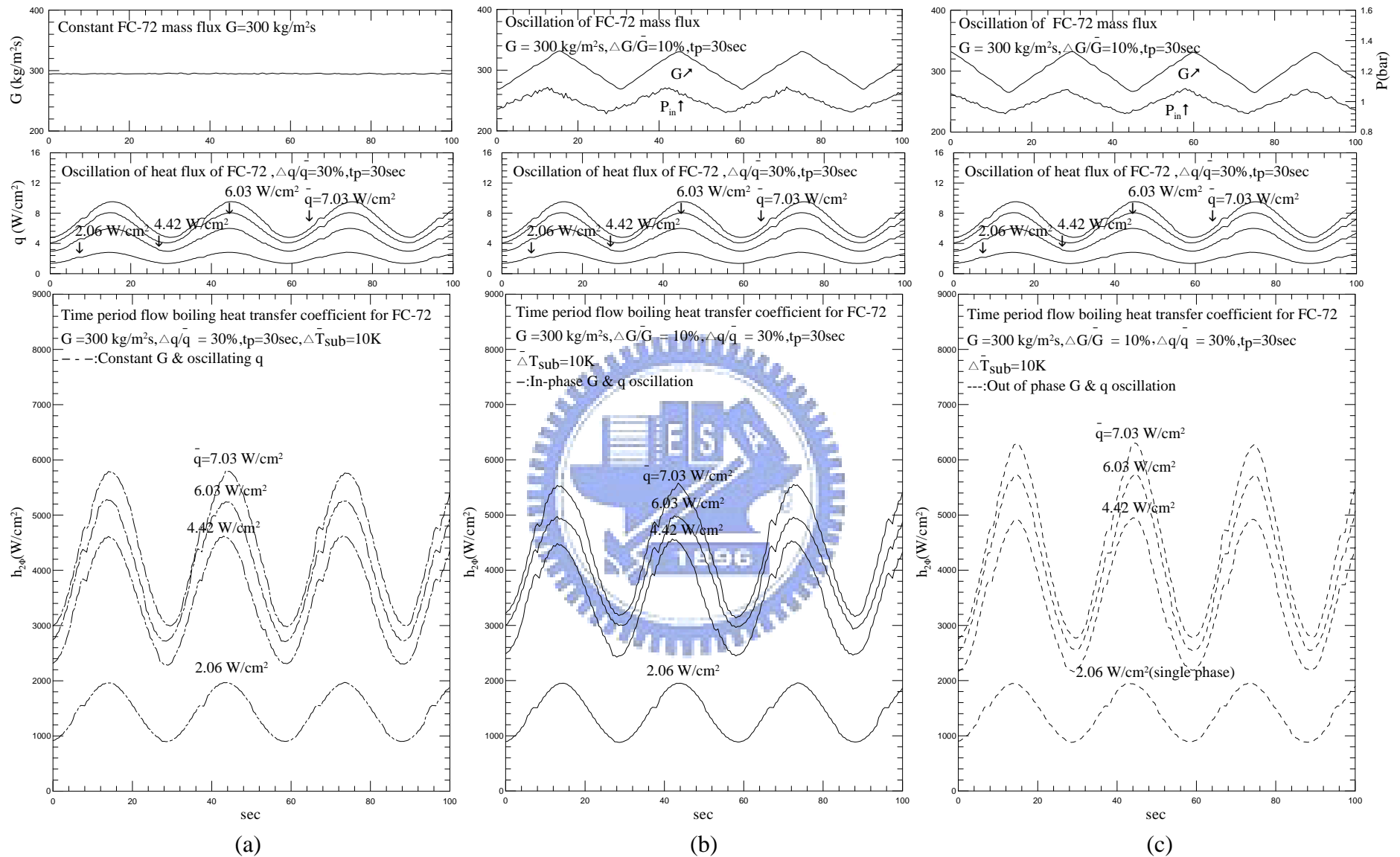


Fig. 5.25 Time variations of the heat transfer coefficient for (a) imposed heat flux oscillation only, (b) in-phase G and q oscillations and (c) out-of-phase G and q oscillations at $\bar{G} = 300$ kg/m²s and $\Delta G/\bar{G} = 10\%$ for $\Delta q/\bar{q} = 30\%$ and $t_p = 30$ sec. for $\Delta T_{sub} = 10$ K.

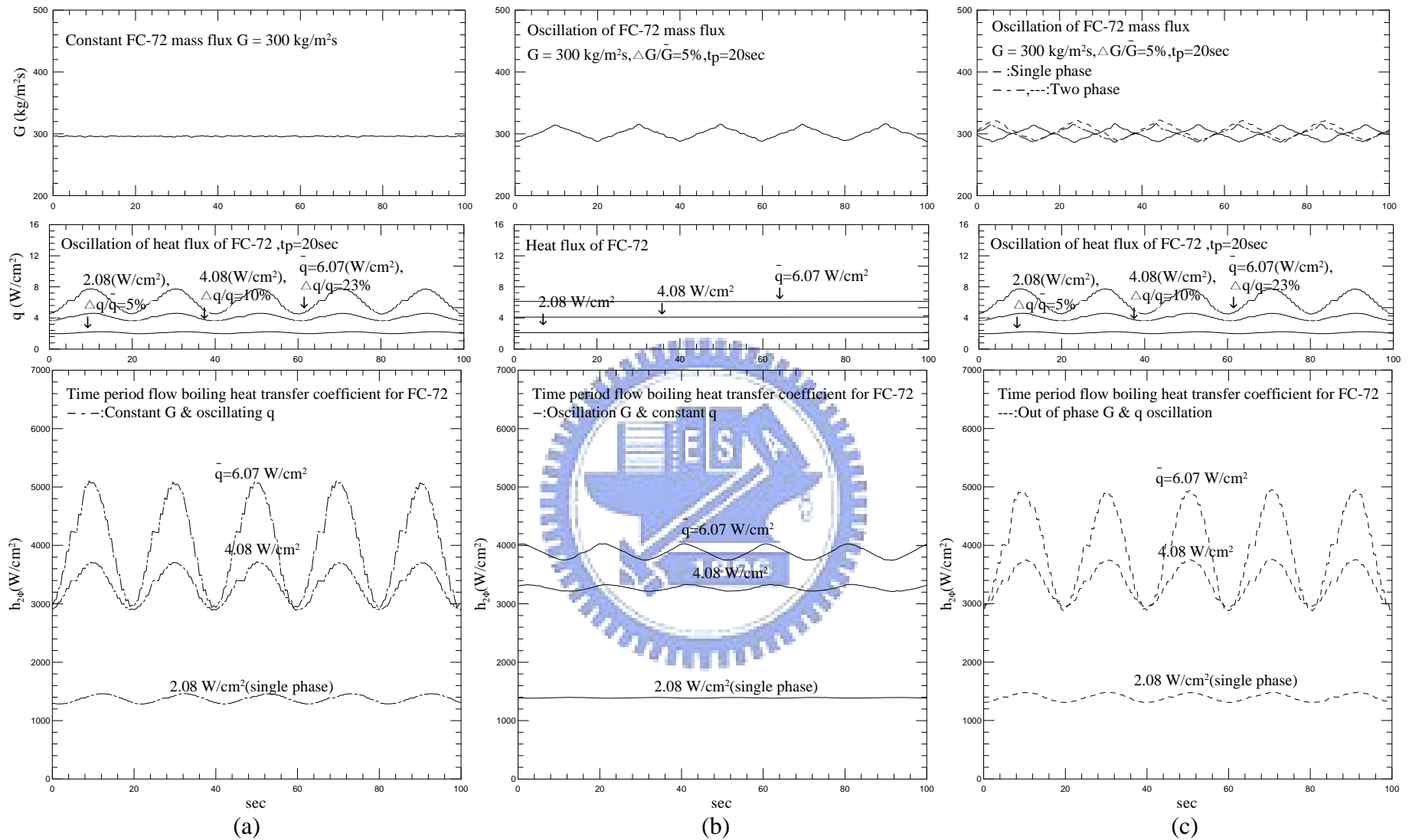


Fig. 5.26 Time variations of the heat transfer coefficient for (a) imposed heat flux oscillation only, (b) imposed mass flux oscillation only and (c) out-of-phase G and q oscillations at $\bar{G} = 300$ kg/m²s and $\Delta G/\bar{G} = 5\%$ for $\Delta q/\bar{q} = 5, 10, 23\%$ and $t_p = 20$ sec. for $\Delta T_{sub} = 10$ K.

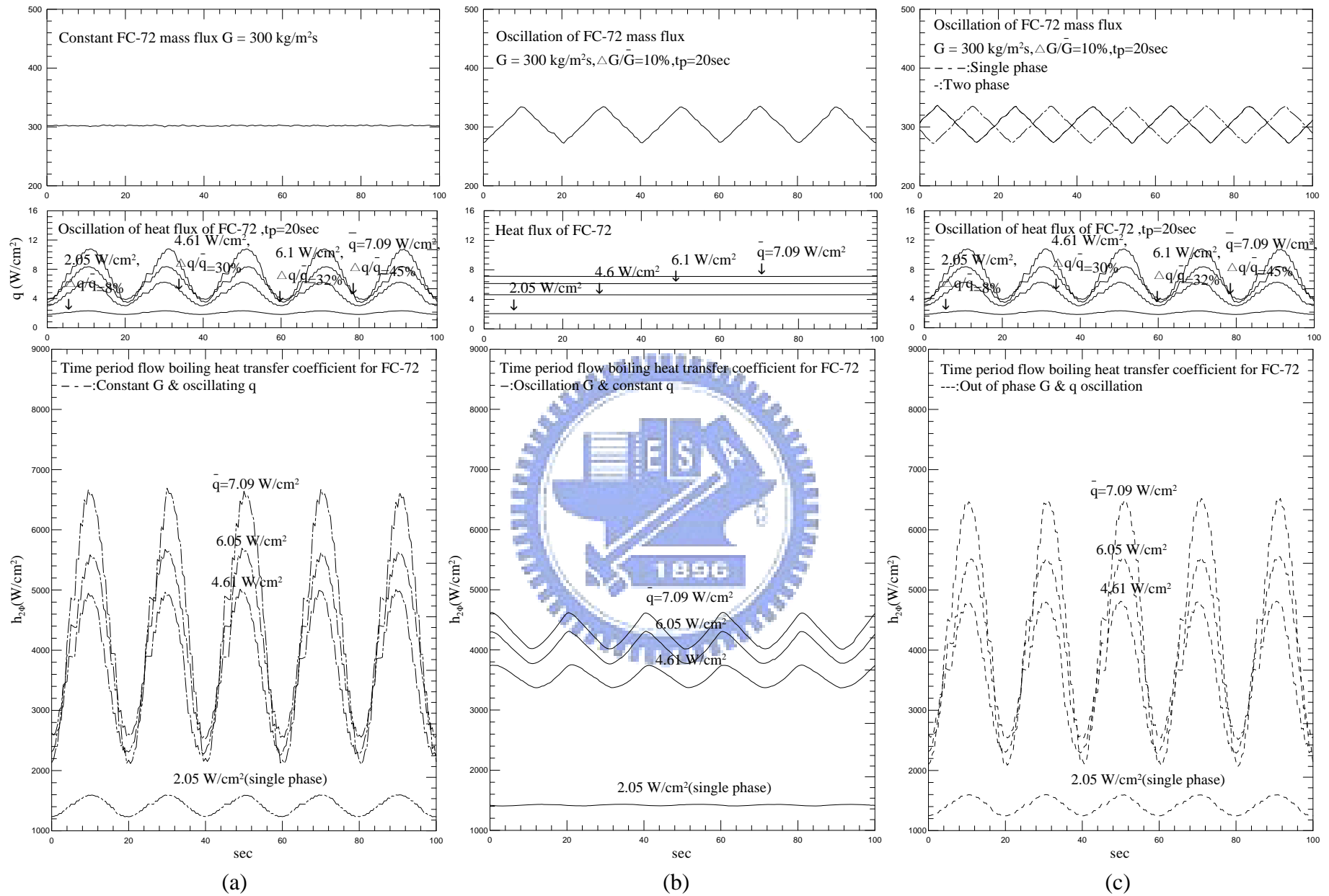


Fig. 5.27 Time variations of the heat transfer coefficient for (a) imposed heat flux oscillation only, (b) imposed mass flux oscillation only and (c) out-of-phase G and q oscillations at $\bar{G} = 300 \text{ kg/m}^2\text{s}$ and $\Delta G/\bar{G} = 10\%$ for $\Delta q/\bar{q} = 8, 30, 32, 45\%$ and $t_p = 20 \text{ sec}$. for $\Delta \bar{T}_{sub} = 10 \text{ K}$.

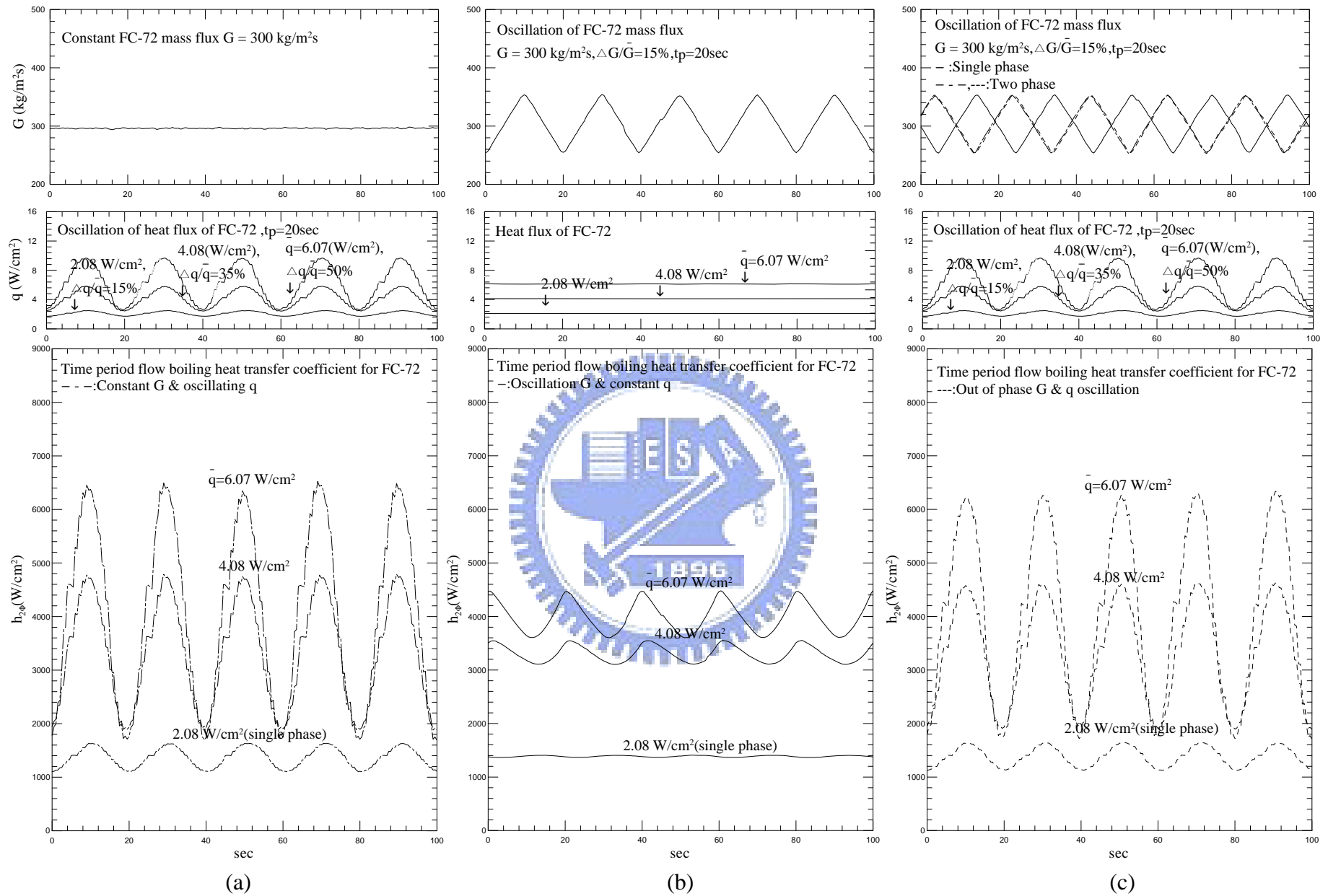


Fig. 5.28 Time variations of the heat transfer coefficient for (a) imposed heat flux oscillation only, (b) imposed mass flux oscillation only and (c) out-of-phase G and q oscillations at $\bar{G} = 300$ kg/m²s and $\Delta G/\bar{G} = 15\%$ for $\Delta q/\bar{q} = 15, 35, 50\%$ and $t_p = 20$ sec. for $\Delta T_{sub} = 10$ K.

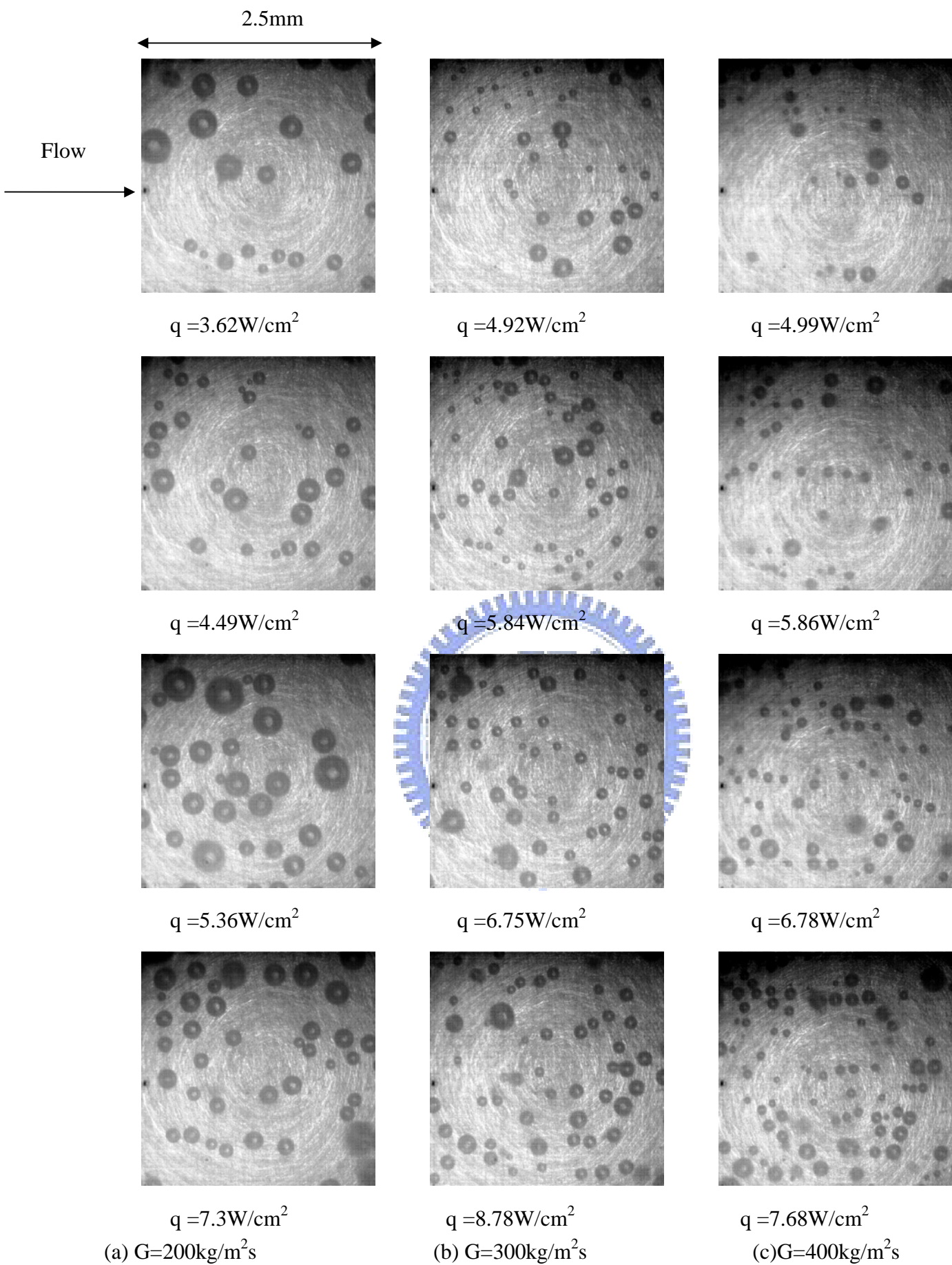


Fig. 5.29 Photos of stable subcooled flow boiling at certain time instants in statistical state for various imposed heat fluxes for (a) $G = 200 \text{ kg/m}^2\text{s}$, (b) $G = 300 \text{ kg/m}^2\text{s}$ and (c) $G = 400 \text{ kg/m}^2\text{s}$ at $\Delta \bar{T}_{sub} = 10 \text{ K}$.

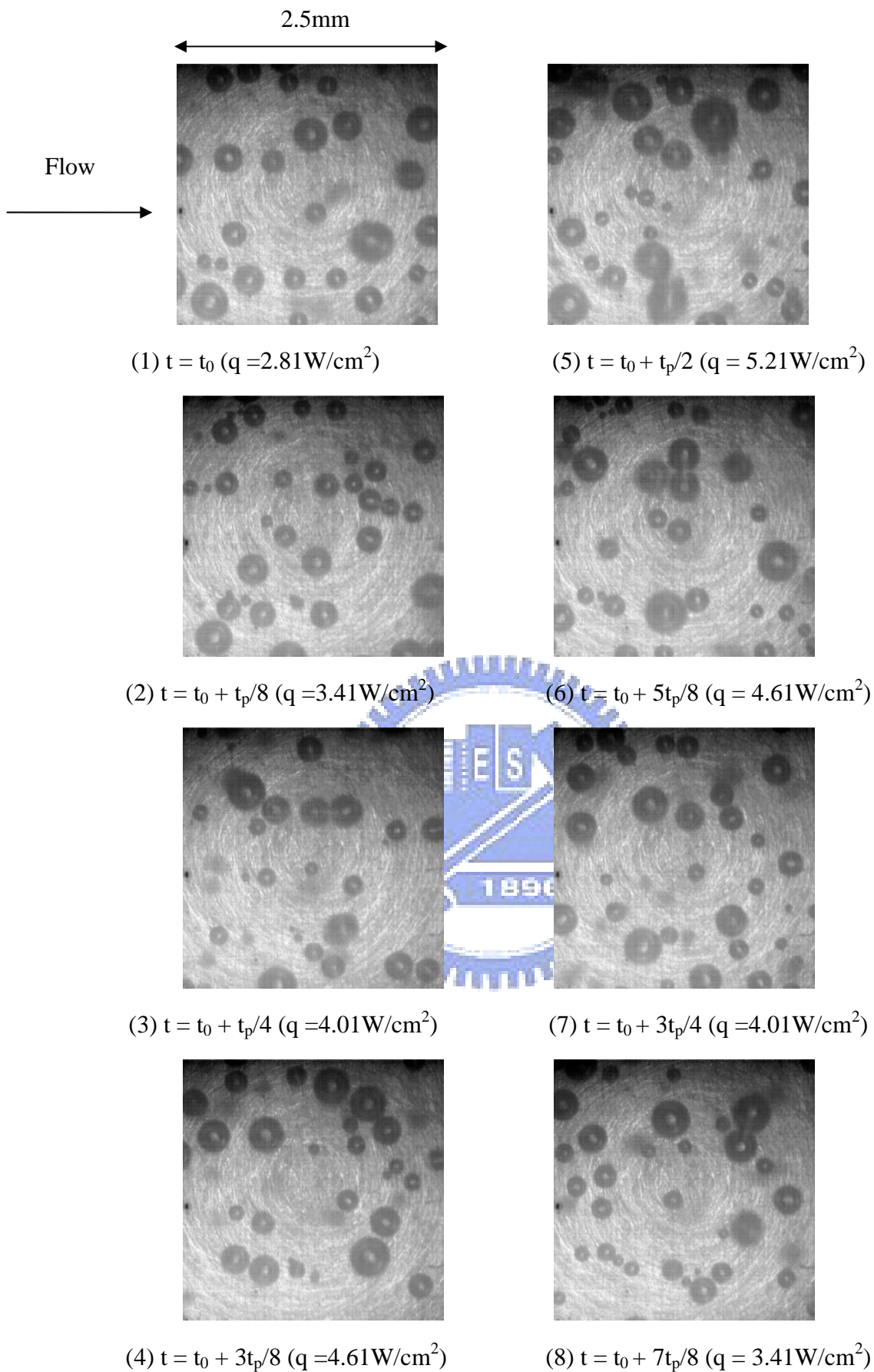


Fig. 5.30 Photos of subcooled flow boiling at certain time instants in a typical time periodic cycle for a constant imposed mass flux at $\bar{q} = 4.01 \text{ W/cm}^2$, $\Delta q/\bar{q} = 30\%$ and $G = 200 \text{ kg/m}^2\text{s}$ with $t_p = 20 \text{ sec}$. and $\Delta \bar{T}_{sub} = 10 \text{ K}$.

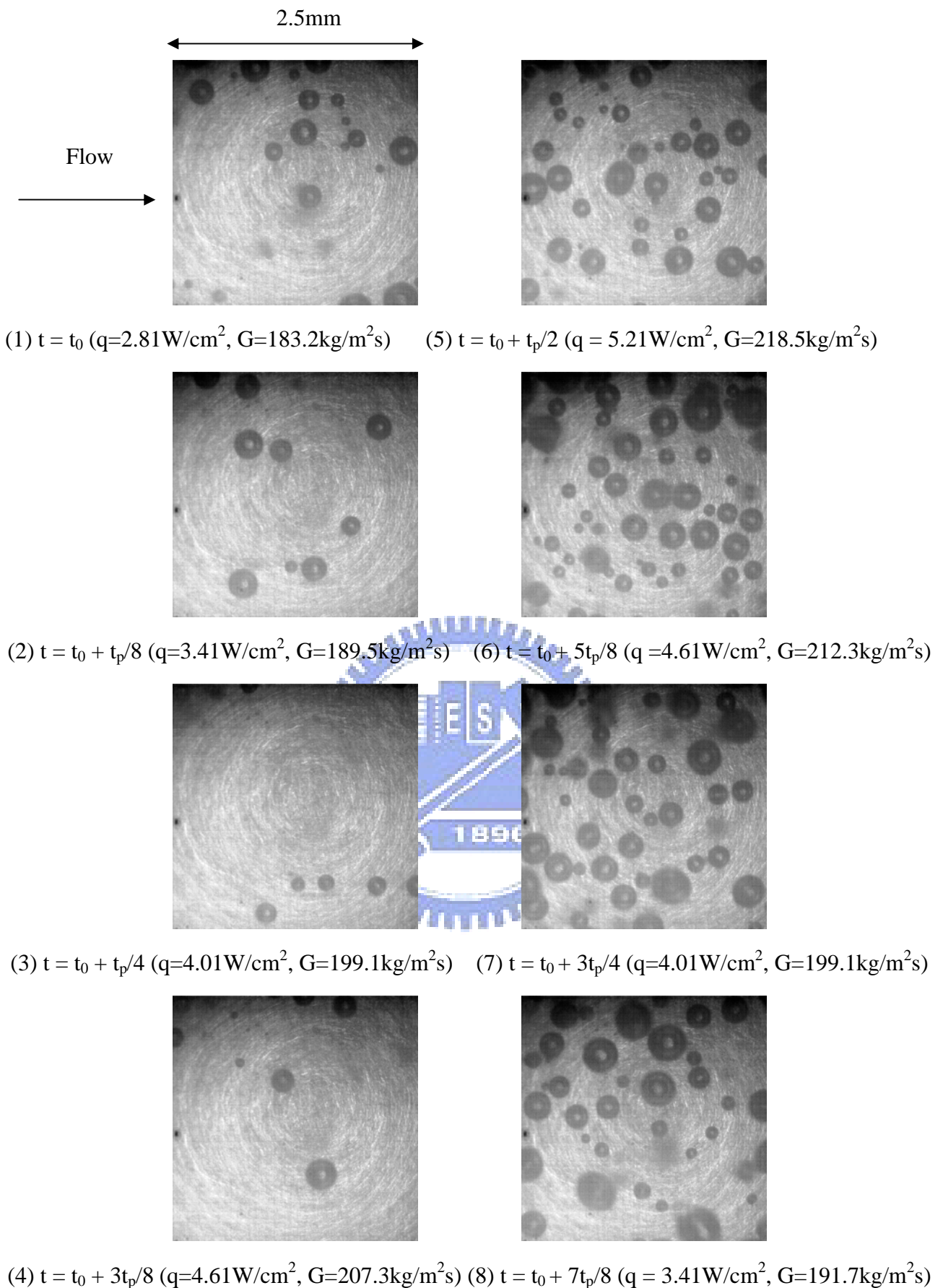


Fig. 5.31 Photos of subcooled flow boiling at certain time instants in a typical time periodic cycle for imposed in-phase G & q oscillations at $\bar{G} = 200\text{kg/m}^2\text{s}$, $\Delta G/\bar{G} = 10\%$, $\bar{q} = 4.01\text{W/cm}^2$ and $\Delta q/\bar{q} = 30\%$ with $t_p = 20\text{sec.}$ and $\Delta \bar{T}_{sub} = 10\text{K.}$

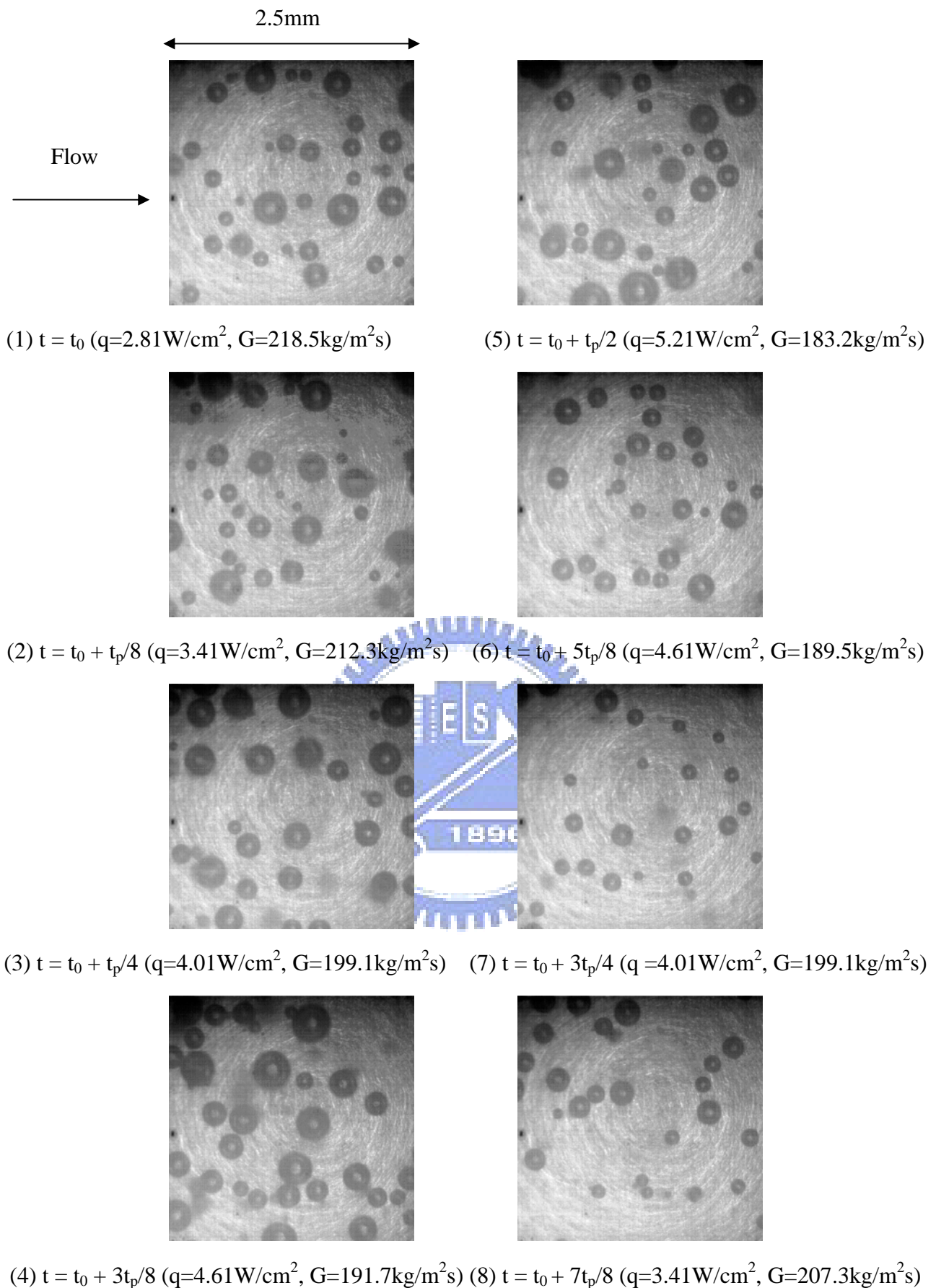


Fig. 5.32 Photos of subcooled flow boiling at certain time instants in a typical time periodic cycle for imposed out-of-phase G & q oscillations at $\bar{G}=200\text{kg/m}^2\text{s}$, $\Delta G/\bar{G}=10\%$, $\bar{q}=4.01\text{W/cm}^2$ and $\Delta q/\bar{q}=30\%$ with $t_p = 20\text{sec.}$ and $\Delta \bar{T}_{sub}=10\text{K.}$

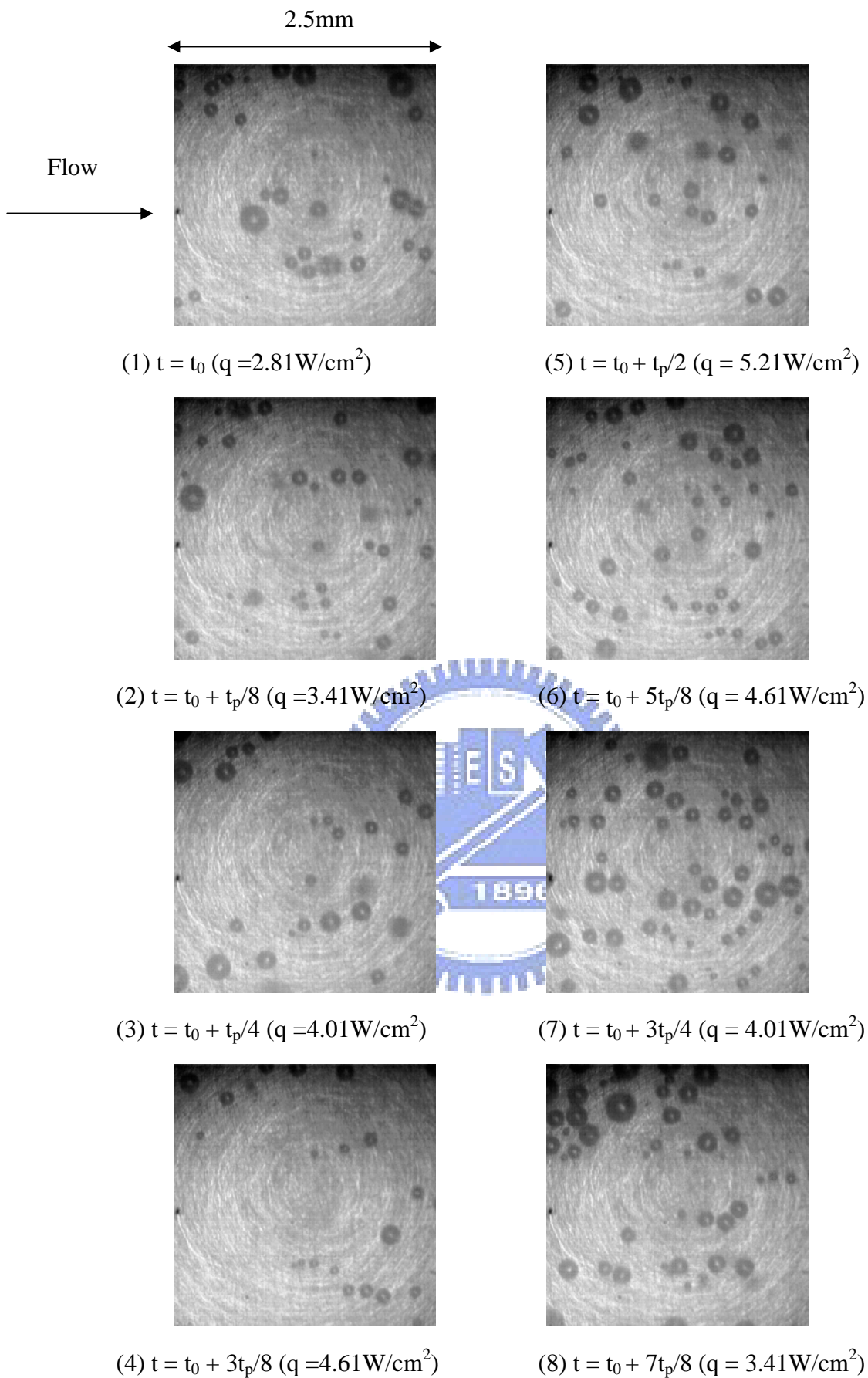


Fig. 5.33 Photos of subcooled flow boiling at certain time instants in a typical time periodic cycle for a constant imposed mass flux at $\bar{q} = 4.01 \text{ W/cm}^2$, $\Delta q/\bar{q} = 30\%$ and $G = 300 \text{ kg/m}^2\text{s}$ with $t_p = 20 \text{ sec}$. and $\Delta T_{sub} = 10 \text{ K}$.

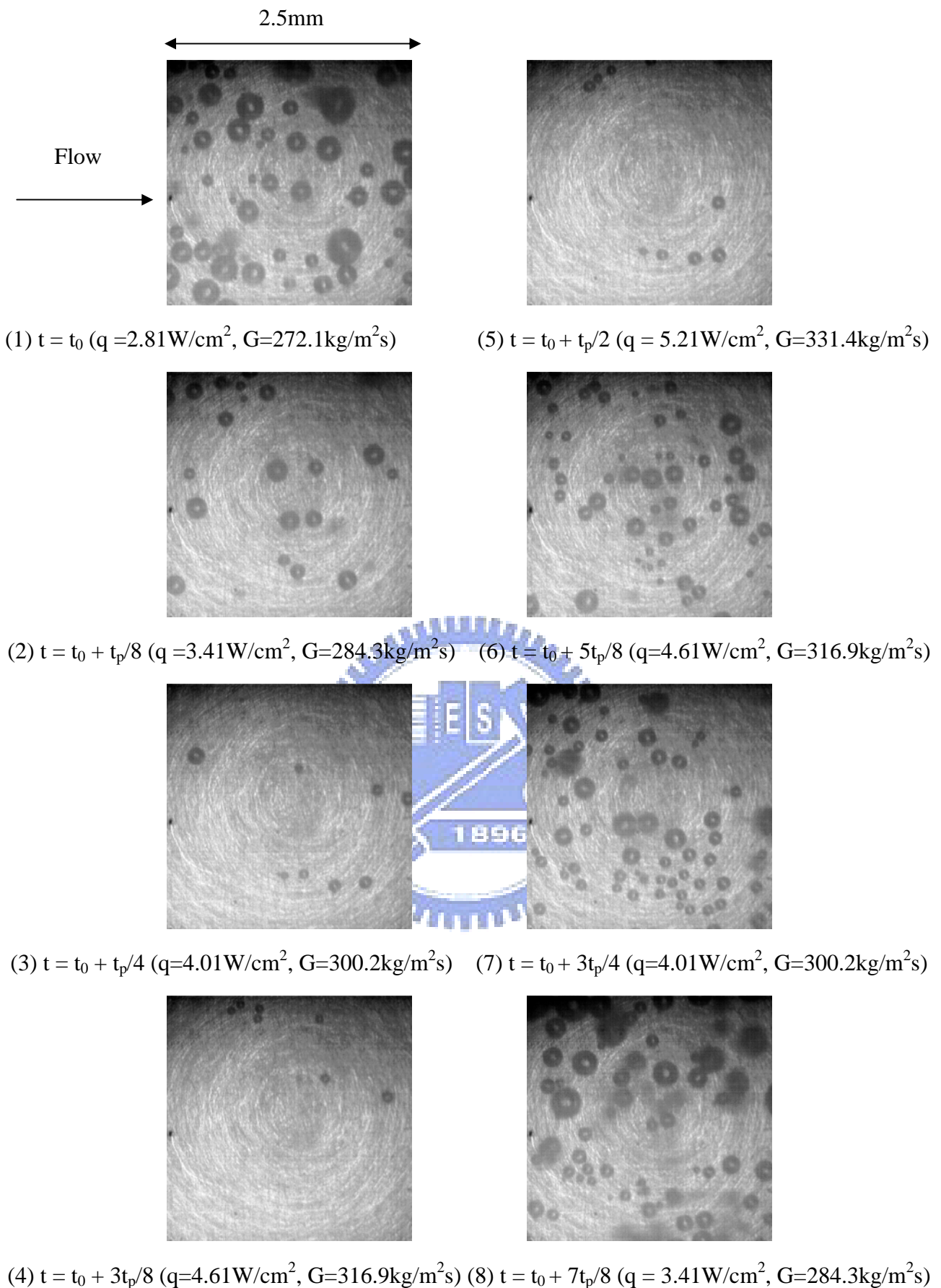


Fig. 5.34 Photos of subcooled flow boiling at certain time instants in a typical time periodic cycle for imposed in-phase G & q oscillations at $\bar{G} = 300 \text{ kg/m}^2\text{s}$, $\Delta G/\bar{G} = 10\%$, $\bar{q} = 4.01 \text{ W/cm}^2$ and $\Delta q/\bar{q} = 30\%$ with $t_p = 20 \text{ sec.}$ and $\Delta \bar{T}_{sub} = 10 \text{ K.}$

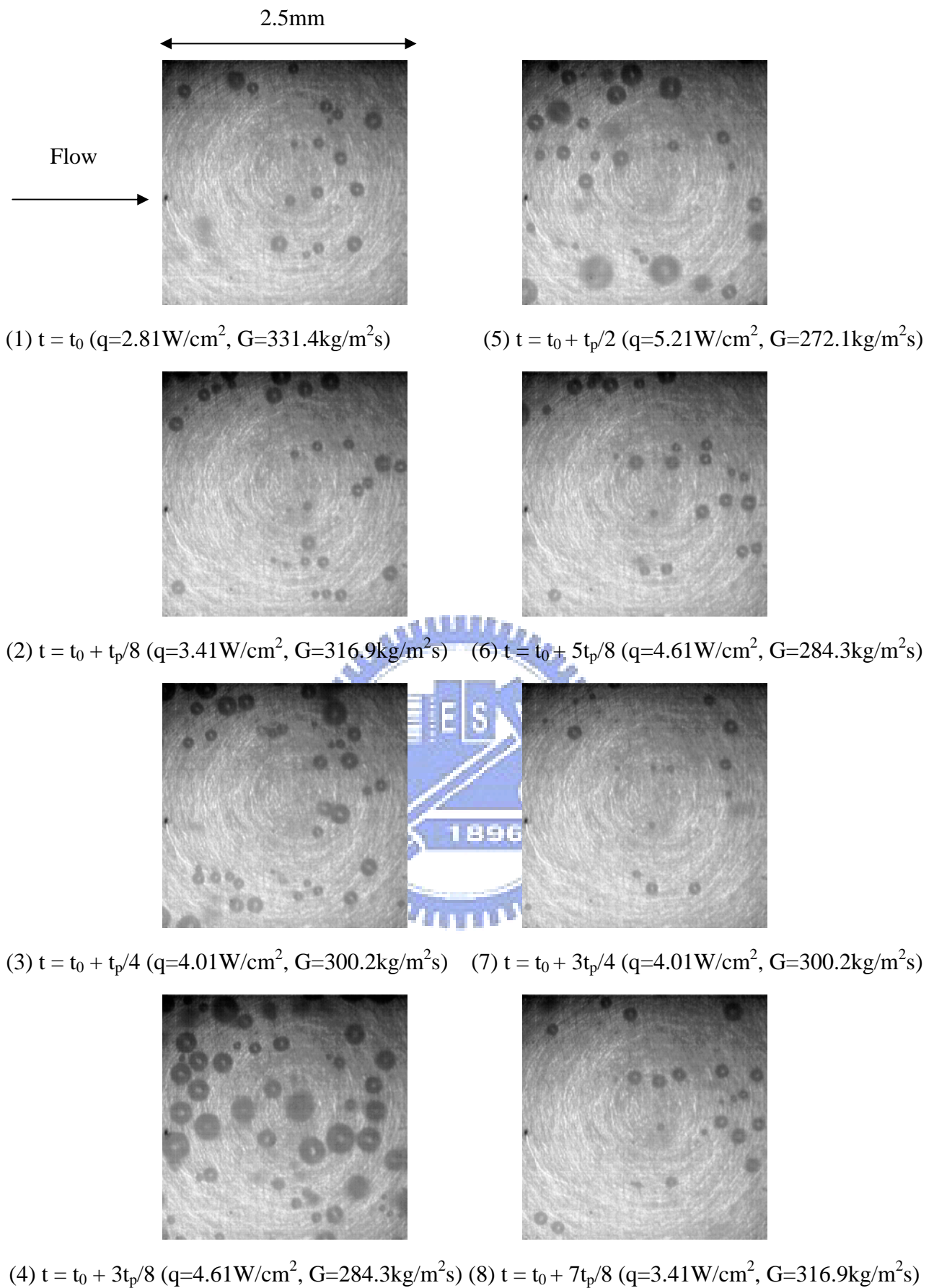


Fig. 5.35 Photos of subcooled flow boiling at certain time instants in a typical time periodic cycle for imposed out-of-phase G & q oscillations at $\bar{G}=300\text{kg/m}^2\text{s}$, $\Delta G/\bar{G}=10\%$, $\bar{q}=4.01\text{W/cm}^2$ and $\Delta q/\bar{q}=30\%$ with $t_p=20\text{sec}$. and $\Delta\bar{T}_{sub}=10\text{K}$.

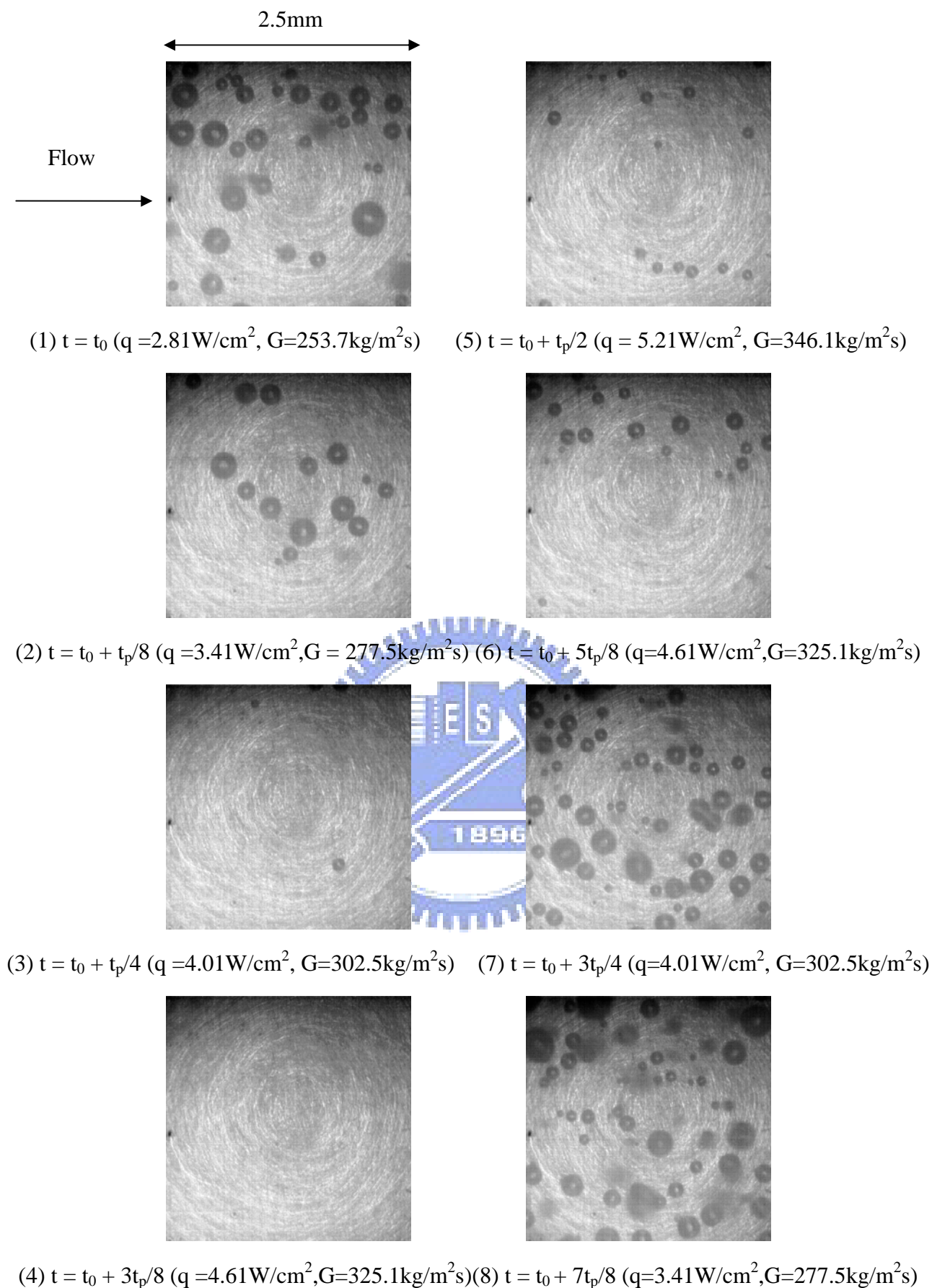


Fig. 5.36 Photos of subcooled flow boiling at certain time instants in a typical time periodic cycle for imposed in-phase G & q oscillations at $\bar{G} = 300 \text{ kg/m}^2\text{s}$, $\Delta G/\bar{G} = 15\%$, $\bar{q} = 4.01 \text{ W/cm}^2$ and $\Delta q/\bar{q} = 30\%$ with $t_p = 20 \text{ sec}$. and $\Delta \bar{T}_{sub} = 10 \text{ K}$.

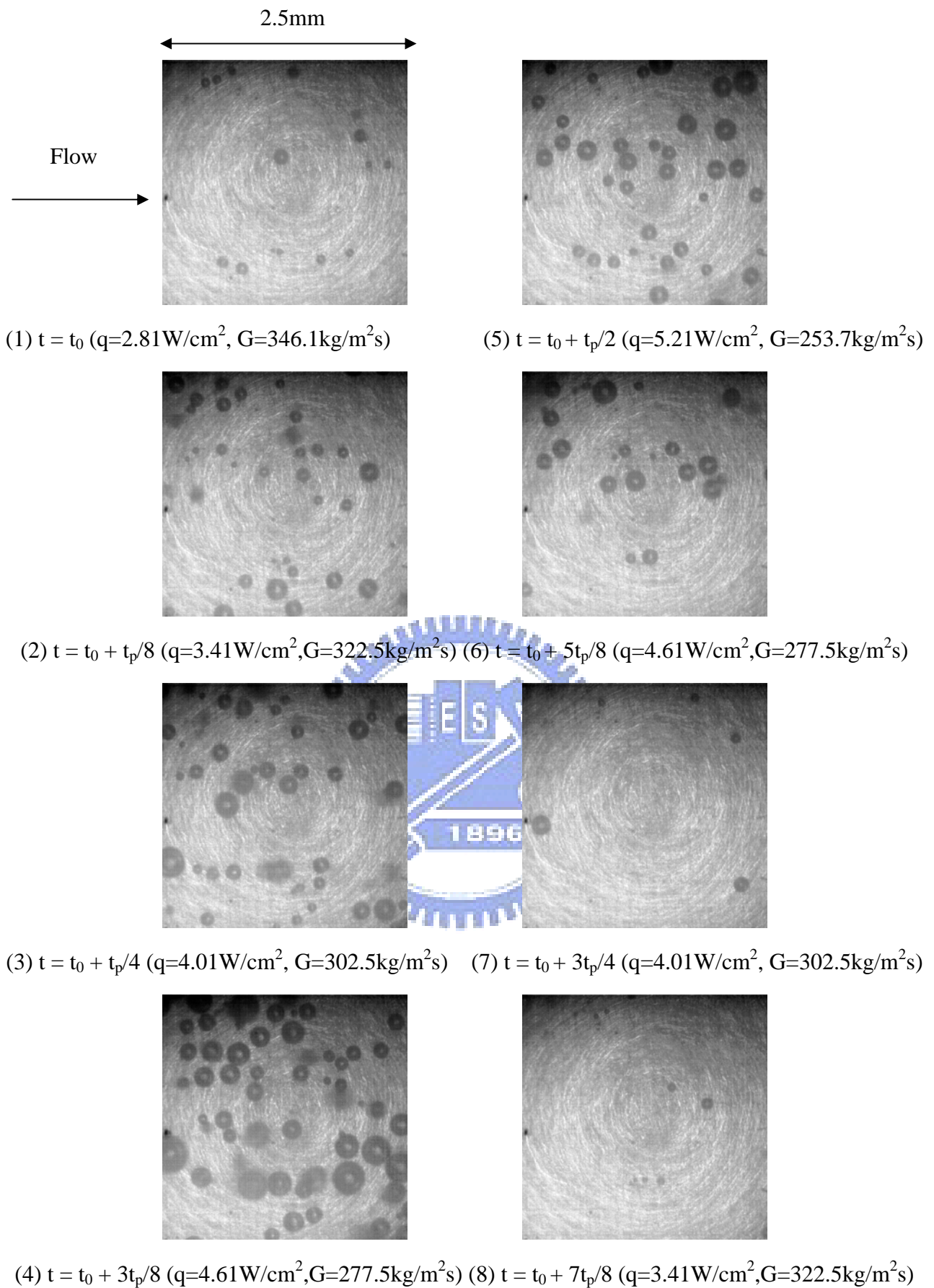


Fig. 5.37 Photos of subcooled flow boiling at certain time instants in a typical time periodic cycle for imposed out-of-phase G & q oscillations at $\bar{G}=300\text{kg/m}^2\text{s}$, $\Delta G/\bar{G}=15\%$, $\bar{q}=4.01\text{W/cm}^2$ and $\Delta q/\bar{q}=30\%$ with $t_p = 20\text{sec.}$ and $\Delta\bar{T}_{sub}=10\text{K.}$

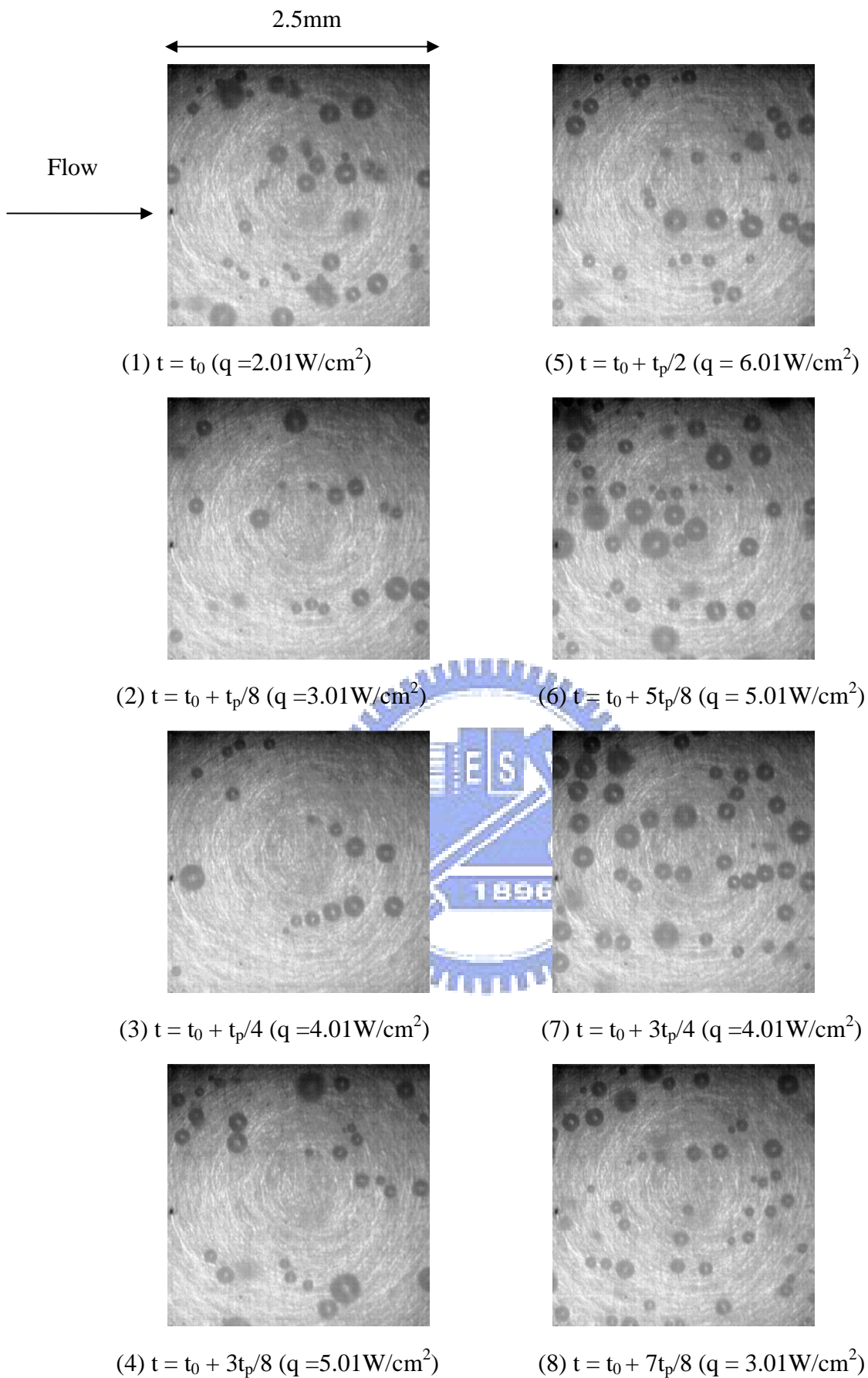


Fig. 5.38 Photos of subcooled flow boiling at certain time instants in a typical time periodic cycle for a constant imposed mass flux at $\bar{q} = 4.01 \text{W/cm}^2$, $\Delta q/\bar{q} = 50\%$ at $G = 300 \text{kg/m}^2\text{s}$ with $t_p = 20 \text{sec}$. and $\Delta \bar{T}_{sub} = 10 \text{K}$.

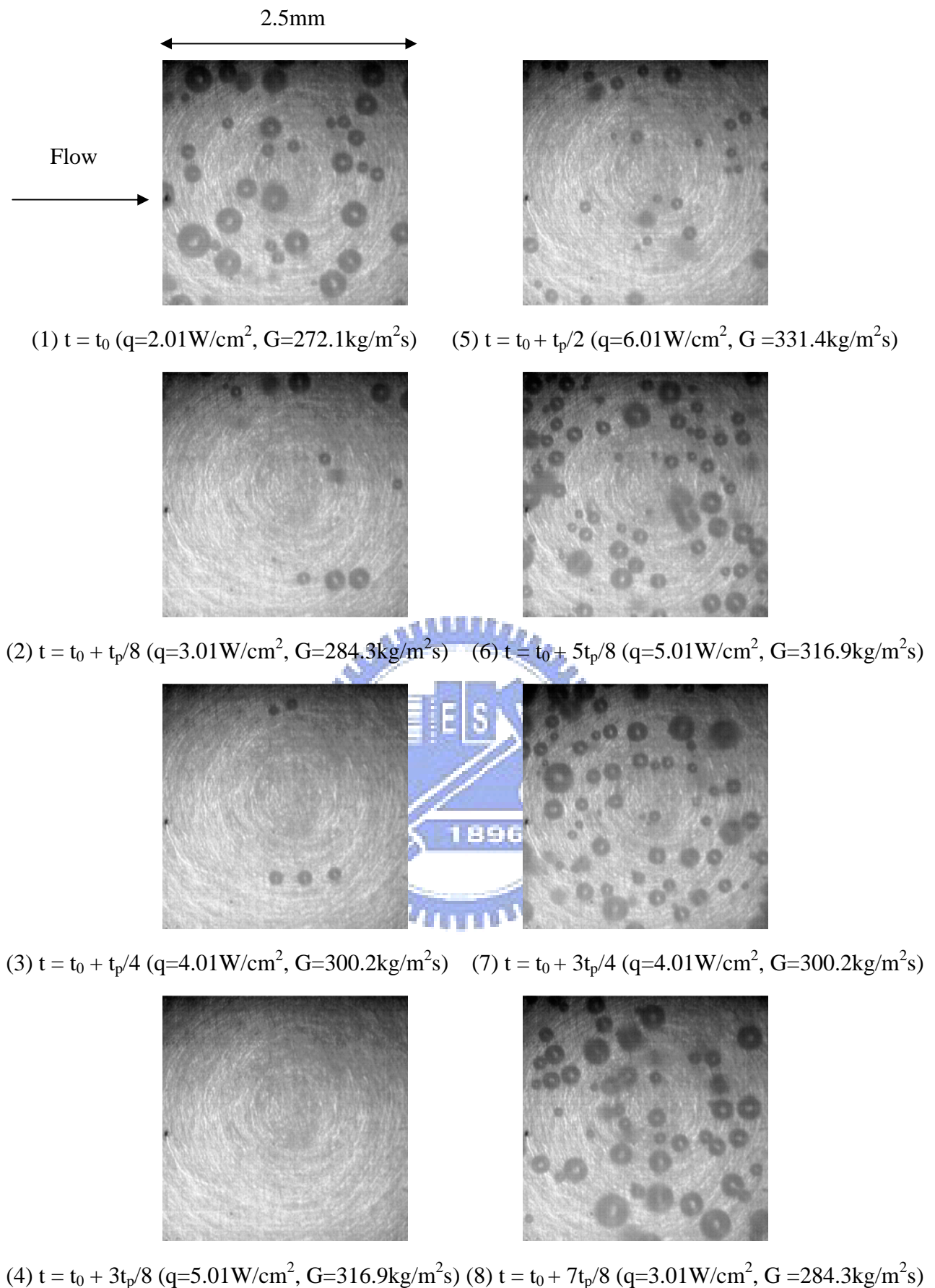


Fig. 5.39 Photos of subcooled flow boiling at certain time instants in a typical time periodic cycle for imposed in-phase G & q oscillations at $\bar{G} = 300\text{kg/m}^2\text{s}$, $\Delta G/\bar{G} = 10\%$, $\bar{q} = 4.01\text{W/cm}^2$ and $\Delta q/\bar{q} = 50\%$ with a $t_p = 20\text{sec}$. and $\Delta T_{sub} = 10\text{K}$.

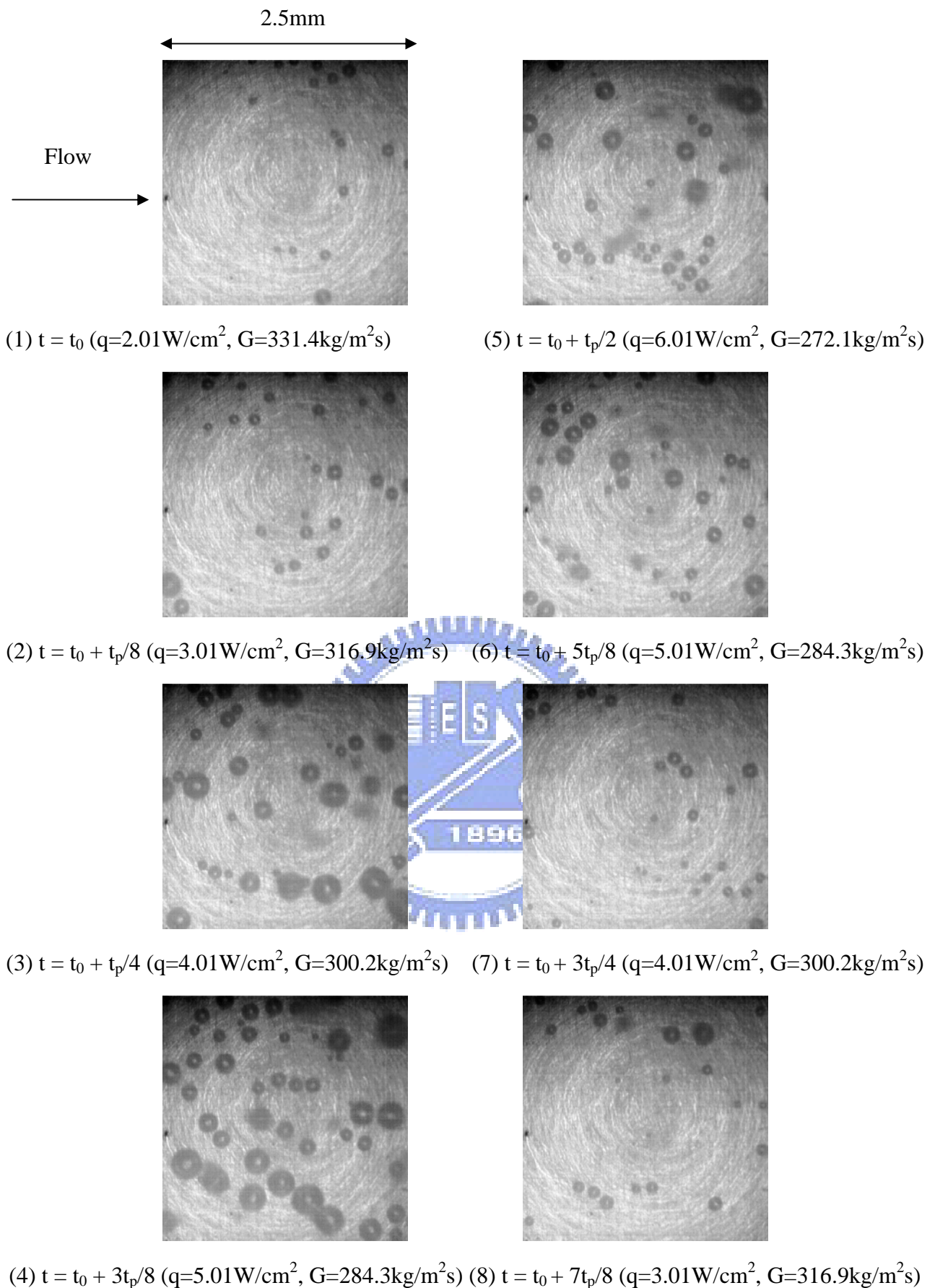


Fig. 5.40 Photos of subcooled flow boiling at certain time instants in a typical time periodic cycle for imposed out-of-phase G & q oscillations at $\bar{G}=300\text{kg/m}^2\text{s}$, $\Delta G/\bar{G}=10\%$, $\bar{q}=4.01\text{W/cm}^2$ and $\Delta q/\bar{q}=50\%$ with a $t_p=20\text{sec}$. and $\Delta T_{sub}=10\text{K}$.

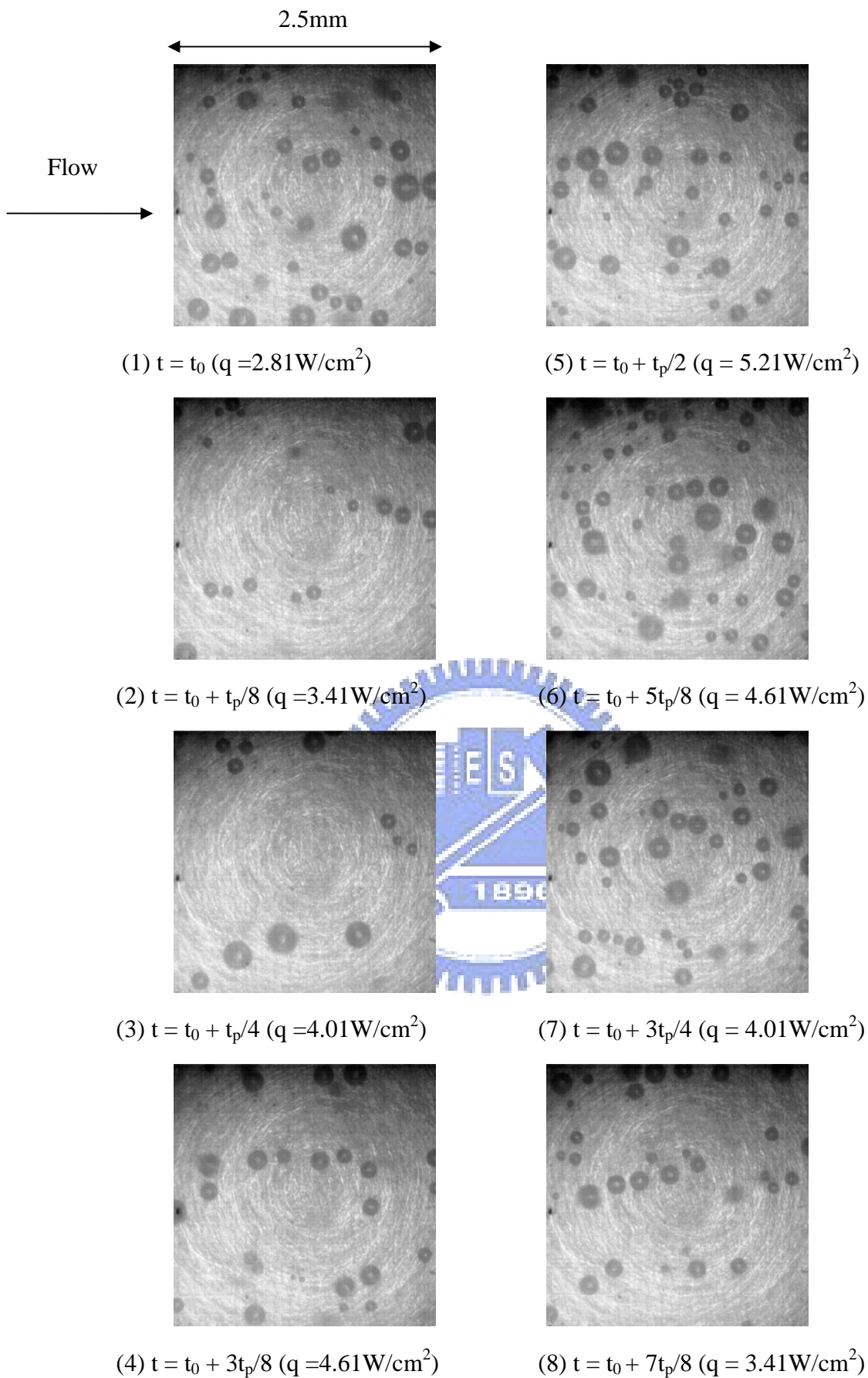


Fig. 5.41 Photos of subcooled flow boiling at certain time instants in a typical time periodic cycle for a constant imposed mass flux at $\bar{q} = 4.01 \text{ W/cm}^2$, $\Delta q/\bar{q} = 30\%$ at $G = 300 \text{ kg/m}^2\text{s}$ with $t_p = 30 \text{ sec}$. and $\Delta \bar{T}_{sub} = 10 \text{ K}$.

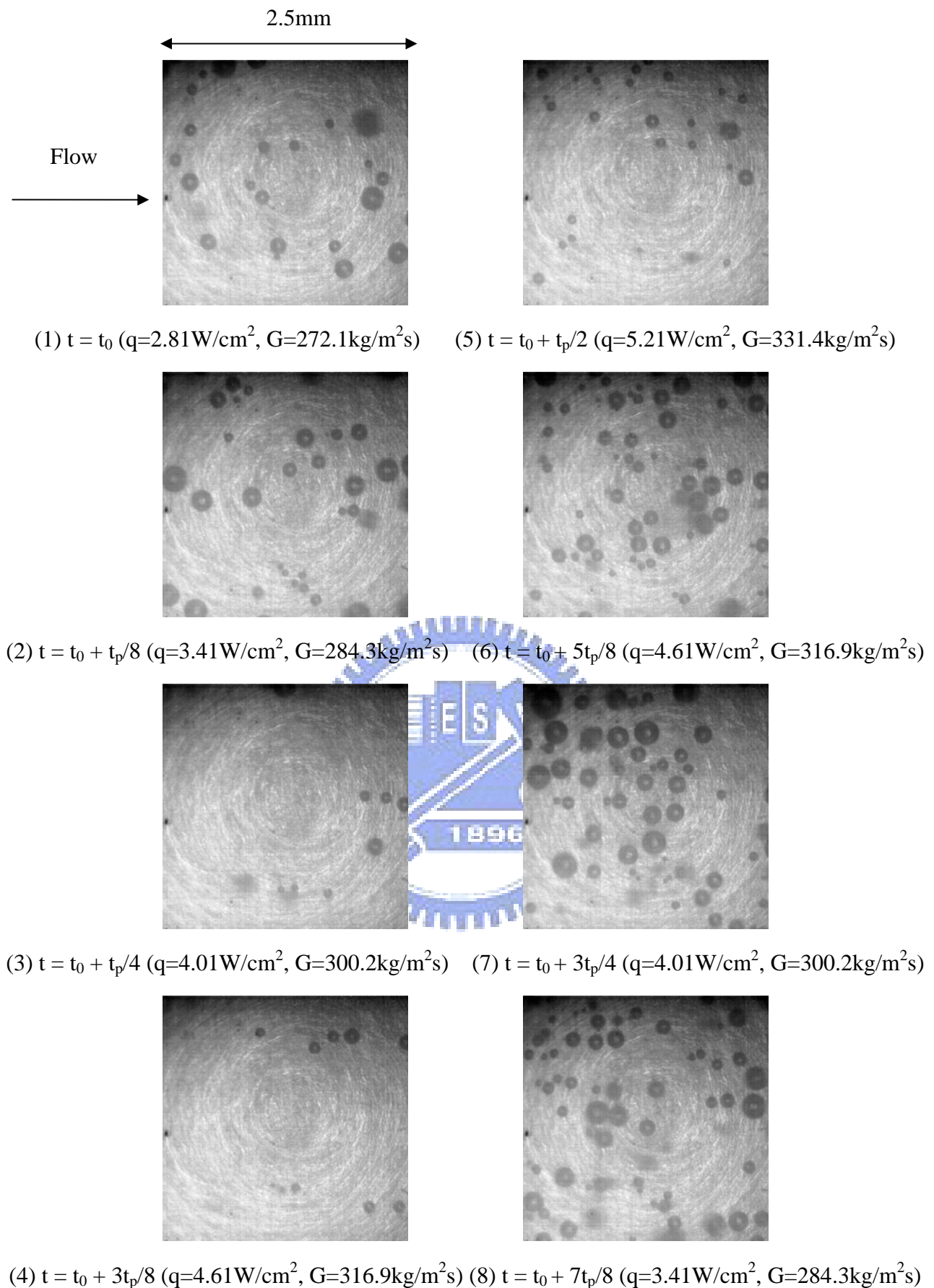


Fig. 5.42 Photos of subcooled flow boiling at certain time instants in a typical time periodic cycle for imposed in-phase G & q oscillations at $\bar{G}=300\text{kg/m}^2\text{s}$, $\Delta G/\bar{G}=10\%$, $\bar{q}=4.01\text{W/cm}^2$ and $\Delta q/\bar{q}=30\%$ with $t_p=30\text{sec}$. and $\Delta\bar{T}_{sub}=10\text{K}$.

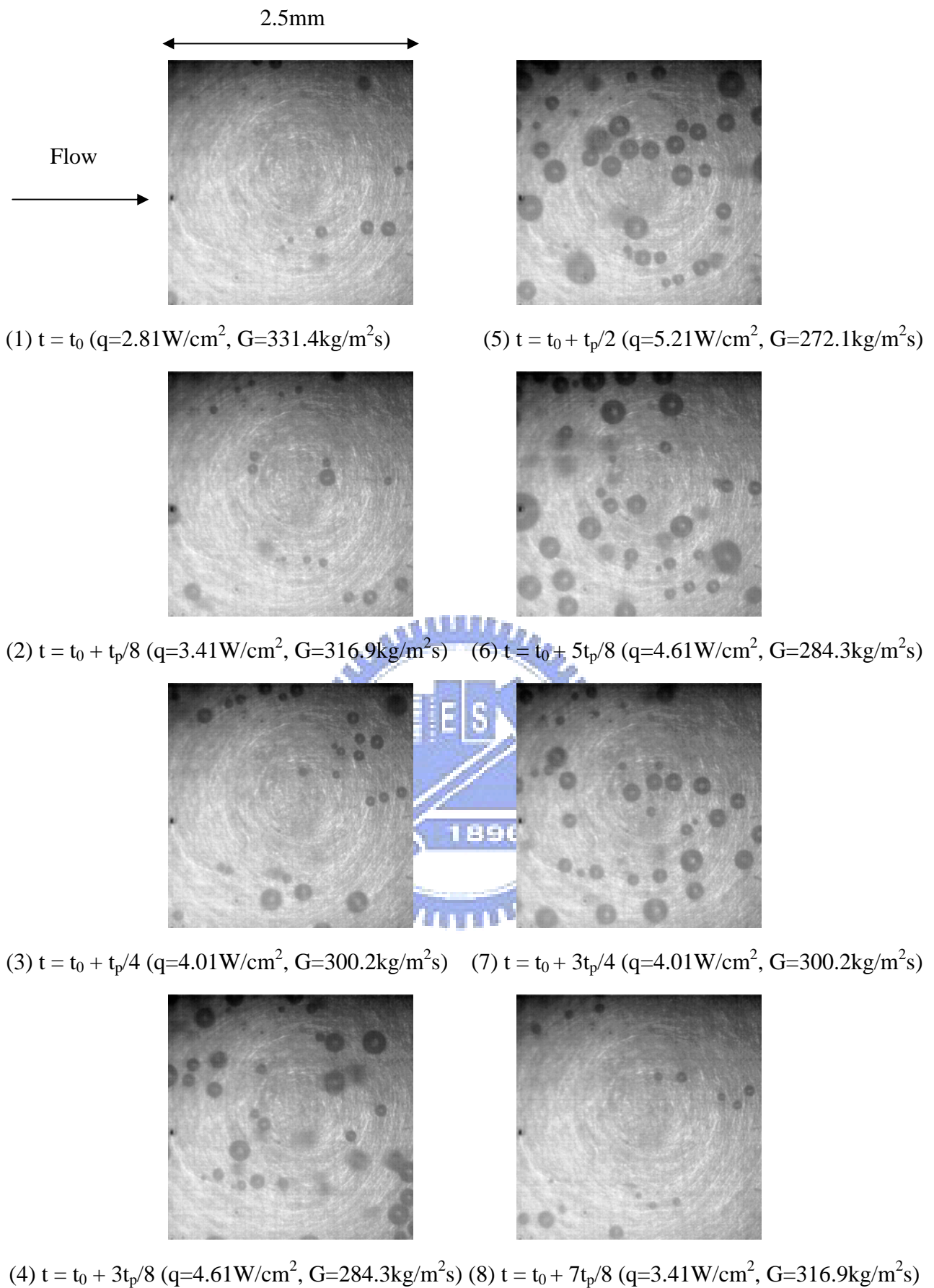


Fig. 5.43 Photos of subcooled flow boiling at certain time instants in a typical time periodic cycle for imposed out-of-phase G & q oscillations at $\bar{G}=300\text{kg/m}^2\text{s}$, $\Delta G/\bar{G}=10\%$, $\bar{q}=4.01\text{W/cm}^2$ and $\Delta q/\bar{q}=30\%$ with $t_p = 30\text{sec.}$ and $\Delta \bar{T}_{sub}=10\text{K.}$

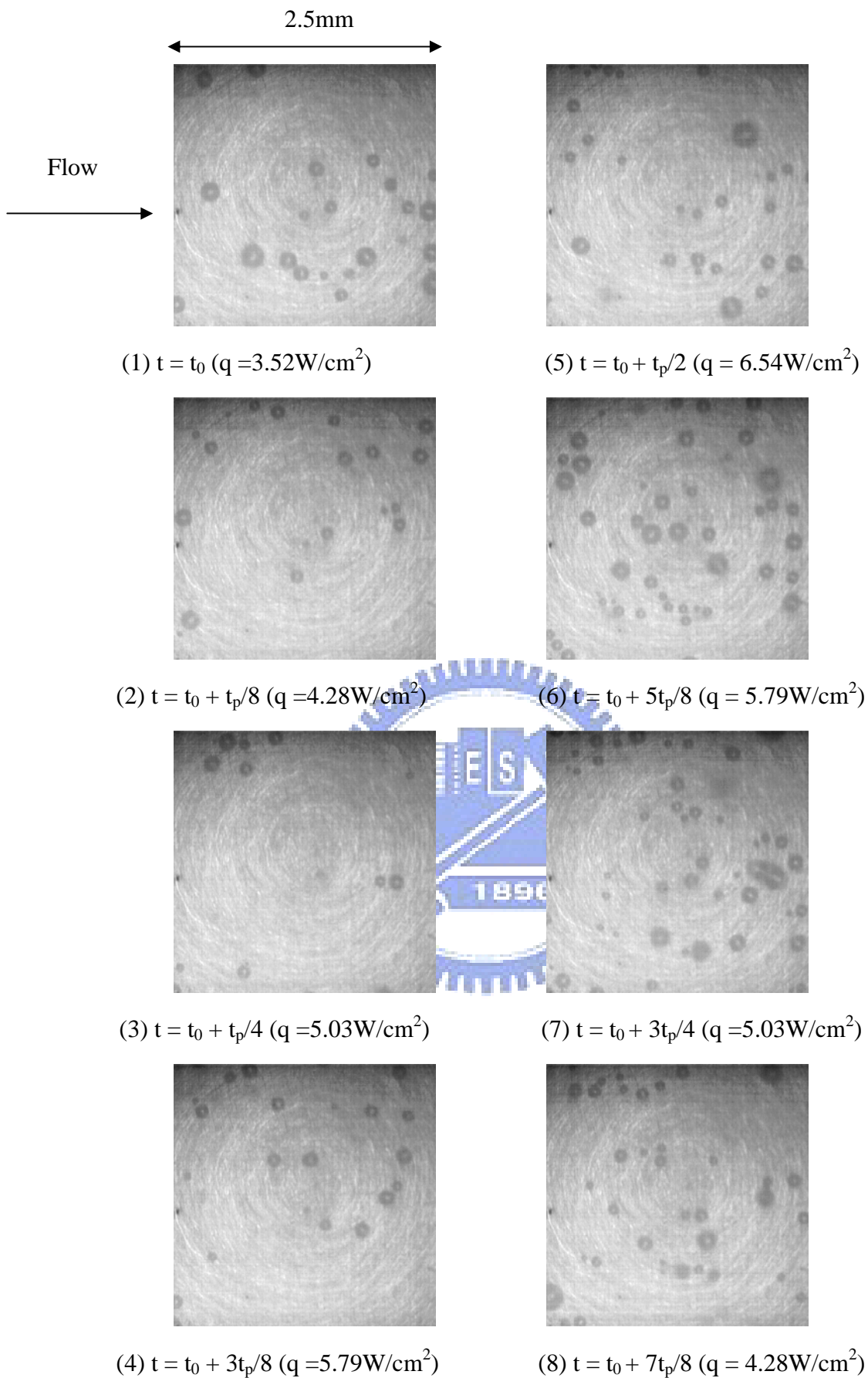


Fig. 5.44 Photos of subcooled flow boiling at certain time instants in a typical time periodic cycle for a constant imposed mass flux at $\bar{q} = 5.03\text{W/cm}^2$, $\Delta q/\bar{q} = 30\%$ at $G = 300\text{kg/m}^2\text{s}$ with $t_p = 20\text{sec}$. and $\Delta\bar{T}_{sub} = 15\text{K}$.

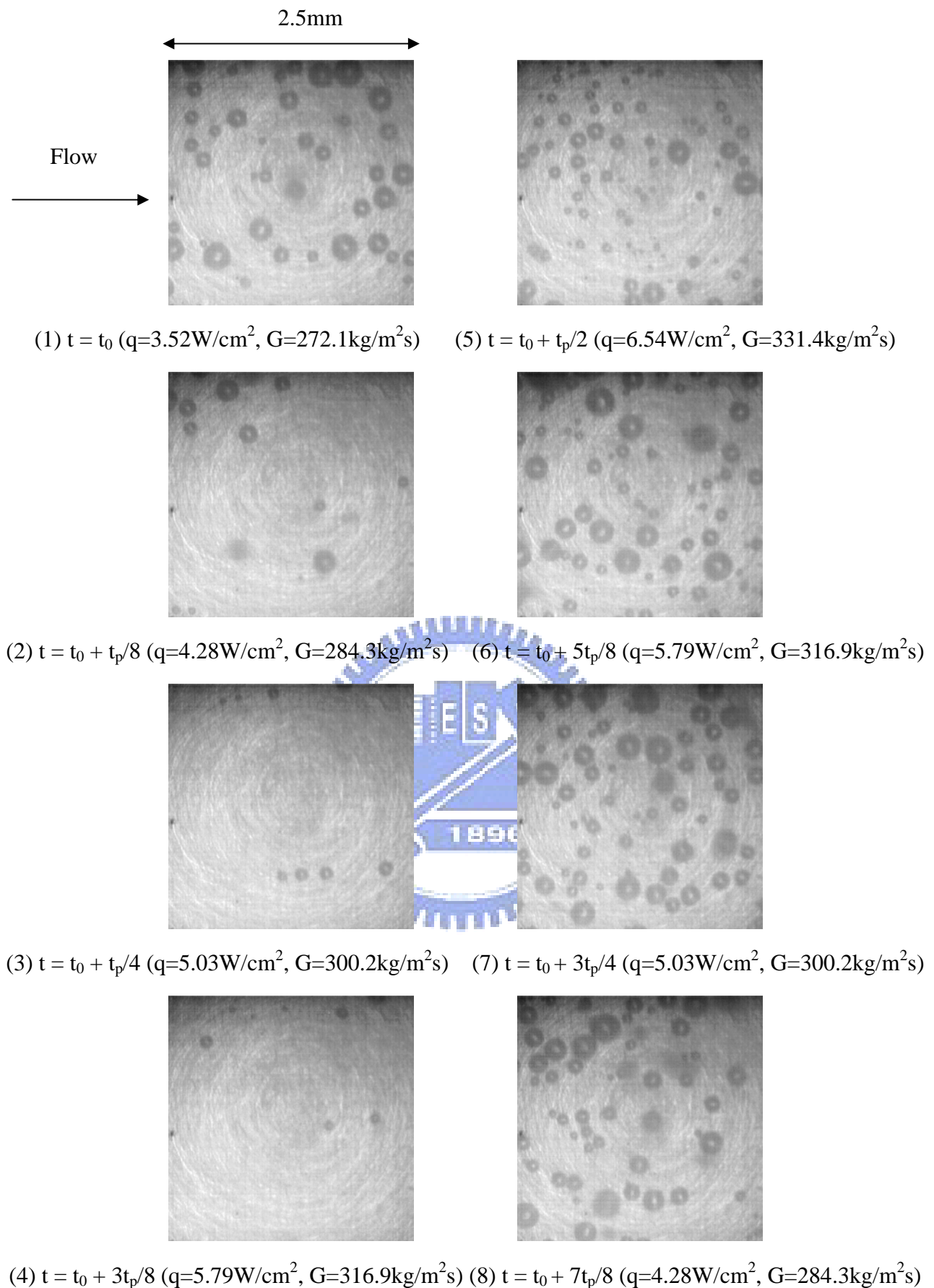


Fig. 5.45 Photos of subcooled flow boiling at certain time instants in a typical time periodic cycle for imposed in-phase G & q oscillations at $\bar{G}=300\text{kg/m}^2\text{s}$, $\Delta G/\bar{G}=10\%$, $\bar{q}=5.03\text{W/cm}^2$ and $\Delta q/\bar{q}=30\%$ with $t_p=20\text{sec.}$ and $\Delta\bar{T}_{sub}=15\text{K.}$

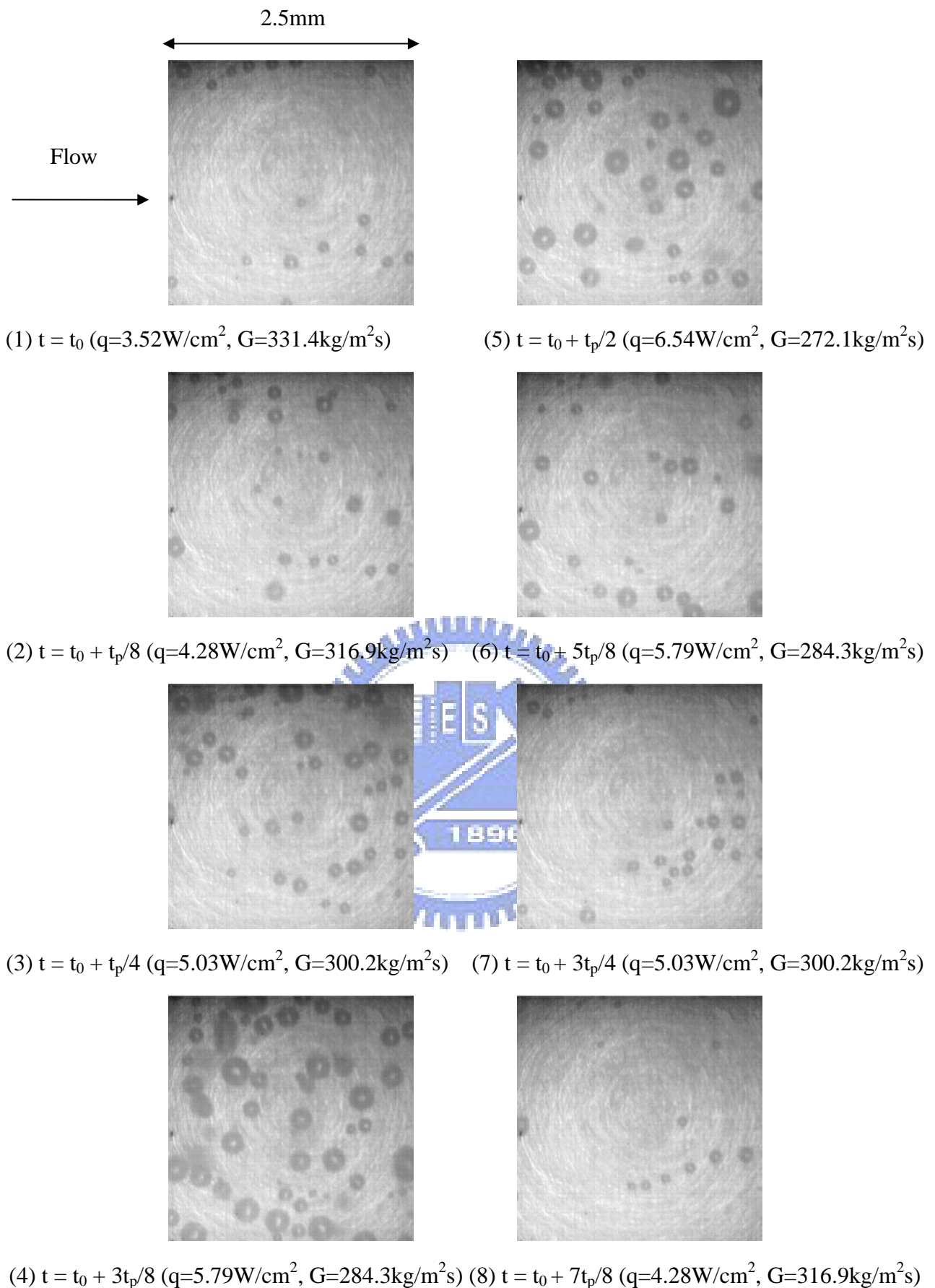


Fig. 5.46 Photos of subcooled flow boiling at certain time instants in a typical time periodic cycle for imposed out-of-phase G & q oscillations at $\bar{G}=300\text{kg/m}^2\text{s}$, $\Delta G/\bar{G}=10\%$, $\bar{q}=5.03\text{W/cm}^2$ and $\Delta q/\bar{q}=30\%$ with $t_p = 20\text{sec.}$ and $\Delta \bar{T}_{sub}=15\text{K.}$

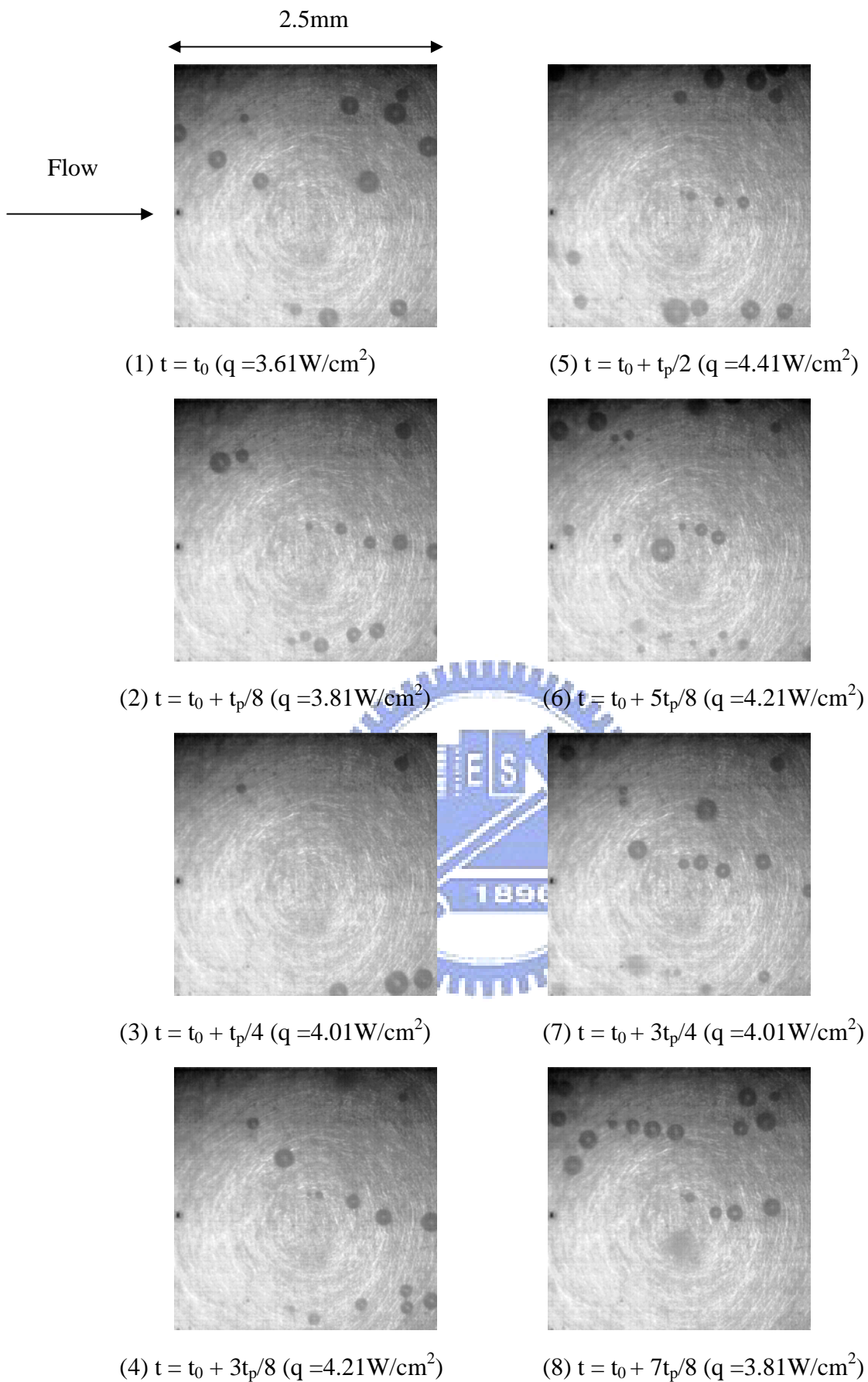


Fig. 5.47 Photos of subcooled flow boiling at certain time instants in a typical time periodic cycle for a constant imposed mass flux at $\bar{q} = 4.01 \text{ W/cm}^2$, $\Delta q/\bar{q} = 10\%$ at $G = 300 \text{ kg/m}^2\text{s}$ with $t_p = 20 \text{ sec}$. and $\Delta \bar{T}_{sub} = 10 \text{ K}$.

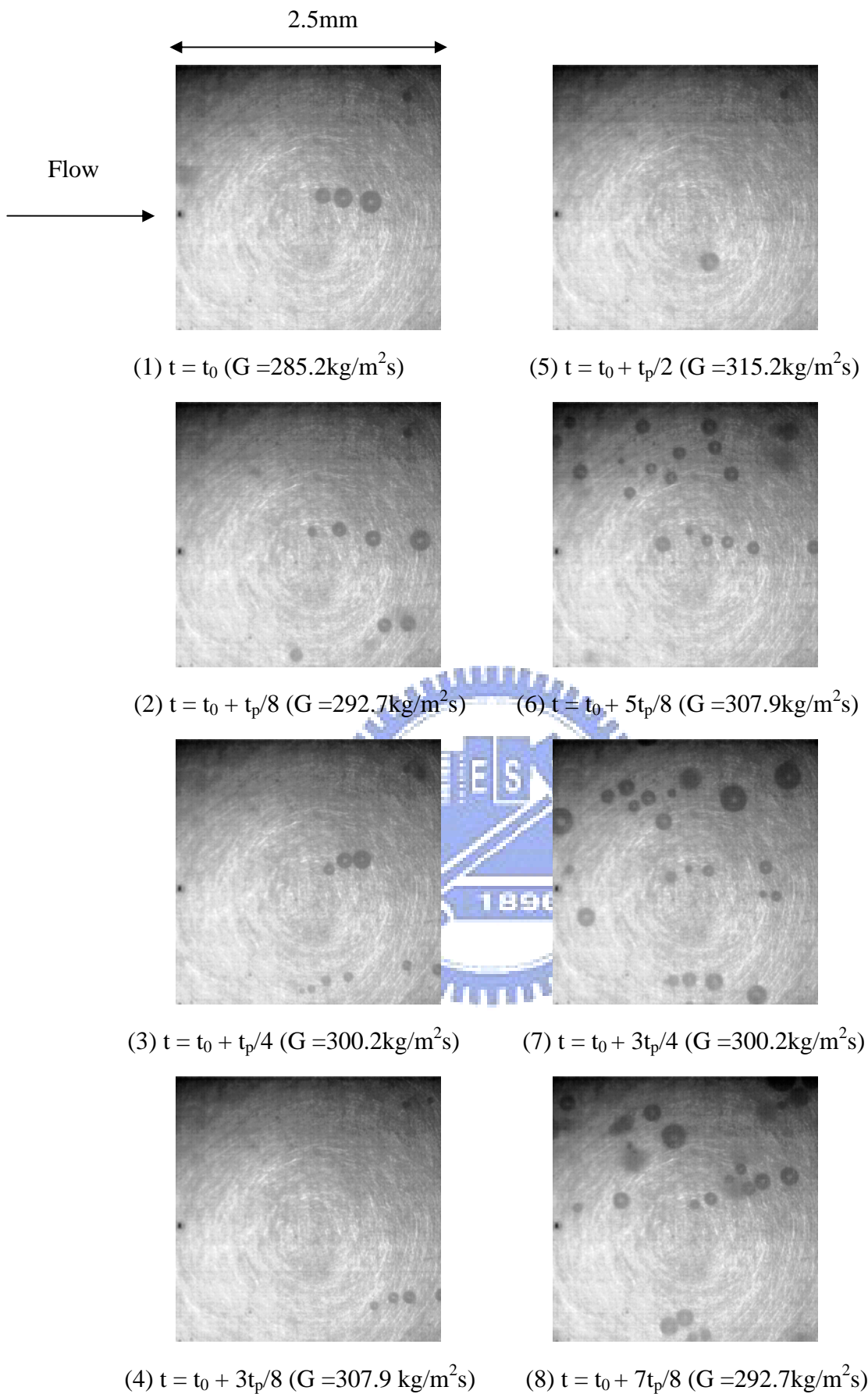


Fig. 5.48 Photos of subcooled flow boiling at certain time instants in a typical time periodic cycle for a constant imposed heat flux at $\bar{q} = 4.01 \text{ W/cm}^2$ at $G = 300 \text{ kg/m}^2 \text{ s}$, $\Delta G/\bar{G} = 5\%$ with $t_p = 20 \text{ sec}$. and $\Delta \bar{T}_{sub} = 10 \text{ K}$.

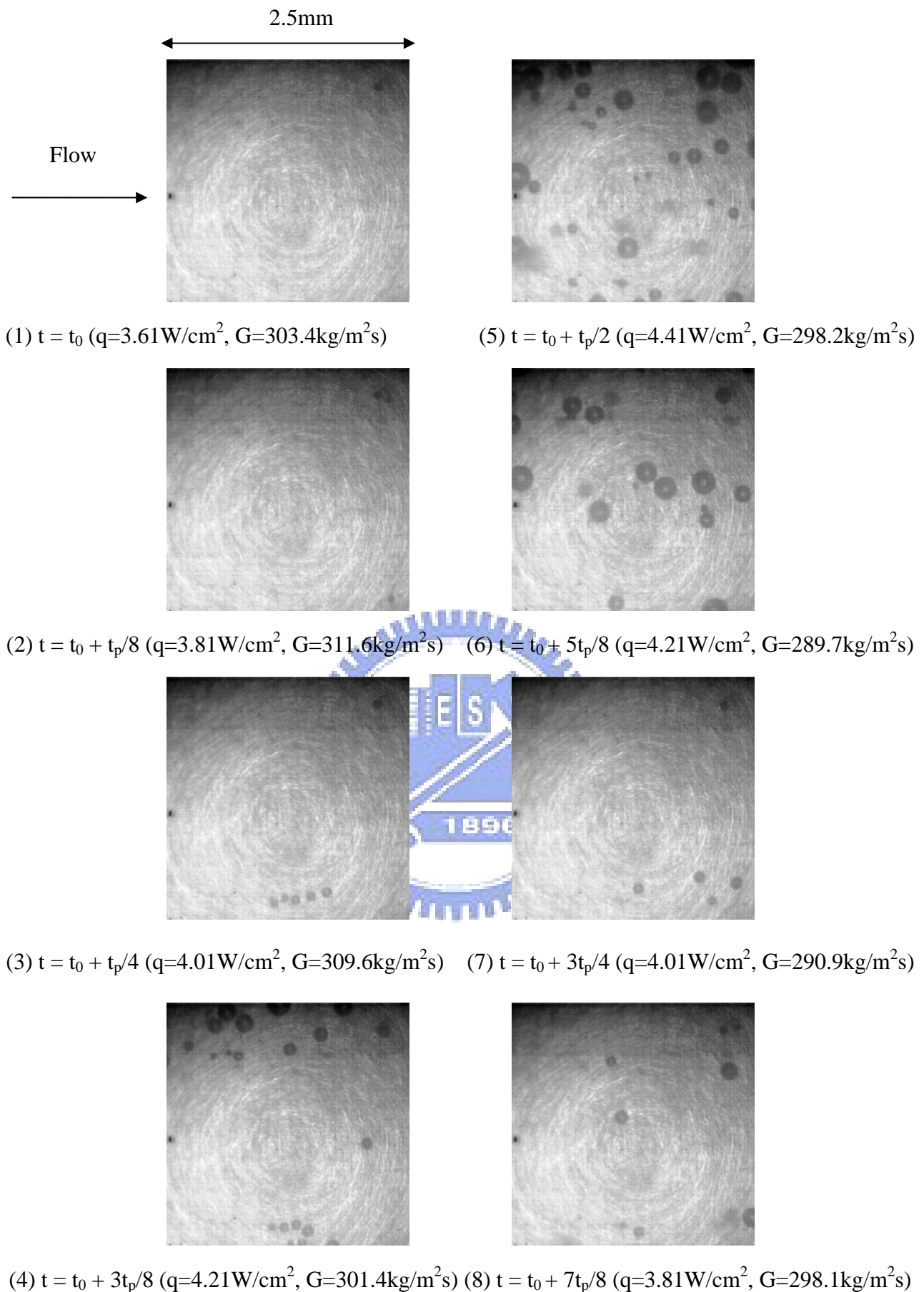


Fig. 5.49 Photos of subcooled flow boiling at certain time instants in a typical time periodic cycle

for imposed out-of-phase G & q oscillations at $\bar{G}=300\text{kg/m}^2\text{s}$, $\Delta G/\bar{G}=5\%$, $\bar{q}=4.01\text{W/cm}^2$ and

$\Delta q/\bar{q}=10\%$ with $t_p = 20\text{sec.}$ and $\Delta T_{sub}=10\text{K.}$

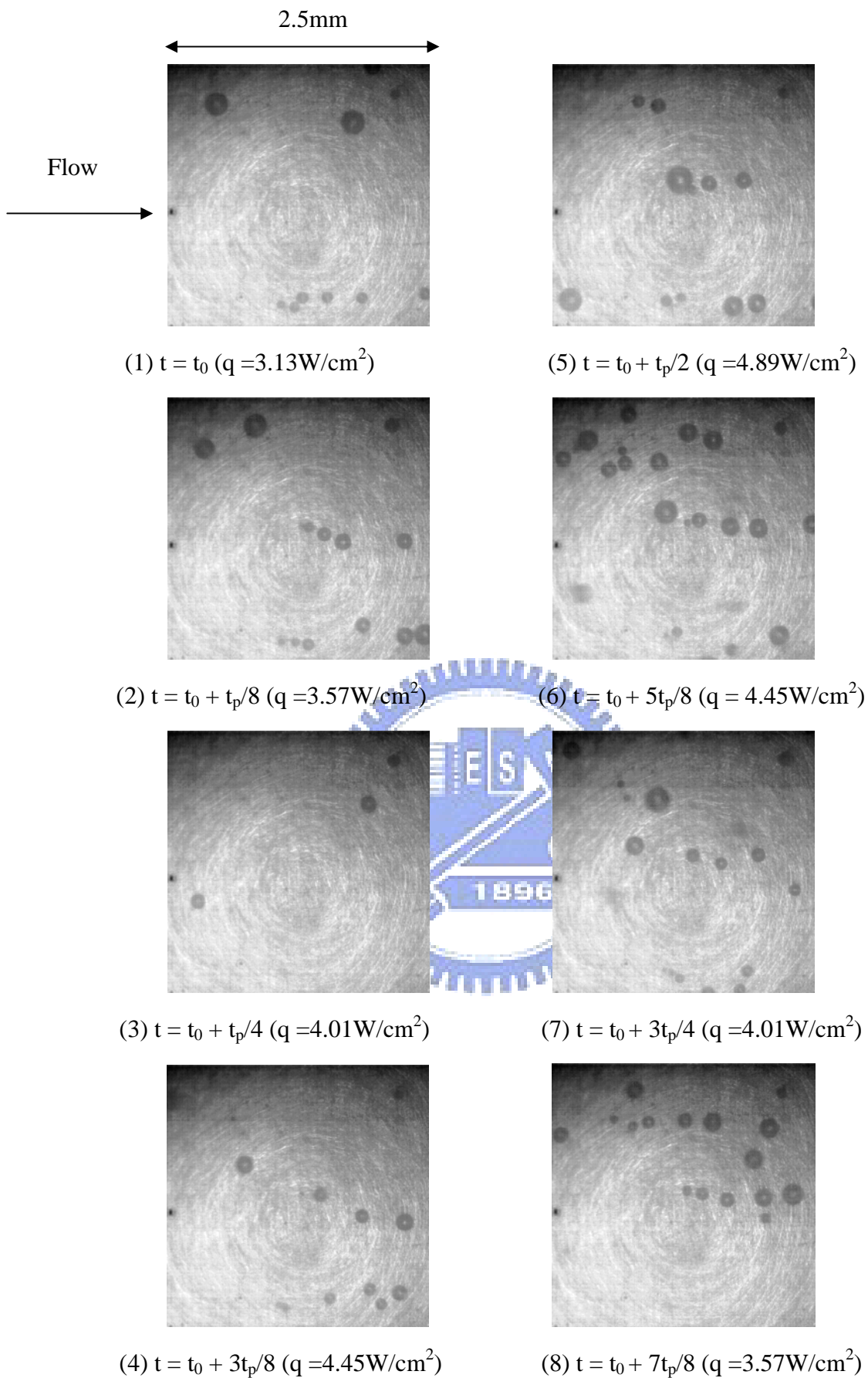


Fig. 5.50 Photos of subcooled flow boiling at certain time instants in a typical time periodic cycle for a constant imposed mass flux at $\bar{q} = 4.01 \text{ W/cm}^2$, $\Delta q/\bar{q} = 22\%$ at $G = 300 \text{ kg/m}^2\text{s}$ with $t_p = 20 \text{ sec}$. and $\Delta \bar{T}_{sub} = 10 \text{ K}$.

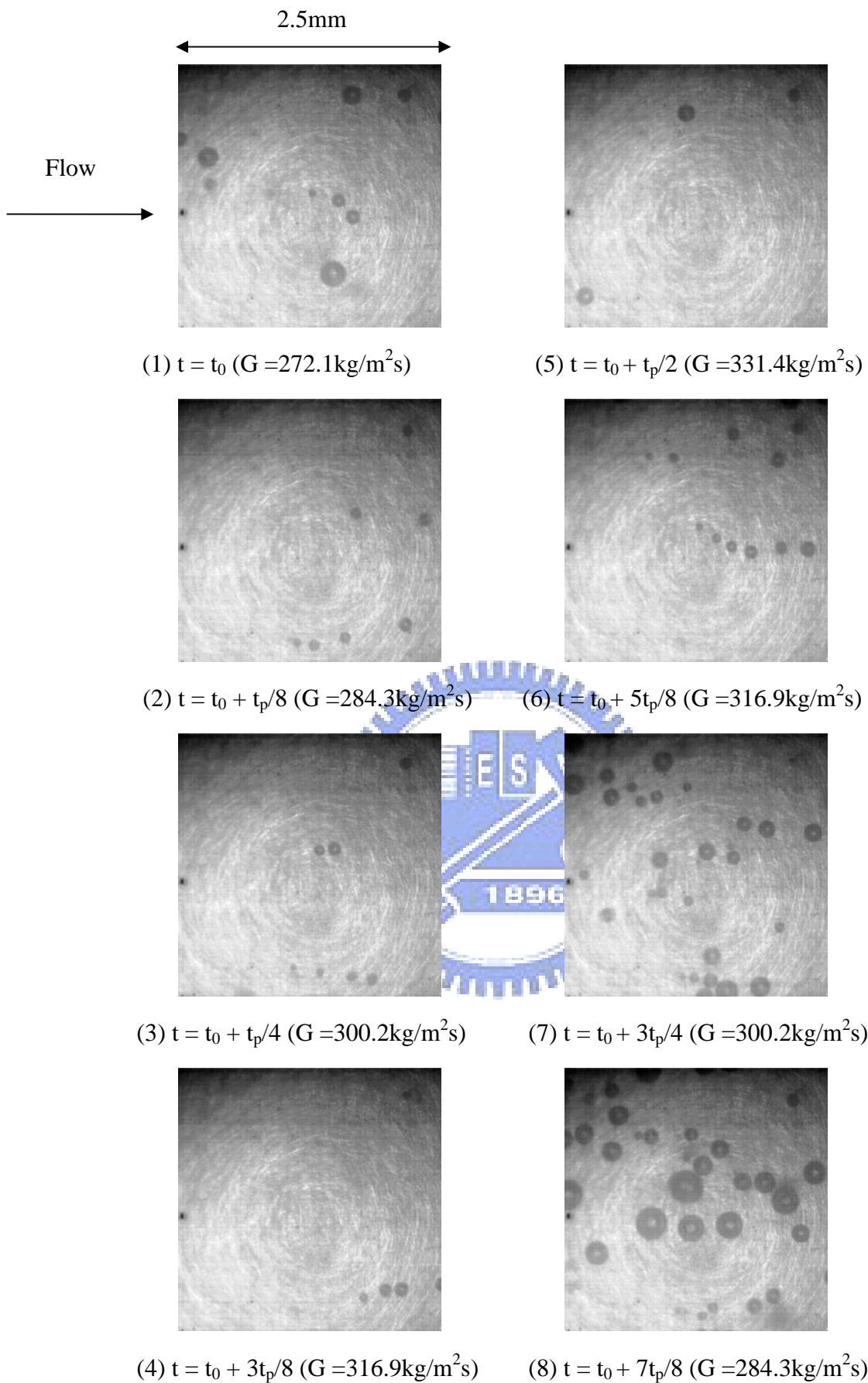


Fig. 5.51 Photos of subcooled flow boiling at certain time instants in a typical time periodic cycle for a constant imposed heat flux at $\bar{q} = 4.01 \text{ W/cm}^2$ at $G = 300 \text{ kg/m}^2\text{s}$, $\Delta G/\bar{G} = 10\%$ with $t_p = 20 \text{ sec}$. and $\Delta \bar{T}_{sub} = 10 \text{ K}$.

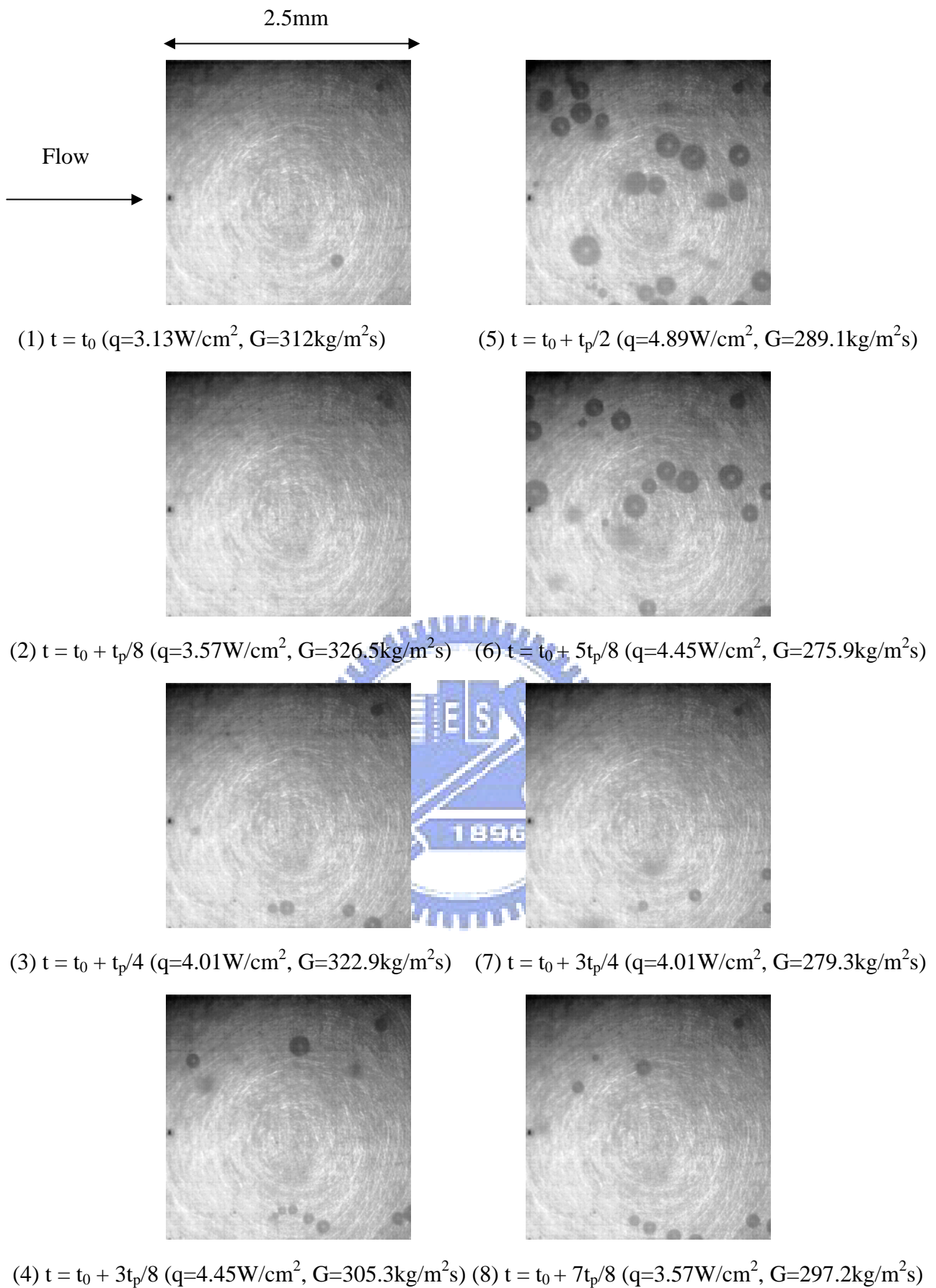


Fig. 5.52 Photos of subcooled flow boiling at certain time instants in a typical time periodic cycle for imposed out-of-phase G & q oscillations at $\bar{G}=300\text{kg/m}^2\text{s}$, $\Delta G/\bar{G}=10\%$, $\bar{q}=4.01\text{W/cm}^2$ and $\Delta q/\bar{q}=22\%$ with $t_p = 20\text{sec.}$ and $\Delta \bar{T}_{sub}=10\text{K.}$

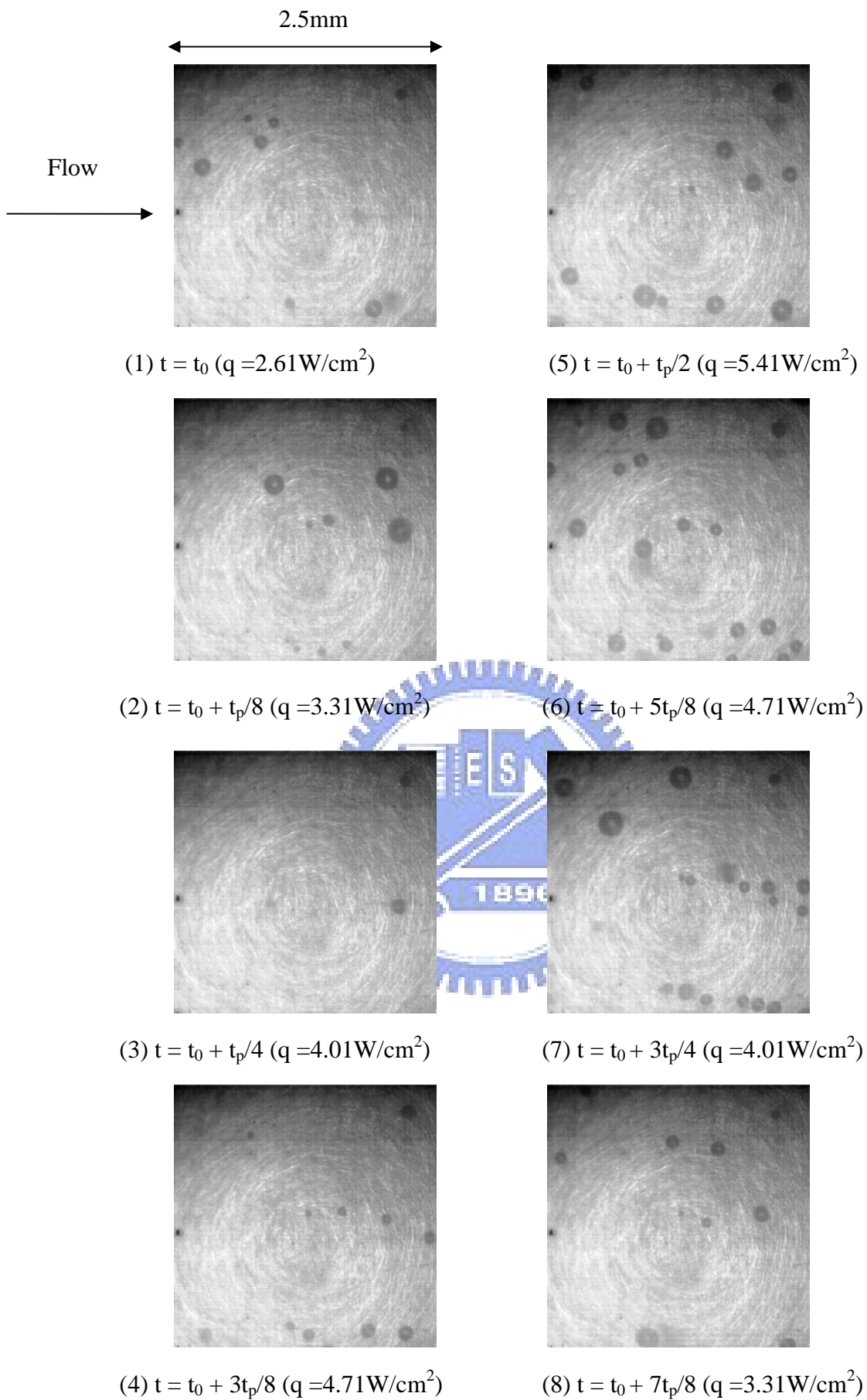


Fig. 5.53 Photos of subcooled flow boiling at certain time instants in a typical time periodic cycle for a constant imposed mass flux at $\bar{q} = 4.01 \text{ W/cm}^2$, $\Delta q / \bar{q} = 35\%$ at $G = 300 \text{ kg/m}^2\text{s}$ with $t_p = 20 \text{ sec}$. and $\Delta \bar{T}_{sub} = 10 \text{ K}$.

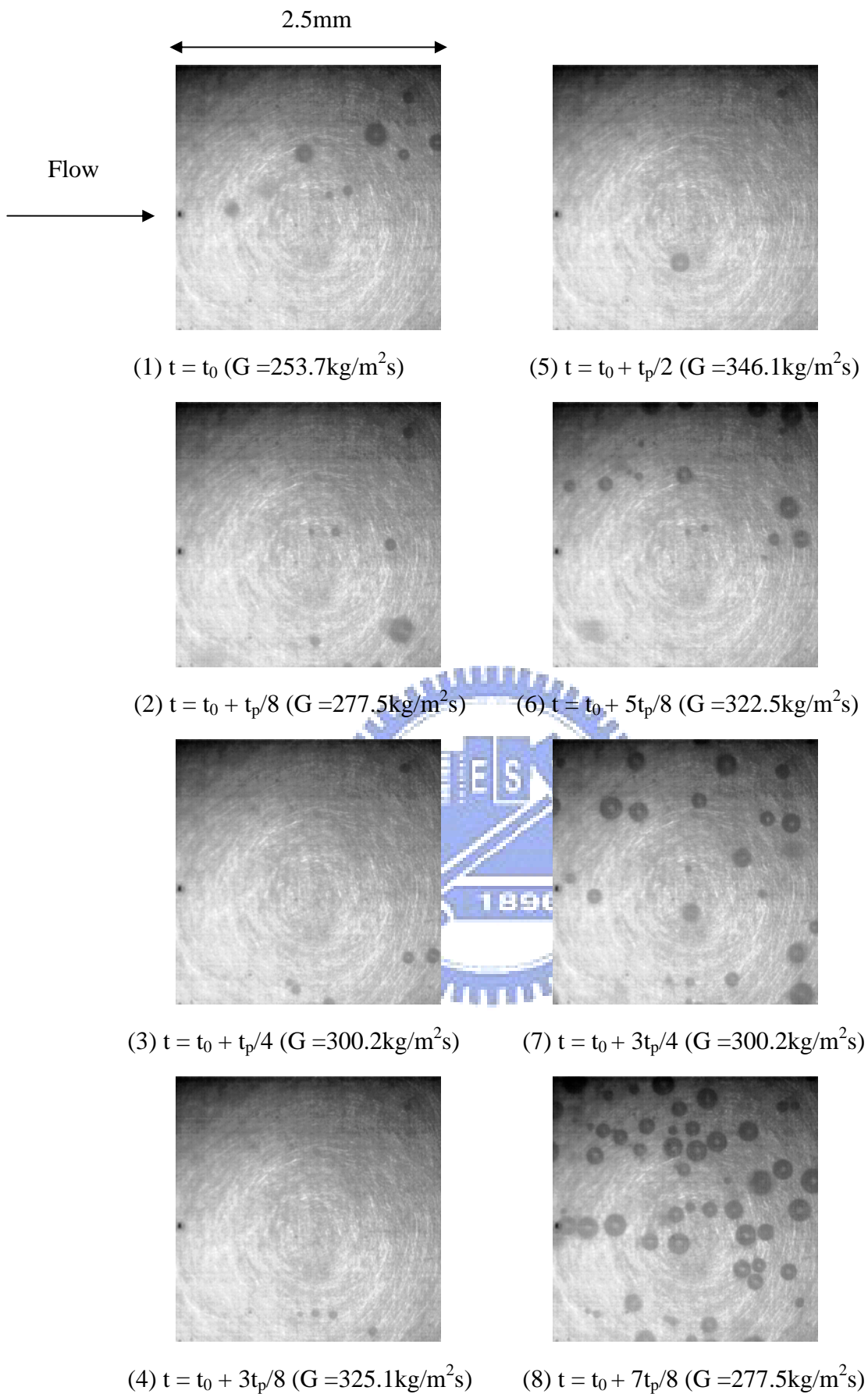


Fig. 5.54 Photos of subcooled flow boiling at certain time instants in a typical time periodic cycle for a constant imposed heat flux at $\bar{q} = 4.01 \text{ W/cm}^2$ at $G = 300 \text{ kg/m}^2\text{s}$, $\Delta G/\bar{G} = 15\%$ with $t_p = 20 \text{ sec}$. and $\Delta \bar{T}_{sub} = 10 \text{ K}$.

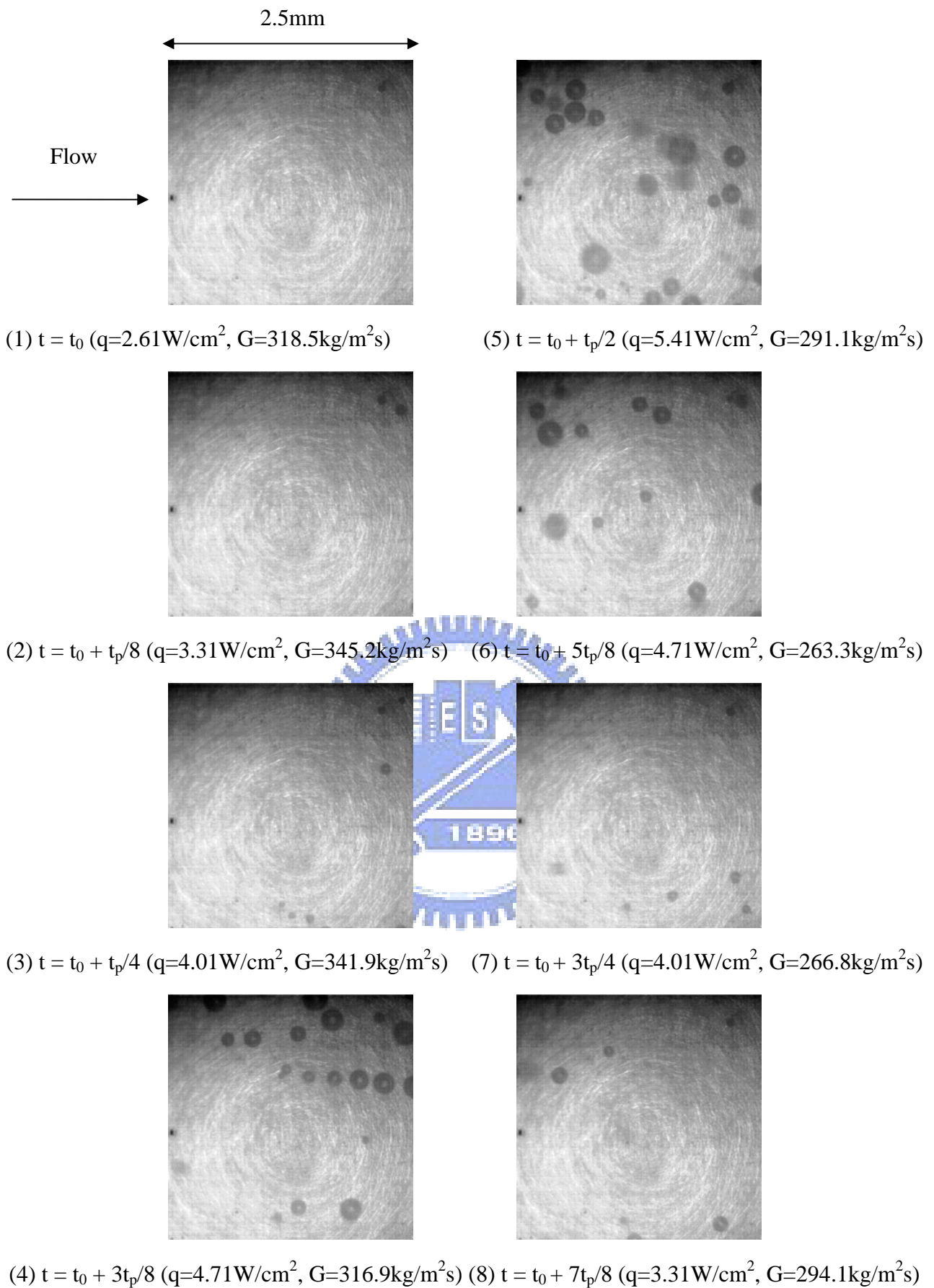


Fig. 5.55 Photos of subcooled flow boiling at certain time instants in a typical time periodic cycle for imposed out-of-phase G & q oscillations at $\bar{G}=300\text{kg/m}^2\text{s}$, $\Delta G/\bar{G}=15\%$, $\bar{q}=4.01\text{W/cm}^2$ and $\Delta q/\bar{q}=35\%$ with $t_p=20\text{sec}$. and $\Delta\bar{T}_{sub}=10\text{K}$.

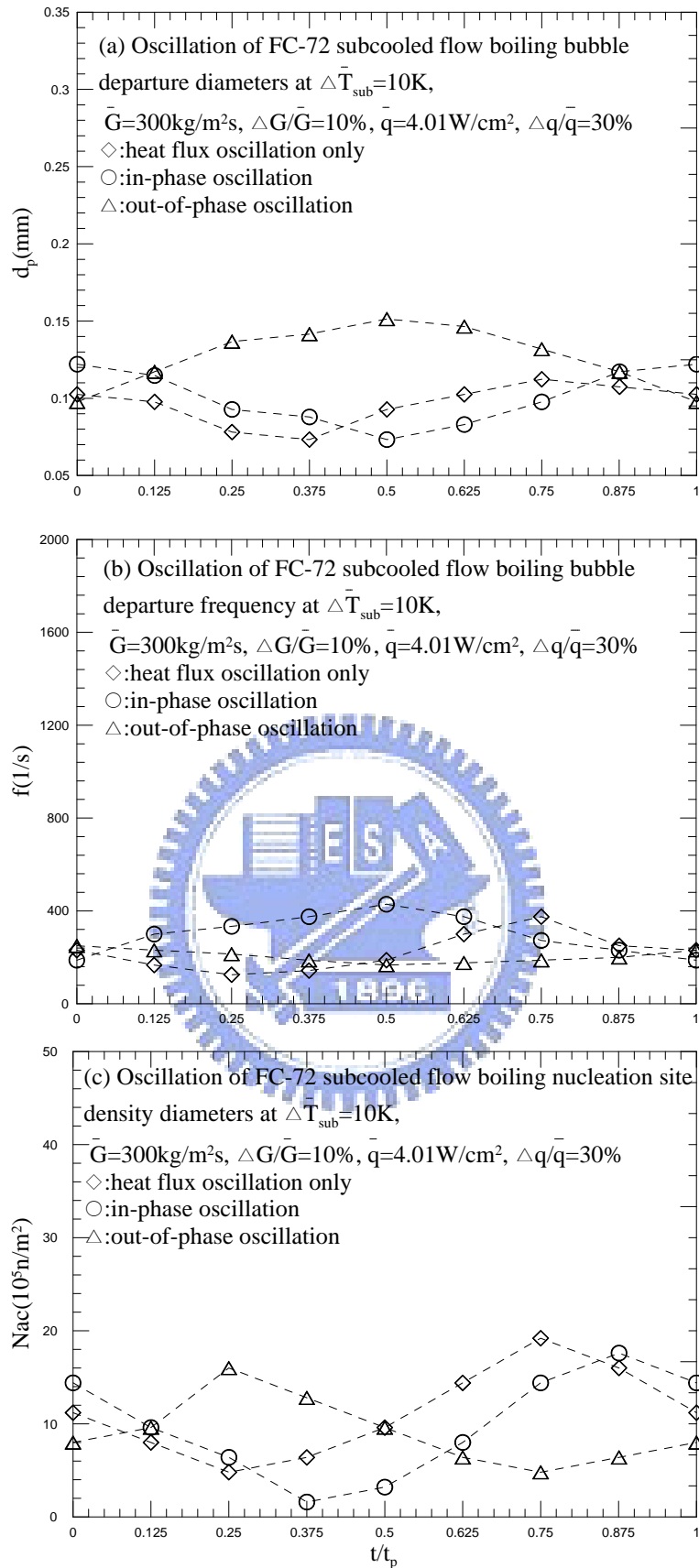


Fig. 5.56 Time period oscillatory subcooled flow boiling of FC-72 with $\bar{q} = 4.01\text{W/cm}^2$, $\Delta q/\bar{q} = 30\%$, $\bar{G}=300\text{kg/m}^2\text{s}$, $\Delta \bar{G}/\bar{G} = 10\%$ and $t_p=20\text{sec}$. for the time variations of bubble characteristics: (a) bubble departure diameter (b) bubble departure frequency (c) active nucleation site density.

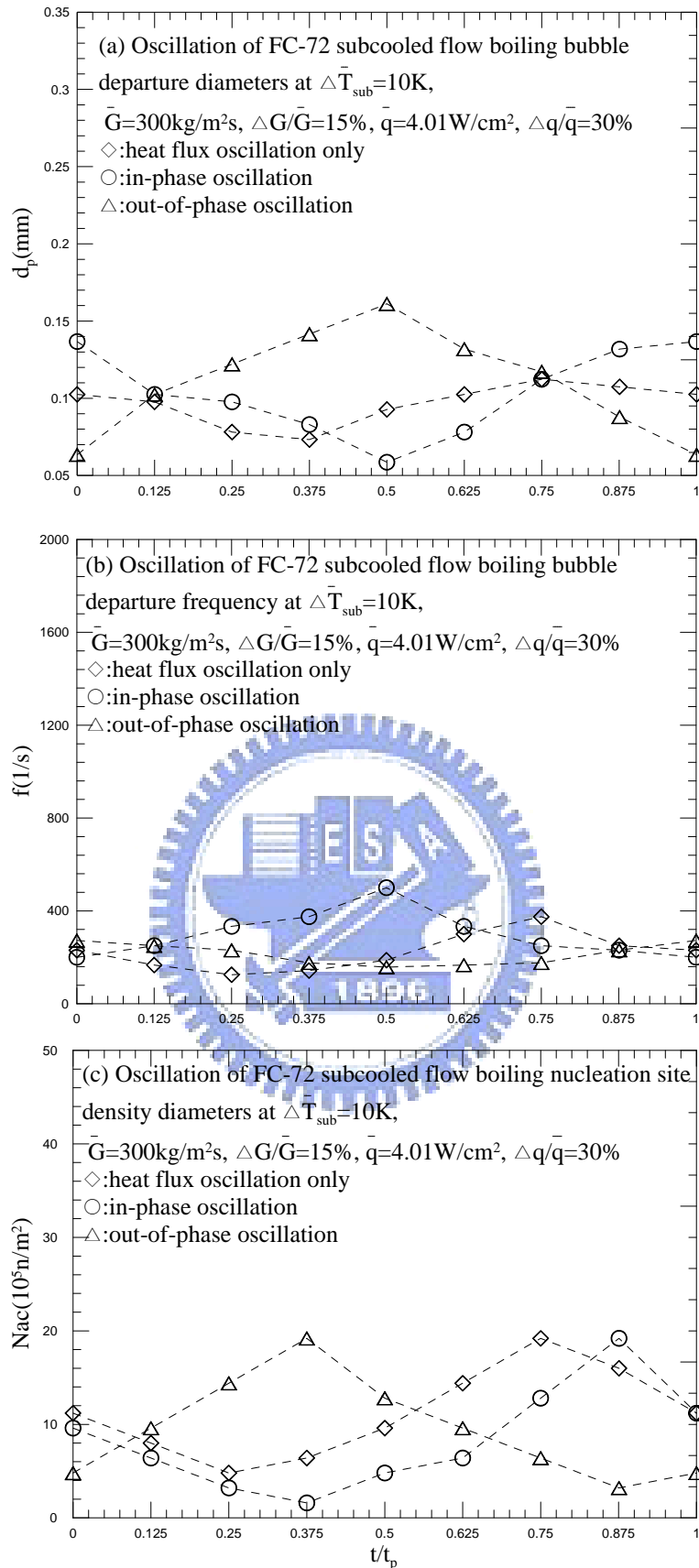


Fig. 5.57 Time period oscillatory subcooled flow boiling of FC-72 with $\bar{q} = 4.01\text{W/cm}^2$, $\Delta q/\bar{q} = 30\%$, $G=300\text{kg/m}^2\text{s}$, $\Delta G/\bar{G} = 15\%$ and $t_p=20\text{sec}$. for the time variations of bubble characteristics: (a) bubble departure diameter (b) bubble departure frequency (c) active nucleation site density.

CHAPTER 6

CONCLUDING REMARKS

The temporal saturated and subcooled flow boiling heat transfer and associated bubble characteristics of FC-72 flow over a small heated circular copper flat plate flush mounted on the bottom of a rectangular channel subject to time periodic heat flux and coolant mass flux oscillating simultaneously in forms of nearly a sinusoidal wave and a triangular wave have been experimentally investigated for both in-phase and out-of-phase G and q oscillations. The effects of the mean level and the oscillation amplitude and period of the imposed heat and mass flux oscillations, inlet liquid subcooling, and the mean coolant mass flux on the time periodic FC-72 flow boiling heat transfer coefficients and associated bubble characteristics such as the mean bubble departure diameter, bubble departure frequency, and active nucleation site density have been examined in detail. Major results presented in Chapters 4 and 5 can be summarized as follows:

- (1) The heated surface is found to also oscillate periodically in time at the same frequency as the imposed G and q oscillations. Besides, the amplitude of the T_w oscillation is generally smaller in the flow boiling when the out-of-phase G and q oscillations are imposed. But in the single-phase flow the T_w oscillation is normally weakened by imposing in-phase G and q oscillation.
- (2) The heated surface temperature oscillation resulting from the imposed heat flux oscillation can be significantly suppressed and even completely wiped out by imposing an out-of-phase G oscillation of suitable amplitude in the flow boiling. For the single-phase flow an in-phase G oscillation should be used. Besides, the time instant of imposing G oscillation should consider the difference in the time lag of T_w due to mass flux and heat flux oscillations.

- (3) An increase in the inlet liquid subcooling results in stronger oscillations in the T_w oscillation. The use of a mass flux oscillation to wipe out the T_w oscillation resulting from the heat flux oscillation is more difficult in the flow boiling especially at a high mean heat flux. But the T_w oscillation can still be suppressed substantially by a suitable choice of a mass flux oscillation.



REFERENCES

1. R. E. Simons, "Thermal Management of Electronic Packages," *Solid State Technology* (1983) 131-137.
2. F. P. Incropera, J. S. Kerby, D. F. Moffatt and S. Ramadhyani, "Convection Heat Transfer from Discrete Heat Sources in a Rectangular Channel," *International Journal of Heat and Mass Transfer* 29 (7) (1986) 1051-1058.
3. K. R. Samant and T. W. Simon, "Heat Transfer from a Small Heated Region to R-113 and FC-72," *Transactions of the ASME Journal of Heat Transfer* 111 (1989) 1053-1059.
4. S. V. Garimella and P. A. Eibeck, "Heat Transfer Characteristics of an Array of Protruding Elements in Single Phase Forced Convection," *International Journal of Heat and Mass Transfer* 33 (12) (1990) 2659-2669.
5. C. O. Gersey and I. Mudawar, "Effects of Orientation on Critical Heat Flux From Chip Arrays During Flow Boiling," *Transactions of the ASME Journal of electronic packaging* 114 (1992) 290-299.
6. T. J. Heindel, F. P. Incropera, and S. Ramadhyani, "Liquid Immersion Cooling of a Longitudinal Array of Discrete Heat Sources in Protruding Substrates : I – Single-Phase Convection," *Transactions of the ASME Journal of Electronic Package* 114 (1992) 55-62.
7. T. J. Heindel, S. Ramadhyani and F. P. Incropera, "Liquid Immersion Cooling of a Longitudinal Array of Discrete Heat Sources in Protruding Substrates : II – Forced Convection Boiling," *Transactions of the ASME Journal of Electronic Packaging* 114 (1992) 63-70.
8. C. P. Tso, K. W. Tou and G. P. Xu, "Numerical Modeling of Turbulent Heat Transfer from Discrete Sources in a Liquid-cooled Channel," *International Journal of Heat and Mass Transfer*, 33 (12) (1998) 1157-1166.
9. T. C. Willingham and I. Mudawar, "Forced-Convection Boiling and Critical Heat Flux from a Linear Array of Discrete Heat Sources," *International Journal of Heat and Mass Transfer* 35 (11) (1992) 2879-2890.

10. R. Hohl, J. Blum, M. Buchholz, T. Luttich, H. Auracher, W. Marquardt, "Model-based Experimental Analysis of Pool Boiling Heat Transfer with Controlled Wall Temperature Transients," *International Journal of Heat Transfer*, Vol. 43 (2001) 2225-52238.
11. A. Sakurai and M. Shiotsu, "Transient Pool Boiling Heat Transfer – I. Incipient Boiling Superheat," *International Journal of Heat Transfer* 99 (1999) 547-553.
12. K. Okuyama, Y. Kozawa, A. Inoue and S. Aoki, "Transient Boiling Heat Transfer Characteristics of R113 at Large Stepwise Power Generation," *International Journal of Heat and Mass Transfer* 31(10) (1988) 2161-2174.
13. K. Okuyama and Y. Iida, "Transient Boiling Heat Transfer Characteristics of Nitrogen (bubble behavior and heat transfer rate at stepwise heat generation)," *International Journal of Heat and Mass Transfer* 33(10) (1990) 2065-2071
14. Marie-Christine Duluc, B. Stutz and M. Lallem, "Transient nucleate boiling under stepwise heat generation for highly wetting fluids," *International Journal of Heat and Mass Transfer* 47 (2004) 5541-5553.
15. H. Auracher and W. Marquardt, "Heat transfer characteristics and mechanisms along entire boiling curves under steady-state and transient conditions," *International Journal of Heat and Fluid Flow* 25 (2004) 223-242.
16. M. Girault and D. Petit, "Resolution of Linear Inverse Forced Convection Problems Using Model Reduction by the Modal Identification Method: Application to Turbulent Flow in parallel-Plate Duct," *International Journal of Heat and Mass Transfer* 47 (2004) 3909-3925.
17. H. Bhowmik and K.W. Tou, "Study of transient forced convection heat transfer from Discrete Heat Sources in a FC-72 Cooled Vertical Channel," *International Journal of Thermal Sciences* 44 (2005) 499-505.
18. H. Bhowmik and K.W. Tou, "Experimental study of transient natural convection heat transfer from simulated electronic chips," *Experimental Thermal and Fluid Science* 29 (2005) 485-492).
19. H. Bhowmik and K.W. Tou, "Thermal Behavior of Simulated Chips During Power-off Transient Period," *Electronics Packaging Technology conference 2003*
20. I. Kataoka, A. Serizawa and A. Sakurai, "Transient Boiling Heat Transfer Under

- Forced Convection,” *International Journal of Heat and Mass Transfer* 26 (1983) 583-595.
21. S. Lin, P.A. Kew and K. Cornwell, “Two-Phase Heat Transfer to a Refrigerant in a 1 mm Diameter Tube,” *International Journal of Refrigeration* 24 (2001) 51-56.
 22. T. Otsuji and A. Kurosawa, “Critical Heat Flux of Forced Convection Boiling in an Oscillating Acceleration Field : I–General Trends,” *Nuclear Engineering and Design*, Vol.71,(1982),pp. 15-26.
 23. T. Otsuji and A. Kurosawa, “Critical Heat Flux of Forced Convection Boiling in an Oscillating Acceleration Field : II–Contribution of flow Oscillation,” *Nuclear Engineering and Design*, Vol.76,(1983),pp. 13-21.
 24. S. Kakac, T. N. Veziroglu, M. M. Padki, L. Q. Fu, and X. J. Chen, “Investigation of Thermal Instability in a Forced Convection Upward Boiling System, ”*Experimental Thermal and Fluid Science*, Vol. 3,(1990),pp. 191-201.
 25. M. M. Padki, H. T. Liu, and Kakac, “Two-Phase Flow Pressure-Drop type and Thermal Oscillations,” *International Journal of Heat and Fluid Flow*, Vol. 12,(1991),pp. 240-248.
 26. Y. Ding, S. Kakac, and X. J. Chen, “Dynamic Instabilities of Boiling Two-Phase Flow in a Single Horizontal Channel, ”*Experimental Thermal and Fluid Science*, Vol. 11,(1995),pp.327-342.
 27. O. Comakli, S. Karsli, and M. Yilmaz, “Experimental Investigate of Two Phase Flow Instability in a Horizontal in-tube Boiling System, ”*Energy Convection and Management*, Vol. 43,(2002),pp.249-268.
 28. P. R. Mawasha and R. J. Gross, “Periodic Oscillations in a Horizontal Single Boiling Channel with Thermal Wall Capacity,” *International Journal of Heat and Fluid Flow* 22 (2001) 643-649.
 29. P. R. Mawasha, R. J. Gross, and D. D. Quinn, “Pressure-Drop Oscillations in a Horizontal Single Boiling Channel,” *Heat Transfer Engineering* 22 (2001) 26-34.
 30. Q. wang, X. J. Chen, S. kakac, and Y. Ding, “Boiling Onset Oscillation : a new type of Dynamic Instability in a Forced-Convection Upflow Boiling System,” *International Journal of Heat and Fluid Flow* 17(1996) 418-423.
 31. D. Brutin, F. Topin, and L. Tadrist, “Experimental Study of Unsteady Convective

- Boiling in Heated Minichannels,” *International Journal of Heat and Mass Transfer* 46 (2003) 2957-2965.
32. D. Brutin and L. Tadrist, “Pressure Drop and Heat Transfer Analysis of Flow Boiling in a Minichannel : Influence of the Inlet Condition on Two-phase Flow Stability,” *International Journal of Heat and Mass Transfer* 47 (2004) 2365-2377.
 33. J. Shuai, R. Kulenovic, and M. Groll, “Pressure Drop Oscillations and Flow Patterns for Flow Boiling of Water in Narrow Channel,” *Proceedings of International Conference on Energy and the Environment, Shanghai, China, May 22-24, 2003.*
 34. S. H. Chang, I. C. Bang and Won-Pil Baek, “A Photographic Study on the Near-wall Bubble Behavior in Subcooled Flow Boiling,” *Int. J. Therm.* 41 (2002) 609-618.
 35. K. Cornwell and P. A. Kew, *Boiling in small parallel channels, Energy Efficiency in Process Technology*, P.A. Pilavachi, Elsevier Applied Science, London, 1993, pp. 624-638.
 36. Y. M. Lie and T. F. Lin, Saturated flow boiling heat transfer and associated bubble characteristics of R-134a in a narrow annular duct, *International Journal of Heat and Mass Transfer* 48(25-26)(2005)5602-5615.
 37. Y. M. Lie and T. F. Lin, Subcooled flow boiling heat transfer and associated bubble characteristics of R-134a in a narrow annular duct, *International Journal of Heat and Mass Transfer* 49(13-14)(2006)2077-2089.
 38. I. C. Bang, S. H. Chang and Won-Pil Baek, “Visualization of the Subcooled Flow Boiling of R-134a in a Vertical Rectangular Channel with an Electrically Heated wall,” *International Journal of Heat and Mass Transfer* 47 (2004) 4349-4363.
 39. S. G. Kandlikar, “Bubble Nucleation and Growth Characteristics in Subcooled Flow Boiling of Water,” *National Heat Transfer Conference HTD-Vol. 342* 4 (1997) 11-18.
 40. R. Maurus, V. Ilchenko and T. Sattelmayer, “Study of the Bubble Characteristics and the Local Void Fraction in Subcooled Flow Boiling Using Digital Imaging and Analyzing Techniques,” *International Journal of Heat and Fluid Flow* 26 (2002) 147-155.
 41. R. Maurus, V. Ilchenko and T. Sattelmayer, “Automated high-speed video analysis of the Bubble Dynamics in Subcooled Flow Boiling,” *International Journal of Heat and Fluid Flow* 25 (2004) 149-158.
 42. R. Maurus and T. Sattelmayer, “Bubble and Boundary Layer Behavior in Subcooled

- Flow Boiling,” *International Journal of Heat and Fluid Flow* 45 (2006) 257-268.
43. G. E. Thorncroft, J. F. Klausner and R. Mei, “An Experimental Investigation of Bubble Growth and Detachment in Vertical Upflow and Downflow Boiling,” *International Journal of Heat and Mass Transfer* 41 (1998) 3857-3871.
 44. T. Okawa, T. Ishida, I. Kataoka, and M. Mori, “An experimental on bubble rise path after the departure from a nucleation site in vertical upflow boiling,” *Experimental Thermal and Fluid Science* 29 (2005) 287-294.
 45. T. Okawa, T. Ishida, I. Kataoka, and M. Mori, “Bubble rise characteristics after the departure from a nucleation site in vertical upflow boiling of subcooled water,” *Nuclear Engineering and Design* 235 (2005) 1149-1161.
 46. T. Okawa, T. Ishida, I. Kataoka, and M. Mori, “On the rise paths of single vapor bubbles after the departure from nucleation sites in subcooled upflow boiling,” *International Journal of Heat and Mass Transfer* 48 (2005) 4446-4459.
 47. R. Situ, T. Hibiki, M. Ishii, and M. Mori, “Photographic study of bubble behaviors in forced convection subcooled boiling,” *International Journal of Heat and Mass Transfer* 47 (2004) 3659-3667.
 48. R. Situ, T. Hibiki, M. Ishii, and M. Mori, “Bubble lift-off size in forced convection subcooled boiling flow,” *International Journal of Heat and Mass Transfer* 48 (2005) 5536-5548.
 49. C. P. Yin, Y. Y. Yan, T. F. Lin. And B. C. Yang, “Subcooled flow boiling heat transfer of R-134a and bubble characteristics in a horizontal annular duct,” *International Journal of Heat and Mass Transfer* 43 (2000) 1885-1896.
 50. 3M company, Kataoka
 51. S. J. Kline and F. A. McClintock, “describing uncertainties in single-sample experiments,” *Mech. Engineering* 75 (1953) 3-8.
 52. 楊政陞, “Transient flow boiling heat transfer of FC-72 and associated bubble characteristic over a small heated plate in a horizontal rectangular channel” 國立交通大學機械工程研究所碩士論文 ,新竹,台灣